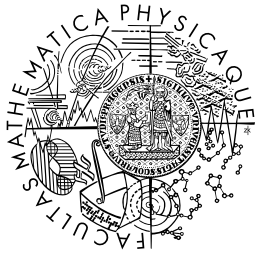

FACULTY
OF MATHEMATICS
AND PHYSICS
Charles University

DOCTORAL THESIS

Petr Kotlařík

Gravitational sources in the vicinity of black holes

Institute of Theoretical Physics

Supervisor of the doctoral thesis: doc. RNDr. Oldřich Semerák, DSc.

Study programme: Physics

Study branch: Theoretical Physics, Astronomy and Astrophysics

Prague 2024

I declare that I carried out this doctoral thesis independently, and only with the cited sources, literature and other professional sources. It has not been used to obtain another or the same degree.

I understand that my work relates to the rights and obligations under the Act No. 121/2000 Sb., the Copyright Act, as amended, in particular the fact that the Charles University has the right to conclude a license agreement on the use of this work as a school work pursuant to Section 60 subsection 1 of the Copyright Act.

In ..... date ....

Author's signature

This thesis could not have been completed without several important individuals. First and foremost, I would like to thank my supervisor, Oldřich Semerák. His lectures on *general relativity* sparked my interest in the field, and his guidance has been invaluable throughout my PhD journey. I also wish to thank my collaborators: David Kofroň, without whom I would be lost in the vast realm of perturbations and Debye potentials, and Che-Yu Chen, who initiated our work on the quasinormal modes, taking this thesis in another intriguing direction.

Additionally, I am grateful to the Institute of Theoretical Physics in Prague for providing a stimulating working environment; the Observatory of Turin, and especially Mariateresa Crosta, for their hospitality during my stay in Italy; the University of the Basque Country for the opportunity to visit Bilbao and meet the local group; and lastly, the RIKEN Institute in Tokyo for the inspiring atmosphere during my stay in Japan.

Finally, I thank my family for their constant support.

Title: Gravitational sources in the vicinity of black holes

Author: Petr Kotlařík

Institute: Institute of Theoretical Physics

Supervisor: doc. RNDr. Oldřich Semerák, DSc., Institute of Theoretical Physics

Abstract: Black holes are among the most intriguing objects in the Universe. When isolated and stationary, they are described by the simple Kerr(-Newman) metric. However, astrophysical black holes are seldom isolated; in fact, we can only know of them through their interaction with the environment. Consequently, the actual gravitational field differs from the Kerr(-Newman) ideal. This thesis investigates the influence of the environment on the gravitational field of black holes. In the stationary (or static) and axially symmetric setting, we derive several analytical models describing a black hole surrounded by a disc or ring. The static problem is solved exactly, yielding the metric in closed form in some cases. Besides the basic physical properties of the results, we analyze the scalar-field quasinormal modes in such a deformed black-hole geometry. Our findings indicate a universal behaviour of the QNM response, which may help in distinguishing the environmental effects from those of modified theories of gravity. In the stationary case, we employ perturbation theory in the tetrad formalism. By introducing the Debye potential, we find the electromagnetic field of a ring source on the rotating black-hole background. We conclude with a discussion of similar treatment of gravitational perturbations.

Keywords: black holes, accretion discs, exact solutions, perturbation theory, quasinormal modes, Debye potential.

CONTENTS

INTRODUCTION

In March, 27$^{\text{th}}$ 2024, the *Event Horizon Telescope Collaboration* (EHT) released an updated image of SgrA*, a supermassive black hole residing at the centre of our galaxy. This remarkable achievement required a unique collaboration of powerful radio telescopes from around the world, resulting in an unprecedented resolution of approximately 50 μas. The new image reveals the linear polarization of the photon ring, providing valuable insights into the surrounding electromagnetic field and offering additional constraints on the black hole parameters. It is worth noting however that "our" black hole is not the first observed. In early 2019, the same collaboration of radio telescopes unveiled the first-ever "silhouette" of a black hole located in the heart of the M87 galaxy. Both images exhibit remarkable agreement with the predictions, once again affirming the power of *general relativity*.

Soon after, the LIGO and VIRGO detectors of gravitational waves will begin their second part of the 4$^{\text{th}}$ observation run (O4), with KAGRA joining in late 2024. It is expected to detect roughly 90 events during the entire O4 run, which is about the same number as has been observed since the famous first detection on 14$^{\text{th}}$ September 2014. And this is certainly not the end. Further instrumental improvements are already planned, which again should double the total number of observations. The new generation of detectors, such as the Einstein Telescope and Cosmic Explorer, are currently being actively discussed. Our exploration will not be limited to the Earth's surface. With a high level of confidence, around the mid-2030s, we should witness the launch of the *Laser Interferometer Space Antenna* (LISA), a space-based gravitational wave detector. LISA will add new intriguing sources to our collection, including intermediate to extreme-mass-ratio-inspirals, compact binaries in our Galaxy, supermassive-black-hole mergers, and possibly the stochastic gravitational-wave background, echo of the early Universe. With the increased precision of this new generation of experiments, we not only expect to test *general relativity* in the strong-field regime, but also to probe the black-hole environment through gravitational waves.

The recent fascinating achievements suggest that we are entering a new golden age of black-hole physics. However, black holes were long seen as a mere mathe-

matical curiosity, solutions to the gravitational equations which could never exist in the real Universe. The general concept of such objects can be traced back to Newtonian times. On 27$^{\text{th}}$ November 1783, a paper in the *Philosophical Transactions of the Royal Society of London* appeared. The author, John Michell, wrote

> *"If there should really exist in nature any bodies, whose density is not less than that of the sun, and whose diameters are more than 500 times the diameter of the sun since their light could not arrive at us; or if there should exist any other bodies of a somewhat smaller size, which are not naturally luminous; of the existence of bodies under either of these circumstances, we could have no information from sight; yet, if any other luminous bodies should happen to revolve about them we might still perhaps from the motions of these revolving bodies infer the existence of the central ones with some degree of probability, ... "*

Of course, the proposed existence of "dark stars" was not taken very seriously back then. However, on 25$^{\text{th}}$ November 1915, exactly 132 years minus two days after Michell's paper, there was a lecture at the *Prussian Academy of Sciences in Berlin*. It was the last of a 6-lecture series that Autumn, where Albert Einstein presented his final form of gravitational equations. By this moment, the completely new theory of gravitation replaced more than 300 years of successful Newton's gravity. In just a month, on 22$^{\text{th}}$ December 1915, Karl Schwarzschild wrote a letter to Einstein reporting that he had found the exact solution for a point source. The letter was written under unbelievable circumstances. At that time, Schwarzschild served in the war stationed on the Russian front. He wrote, *"As you see, the war treated me kindly enough, in spite of the heavy gunfire, to allow me to get away from it all and take this walk in the land of your ideas."* Pleasantly surprised Einstein *"had not expected that one could formulate the exact solution of the point problem in such a simple way."*

This was the first exact mathematical description of a black hole, namely spherically symmetric one. In the spherical Schwarzschild coordinates, the solution has some surprising features. Apart from the expected singularity at $r = 0$ (after all, it is merely a point source), there is another singularity[1] present at $r = 2GM/c^2$, where M is the mass of the source, G is the gravitational constant, and c is the speed of light. Curiously, it is the same value that Michell found for the radius of a dark star. Photons radiated below this sphere can not escape to radial infinity. However, it still took 50 years from the Schwarzschild discovery until black holes appeared in decent astrophysical conferences. Even though, already in the 1930s, relativists predicted that a star more massive than about 1.5 times the solar mass must undergo extreme contraction and that Einstein's equations predict gravitational collapse, the change was mainly due to the observational discoveries of relativistic compact objects.

In 1962, astronomers discovered strong X-ray sources, quasars in 1963, and pulsars in 1967. Strong gamma-ray bursts were also observed around the same

[1]Today, we know that it is an example of a *coordinate* singularity, not a physical singularity. Nevertheless, the radius represents a mathematical boundary that causally disconnects the interior from the outside; it is called the *event horizon*.

time. Simultaneously, in 1963, Kerr solved the Einstein equations for a rotating black hole, which stimulated another rapid theoretical development. These speculative compact objects quickly became suitable candidates for the newly observed high-energy phenomena. Most pulsars were soon identified as neutron stars, and other observations strongly pointed towards black holes. Although we cannot directly see black holes, their presence is revealed through their interaction with the surroundings. As sources of extreme gravity, black holes pull matter which accelerates to high velocities often approaching the speed of light. The infalling matter, however, does not reach the black hole's horizon radially; instead, it is captured by the gravity of the compact object, typically forming an accretion disc. In this disc, a (quasi-)equilibrium is achieved through the mutual balancing of gravitational and centrifugal forces. Due to the steep radial gradient of the orbital velocity, the accreting matter is heated by the viscous friction of the neighbouring layers to very high temperatures, emitting a significant amount of energy in the form of radiation. Another source of activity is the formation of relativistic jets: stable, collimated ejections of highly accelerated matter along the rotational axis of the central black hole. The mechanism behind their formation is still not fully understood, but the magnetic field likely plays a crucial role. The total energy radiated from such systems can often be many orders of magnitude larger than the integrated radiated energy from all the stars in the Milky Way galaxy. Black holes drive the most powerful engines we know of!

In this thesis, we will study spacetimes that contain a black hole surrounded by additional gravitating sources, specifically a ring or thin disc. However, the non-linear nature of the Einstein equations makes the problem rather involved. Properly modelling accretion requires advanced and computationally expensive numerical methods. Nevertheless, if suitably simplified, there are still problems that can be tackled analytically. The simplifications we consider are stationarity, axial symmetry, and circularity. Such spacetimes can approximate steadily rotating astrophysical bodies. There are two additional complications in *general relativity* compared to Newton's theory: self-gravitation, where the source feels its own gravity, leading to a much more constrained system, and the (frame-)dragging of the spacetime associated with rotation.

If we neglect the latter effect and consider only static spacetimes, the metric outside of sources (in vacuum) can be described by just two functions. One of these functions satisfies the linear Laplace equation, while the other is determined by a quadrature. In this case, we can find exact and closed-form solutions for certain "superposition" problems involving multiple gravitating sources. But extra caution must be taken. Even a simple source with a direct Newtonian counterpart can result in a spacetime with rather peculiar properties, and the superposition of such sources may lead to singularities or other pathologies, sometimes with unclear physical interpretation.

In real astrophysical systems, however, the rotation is ubiquitous, and the associated dragging effects introduce much more complexity to the problem. It is highly unlikely to find an exact superposition of rotating sources, even in the stationary regime. Instead, we must rely on approximation methods, such as perturbations.

The thesis is organised as follows: The first chapter will be dedicated to the basic concepts of stationary and axially symmetric (and circular) spacetimes. In

the second chapter, we will present several results describing static superpositions of a black hole with a disc or ring. The third chapter will focus on an astrophysically motivated application, we will study the quasinormal response of such a black hole. Then, in the last chapter, we will delve into the topic of stationary perturbations of rotating black holes. After introducing the tetrad formalism, we will provide an explicit solution describing the electromagnetic field of a ring source on the Kerr background. Finally, we will outline a similar procedure for the gravitational perturbations, and conclude with a brief summary in the Conclusions section. At the end of each chapter, we attach publications in the Astrophysical Journal and Physical Review D. For the latter, preprints are included due to the license restrictions of the journal.

Notation

We use metric tensor $g_{\mu\nu}$ with signature $(-+++)$. All quantities are given in geometrized units in which $c = G = 1$. Greek indices go through $0 - 3$. We employ Einstein's summation convention and use the index-posed comma to denote partial derivative and the semicolon to denote covariant derivative. We also use the operator notation for both derivatives ∂_μ, ∇_μ, particularly in the context of tetrad formalism. Riemann tensor is defined according to $V_{\nu;\kappa\lambda} - V_{\nu;\lambda\kappa} = R^{\mu}{}_{\nu\kappa\lambda} V_\mu$, where V_μ is an arbitrary covector. Ricci tensor is defined by $R_{\nu\lambda} = R^{\kappa}{}_{\nu\kappa\lambda}$. We use standard notation for complete elliptic integrals

$$K(k) = \int_0^{\frac{\pi}{2}} \frac{\mathrm{d}\varphi}{\sqrt{1 - k^2 \sin^2 \varphi}}\,, \qquad E(k) = \int_0^{\frac{\pi}{2}} \sqrt{1 - k^2 \sin^2 \varphi}\,\mathrm{d}\varphi\,,$$

$$\Pi(n, k) = \int_0^{\frac{\pi}{2}} \frac{\mathrm{d}\varphi}{(1 - n \sin^2 \varphi)\sqrt{1 - k^2 \sin^2 \varphi}}\,,$$

where k is the modulus.

CHAPTER

1

CIRCULAR SPACETIMES

Circular spacetimes are of clear interest in general relativity since they describe the gravitational field of axially symmetric rotating bodies. In this chapter, we will introduce some basic concepts of such spacetimes. Apart from the features presented in what follows, we will also assume that the spacetime is **asymptotically flat**, i.e., it approaches the Minkowski metric at spatial infinity. Moreover, we will not deal with the **cosmological constant** Λ, which is set to zero.

Stationary and axially symmetric spacetime is a spacetime that admits two commuting[1] Killing vectors fields, one of them being asymptotically timelike $\xi^{\mu}_{(t)}$ and the other, $\xi^{\mu}_{(\phi)}$, asymptotically spacelike with closed orbits. In the adapted coordinates (t, ϕ, x^2, x^3), such that $\xi^{\mu}_{(t)} \equiv \partial^{\mu}_{t}$ and $\xi^{\mu}_{(\phi)} \equiv \partial^{\mu}_{\phi}$, the metric is time independent and invariant under rotations, i.e.,

$$\mathrm{d}s^2 = g_{\mu\nu}(x^2, x^3)\,\mathrm{d}x^{\mu}\,\mathrm{d}x^{\nu}\,. \tag{1.1}$$

We also presume existence of the rotation axis, which is a set of points where $\xi^{\mu}_{(\phi)}$ vanishes, so the integral-line circumference $\oint \sqrt{g_{\phi\phi}}\,\mathrm{d}\phi = 2\pi\sqrt{g_{\phi\phi}} = 0$ there as the invariant norm $g_{\phi\phi} \equiv g_{\alpha\beta}\xi^{\alpha}_{(\phi)}\xi^{\beta}_{(\phi)} \to 0$. The axis should also be **elementary flat**, in other words, the length of a closed orbit of $\xi^{\mu}_{(\phi)}$ should approach 2π times the proper perpendicular distance of the orbit from the axis. Thus, the gradient of the "circumferential radius" $\sqrt{g_{\phi\phi}}$ should satisfy (Stephani et al., 2003)

$$\frac{(g_{\phi\phi})_{,\alpha}(g_{\phi\phi})^{,\alpha}}{4g_{\phi\phi}} \longrightarrow 1 \tag{1.2}$$

in the limit at the rotation axis. Such a condition ensures that the axis is regular and free of conical singularities.

[1] Carter (1970) showed that the commutative property is indeed general in the asymptotically flat spacetimes.

Static spacetime is stationary and invariant under time reversal. Geometrically, it is true when the Killing vector field $\xi^\mu_{(t)}$ is hypersurface orthogonal, which implies $g_{ti} = 0$ in the adapted coordinates.

The condition of circularity means that all elements of sources move only in the directions given by the two Killing vector fields $\xi^\mu_{(t)}$ and $\xi^\mu_{(\phi)}$. In other words, the metric is invariant under the simultaneous transformation $(t \to -t, \phi \to -\phi)$. It is the best generalization of *circular motion*. In the language of differential geometry, such a symmetry is called **orthogonal transitivity**, and it is expressed by the condition

$$\xi^\alpha_{(t)} R^{[\beta}_\alpha \xi^\gamma_{(t)} \xi^{\delta]}_{(\phi)} = 0 = \xi^\alpha_{(\phi)} R^{[\beta}_\alpha \xi^\gamma_{(\phi)} \xi^{\delta]}_{(t)} \,, \tag{1.3}$$

where $R_{\mu\nu}$ is the Ricci tensor. If the condition (1.3) holds, and there exists the rotation axis where $\xi^\mu_{(\phi)} = 0$[2], then the 2-spaces which are orthogonal to both $\xi^\mu_{(t)}$ and $\xi^\mu_{(\phi)}$ are integrable (Wald, 1984). Then, we may choose the remaining coordinates (x^2, x^3) in one of the integral 2-spaces and propagate them to the rest of the spacetime along the integral lines of the Killing vector fields. Thus, the metric takes a block diagonal form

$$\mathrm{d}s^2 = g_{pq}\,\mathrm{d}x^p\,\mathrm{d}x^q + g_{ij}\,\mathrm{d}x^i\,\mathrm{d}x^j \,, \tag{1.4}$$

where $p, q = (t, \phi)$ and $i, j = (2, 3)$.

1.1 The metric and Einstein equations

Every 2-dimensional Riemannian manifold is conformally flat, so we can choose the coordinates (x^2, x^3) in such a way that the $g_{ij}\,\mathrm{d}x^i\,\mathrm{d}x^j$ part of (1.4) is diagonal. These coordinates are called canonical Weyl coordinates ($\rho \equiv x^2, z \equiv x^3$) and the metric in the Carter-Thorne-Bardeen form reads

$$\mathrm{d}s^2 = g_{tt}\,\mathrm{d}t^2 + 2g_{t\phi}\,\mathrm{d}t\,\mathrm{d}\phi + g_{\phi\phi}\,\mathrm{d}\phi^2 + g_{22}\delta_{ij}\,\mathrm{d}x^i\,\mathrm{d}x^j \tag{1.5}$$

$$= -e^{2\nu}\,\mathrm{d}t^2 + B^2\rho^2 e^{-2\nu}(\mathrm{d}\phi - \omega\,\mathrm{d}t)^2 + e^{2\lambda-2\nu}(\mathrm{d}\rho^2 + \mathrm{d}z^2) \,. \tag{1.6}$$

The symmetries reduced the problem to finding just 4 metric functions B, ν, ω, and λ, which depend only on the coordinates (ρ, z). The Killing-part metric functions are invariants,

$$g_{tt} \equiv g_{\alpha\beta}\xi^\alpha_{(t)}\xi^\beta_{(t)} \,, \quad g_{t\phi} \equiv g_{\alpha\beta}\xi^\alpha_{(t)}\xi^\beta_{(\phi)} \,, \quad g_{\phi\phi} \equiv g_{\alpha\beta}\xi^\alpha_{(\phi)}\xi^\beta_{(\phi)} \,, \tag{1.7}$$

thus

$$e^{2\nu} \equiv -g_{tt} - g_{t\phi}\omega \,, \quad \omega \equiv -\frac{g_{t\phi}}{g_{\phi\phi}} \tag{1.8}$$

also have invariant meaning. The function e^ν is known as the lapse function[3] and ω is the angular velocity which the local inertial systems "co-rotate" with the sources. The function ν is also commonly referred to as the *gravitational potential* because, in the static limit, it is the counterpart of the Newtonian gravitational potential.

[2] In fact, this condition can be relaxed to the spacetimes where $\xi_{(t)[\mu}\xi_{(\phi)\nu}\nabla_\kappa\xi_{(t)\delta]}$ and $\xi_{(t)[\mu}\xi_{(\phi)\nu}\nabla_\kappa\xi_{(\phi)\delta]}$ vanish in at least one point (Wald, 1984).

[3] A normalization factor of the future-oriented unit normal to $t =$ const hypersurfaces.

The gravitational field described by the metric (1.6) is locally determined by the Einstein equations, which link the Ricci curvature tensor $R_{\mu\nu}$ to the stress-energy tensor $T_{\mu\nu}$ via

$$R_{\mu\nu} - \frac{1}{2} R g_{\mu\nu} = 8\pi T_{\mu\nu}\,, \tag{1.9}$$

where $R \equiv R^{\alpha}{}_{\alpha}$, and where we set the cosmological constant Λ to zero. For the circular metric (1.6), Einstein equations are reduced to a system of 6 coupled nonlinear partial differential equations

$$\nabla \cdot (\rho \nabla B) = 8\pi B \rho (T_{\rho\rho} + T_{zz})\,, \tag{1.10}$$

$$\nabla \cdot (B \nabla \nu) - \frac{B^3 \rho^2}{2e^{4\nu}} (\nabla \omega)^2 = 4\pi B e^{2\lambda - 2\nu} (T^i_i - 2\omega T^t_\phi - T^t_t)\,, \tag{1.11}$$

$$\nabla \cdot (B^3 \rho^2 e^{-4\nu} \nabla \omega) = -16\pi B e^{2\lambda - 2\nu} T^t_\phi\,, \tag{1.12}$$

$$\lambda_{,\rho\rho} + \lambda_{,zz} + \nu_{,\rho}^2 + \nu_{,z}^2 - \frac{3B^2\rho^2}{4e^{4\nu}} \left[\omega_{,\rho}^2 + \omega_{,z}^2\right] = 8\pi e^{2\lambda - 2\nu} (T^\phi_\phi - \omega T^t_\phi)\,, \tag{1.13}$$

$$\begin{aligned} \lambda_{,\rho}(B\rho)_{,\rho} - \lambda_{,z}(B\rho)_{,z} - B\rho \left[\nu_{,\rho}^2 + \nu_{,z}^2\right] - \frac{1}{2}\left[(B\rho)_{,\rho\rho} - (B\rho)_{,zz}\right] + \\ + \frac{1}{4} B^3 \rho^3 e^{-4\nu} \left(\omega_{,\rho}^2 - \omega_{,z}^2\right) = 4\pi B \rho (T_{\rho\rho} - T_{zz})\,, \end{aligned} \tag{1.14}$$

$$\lambda_{,\rho}(B\rho)_{,z} + \lambda_{,z}(B\rho)_{,\rho} - 2B\rho\nu_{,\rho}\nu_{,z} - (B\rho)_{,\rho z} + \frac{1}{2} B^3 \rho^3 e^{-4\nu} \omega_{,\rho}\omega_{,z} = 8\pi B \rho T_{\rho z}\,, \tag{1.15}$$

where ∇ and $\nabla\cdot$ are the standard gradient and divergence in the flat 3D space in cylindrical coordinates (ρ, ϕ, z). The number of independent equations is further reduced by one (let's say (1.13)) thanks to the Bianchi identities. When B, ν, and ω are known, the remaining function λ follows from the line-integration (1.14) and (1.15).

1.2 Boundary conditions and basic features of the spacetime

On the *rotation axis*, the condition (1.2) translates to

$$\lim_{\rho \to 0} \frac{e^\lambda}{B} = 1\,, \tag{1.16}$$

which also ensures that the azimuthal coordinate ϕ is normalized to the usual interval $[0, 2\pi)$. Regular, i.e., strut-free axis, also requires vanishing derivatives of the metric functions

$$\nu_{,\rho},\ B_{,\rho},\ \omega_{,\rho},\ \lambda_{,\rho} \xrightarrow[\rho\to 0]{} 0\,. \tag{1.17}$$

In *radial infinity*, we naturally assume that the spacetime is asymptotically flat if dealing with isolated bodies. This means a particular asymptotic form of the metric functions

$$\begin{aligned} \nu &= -\frac{M}{r} + \mathcal{O}(r^{-2})\,, & \omega &= \frac{2J}{r^3} + \mathcal{O}(r^{-4})\,, \\ B &= 1 + \mathcal{O}(r^{-2})\,, & \lambda &= \mathcal{O}(r^{-2})\,, \end{aligned} \tag{1.18}$$

where r is any radial coordinate which is asymptotically $\sqrt{\rho^2+z^2}$, and constants M and J are interpreted as the total mass and angular momentum contained in the spacetime. They follow from the notion of total energy and angular momentum on a hypersurface in the asymptotic flat infinity motivated by the Hamiltonian formulation of general relativity by Arnowitt, Deser & Misner (ADM) in (Arnowitt et al., 1962). More "covariant" prescription of those properties is due to Komar (1959). The Komar mass and angular momentum are defined as conserved quantities associated with the Killing symmetries $\xi^\mu_{(t)}$ and $\xi^\mu_{(\phi)}$ respectively. In particular

$$M_{\rm K} = \frac{1}{8\pi}\oint_{S_\infty} \xi^{\alpha;\beta}_{(t)}\,\mathrm{d}S_{\alpha\beta}\,, \tag{1.19}$$

$$J_{\rm K} = -\frac{1}{16\pi}\oint_{S_\infty} \xi^{\alpha;\beta}_{(\phi)}\,\mathrm{d}S_{\alpha\beta}\,, \tag{1.20}$$

where we integrate over some 2-surface S_∞ in the asymptotic infinity[4]. Note, however, that while the ADM quantities can be defined in any asymptotically flat spacetime, the Komar analogues require additional symmetries.

In the following, we will be mainly interested in spacetimes, where a black hole is one of the sources. The classical definition of a black hole (Misner et al., 2017) could go like this: *A black hole is a region of spacetime from which no signal (timelike or null) can escape and be detected a distant observer.* The boundary of that region is called the **event horizon**. In circular spacetimes, it is invariantly given by vanishing lapse function (Carter, 1969)

$$0 = -g_{\alpha\beta}(\xi^\alpha_{(t)}+\omega\xi^\alpha_{(\phi)})(\xi^\beta_{(t)}+\omega\xi^\beta_{(\phi)}) = -g_{tt}-g_{t\phi}\omega = e^{2\nu}\,. \tag{1.21}$$

On the stationary horizon, the function ω is a constant $\omega_{\rm H}$, i.e., the horizon "rotates" with respect to the infinity as a rigid body. Thus, the event horizon is also the **Killing horizon** as the Killing vector field $\xi^\mu_{(t)}+\omega_{\rm H}\xi^\mu_{(\phi)}$ becomes null there. The metric coefficients should be regular on the horizon, thus because $e^{2\nu}=0$ and $\omega=\text{const}\equiv\omega_{\rm H}$, it follows from the regularity of $g_{\phi\phi}$ and $g_{\rho\rho}=g_{zz}$ that

$$B\rho \underset{\to{\rm H}}{\longrightarrow} 0\,,\quad e^{2\lambda}\underset{\to{\rm H}}{\longrightarrow} 0\,. \tag{1.22}$$

1.3 $T_{\rho\rho}+T_{zz}=0$ case

For a special case of the stress-energy tensor, where $T_{\rho\rho}+T_{zz}=0$, which is valid, in particular, for dust or vacuum, the first Einstein equation (1.10) reduces to an axially symmetric Laplace equation in 4 dimensions

$$\Delta B \equiv B_{,\rho\rho}+\frac{2B_{,\rho}}{\rho}+B_{,zz}=0\,. \tag{1.23}$$

Any nontrivial solution of the above equation can be used, except $B=\rho^{-1}$ which does not preserve the axial symmetry, but leads to plane waves. The simplest

[4]Different signs origin in opposite normalization of $\xi^\mu_{(t)}$ and $\xi^\mu_{(\phi)}$, while factor 2 is justified from an additional boundary term in the covariant Hamiltonian formalism (Wald, 1993).

solution $B = 1$ is commonly used, and it will be mostly employed in this thesis. However, general $B \neq 1$ is related by a coordinate transformation

$$\rho' = \rho B\,, \quad z' = \pm \int \rho B_{,z}\,\mathrm{d}\rho - (\rho B)_{,\rho}\,\mathrm{d}z\,, \tag{1.24}$$

where the coordinates which correspond to $B = 1$ are denoted by primes (ρ', z'). The form (1.24) follows from the metric coefficient $g_{\phi\phi}$ and the redefinition of z is chosen in a way that the (ρ, z) part of the metric remains isotropic. With such a coordinate change, the metric function λ (recall that $g_{\rho\rho} = g_{zz} = e^{2\lambda-2\nu}$) transforms as

$$\lambda' = \lambda - \frac{1}{2}\log\left[(\rho B_{,z})^2 + (\rho B)_{,\rho}^2\right]. \tag{1.25}$$

The case $T_{\rho\rho} + T_{zz} = 0$ and $B = 1$ is often considered in the Weyl-Papapetrou form of the metric

$$\mathrm{d}s^2 = -f(\mathrm{d}t - A\,\mathrm{d}\phi)^2 + f^{-1}\rho^2\,\mathrm{d}\phi^2 + e^{2\gamma}f^{-1}(\mathrm{d}\rho^2 + \mathrm{d}z^2)\,, \tag{1.26}$$

where, instead of ν, ω, and λ, we have f, A, and γ, which are related by

$$f = e^{2\nu} - \rho^2 e^{-2\nu}\omega^2\,, \quad A = -\frac{\rho^2 e^{-2\nu}\omega}{f}\,, \quad e^{2\gamma} = f e^{2\lambda-2\nu}\,. \tag{1.27}$$

1.4 Black holes

Mysterious, yet "simple" are isolated stationary black holes. In general, they are fully characterized just by three parameters: mass, angular momentum, and electric charge (if we ignore a hypothetical magnetic monopole). Relativists say, they have "no-hair" – they are independent of any additional parameter. In this thesis, we will consider only vacuum black holes (with no electric charge) which will later be perturbed by some matter *outside* the horizon.

1.4.1 Schwarzschild solution

Any spherically symmetric vacuum spacetime is described by the Schwarzschild metric (Schwarzschild, 1916; Birkhoff & Langer, 1923). In Weyl coordinates, it is given by

$$\nu_{\mathrm{Schw}} = \frac{1}{2}\log\frac{R_+ + R_- - 2M}{R_+ + R_- + 2M}\,, \tag{1.28}$$

$$\lambda_{\mathrm{Schw}} = \frac{1}{2}\log\frac{(R_+ + R_-)^2 - 4M^2}{4R_+R_-}\,, \tag{1.29}$$

$$B = 1\,, \tag{1.30}$$

where M represents the total mass of the source and

$$R_\pm = \sqrt{\rho^2 + (|z| \mp M)^2}\,. \tag{1.31}$$

For a point-like source – meaning that $T_{\mu\nu} = 0$ everywhere except at the very centre – it represents a static and spherically symmetric black hole. However,

Weyl coordinates (involving the choice $B = 1$) do not cover the black hole interior, and the functions (1.28) and (1.29) do not exhibit the spherical symmetry explicitly. Instead, the horizon is rendered as a singular rod of length $2M$ placed symmetrically on the z axis ($\rho = 0, |z| \leq M$). To recover the explicit spherical symmetry, we can transform to the Schwarszchild coordinates (r, θ) defined by

$$\rho = \sqrt{r(r-2M)}\sin\theta\,, \qquad z = (r-M)\cos\theta\,, \tag{1.32}$$

leading to the metric functions

$$\nu_{\rm Schw} = \frac{1}{2}\log\left(1-\frac{2M}{r}\right)\,, \quad \lambda_{\rm Schw} = \frac{1}{2}\log\frac{r(r-2M)}{r(r-2M)+M^2\sin^2\theta}\,. \tag{1.33}$$

By such a coordinate transformation, we recover the Schwarzschild metric in a standard "textbook" form with the spherical horizon located at $r = 2M$,

$$\mathrm{d}s^2 = -\left(1-\frac{2M}{r}\right)\mathrm{d}r^2 + \frac{\mathrm{d}r^2}{1-\frac{2M}{r}} + r^2\,\mathrm{d}\theta^2 + r^2\sin^2\theta\,\mathrm{d}\phi^2\,. \tag{1.34}$$

Another possibility is to use spherical coordinates (R, ϑ) defined by a simple transformation

$$\rho = R\sin\vartheta\,, \qquad z = R\cos\vartheta\,. \tag{1.35}$$

However, if we keep $B = 1$, the horizon would be at $R = 0$, which does not improve the situation that much. But, since the location of the horizon is given by $B\rho = 0$ (1.22), another option is to use a coordinate system where B vanishes on the horizon instead of ρ. Let say that it happens at $R = \text{const} \equiv \frac{M}{2}$. The simplest solution of (1.23) which satisfies this condition is

$$B = 1 - \frac{M^2}{4(\rho^2+z^2)} \equiv 1 - \frac{M^2}{4R^2}\,. \tag{1.36}$$

These new coordinates are commonly referred to as isotropic coordinates since the metric functions become (taking into account (1.25))

$$\nu_{\rm Schw} = \log\frac{2R-M}{2R+M}\,, \quad \lambda_{\rm Schw} = \log\left(1-\frac{M^2}{4R^2}\right)\,, \tag{1.37}$$

and the metric itself acquires the isotropic form

$$\mathrm{d}s^2 = -\left(\frac{2R-M}{2R+M}\right)^2\mathrm{d}t^2 + \left(1+\frac{M}{2R}\right)^4(\mathrm{d}R^2 + R^2\,\mathrm{d}\vartheta^2 + R^2\sin^2\vartheta\,\mathrm{d}\phi^2)\,. \tag{1.38}$$

1.4.2 Kerr solution

Arguably more significant from the astrophysical point of view is a black hole, which includes not only the mass but also a rotational angular momentum. Its geometry is described by the famous Kerr metric (Kerr, 1963) – see also a recent review by Teukolsky (2015). In the Weyl coordinates, the metric functions read

$$\nu_{\rm Kerr} = \frac{1}{2}\log\frac{\Sigma\Delta}{\mathcal{A}}\,, \qquad \omega_{\rm Kerr} = \frac{aM(2M+R_+ + R_-)}{\mathcal{A}}\,, \tag{1.39}$$

$$B = 1\,, \qquad \lambda_{\rm Kerr} = \frac{1}{2}\log\frac{\Delta\Sigma^2}{\mathcal{A}} R_+ R_-\,, \tag{1.40}$$

where

$$\Delta = a^2 - M^2 + \frac{1}{4}(R_+ + R_-)^2\,, \tag{1.41}$$

$$\Sigma = \frac{4a^2(M+R_+)(M+R_-) - M^2(2M+R_++R_-)^2}{4(a^2-M^2)}\,, \tag{1.42}$$

$$\mathcal{A} = \frac{1}{16}\left\{\left[4a^2 + (2M+R_++R_-)^2\right]^2 - 4a^2\Delta\left[4 + \frac{(R_+-R_-)^2}{a^2-M^2}\right]\right\}\,, \tag{1.43}$$

$$R_\pm = \sqrt{\rho^2 + (z \mp \sqrt{M^2-a^2})^2}\,. \tag{1.44}$$

We use the standard notation: M represents the mass of the black hole, and $J = Ma$ is the rotational angular momentum. In the limit $a \to 0^+$, the solution goes to the Schwarszchild metric. The (outer) horizon is again rendered as a massive line segment ($\rho = 0, |z| \le \sqrt{M^2-a^2}$).

Similarly to the Schwarzschild case, when discussing the horizon, it is better to use more suitable coordinates, which cover also the interior of the black hole. The standard choice is the minimal generalization of Schwarszchild coordinates – spheroidal Boyer-Lindquist coordinates (r, θ) – related to the Weyl ones by

$$\rho = \sqrt{r^2 - 2Mr + a^2}\sin\theta\,, \qquad z = (r-M)\cos\theta\,. \tag{1.45}$$

Then (1.41)-(1.43) simplifies to

$$\begin{aligned} \Delta &= r^2 - 2Mr + a^2\,, & \Sigma &= r^2 + a^2\cos^2\theta\,, \\ \mathcal{A} &= (r^2+a^2)^2 - \Delta a^2\sin^2\theta\,, & \omega_{\rm Kerr} &= \frac{2aMr}{\mathcal{A}} \end{aligned} \tag{1.46}$$

and the metric acquires the form

$$\mathrm{d}s^2 = -\frac{\Sigma\Delta}{\mathcal{A}}\,\mathrm{d}t^2 + \frac{\mathcal{A}}{\Sigma}\sin^2\theta(\mathrm{d}\phi - \omega\,\mathrm{d}t)^2 + \frac{\Sigma}{\Delta}\,\mathrm{d}r^2 + \Sigma\,\mathrm{d}\theta^2\,. \tag{1.47}$$

recovering actually two horizons located at $\Delta = 0 \Leftrightarrow r_\pm = M \pm \sqrt{M^2-a^2}$.

It is also possible to use the isotropic coordinates (1.35) with a slightly different choice of B,

$$B = 1 - \frac{|M^2-a^2|}{4(\rho^2+z^2)^2} = 1 - \frac{|M^2-a^2|}{4R^2}\,, \tag{1.48}$$

with the (outer) horizon is located at $R = \frac{\sqrt{M^2-a^2}}{2}$.

1.5 Thin discs and singular surfaces

When there are other sources around the black hole, we have to specify the boundary conditions on their surfaces, and eventually also find their inner solution for the full discussion. For simplicity, we will consider *infinitesimally thin discs*, i.e., discs whose typical thickness is negligible compared to their radius. In such a case, the stress-energy tensor $T_{\mu\nu}$ is zero everywhere except a singular 2-surface,

where it is proportional to a delta distribution. For a proper definition of the *surface stress-energy tensor*, we will follow the approach due to Israel (1966), see also Ledvinka & Bičák (2019).

Consider a singular 2-surface Σ located on the equatorial plane $z = 0$, which separates the spacetime into two regions $\mathscr{M}^+$ and $\mathscr{M}^-$ with unit normals ${}^{\pm}n^{\alpha}$ in $\mathscr{M}^{\pm}$ respectively,

$$ {}^{\pm}n^{\alpha} = \pm e^{\nu-\lambda}\delta^{\alpha}_{z} \,. \tag{1.49} $$

Let us denote the projection tensor to the surface Σ as

$$ {}^{\pm}h_{\alpha\beta} = g_{\alpha\beta} - {}^{\pm}n_{\alpha}\,{}^{\pm}n_{\beta} \,, \tag{1.50} $$

and the extrinsic curvature of Σ in $\mathscr{M}^+$ and $\mathscr{M}^-$

$$ {}^{\pm}K_{\alpha\beta} = {}^{\pm}h^{\gamma}_{\alpha}\,{}^{\pm}h^{\delta}_{\beta}\nabla_{\gamma}\,{}^{\pm}n_{\delta} \,. \tag{1.51} $$

If the difference of the extrinsic curvatures $[K^{\alpha}_{\beta}] \equiv {}^{-}K^{\alpha}_{\beta} - {}^{+}K^{\alpha}_{\beta} \neq 0$, we define the surface stress-energy tensor as

$$ S^{\alpha}_{\beta} = \frac{1}{8\pi}\left([K^{\alpha}_{\beta}] - [K^{\gamma}_{\gamma}]h^{\alpha}_{\beta}\right) , \qquad K^{\gamma}_{\gamma} = g^{\gamma\delta}K_{\gamma\delta} \,. \tag{1.52} $$

We consider the spacetime to be reflection symmetric with respect to the surface Σ, thus the extrinsic curvatures are the same with opposite signs due to the opposite orientation of the normal vectors, i.e., $[K^{\mu}_{\nu}] = -2\,{}^{+}K^{\mu}_{\nu}$. It can then be shown that $S_{\mu\nu}$ corresponds to the integral of the full stress-energy tensor $T_{\mu\nu}$ over the infinitesimal thickness of the source Israel (1966),

$$ S_{\mu\nu} = \lim_{\epsilon\to 0^+}\int_{-\epsilon}^{+\epsilon} T_{\mu\nu}\sqrt{g_{zz}}\,\mathrm{d}z \quad \Longleftrightarrow \quad T_{\mu\nu}\sqrt{g_{zz}} = S_{\mu\nu}\delta(z) \,, \tag{1.53} $$

which justifies the name *surface stress-energy tensor*. Its components read explicitly

$$ 8\pi B e^{\lambda-\nu}S^{t}_{t} = 2B_{,z} + 2B(\lambda_{,z} - 2\nu_{,z}) + e^{-4\nu}B^3\rho^2\omega\omega_{,z} \,, \tag{1.54} $$

$$ 8\pi B e^{\lambda-\nu}S^{t}_{\phi} = -e^{-4\nu}B^3\rho^2\omega_{,z} \,, \tag{1.55} $$

$$ 8\pi B e^{\lambda-\nu}S^{\phi}_{t} = 2\omega(B_{,z} - 2B\nu_{,z}) + B\omega_{,z}(1 + e^{-4\nu}B^2\rho^2\omega^2) \,, \tag{1.56} $$

$$ 8\pi B e^{\lambda-\nu}S^{\phi}_{\phi} = 2B\lambda_{,z} - e^{-4\nu}B^3\rho^2\omega\omega_{,z} \,, \tag{1.57} $$

$$ 4\pi B e^{\lambda-\nu}S^{\rho}_{\rho} = B_{,z} \,, \tag{1.58} $$

$$ S^{\rho}_{z} = 0 \,, \tag{1.59} $$

$$ S^{z}_{z} = 0 \,, \tag{1.60} $$

where all quantities are computed in the limit $z \to 0^+$.

Now, we want to physically interpret the obtained surface stress-energy tensor. This can be easily done if S^{μ}_{ν} is in diagonal form. That involves solving the eigenvalue problem

$$ (S^{\mu}_{\alpha} - \chi\delta^{\mu}_{\alpha})V^{\alpha} = 0 \,. \tag{1.61} $$

We find the eigenvalues

$$ \chi_{(\pm)} = \frac{1}{2}\left[S^{t}_{t} + S^{\phi}_{\phi} \pm \sqrt{\mathscr{D}}\right] , \qquad \chi_{(\rho)} = S^{\rho}_{\rho} \,, \qquad \chi_{(z)} = 0 \,, \tag{1.62} $$

where the discriminant is

$$\mathscr{D} = (S^\phi_\phi - S^t_t)^2 + 4S^t_\phi S^\phi_t = (S^A_A)^2 - 4\det S^A_B \,. \tag{1.63}$$

Indices with the capital letters denote $A, B = (t, \phi)$. Components of the corresponding eigenvectors are

$$V^\mu = V^t(1, \Omega, 0, 0)\,, \qquad W^\mu = \mathcal{W}(g_{t\phi} + g_{\phi\phi}\Omega, -g_{tt} - g_{t\phi}\Omega, 0, 0)\,, \tag{1.64}$$

$$V^\mu_{(\rho)} = e^{\nu-\lambda}(0, 0, 1, 0)\,, \qquad V^\mu_{(z)} = e^{\nu-\lambda}(0, 0, 0, 1)\,, \tag{1.65}$$

where

$$\Omega = \frac{S^\phi_\phi - S^t_t - \sqrt{\mathscr{D}}}{2S^t_\phi}\,, \tag{1.66}$$

$$V^t = \frac{1}{\sqrt{-g_{tt} - 2g_{t\phi}\Omega - g_{\phi\phi}\Omega^2}} = \frac{1}{\sqrt{e^{2\nu} - g_{\phi\phi}(\Omega - \omega)^2}} = \frac{e^{-\nu}}{\sqrt{1 - v^2}}\,, \tag{1.67}$$

$$\mathcal{W} = \frac{V^t}{\sqrt{g^2_{t\phi} - g_{\phi\phi}g_{tt}}} = \frac{V^t}{B\rho}\,, \tag{1.68}$$

and $v = \sqrt{g_{\phi\phi}}e^{-\nu}(\Omega - \omega)$, represents a relative velocity of the disc element locally measured by a ZAMO observer. If $\mathscr{D} \geq 0$, all eigenvalues are real, thus the surface stress-energy tensor can be written in the form of an *ideal fluid*,

$$S^{\mu\nu} = \sigma V^\mu V^\nu + p_{(\phi)} W^\mu W^\nu + p_{(\rho)} V^\mu_{(\rho)} V^\nu_{(\rho)}\,, \tag{1.69}$$

with

- the surface energy density $\sigma \equiv -\chi_{(-)}$,
- azimuthal pressure $p_{(\phi)} \equiv \chi_{(+)}$,
- and radial pressure $p_{(\rho)} \equiv \chi_{(\rho)}$,

interpreted in the rest system of the fluid. The fluid four-velocity is the unit timelike vector V^μ, while W^μ is the four-vector perpendicular to V^μ pointing in the azimuthal direction, and $V^\mu_{(\rho)}$, $V^\mu_{(z)}$ span the remaining two spatial directions. The quantity Ω represents an angular velocity of the fluid with respect to the flat infinity. The zero eigenvalue $\chi_{(z)} = 0$ reflects the fact that no pressure can act in the direction perpendicular to the disc. Notice that if $B = 1$, it automatically follows from (1.58) that $S^\rho_\rho = 0$, thus the disc can not have radial pressure for this choice of B.

If $\mathscr{D} < 0$, the eigenvalues and eigenvectors are complex and the interpretation as an ideal fluid no longer applies. Moreover, since $\mathscr{D} = (S^\alpha_\beta u^\beta_1 u_{1\alpha})(S^\alpha_\beta u^\beta_2 u_{2\alpha})$ for certain null vectors u^α_1 and u^α_2, the case $\mathscr{D} < 0$ violates the weak energy condition. Then one of the observers in the limit near u^μ_1, or u^μ_2 would measure negative energy density (more on the energy conditions in Sec. 1.7).

1.6 Circular orbits and counter-rotating interpretation

Circular orbits are the most prominent and "natural" type of motion in axially symmetric and stationary spacetimes. Such a motion respects the Killing symmetries, which in the Weyl coordinates means orbits ($\rho = \text{const}, z = \text{const}$) with steady angular velocity

$$\Omega = \frac{\mathrm{d}\phi}{\mathrm{d}t}\,. \tag{1.70}$$

The corresponding four-velocity reads

$$u^\mu = \frac{\xi^\mu_{(t)} + \Omega\xi^\mu_{(\phi)}}{|\xi^\mu_{(t)} + \Omega\xi^\mu_{(\phi)}|} = u^t(1, \Omega, 0, 0)\,, \tag{1.71}$$

where[5]

$$u^t = \frac{1}{\sqrt{-g_{tt} - 2g_{t\phi}\Omega - g_{\phi\phi}\Omega^2}} = \frac{1}{\sqrt{e^{2\nu} - g_{\phi\phi}(\Omega - \omega)^2}} \equiv \frac{e^{-\nu}}{\sqrt{1 - v^2}}\,. \tag{1.72}$$

If the motion is "free", i.e., the particle follows a geodesic, the four-acceleration a^μ of the orbit

$$a_\mu = u_{\mu;\alpha}u^\alpha = \frac{1}{2}\frac{g_{tt,\mu} + 2g_{t\phi,\mu}\Omega - g_{\phi\phi,\mu}\Omega^2}{g_{tt} + 2g_{t\phi}\Omega + g_{\phi\phi}\Omega^2} \tag{1.73}$$

must vanish. The symmetries require that the components a_t and a_ϕ are identically zero everywhere and in the equatorial plane $a_z = 0$ as well. Thus, the only non-vanishing component is a_ρ. Requiring $a_\rho = 0$ gives the allowed angular velocities

$$\begin{aligned}\Omega_\pm &= -\frac{g_{t\phi,\rho}}{g_{\phi\phi,\rho}} \pm \sqrt{\left(\frac{g_{t\phi,\rho}}{g_{\phi\phi,\rho}}\right)^2 - \frac{g_{tt,\rho}}{g_{\phi\phi,\rho}}} = \\ &= \omega + \frac{g_{\phi\phi}}{g_{\phi\phi,\rho}}\omega_{,\rho} \pm \sqrt{\left(\frac{g_{\phi\phi}}{g_{\phi\phi,\rho}}\right)^2 \omega^2_{,\rho} + \frac{2\nu_{,\rho}e^{2\nu}}{g_{\phi\phi,\rho}}}\,,\end{aligned} \tag{1.74}$$

where all the functions are taken in the $z = 0$ limit. Such a value of the angular velocity exists only if the expression under the square root is non-negative. Hence, the basic condition for the free circular motion reads

$$4e^{4\nu}\nu_{,\rho}\left[(\rho B)_{,\rho} - \rho B\nu_{,\rho}\right] + \rho^3 B^3 \omega^2_{,\rho} \geq 0\,. \tag{1.75}$$

When (1.75) is not fulfilled, the particle is pulled "outwards" too strongly so no value of Ω is sufficiently small.

While the axial symmetry is "natural" to disc sources, the stationarity condition is more subtle. Such a state requires precise equilibrium of the gravitational, inertial, and pressure forces. We have seen one interpretation of a thin disc in the previous section, in particular, it led to an understanding of the disc as an

[5] Analogously to (1.67), v represents a local relative velocity of the particle on the circular orbit with respect to a ZAMO observer.

ideal fluid with azimuthal and radial stresses. However, there is another option used more in the astrophysical context. When the radial pressure vanishes ($S^\rho_\rho = 0$) $\Leftrightarrow$ $p_{(\rho)} = 0$, we can interpret the disc as it consisting of two counter-rotating streams of dust on circular geodesics. The surface stress-energy tensor can be decomposed into

$$S^{\mu\nu} = \sigma_+ U^\mu_+ U^\nu_+ + \sigma_- U^\mu_- U^\nu_- \,, \tag{1.76}$$

where the sign $\pm$ refers to the direction of the stream with respect to the azimuthal coordinate ϕ. The components of the four-velocities are simply (1.71) with the geodesic values of $\Omega_\pm$ (1.74), namely

$$U^\mu_\pm = U^t_\pm (1, \Omega_\pm, 0, 0) \,, \qquad U^t_\pm = \frac{1}{\sqrt{-g_{tt} - 2g_{t\phi}\Omega_\pm - g_{\phi\phi}\Omega^2_\pm}} \equiv \frac{e^{-\nu}}{\sqrt{1 - v^2_\pm}} \,. \tag{1.77}$$

Clearly, the double-stream interpretation is only possible if the condition (1.75) holds. From (1.76) we have

$$\sigma_\pm = \pm (g_{tt} + 2g_{t\phi}\Omega_\pm + g_{\phi\phi}\Omega^2_\pm) \frac{S^{\phi\phi} - S^{tt}\Omega^2_\mp}{\Omega^2_- - \Omega^2_+} \,. \tag{1.78}$$

By equating (1.69) – with $p_{(\rho)} = 0$ – and (1.76),

$$\sigma V^\mu V^\nu + p_{(\phi)} W^\mu W^\nu = \sigma_+ U^\mu_+ U^\nu_+ + \sigma_- U^\mu_- U^\nu_- \tag{1.79}$$

we can identify the connection between both interpretations, namely from the trace of the stress-energy tensor it immediately follows

$$\sigma_+ + \sigma_- = \sigma - p_{(\phi)} \,. \tag{1.80}$$

From the projection onto $V^\mu V^\nu$, $W^\mu W^\nu$, and $V^\mu W^\nu$ we have

$$\begin{aligned}
\sigma &= \sigma_+ (U^\alpha_+ V_\alpha)^2 + \sigma_- (U^\beta_- V_\beta)^2 \\
&= \frac{1}{1 - v^2} \left[\frac{(1 - v v_-)^2}{1 - v^2_-} \sigma_- + \frac{(1 - v v_+)^2}{1 - v^2_+} \sigma_+ \right] , \qquad (1.81) \\
p_{(\phi)} &= \sigma_+ (U^\alpha_+ W_\alpha)^2 + \sigma_- (U^\beta_- W_\beta)^2 \\
&= \frac{1}{1 - v^2} \left[\frac{(v - v_-)^2}{1 - v^2_-} \sigma_- + \frac{(v - v_+)^2}{1 - v^2_+} \sigma_+ \right] , \qquad (1.82) \\
0 &= \sigma_+ (U^\alpha_+ V_\alpha)(U^\beta_+ W_\beta) + \sigma_- (U^\alpha_- V_\alpha)(U^\beta_- W_\beta) \\
&= \frac{1}{1 - v^2} \left[\frac{(1 - v v_-)(v - v_-)}{1 - v^2_-} \sigma_- + \frac{(1 - v v_+)(v - v_+)}{1 - v^2_+} \sigma_+ \right] . \qquad (1.83)
\end{aligned}$$

To summarize, there are two possible physical interpretations of thin discs with no radial pressure:

- a single-component ideal fluid of the surface density σ and azimuthal pressure $p_{(\phi)}$ – set of hoops with an internal pressure,
- two counter-rotating streams of dust following circular geodesics with the surface densities σ_+ and σ_-.

1.7 Energy conditions and physical properties

Not any value of the density or pressure is considered physically acceptable. First of all, all the disc elements should move with subluminal velocities. In other words, V^μ should be normalized to -1, thus V^t must be real. From (1.67) it follows that it is true if $|v| \leq 1$. The same should also hold for the counter-rotating streams, i.e., $|v_\pm| \leq 1$.

The common additional requirements are energy conditions which attempt to express the fact that any time-like (or null) observer u^μ should agree that gravity is attractive. More formulations are possible:

- *weak energy condition (WEC)*: the energy density measured by any observer is non-negative, $T_{\alpha\beta}u^\alpha u^\beta \geq 0$,
- *dominant energy condition (DEC)*: the current of energy $(-T^\mu{}_\alpha\, u^\alpha)$ should be time-like or null, i.e., $T^\beta{}_\alpha\, T_{\beta\gamma}\, u^\alpha u^\gamma \leq 0$,
- *strong energy condition (SEC)*: gravity is never repulsive, which requires $\left(T_{\alpha\beta} - \frac{1}{2}T g_{\alpha\beta}\right) u^\alpha u^\beta = T_{\alpha\beta}u^\alpha u^\beta + \frac{1}{2}T \geq 0$.

For the stress-energy tensor (1.69) the energy conditions in terms of physical characteristics read

$$\begin{aligned}
\text{WEC} &\iff \sigma \geq 0\,, \quad \sigma + p_{(\phi)} \geq 0\,, \quad \sigma + p_{(\rho)} \geq 0\,,\\
\text{DEC} &\iff \sigma \geq 0\,, \quad p_{(\phi)}^2 + p_{(\rho)}^2 \leq \sigma^2\,,\\
\text{SEC} &\iff \sigma + p_{(\phi)} \geq 0\,, \quad \sigma + p_{(\rho)} \geq 0\,, \quad \sigma + p_{(\phi)} + p_{(\rho)} \geq 0\,.
\end{aligned}$$

In the case of the counter-rotating interpretation (for which we assume $p_{(\rho)} = 0$), all energy conditions require $\sigma_+ \geq 0$ and $\sigma_- \geq 0$. It also implies that the subdeterminant of S_B^A should be negative,

$$\det(S_B^A) = -\sigma p_{(\phi)} = -\frac{(v_+ - v_-)^2}{(1-v_+^2)(1-v_-^2)}\sigma_+\sigma_- \leq 0\,. \tag{1.84}$$

Hence, as expected, the counter-rotating interpretation is more restrictive, requiring also $p_{(\phi)} \geq 0$.

Finally, we remark that orbits in the counter-rotating interpretation should be stable against radial and vertical perturbations. We will not discuss these issues in this thesis, but we refer the reader to Semerák & Žáček (2000) and the references therein. One should also check some general spacetime properties such as the existence of singularities, closed timelike curves, or asymptotic behavior.

1.8 Mass and angular momentum

Assuming asymptotically flat spacetime, one way to obtain the total mass and angular momentum contained within that spacetime is to read them out from the asymptotic behaviour of the metric functions (1.18). However, using the symmetries – stationarity and axial symmetry in this case – Komar integrals (1.19) and (1.20) allow to assign both properties directly to the disc source. By applying the Stokes theorem, the identity valid for any Killing vector field

$\xi^{\mu;\beta}{}_{\beta} = -R^{\mu}_{\beta}\xi^{\beta}$ and the "trace-reversed" Einstein equations $R^{\mu}_{\nu} = 4\pi(2T^{\mu}_{\nu} - T\delta^{\mu}_{\nu})$, we get

$$\mathcal{M}_{\mathrm{K}} = \frac{1}{8\pi}\oint_{\partial\Sigma}\xi^{\alpha;\beta}_{(t)}\,\mathrm{d}S_{\alpha\beta} = \frac{1}{4\pi}\int_{\Sigma}\xi^{\alpha;\beta}_{(t)\beta}\,\mathrm{d}\Sigma_{\alpha} = -\int_{\Sigma}(2T^{\alpha}_{\beta}\xi^{\beta}_{(t)} - T\xi^{\alpha}_{(t)})\,\mathrm{d}\Sigma_{\alpha}\,, \quad (1.85)$$

$$\mathcal{J}_{\mathrm{K}} = -\frac{1}{16\pi}\oint_{\partial\Sigma}\xi^{\alpha;\beta}_{(\phi)}\,\mathrm{d}S_{\alpha\beta} = -\frac{1}{8\pi}\int_{\Sigma}\xi^{\alpha;\beta}_{(\phi)\beta}\,\mathrm{d}\Sigma_{\alpha} = \frac{1}{2}\int_{\Sigma}(2T^{\alpha}_{\beta}\xi^{\beta}_{(\phi)} - T\xi^{\alpha}_{(\phi)})\,\mathrm{d}\Sigma_{\alpha}\,. \quad (1.86)$$

In the Weyl coordinates, we take the natural volume element of a slice $t = \text{const}$, that is $\mathrm{d}\Sigma_{\mu} = \delta^{t}_{\mu}\sqrt{-g}\,\mathrm{d}^3x = \delta^{t}_{\mu}B\rho e^{2\lambda-2\nu}\,\mathrm{d}\rho\,\mathrm{d}z\,\mathrm{d}\phi$. For a thin disc characterized by the surface stress-energy tensor (1.53), i.e., $T_{\mu\nu}\sqrt{g_{zz}} = T_{\mu\nu}e^{\lambda-\nu} = S_{\mu\nu}\delta(z)$, we can perform the integration over z and ϕ coordinates resulting in

$$\mathcal{M}_{\mathrm{K}} = 2\pi\int_{-\infty}^{\infty}(S^{\rho}_{\rho} + S^{\phi}_{\phi} - S^{t}_{t})B\rho e^{\lambda-\nu}\,\mathrm{d}\rho\,, \quad (1.87)$$

$$\mathcal{J}_{\mathrm{K}} = 2\pi\int_{-\infty}^{\infty}S^{t}_{\phi}B\rho e^{\lambda-\nu}\,\mathrm{d}\rho\,. \quad (1.88)$$

Substituting (1.54)-(1.58), we get the Komar mass and angular momentum in terms of the metric functions and their normal derivatives to the disc plane,

$$\mathcal{M}_{\mathrm{K}} = \frac{1}{2}\int_{-\infty}^{\infty}(2\nu_{,z} - B^2\rho^2e^{-4\nu}\omega\omega_{,z})B\rho\,\mathrm{d}\rho\,, \quad (1.89)$$

$$\mathcal{J}_{\mathrm{K}} = -\frac{1}{4}\int_{-\infty}^{\infty}B^3\rho^3e^{-4\nu}\omega_{,z}\,\mathrm{d}\rho\,. \quad (1.90)$$

CHAPTER

2

WEYL (STATIC) SPACETIMES

In this chapter, we focus on the static limit, i.e., when $\omega = 0$, commonly referred to as Weyl spacetimes. While most astrophysical objects presumably carry some angular momentum, when the net rotation in the spacetime is negligible, or compensated, it is an adequate approximation. Moreover, it may already help us to understand some interesting implications of the disc's gravity without the need to deal with the mathematical complexity of the stationary case.

The Weyl metric reads

$$\mathrm{d}s^2 = -e^{2\nu}\,\mathrm{d}t^2 + B^2\rho^2 e^{-2\nu}\,\mathrm{d}\phi^2 + e^{2\lambda-2\nu}(\mathrm{d}\rho^2 + \mathrm{d}z^2)\,. \tag{2.1}$$

Our attention will go towards the case $T_{\rho\rho} + T_{zz} = 0$. As we discussed in Sec. 1.3, then we can choose $B = 1$, which reduces the Einstein equations to

$$\Delta\nu = 4\pi e^{2\lambda-2\nu}(T^{\phi}_{\phi} - T^{t}_{t})\,, \tag{2.2}$$

$$\lambda_{,\rho} - \rho\left(\nu_{,\rho}^2 - \nu_{,z}^2\right) = 4\pi\rho(T_{\rho\rho} - T_{zz})\,, \tag{2.3}$$

$$\lambda_{,z} - 2\rho\nu_{,\rho}\nu_{,z} = 8\pi\rho T_{\rho z}\,, \tag{2.4}$$

where Δ is the standard 3D Laplace operator in cylindrical coordinates. What a remarkable result! In vacuum (where $T_{\mu\nu} = 0$), the metric function ν satisfies the Laplace equation. Thus, any vacuum axially symmetric gravitational field known from Newton's theory is a valid solution for ν in GR. However, the function ν does not tell the whole story, as there is also another function λ present in the metric. This can significantly deviate from the Newtonian picture. The second metric function λ is determined by a line integration going through a vacuum region,

$$\lambda = \int \rho\left(\nu_{,\rho}^2 - \nu_{,z}^2\right)\mathrm{d}\rho + 2\rho\nu_{,\rho}\nu_{,z}\,\mathrm{d}z\,, \tag{2.5}$$

where the integration usually starts at the symmetry axis where $\lambda = 0$ from the regularity condition (1.16). Because the Laplace equation $\Delta\nu = 0$ is also the

integrability condition for (2.5), the metric function λ is, in principle, obtainable for any Newtonian potential ν. Notice that while the Laplace equation is linear, the non-linearity of the Einstein equations is manifested in the equations for λ.

Even though the problem of finding a static and axially symmetric solution to the Einstein equations is partially Newtonian, one has to be careful about the physical interpretation of the obtained metric. For example, the simplest solution of the Laplace equation is the Newtonian potential of a point mass $\mathcal{M}$ located at the origin

$$\nu = -\frac{\mathcal{M}}{\sqrt{\rho^2 + z^2}}\,. \tag{2.6}$$

This potential is spherically symmetric, but the second metric function

$$\lambda = \frac{-\mathcal{M}^2\rho^2}{2(\rho^2 + z^2)^2} \tag{2.7}$$

is not! The solution was first considered by Curzon (1925) and Chazy (1924) and as it later turned out, its interpretation is rather challenging. It describes an asymptotically flat spacetime with a curvature singularity at $\rho = 0, z = 0$ not covered by the horizon, although it is black due to the vanishing lapse function. But the singularity is not point-like, instead the metric can be smoothly (but not analytically) prolonged to a new asymptotically flat region which is more consistent with a ring-like singularity – for more details see Griffiths & Podolský (2009) and the references therein.

2.1 Axially symmetric Green function and the Bach-Weyl ring

The axially symmetric Green function for the Laplace equation reads

$$\mathscr{G}(\rho, z|\rho_0, z_0) = -\frac{1}{2\pi}\int_0^\pi \frac{\mathrm{d}\phi}{\sqrt{(z - z_0)^2 + \rho^2 + \rho_0^2 - 2\rho\rho_0\cos\phi}}\,, \tag{2.8}$$

where the integration over ϕ gives

$$\mathscr{G}(\rho, z|\rho_0, z_0) = -\frac{K(k)}{\pi\sqrt{(\rho + \rho_0)^2 + (z - z_0)^2}}\,, \quad k = \frac{2\sqrt{\rho\rho_0}}{(\rho + \rho_0)^2 + (z - z_0)^2}\,. \tag{2.9}$$

The function $K(k)$ is the complete elliptic integral of the first kind with modulus k. Physically, the Green function describes the Newtonian potential of a singular ring of constant linear density ρ_0^{-1}.

In GR, such a ring was first considered by Bach & Weyl (1922). In particular, the homogeneous singular ring with the mass $\mathcal{M}$ located in the equatorial plane ($z_0 = 0$) at the Weyl radius $\rho_0 = b$ is described by

$$\nu_{\mathrm{BW}} = -\frac{2\mathcal{M}K(k)}{\pi\sqrt{(\rho + b)^2 + z^2}}\,, \tag{2.10}$$

$$\lambda_{\mathrm{BW}} = -\frac{\mathcal{M}^2}{4\pi^2 b^2\rho}\left\{(\rho + b)\left[E(k) - K(k)\right]^2 + \frac{(\rho - b)\left[E(k) - k'^2K(k)\right]^2}{k'^2}\right\}, \tag{2.11}$$

where E is the complete elliptic integral of the second kind with the same modulus as in (2.9) and k' denotes the complementary modulus $k'^2 = 1 - k^2$.

The Bach-Weyl ring is another example of how a perfectly reasonable Newtonian solution, when generalized to GR, possesses rather unexpected properties. Namely, due to the second metric function λ, the ring singularity is strongly directional, meaning that the meridional sections close to the ring are not isotropic. The proper radius $\int_0^b \sqrt{g_{\rho\rho}}\,\mathrm{d}\rho$ of the ring is infinite, while the proper distance from the outer half-plane $\rho \geq b$ to the ring is always finite (Semerák, 2016). D'Afonseca et al. (2005) studied the geodesic structure finding that the ring is more attractive from the inner part, but the test particles never reach the ring there, because it is an infinite distance for them. In the limit $b \to 0^+$, both elliptic integrals approach $\pi/2$ and the Bach-Weyl solution goes over to the Chazy-Curzon solution, which preserves the directional property of the singularity as we briefly discussed in the previous section.

2.2 Appell ring

Although the solutions to the Laplace equation are unique, which ensures that the Bach-Weyl ring is the only correct "singular ring", there are more exact solutions which can be interpreted as ring-like. One of them is an old Appell ring obtained (within electrostatics) already in the 19th century (Appell, 1887). It is described by a potential of a point particle of mass $\mathcal{M}$ located at an imaginary extension of the z axis ($\rho = 0, z = ib$), in particular

$$\nu_{\mathrm{App}} = -\frac{\mathcal{M}}{\sqrt{\rho^2 + (z - ib)^2}}\,. \tag{2.12}$$

Thanks to the linearity of the Laplace equation, the real part of such a Newtonian potential is also a solution, singular at $\rho = b$ in the equatorial plane $z = 0$. This "ring" was first studied in GR by Gleiser & Pullin (1989), the metric functions read explicitly

$$\nu_{\mathrm{App}} = -\mathrm{Re}\left[\frac{\mathcal{M}}{\sqrt{\rho^2 + (z - ib)^2}}\right] = -\frac{\mathcal{M}}{\sqrt{2}\Sigma}\sqrt{\Sigma + \rho^2 + z^2 - b^2}\,, \tag{2.13}$$

$$\lambda_{\mathrm{App}} = \frac{\mathcal{M}^2}{8b^2}\left[1 - \frac{\rho^2 + z^2 + b^2}{\Sigma} - \frac{2b^2\rho^2(\Sigma^2 - 8z^2b^2)}{\Sigma^4}\right], \tag{2.14}$$

where $\Sigma = \sqrt{(\rho^2 - b^2 + z^2)^2 + 4b^2z^2}$. As pointed out by Semerák et al. (1999), the Appell ring has many similarities to the Kerr singularity, although no dragging effects are present as the spacetime is static. It can be interpreted as an intrinsically flat disc ($\rho \leq b, z = 0$) with an effective negative surface mass density

$$\sigma = -\frac{\mathcal{M}b}{2\pi(b^2 - \rho^2)^{3/2}} \tag{2.15}$$

diverging towards the rim ($\rho = b, z = 0$) to $-\infty$ while jumping to $+\infty$ precisely at the rim, so the total mass remains positive and finite. The second option is that it represents a singular ring of mass $\mathcal{M}$ if the metric is smoothly extended

through the inner (flat, disc-like) region to a new asymptotically flat manifold where, however, the ring has a negative mass $-\mathcal{M}$. In the limit $b \to 0^+$, we again recover the Chazy-Curzon solution.

Regardless of the interpretation, it is clear that the ring sources are problematic in GR. Especially if they should represent a limit of a real extended (toroidal) astrophysical object. However, the situation is much better for infinitesimally thin discs as we will see in the next sections.

2.3 Thin discs

Consider a thin (infinite or finite) axially symmetric disc lying in the equatorial plane ($z_0 = 0$) with the Newtonian surface density $w(\rho)$. Then the solution of the Poisson equation $\Delta\nu = 4\pi w(\rho)\delta(z)$ is given by an integral of the Green function (2.8) over the disc density

$$\nu_{\rm disc}(\rho, z) = 4\pi \int_0^\infty \mathscr{G}(\rho, z|\rho_0, 0)\rho_0 w(\rho_0)\,\mathrm{d}\rho_0 \tag{2.16}$$

$$= -4 \int_0^\infty \frac{\rho_0 w(\rho_0)}{\sqrt{(\rho+\rho_0)^2 + z^2}} K\left(\frac{2\sqrt{\rho\rho_0}}{\sqrt{(\rho+\rho_0)^2 + z^2}}\right) \mathrm{d}\rho_0\,. \tag{2.17}$$

The second metric function is then determined from (2.5). From the knowledge of the Newtonian potential $\nu_{\rm disc}$, we can recover the density by

$$w(\rho) = \frac{1}{2\pi} \lim_{z\to 0^+} \nu_{,z}\,, \tag{2.18}$$

which follows from integrating the Poisson equation over the z coordinate, assuming that the spacetime is reflection symmetric.

Solving (2.17) directly is mostly not feasible, thus several other approaches have been applied in the literature. One way is to start at the symmetry axis where $K(k) = \pi/2$ and solve much simpler integration there. If the potential on the axis can be expanded in power series of z, the solution may be constructed everywhere. In particular, if

$$\nu_{\rm disc}(\rho = 0, z) = -2\pi \int_0^\infty \frac{\rho_0 w(\rho_0)}{\sqrt{\rho_0^2 + z^2}}\,\mathrm{d}\rho_0 = \sum_{j=0}^\infty \alpha_j z^j + \beta_j z^{-j}\,, \tag{2.19}$$

where α_j, β_j are constant coefficients, then the potential at a generic location (ρ, z) is given by

$$\nu_{\rm disc}(\rho, z) = \sum_{j=0}^\infty \left[\alpha_j \left(\sqrt{\rho^2 + z^2}\right)^j + \beta_j \left(\sqrt{\rho^2 + z^2}\right)^{-j}\right] P_j\left(\frac{z}{\sqrt{\rho^2 + z^2}}\right)\,, \tag{2.20}$$

where P_j are the Legendre polynomials. However, the above recipe usually results in the metric with infinite Legendre series with a rather poor convergence.

There is one exception found by Morgan & Morgan (1969), where the series is finite. They used the fact that the axially symmetric Laplace equation is separable in *oblate spheroidal coordinates* (ζ, ξ) defined as

$$\rho^2 = b^2(1+\zeta^2)(1-\xi^2)\,, \quad z = b\zeta\xi\,, \tag{2.21}$$

where b is a constant with the dimension of length. For an isolated thin disc stretching from the origin ($\rho = 0, z = 0$) to some Weyl radius ($\rho = b, z = 0$), the general form of the potential reads

$$\nu_{\rm MM}(\zeta,\xi) = -\frac{\mathcal{M}}{b}\sum_{j=0}^{\infty} C_{2j}{\rm i}Q_{2j}({\rm i}\zeta)P_{2j}(\xi)\,, \tag{2.22}$$

where P_{2j} and Q_{2j} are the Legendre polynomials of the first and second kind and C_{2j} are constants determined by the source. From (2.18) it follows that

$$w_{\rm MM}(\rho \le b) = \frac{\mathcal{M}}{2\pi b}\frac{1}{\sqrt{b^2-\rho^2}}\sum_{j=0}^{\infty}(2j+1)C_{2j}Q_{2j+1}(0)P_{2j}\left(\sqrt{1-\frac{\rho^2}{b^2}}\right)\,. \tag{2.23}$$

By setting

$$C_{2j}^{(n)} = \begin{cases} \frac{(-1)^j(4j+1)(2j)!(n+j)!}{(j!)^2(n-j)!(2n+2j+1)!}\,, & j \le n\,,\\ 0\,, & j > n\,, \end{cases}$$

for an integer n, we obtain the Morgan-Morgan family of discs characterized by the Newtonian surface density

$$w_{\rm MM}^{(n)}(\rho \le b) = \frac{(2n+1)\mathcal{M}}{2\pi b^2}\left(1-\frac{\rho^2}{b^2}\right)^{n-1/2}\,. \tag{2.24}$$

The second metric function can also be obtained in closed form by directly solving case by case the vacuum Einstein equations (2.3) and (2.4) transformed to the oblate spheroidal coordinates (2.21)

$$\frac{\zeta^2+\xi^2}{\xi^2-1}\lambda_{,\zeta} = -\zeta(\xi^2-1)\nu_{,\xi}^2 - \zeta(\zeta^2+1)\nu_{,\zeta}^2 + 2\xi(\zeta^2+1)\nu_{,\zeta}\nu_{,\xi}\,, \tag{2.25}$$

$$\frac{\zeta^2+\xi^2}{\zeta^2+1}\lambda_{,\xi} = \xi(\zeta^2+1)\nu_{,\zeta}^2 + \xi(\xi^2-1)\nu_{,\xi}^2 - 2\zeta(\xi^2-1)\nu_{,\zeta}\nu_{,\xi}\,. \tag{2.26}$$

Thanks to the integrability condition $\Delta\nu = 0$, it is sufficient to integrate the second equation over ξ starting at the axis $\xi = 1$ where $\lambda = 0$. The integration over ζ would give the same result.

If interested in annular discs, we can use another symmetry of the Laplace equation – inversion with respect to a sphere, so-called **Kelvin transformation**. Given a sphere of radius b, the inversion of a point (ρ, z) means the coordinate transformation

$$\rho \longrightarrow \frac{b^2\rho}{\rho^2+z^2}\,, \quad z \longrightarrow \frac{b^2 z}{\rho^2+z^2}\,. \tag{2.27}$$

Then, if ν satisfies the Laplace equation, the function

$$\mathcal{K}\nu(\rho,z) \equiv \frac{b}{\sqrt{\rho^2+z^2}}\nu\left(\frac{b^2\rho}{\rho^2+z^2}, \frac{b^2 z}{\rho^2+z^2}\right) \tag{2.28}$$

solves the Laplace equation as well. Such a transformation maps spheres into spheres and, in particular, the interior of the sphere is mapped into its exterior and vice versa. Thus, a thin disc is transformed into a thin disc with a different Newtonian density profile

$$w(\rho) \longrightarrow \frac{b^3}{\rho^3}w\left(\frac{b^2}{\rho}\right)\,. \tag{2.29}$$

Inverting the Morgan-Morgan discs leads to new disc solutions with the Newtonian density

$$w^{(n)}_{\mathrm{iMM}}(\rho \geq b) = \frac{2^{2n}(n!)^2}{(2n)!\pi^2}\frac{\mathcal{M}b}{\rho^3}\left(1-\frac{b^2}{\rho^2}\right)^{n-1/2} . \tag{2.30}$$

They are spatially infinite, stretching from $\rho = b$ to infinity, although having a *finite* total mass $\mathcal{M}$. These discs were first considered by Lemos & Letelier (1994), where they were also superposed with a Schwarzschild black hole, see also Semerák & Žáček (2000); Žáček & Semerák (2002); Semerák (2003) for a detailed study of physical properties, including stability. The second metric function λ has not been obtained analytically, until our recent work Kofroň et al. (2023) – see Sec. 2.6.3.

2.4 Physical properties of static thin discs

When the spacetime is static and no radial pressure is present ($p_{(\rho)} = 0$), the stress-energy tensor (1.54)-(1.60) has only two non-zero components

$$S^t_t = -\frac{e^{\nu-\lambda}}{2\pi}\nu_{,z}(1-\rho\nu_{,\rho}) , \quad S^\phi_\phi = \frac{e^{\nu-\lambda}}{2\pi}\rho\nu_{,z}\nu_{,\rho} , \tag{2.31}$$

where we used the vacuum Einstein equation (2.4) and assumed that $B = 1$. The expression for density and azimuthal pressure becomes very simple,

$$\sigma + p_{(\phi)} = S^\phi_\phi - S^t_t = e^{\nu-\lambda}\frac{\nu_{,z}}{2\pi} = e^{\nu-\lambda}w(\rho) , \tag{2.32}$$

$$p_{(\phi)} = S^\phi_\phi = e^{\nu-\lambda}\rho w(\rho)\nu_{,\rho} , \tag{2.33}$$

where $w(\rho)$ is the Newtonian surface density (2.18). As expected, this Newtonian quantity is related to the sum of the physical density and pressure. The eigenvectors of the stress-energy tensor are

$$V^\mu = e^{-\nu}(1,0,0,0) , \qquad W^\mu = \frac{e^\nu}{\rho}(0,1,0,0) \tag{2.34}$$

and the counter-rotating parameters are simplified to

$$\Omega_\pm = \pm e^{2\nu}\sqrt{\frac{1}{\rho}\cdot\frac{\nu_{,\rho}}{1-\rho\nu_{,\rho}}} , \qquad U^\mu_\pm = e^{-\nu}\sqrt{\frac{1-\rho\nu_{,\rho}}{1-2\rho\nu_{,\rho}}}(1,\Omega_\pm,0,0) , \tag{2.35}$$

and

$$\sigma_\pm = \frac{\sigma}{2} = \frac{1}{2}e^{\nu-\lambda}w(\rho)(1-\rho\nu_{,\rho}) , \qquad v^2_\pm = \frac{\rho\nu_{,\rho}}{1-\rho\nu_{,\rho}} = \frac{p_{(\phi)}}{\sigma} . \tag{2.36}$$

Finally, all the energy conditions discussed in Sec. 1.7 are satisfied for both interpretations if the linear velocities acquire timelike values $0 \leq |v_\pm| < 1$.

The total angular momentum is, of course, zero and the total mass of the disc matches the Newtonian expression

$$\mathcal{M}_{\mathrm{K}} = \int_{-\infty}^{\infty}\nu_{,z}\rho\,\mathrm{d}\rho = 2\pi\int_{-\infty}^{\infty}w(\rho)\rho\,\mathrm{d}\rho . \tag{2.37}$$

2.5 Superposition of multiple sources

The static and axially symmetric problem is partially linear – it is possible to use the superposition principle for the gravitational potential ν. However, the second metric function λ does not "superpose" that simply. Even vacuum equations (2.3), (2.4) are non-linear (quadratic in ν). Indeed, imagine two sources described by the metric function ν_1, ν_2 and λ_1, λ_2 satisfying (2.5) respectively. Then, their common gravitational field is given by

$$\nu = \nu_1 + \nu_2 \,, \qquad \lambda = \lambda_1 + \lambda_2 + \lambda_{\rm int} \,, \tag{2.38}$$

where the "interaction" part $\lambda_{\rm int}$ satisfies

$$\lambda_{{\rm int},\rho} = 2\rho(\nu_{1,\rho}\nu_{2,\rho} - \nu_{1,z}\nu_{2,z}) \,, \tag{2.39}$$

$$\lambda_{{\rm int},z} = 2\rho(\nu_{1,\rho}\nu_{2,z} + \nu_{1,z}\nu_{2,\rho}) \,. \tag{2.40}$$

Typically, we will consider the Schwarzschild black hole (1.28), (1.29) as one of the sources, and a static thin disc as the other.

2.6 Particular results

2.6.1 Polynomial and power-law discs

For a specific Newtonian density profile, the integration (2.17) can be performed directly. However, we need to re-express the Green function in a more suitable form. Already in electrostatics, then considered by Toomre (1963) and, more recently, by Conway (2000) and us in Kotlařík et al. (2022), the axially symmetric Green function (2.8) can be cast into the form

$$\mathscr{G}(\rho, z|\rho_0, z_0) = -2\pi\rho_0 \int_0^\infty J_0(s\rho_0)J_0(s\rho)e^{-s|z-z_0|}\,{\rm d}s \,, \tag{2.41}$$

where J_0 is the Bessel function of the order zero, and s is an auxiliary real parameter with the dimension of inverse length. The Newtonian potential of a thin disc lying in the equatorial plane $z_0 = 0$ reads

$$\nu_{\rm disc} = -2\pi \int_0^\infty \int_0^\infty \rho_0 w(\rho_0) J_0(s\rho_0)J_0(s\rho)e^{-s|z|}\,{\rm d}s\,{\rm d}\rho_0 \,. \tag{2.42}$$

Remarkably, for the density profiles which are given as a general combination of the even powers in $\rho_0 \in (0, b)$, the radial integration can be evaluated analytically and expressed, again, in terms of the Bessel functions. In the end, the problem is reduced to integrals of the type

$$\mathcal{I}_{(\alpha,\beta,\gamma)} = \int_0^\infty s^\alpha J_\beta(sb)J_\gamma(s\rho)e^{-s|z|}\,{\rm d}s \,, \qquad \alpha \in {\rm Z}, \text{ and } \beta, \gamma \in {\rm N}_0. \tag{2.43}$$

These "Laplace transformations of the Bessel functions products" were studied by Conway (2000) thoroughly. In particular, general $\mathcal{I}_{(\alpha,\beta,\gamma)}$ leads to a specific combination of the complete elliptic integrals. Gravitational potentials corresponding to the negative powers ρ_0^{-2l-3} in the Newtonian density can also be found as they follow from the Kelvin transformation (2.27), (2.28). Then, using the linearity

of the Laplace equation, we obtained in Kotlařík et al. (2022) closed-form potentials of the finite polynomial and infinite and finite annular power-law discs of the Newtonian density profiles

$$\sigma_{\rm pol}^{(m,2l)}(\rho \leq b) = \binom{m+\frac{1}{l}}{m} \frac{\mathcal{M}}{\pi b^2} \left(1 - \frac{\rho^{2l}}{b^{2l}}\right)^m , \tag{2.44}$$

$$\sigma_{\rm pl}^{(m,2l)}(\rho \geq b) = \binom{m+\frac{1}{2l}}{m} \frac{\mathcal{M}b}{2\pi\rho^3} \left(1 - \frac{b^{2l}}{\rho^{2l}}\right)^m , \tag{2.45}$$

$$\sigma_{\rm bump}^{(L)}(b_{\rm in} \leq \rho \leq b_{\rm out}) = -W_0 + \sum_{j=0}^{L} (-1)^j \frac{W_{-3-2j}}{\rho^{3+2j}} , \tag{2.46}$$

where $l, L, m \in \mathrm{N}_0$. In that paper, we list some explicit examples of the potentials and check several basic physical properties.

2.6.2 Fully relativistic solution of a black hole encircled by a thin disc

Kuzmin (1956) formulated a simple yet very useful method for deriving thin disc solutions. Imagine a point mass $\mathcal{M}$ below the equatorial plane ($z = 0$) sitting on the symmetry axis $\rho = 0$ at a distance b. Then, if we cut the resulting gravitational field through the plane $z = 0$ and reflect the positive-z half-space to the negative-z half-space, we obtain discontinuous normal derivatives of the metric over the plane $z = 0$. That results in a surface mass density on that plane. In particular, the Newtonian potential and the corresponding Newtonian surface density read

$$\nu_{\rm Kuz}(\rho, z) = -\frac{\mathcal{M}}{\sqrt{\rho^2 + (|z| + b)^2}} , \quad w_{\rm Kuz}(\rho) = \lim_{z\to 0^+} \frac{\nu_{,z}}{2\pi} = \frac{1}{2\pi} \frac{\mathcal{M}b}{(\rho^2 + b^2)^{3/2}} . \tag{2.47}$$

Evans & de Zeeuw (1992) showed that the Kuzmin solution can actually be used as a building block for other axially symmetric discs. The interpretation of the method could be twofold: (*i*) constructing new discs by a superposition of Kuzmin discs with different b weighted by different weights $W(b)$, or, (*ii*) considering a gravitational field of a line distribution of matter described by the weight function $W(b)$, cut and reflected with respect to the equatorial plane. The gravitational potential and the associated Newtonian surface density is

$$\nu = -\int_0^\infty \frac{W(b)\,\mathrm{d}b}{\sqrt{\rho^2 + (|z| + b)^2}} , \quad w(\rho) = \frac{1}{2\pi} \int_0^\infty \frac{W(b) b\,\mathrm{d}b}{(\rho^2 + b^2)^{3/2}} . \tag{2.48}$$

Bičák et al. (1993a,b) introduced the technique to GR and derived the whole metric for various classical discs such as Kuzmin-Toomre (Toomre, 1963), Kalnajs-Mestel (Kalnajs, 1976; Mestel, 1963) and Schwarzschild discs (the latter corresponds to a constant weight function $W(b) = \mathrm{const}$).

In Kotlařík & Kofroň (2022), we took a certain combination of Kuzmin-Toomre solutions proposed by Vogt & Letelier (2009), describing infinite thin discs with the Newtonian density profiles

$$w_{\rm VL}^{(m,n)}(\rho) = \frac{\mathcal{M}b^{2m+1}(2m+1)}{2\pi} \binom{m+n+1/2}{n} \frac{\rho^{2n}}{(\rho^2 + b^2)^{m+n+3/2}} , \tag{2.49}$$

where $\mathcal{M}$ is the total mass of the disc, and $m, n \in \mathrm{N}_0$. When $n \geq 1$, the density drops to zero on the axis $\rho = 0$, thus the disc has an annular character. For such discs, we derived the second metric function λ and superposed them with the Schwarzschild black hole placed in their empty centre. The resulting superposed metric is analytical and was found in closed form.

2.6.3 A new generic method for generating thin disc solutions

Inspired by the Kuzmin trick (2.47), we developed a new method for generating thin-disc solutions in GR (Kofroň et al., 2023). As the building block, instead of a point particle on the negative half of the z axis, we use the Appell potential (2.12). Assume a line distribution of matter along the imaginary part of the z axis described by a real weight function $f(q)$, and cut and reflect the resulting gravitational field with respect to the equatorial plane ($z = 0$). The (complex) potential simply reads[1]

$$\nu_f(\rho, z) = -\int_0^\infty \frac{f(q)\,\mathrm{d}q}{\sqrt{\rho^2 + (|z| + \mathrm{i}q)^2}}\,. \tag{2.50}$$

Both the real and imaginary parts of (2.50) are solutions to the Laplace equation which correspond to a layer of matter in the equatorial plane. However, from the asymptotic behaviour of the potential, only the real part corresponds to the physical mass, while the imaginary part represents a nonphysical dipole. In particular, using the oblate spherical coordinates (2.21) we have

$$\frac{f(q)}{\sqrt{\rho^2 + (|z| + \mathrm{i}q)^2}} \approx -\frac{f(q)}{b\zeta} + \frac{\mathrm{i}b\xi f(q)}{b^2\zeta^2} + \mathcal{O}(\zeta^{-3}) \tag{2.51}$$

for large $\zeta \gg 1$. Thus, $\int_0^\infty f(q)\,\mathrm{d}q$ may be interpreted as the total mass of the disc, while we omit the imaginary part from further considerations.

Under reasonable conditions on the weight function $f(q)$, we can show that the resulting Newtonian surface density is given by an Abel transformation of the weight function,

$$w_f(\rho) = -\frac{1}{2\pi}\int_\rho^\infty \frac{\mathrm{d}f}{\mathrm{d}q}\,\frac{\mathrm{d}q}{\sqrt{q^2 - \rho^2}}\,, \tag{2.52}$$

and the inverted relation

$$f(q) = 4\int_q^\infty \frac{\rho w_f(\rho)\,\mathrm{d}\rho}{\sqrt{\rho^2 - q^2}}\,. \tag{2.53}$$

Hence, from the desired Newtonian density we can find the weight function $f(q)$ using (2.53) and then take the real part of the gravitational potential ν_f from the integration (2.50). All the disc solutions discussed in the previous sections can be reformulated in this way. Namely, the approach proved useful when deriving the second metric function λ. We have been able to complete the metric for the inverted Morgan-Morgan discs (2.30), including the case when they are superposed

[1]Note that we use a slightly different notation in Kofroň et al. (2023), where we integrate over a real variable w (not to confuse with the density $w(\rho)$), rather than q.

with the Schwarzschild black hole. We also considered a more general family of Morgan-Morgan discs (Letelier, 2007) – holey Morgan-Morgan discs – and their inversions

$$w^{(m,n)}_{\mathrm{hMM}}(\rho \leq b) = \frac{\mathcal{M}}{2\pi b^{2+2m}} \frac{\left(\frac{3}{2}\right)_{m+n}}{m!\left(\frac{1}{2}\right)_n} \rho^{2m} \left(1 - \frac{\rho^2}{b^2}\right)^{n-1/2}, \tag{2.54}$$

$$w^{(m,n)}_{\mathrm{ihMM}}(\rho \geq b) = \frac{b^{2m+1}(m+n)!}{\pi^2 \left(\frac{1}{2}\right)_m \left(\frac{1}{2}\right)_n} \frac{\mathcal{M}}{\rho^{2m+3}} \left(1 - \frac{b^2}{\rho^2}\right)^{n-1/2}. \tag{2.55}$$

Both metric functions were derived in closed forms. Notice that similarly to the Vogt-Letelier discs (2.49), the densities (2.54) drop to zero on the axis $\rho = 0$ when $m \geq 1$, so a physically reasonable superposition with a black hole is also possible for them.

The Astrophysical Journal, 931:161 (16pp), 2022 June 1 https://doi.org/10.3847/1538-4357/ac6027

Static Thin Disks with Power-law Density Profiles*

P. Kotlařík, D. Kofroň, and O. Semerák
Institute of Theoretical Physics, Faculty of Mathematics and Physics, Charles University, Prague, Czech Republic
Received 2022 February 15; revised 2022 March 19; accepted 2022 March 21; published 2022 June 7

Abstract

The task of finding the potential of a thin circular disk with power-law radial density profile is revisited. The result, given in terms of infinite Legendre-type series in the above reference, has now been obtained in closed form thanks to the method of Conway employing Bessel functions. Starting from a closed-form expression for the potential generated by the elementary density term ρ^{2l}, we cover more generic—finite solid or infinite annular—thin disks using superposition and/or inversion with respect to the rim. We check several specific cases against the series-expansion form by numerical evaluation at particular locations. Finally, we add a method to obtain a closed-form solution for *finite* annular disks whose density is of "bump" radial shape, as modeled by a suitable combination of several powers of radius. Density and azimuthal pressure of the disks are illustrated on several plots, together with radial profiles of free circular velocity.

Unified Astronomy Thesaurus concepts: Relativistic disks (1388); Black holes (162)

1. Introduction

Disk sources of gravitation have a clear astrophysical importance. Disk configurations typically result from the combined effect of central attraction—due to a central body or due to the disk itself—and centrifugal force due to orbital motion of the disk matter. In Newton's theory, the gravitational field is fully represented by potential, given by mass density through the Poisson equation. In general relativity, where mass *currents* also contribute to the field, one has to also specify how the matter *moves*—i.e., how it orbits in the disk case. Unfortunately, when there is some overall net rotation, Einstein equations lead to a difficult problem, usually not solvable by analytical methods. On the other hand, if rotation can be neglected, or if it is compensated as in the case of two equal counter-orbiting streams, the situation is much simpler. More specifically, in the *static* and *axially symmetric* vacuum (or possibly electro-vacuum) case, the gravitational field can always be described by the spacetime metric of the Weyl type[1]

$$ds^2 = -e^{2\nu}dt^2 + \rho^2 e^{-2\nu}d\phi^2 + e^{2\lambda-2\nu}(d\rho^2 + dz^2), \tag{1}$$

where t, ρ, ϕ, and z are the Weyl cylindrical coordinates, ν (counterpart of the Newtonian gravitational potential) is given by the Laplace equation (so it behaves linearly), and λ is found (from ν) by quadrature

$$\lambda = \int_{\text{axis}}^{\rho,z} \rho\,[(\nu_{,\rho}^{\,2} - \nu_{,z}^{\,2})d\rho + 2\nu_{,\rho}\nu_{,z}\,dz], \tag{2}$$

computed along any path going through the (electro-)vacuum region.

Therefore, the Laplace equation is the key to the external field in Newtonian gravitation, in electrostatics, as well as in *static* general relativity. In the last case, however, the field is *not* in general represented completely by the thus determined potential; in the axially symmetric case, specifically, it also depends on the second metric function λ, which influences the geometry of meridional (ρ, z) sections and which can deviate the whole picture from the Newtonian form significantly. Still, the linearity of the Laplace equation is a tremendous simplification, permitting, in particular, to obtain the field of multicomponent systems by mere superposition. One can thus find, even in general relativity, the field of a static and axisymmetric system of a body encircled by a disk or a ring, as an approximation of, e.g., a black hole surrounded by an accretion disk. Regarding the gravitational dominance of such a compact source as the black hole, the matter in its surroundings is often treated as a test (non-gravitating), but higher (than first) derivatives of the metric/potential are generally prone to subtle effects of "self-gravitation," and since these are crucial for stability of the motion, the (self-)gravitating matter may sometimes assume a considerably different configuration than the test matter.

The paper is organized as follows. First, we recall in Section 2 how the Poisson integral solution of the Laplace equation appears in the case of a thin circular disk. Following the method suggested by Conway (2000), we then, in Section 3, rewrite that integral in terms of Bessel functions and solve it for a simple power-law density profile. The case of more general power-law (polynomial) density profiles is solved, in a closed form, in Section 4, both for solid and annular disks. In Section 5, the closed-form result is

* Dedicated to our teacher, Professor Jiří Bičák, on the occasion of his 80th birthday. For O.S., Jiří's interest in thin disks was, 30 yr ago (Bičák et al. 1993), the first motivation to study the topic.

[1] We use the $(-+++)$ signature of the metric, and geometrized units in which $c = 1$, $G = 1$.

numerically checked against the series-expansion solution presented in Semerák (2004). After briefly explaining, in Section 6, why the procedure only works for a density involving even powers of radius, we add in Section 7 how to obtain the potential of a *finite* disk with "bump"-type density profile. Physical properties of the disk sources are illustrated in Sections 8 (radial profiles of density and of azimuthal pressure) and 9 (radial profile of circular-geodesic velocity). Finally, we make several remarks in Section 10, mainly mentioning similar results that have appeared in the literature recently.

2. Static Thin Circular Disks

Computation of the potential of static thin circular disks is a classical problem of the potential theory. In Newton's theory of gravitation, it is mostly solved while modeling the gravitational field of galactic disks, while in general relativity, one mostly tackles it when modeling accretion disks around compact objects. Although it reduces to the Laplace equation in both theories, in the static case, it remains a challenge, as it is best illustrated by the "trivial" case of uniform surface density when the result still involves elliptic integrals of all three kinds (e.g., Lass & Blitzer 1983). For a thin disk lying in the equatorial plane ($z=0$), with an outer rim situated on some Weyl radius b, the Poisson integral for ν reads

$$\nu(\rho, z) = -2\int_0^{\pi}\int_0^{b} \frac{w(\rho')\rho' d\rho' d\phi}{\sqrt{\rho^2+z^2+\rho'^2-2\rho\rho'\cos\phi}}. \tag{3}$$

Integration with respect to ρ' leads to an expression containing Appell's hypergeometric function of two variables, while that with respect to ϕ yields

$$\nu(\rho, z) = -4\int_0^{b} \frac{w(\rho')\rho'}{\sqrt{(\rho+\rho')^2+z^2}} K\left(\frac{2\sqrt{\rho\rho'}}{\sqrt{(\rho+\rho')^2+z^2}}\right) d\rho'. \tag{4}$$

On the symmetry axis ($\rho=0$), it simplifies considerably, because the complete elliptic integral of the first kind $K(k)$ reduces to $\pi/2$. In the axisymmetric case, knowledge of ν on the axis is crucial, since if the latter can be expanded as a power series in z,

$$\nu(z) = -\frac{\mathcal{M}}{b}\sum_{j=0}^{\infty}\left(\alpha_j\frac{z^j}{b^j}+\beta_j\frac{b^{j+1}}{z^{j+1}}\right), \tag{5}$$

the potential at general location is obtained just by replacing z with $\sqrt{\rho^2+z^2}$ in the above sum and multiplying each of its terms by the Legendre polynomial $P_j\left(\frac{z}{\sqrt{\rho^2+z^2}}\right)$. In (5), α_j and β_j are coefficients and $\mathcal{M}$ represents the disk mass in our case.

If interested in *annular* disks rather than in finite solid ones, one can perform an inversion with respect to the rim at $\rho=b$ (also called the Kelvin transformation),

$$\rho \to \frac{b^2\rho}{\rho^2+z^2}, \qquad z \to \frac{b^2 z}{\rho^2+z^2}; \qquad \nu(\rho, z) \longrightarrow \frac{b}{\sqrt{\rho^2+z^2}}\,\nu\left(\frac{b^2\rho}{\rho^2+z^2}, \frac{b^2 z}{\rho^2+z^2}\right). \tag{6}$$

Actually, such a transformation leaves the solution of the Laplace equation a solution, just that it corresponds then to an annular disk, stretching from $\rho=b$ to radial infinity.

Two additional features are required naturally: the spacetime should be reflection symmetric, so z must appear as $|z|$ in odd powers; and the potential should be finite everywhere, at the origin ($\sqrt{\rho^2+z^2}=0$) and at infinity ($\sqrt{\rho^2+z^2}\to\infty$) in particular. Anyway, the above recipe yields the result in terms of the Legendre-type series, which is not ideal, due to rather bad convergence properties. A closed-form formula would definitely be more desirable. Unfortunately, such has been found only rarely, because the Poisson integral (4) usually is not elementary. One of the simple exceptions is the Morgan–Morgan family of solutions (Morgan & Morgan 1969), which corresponds, after inversion with respect to the rim, to the surface densities

$$w^{(m)}_{\mathrm{iMM}}(\rho) = \frac{2^{2m}(m!)^2\mathcal{M}b}{(2m)!\,\pi^2\rho^3}\left(1-\frac{b^2}{\rho^2}\right)^{m-1/2}. \tag{7}$$

The corresponding ν potentials are expressed in terms of *finite* Legendre series (with $m+1$ terms), so there is no truncation issue. The superposition of the Morgan–Morgan disks with a Schwarzschild-type black hole was studied by, e.g., Lemos & Letelier (1994) and Semerák (2003).

In Semerák (2004), we derived the potentials for similar (also annular) disks with densities of the power-law form

$$w_{\mathrm{i}}^{(m,n)}(\rho) = \binom{m+\frac{1}{n}}{m}\frac{\mathcal{M}b}{2\pi\rho^3}\left(1-\frac{b^n}{\rho^n}\right)^m, \tag{8}$$

where m and n are natural numbers and the first parenthesis stands for binomial coefficient. These behave somewhat more regularly at the inner rim and do not involve the square root. We were able to find the potential in closed form on the axis, but elsewhere it was

only given in terms of an infinite Legendre sum. The purpose of the present paper is to show that it can be written in a closed form. The key feature will be the relation between a complete elliptic integral of the first kind and an integral over a product of Bessel functions and exponentials.

3. Potential in Terms of the Bessel Functions

The alternative formulation we will build on first appeared within electrodynamics and later was applied to galactic disks by Toomre (1963). More recently, Conway (2000) developed it to obtain closed-form solutions for the potential of matter confined within axisymmetric boundaries. It consists of expressing the axisymmetric Green function, i.e., the potential due to an infinitesimally thin circular loop placed at (ρ', z'), as

$$\nu_{\rm loop}(\rho, z) = -2\pi\rho' \int_0^\infty J_0(s\rho')J_0(s\rho)e^{-s|z-z'|}\, ds, \tag{9}$$

where J_0 is the zero-order Bessel function of the first kind and s is an auxiliary real variable. The potential due to a thin source of surface density $w(\rho')$, placed at $z' = 0$, can thus be written as

$$\nu(\rho, z) = -2\pi \int_0^\infty \int_0^\infty \rho' w(\rho')J_0(s\rho')J_0(s\rho)e^{-s|z|}\, ds\, d\rho'. \tag{10}$$

The double integration of (10) looks more complicated than the single one in (4), but this is outweighed by having much better knowledge of integrals involving Bessel functions.

3.1. Potential for Power-law Density Terms: Convolution with the Bessel Functions

Consider the density given by an even power of ρ' within some finite radial range $(0, b)$,

$$w(\rho') = (\rho')^{2l}, \qquad 0 < \rho' < b, \qquad l > 0 \text{ integer}.$$

In such a case, the radial integration in (10) yields

$$\int_0^b \rho' w(\rho')J_0(s\rho')d\rho' = \frac{b^{2l+2}}{2l+2}\, {}_1F_2\left(1+l;\, 2+l,\, 1;\, -\frac{b^2s^2}{4}\right), \tag{11}$$

with ${}_1F_2$ the "1,2" generalized hypergeometric function. Employing the contiguous relation

$$c\, {}_1F_2(a;\, b+1,\, c;\, z) = b\, {}_1F_2(a;\, b,\, c+1;\, z) - (b-c)\, {}_1F_2(a;\, b+1,\, c+1;\, z), \tag{12}$$

we can express ${}_1F_2$ in terms of ${}_0F_1$, and thus, thanks to the identity

$${}_1F_2\left(a;\, a,\, c;\, -\frac{z^2}{4}\right) = {}_0F_1\left(-;c;\, -\frac{z^2}{4}\right) = \left(\frac{z}{2}\right)^{1-c}\Gamma(c)J_{c-1}(z), \tag{13}$$

as a combination of Bessel functions, with a and c integers. In particular, regarding the symmetry ${}_1F_2(a; b, c; z) = {}_1F_2(a; c, b; z)$, we have

$$\begin{aligned}
&{}_1F_2\left(1+l;\, 2+l,\, 1;\, -\frac{b^2s^2}{4}\right)\\
&\quad = \sum_{j=1}^{l}(-1)^{j+1}\binom{l+1}{j}\, {}_1F_2\left(1+l;\, 1+l, j+1;\, -\frac{b^2s^2}{4}\right) + (-1)^l\, {}_1F_2\left(1+l;\, 2+l,\, 1+l;\, -\frac{b^2s^2}{4}\right)\\
&\quad = (l+1)!\sum_{j=1}^{l+1}\frac{(-1)^{j+1}}{(l+1-j)!}\left(\frac{2}{bs}\right)^j J_j(bs).
\end{aligned} \tag{14}$$

Using the above relations, we can write the potential (10) of the power-law density term $w(\rho') = (\rho')^{2l}$ as

$$\nu^{(2l)}(\rho, z) = -\pi\, \frac{b^{2l+2}}{l+1}\int_0^\infty {}_1F_2\left(1+l;\, 2+l,\, 1;\, -\frac{b^2s^2}{4}\right)J_0(s\rho)e^{-s|z|}\, ds = \pi\, b^{2l+2}l!\sum_{j=1}^{l+1}\frac{(-2)^j}{b^j(l+1-j)!}\,\mathcal{I}_{(-j,j,0)}, \tag{15}$$

where we have denoted

$$\mathcal{I}_{(\alpha,\beta,\gamma)} \coloneqq \int_0^\infty s^\alpha J_\beta(sb) J_\gamma(s\rho) e^{-s|z|}\, ds. \tag{16}$$

Conway (2000) studied this kind of "Bessel–Laplace" integral in his Appendix B.[2] We collect the main results here. The lowest of the integrals can be computed directly (see the Appendix of Conway 2001):[3]

$$\mathcal{I}_{(0,0,0)} = \frac{kK(k)}{\pi\sqrt{b\rho}}, \tag{17}$$

$$\mathcal{I}_{(0,1,1)} = \frac{1}{\pi k\sqrt{b\rho}}[(2-k^2)K(k) - 2E(k)], \tag{18}$$

$$\mathcal{I}_{(0,1,0)} = -\frac{k|z|}{2\pi b\sqrt{b\rho}}\left[\frac{b-\rho}{b+\rho}\,\Pi\left(\frac{4b\rho}{(b+\rho)^2}, k\right) + K(k)\right] + \frac{1}{b}H(b-\rho), \tag{19}$$

where

$$k \coloneqq \frac{2\sqrt{b\rho}}{\sqrt{(\rho+b)^2+z^2}} \tag{20}$$

and H is the Heaviside step function. A general $\mathcal{I}_{(\alpha,\beta,\gamma)}$ can be obtained using the recurrence relations[4]

$$\mathcal{I}_{(\alpha,\beta,\gamma)} = \frac{b}{2\beta}[\mathcal{I}_{(\alpha+1,\beta+1,\gamma)} + \mathcal{I}_{(\alpha+1,\beta-1,\gamma)}], \tag{21}$$

$$\mathcal{I}_{(0,\beta,\gamma)} = \frac{2(\gamma+1)|z|}{(\gamma+1-\beta)\rho}\mathcal{I}_{(0,\beta,\gamma+1)} - \frac{2(\gamma+1)b}{(\gamma+1-\beta)\rho}\mathcal{I}_{(0,\beta-1,\gamma+1)} + \frac{\gamma+1+\beta}{\gamma+1-\beta}\mathcal{I}_{(0,\beta,\gamma+2)}, \tag{22}$$

$$\mathcal{I}_{(0,\gamma+1,\gamma)} = \frac{\rho}{b}\mathcal{I}_{(0,\gamma,\gamma-1)} + \frac{\rho}{2\gamma}[\mathcal{I}_{(1,\gamma+1,\gamma+1)} - \mathcal{I}_{(1,\gamma-1,\gamma-1)}], \tag{23}$$

$$\mathcal{I}_{(1,\gamma,\gamma)} = \frac{(2\gamma-1)|z|k^2}{8b\rho(1-k^2)}[k^2\mathcal{I}_{(0,\gamma-1,\gamma-1)} - (2-k^2)\mathcal{I}_{(0,\gamma,\gamma)}], \tag{24}$$

$$\mathcal{I}_{(0,\gamma,\gamma)} = \frac{4(\gamma-1)}{2\gamma-1}\frac{2-k^2}{k^2}\mathcal{I}_{(0,\gamma-1,\gamma-1)} - \frac{2\gamma-3}{2\gamma-1}\mathcal{I}_{(0,\gamma-2,\gamma-2)} \ldots = \frac{1}{\pi\sqrt{b\rho}}\,Q_{\gamma-1/2}\left(\frac{\rho^2+b^2+z^2}{2b\rho}\right) \quad (\gamma > -1/2), \tag{25}$$

where $Q_{\gamma-1/2}$ are Legendre functions of the second kind (toroidal functions).

For our potential formula (15), we first reduce the first index of $\mathcal{I}_{(-j,j,0)}$ to zero using (21) and then also do the same with the remaining indices using (22)–(25) successively. Since $\mathcal{I}_{(0,-1,-1)} = \mathcal{I}_{(0,1,1)}$, one ends up with just a combination of (17)–(19), which means that $\nu^{(2l)}$ is obtained in closed form. However, the procedure grows cumbersome for higher exponents, because the order of the polynomial "coefficients" in front of the resulting elliptic integrals gradually grows. It is thus useful to create, for evaluation of a generic-case potential, a package in some symbolic-manipulation software; we have used Mathematica for that purpose.

Let us illustrate how the result (15) appears in specific cases. For $l = 0$, the density is just constant, which leads to the well-known solution derived by, e.g., Lass & Blitzer (1983):

$$\nu^{(0)}(\rho, z) = 2\pi|z|H(b-\rho) - \frac{4\sqrt{b\rho}}{k}E(k) - \frac{b^2-\rho^2}{\sqrt{b\rho}}kK(k) - \frac{b-\rho}{b+\rho}\frac{z^2k}{\sqrt{b\rho}}\,\Pi\left(\frac{4b\rho}{(b+\rho)^2}, k\right). \tag{26}$$

For $l \geqslant 1$, the potential can be expressed in a similar but generalized form,[5]

$$\nu^{(2l)}(\rho, z) = 2\pi|z|\mathcal{P}_H^{(2l)}H(b-\rho) - \frac{4\sqrt{b\rho}}{k}\mathcal{P}_E^{(2l)}E(k) - \frac{k}{\sqrt{b\rho}}\mathcal{P}_K^{(2l)}K(k) - \frac{b-\rho}{b+\rho}\frac{z^2k}{\sqrt{b\rho}}\mathcal{P}_\Pi^{(2l)}\Pi\left(\frac{4b\rho}{(b+\rho)^2}, k\right), \tag{27}$$

[2] Eason et al. (1955) called them "Lipschitz–Hankel" integrals for products of Bessel functions. They actually represent Laplace transform of products of two Bessel functions—see also Hanson & Puja (1997) and Kausel & Baig (2012) for thorough treatments.

[3] Conway writes $\mathcal{I}_{(0,1,0)}$ in terms of the Heuman lambda function, whereas we use its relation to complete elliptic integral of the third kind (Eason et al. 1955)

$$\Lambda_0\left(\arcsin\frac{z}{\sqrt{(b-\rho)^2+z^2}}, k\right) = \frac{2}{\pi}\frac{|b-\rho|}{b+\rho}\frac{|z|}{\sqrt{(b+\rho)^2+z^2}}\,\Pi\left(\frac{4b\rho}{(b+\rho)^2}, k\right) = \frac{1}{\pi}\frac{|b-\rho|}{b+\rho}\frac{k|z|}{\sqrt{b\rho}}\,\Pi\left(\frac{4b\rho}{(b+\rho)^2}, k\right).$$

[4] Expressions (B27) (B26), (B23), (B12), and (B7) in Appendix B in Conway (2000).

[5] The factor $(b^2-\rho^2)$ is really not present in front of $K(k)$ anymore.

where $\mathcal{P}^{(2l)}$ are polynomials in ρ and z. Generally, $\mathcal{P}^{(2l)}$ are even polynomials of the order $2l$ in the case of $\mathcal{P}^{(2l)}_{H,\Pi,E}$, and of the order $2l+2$ in the case of $\mathcal{P}^{(2l)}_{K}$. For the first few cases, the polynomials read

$$\mathcal{P}^{(2)}_{H,\Pi} = \frac{1}{(1\cdot 3)^1}(3\rho^2 - 2z^2), \tag{28}$$

$$\mathcal{P}^{(2)}_{E} = \frac{1}{(1\cdot 3)^2}(b^2 + 4\rho^2 - 11z^2), \tag{29}$$

$$\mathcal{P}^{(2)}_{K} = \frac{1}{(1\cdot 3)^2}(5b^4 - b^2\rho^2 - 4\rho^4 + 4b^2z^2 + 16\rho^2z^2 + 5z^4), \tag{30}$$

$$\mathcal{P}^{(4)}_{H,\Pi} = \frac{1}{(3\cdot 5)^1}(15\rho^4 - 40\rho^2z^2 + 8z^4), \tag{31}$$

$$\mathcal{P}^{(4)}_{E} = \frac{1}{(3\cdot 5)^2}(9b^4 + 16b^2\rho^2 + 64\rho^4 - 47b^2z^2 - 607\rho^2z^2 + 274z^4), \tag{32}$$

$$\mathcal{P}^{(4)}_{K} = \frac{1}{(3\cdot 5)^2}(81b^6 - b^4\rho^2 - 16b^2\rho^4 - 64\rho^6 + 8b^4z^2 + 192b^2\rho^2z^2 + 768\rho^4z^2 - 107b^2z^4 - 267\rho^2z^4 - 154z^6), \tag{33}$$

$$\mathcal{P}^{(6)}_{H,\Pi} = \frac{1}{(5\cdot 7)^1}(35\rho^6 - 210\rho^4z^2 + 168\rho^2z^4 - 16z^6), \tag{34}$$

$$\mathcal{P}^{(6)}_{E} = \frac{1}{(5\cdot 7)^2}(25b^6 + 36b^4\rho^2 + 64b^2\rho^4 + 256\rho^6 - 107b^4z^2 - 631b^2\rho^2z^2 - 5175\rho^4z^2 + 306b^2z^4 + 8132\rho^2z^4 - 1452z^6), \tag{35}$$

$$\begin{aligned}\mathcal{P}^{(6)}_{K} = \frac{1}{(5\cdot 7)^2}(&325b^8 - b^6\rho^2 - 4b^4\rho^4 - 64b^2\rho^6 - 256\rho^8 + 12b^6z^2 + 80b^4\rho^2z^2 + 1536b^2\rho^4z^2 + 6144\rho^6z^2 - 59b^4z^4\\ &- 2819b^2\rho^2z^4 - 10307\rho^4z^4 + 586b^2z^6 - 800\rho^2z^6 + 892z^8).\end{aligned} \tag{36}$$

Although the expressions show some clear combinatorial-type patterns, we have not been able to arrange them completely in a simple closed formula, so it is better to keep the expanded form.

We may also add that, in the equatorial plane ($z=0$), the exponential $e^{-s|z|}$ reduces to unity and integral (16) can be expressed in terms of a hypergeometric function as

$$\int_0^\infty s^\alpha J_\beta(sb)J_\gamma(s\rho)ds = \frac{2^\alpha}{\gamma!}\,\frac{\rho^\gamma}{b^{\alpha+\gamma+1}}\,\frac{\Gamma\left(\frac{\alpha+\beta+\gamma+1}{2}\right)}{\Gamma\left(\frac{\beta-\alpha-\gamma+1}{2}\right)}\,{}_2F_1\left(\frac{\alpha-\beta+\gamma+1}{2}, \frac{\alpha+\beta+\gamma+1}{2}; \gamma+1; \frac{\rho^2}{b^2}\right), \tag{37}$$

where it is assumed that $\alpha<1$, $\alpha+\beta+\gamma+1>0$, and $0<\rho<b$. (For $\rho>b>0$, one just swaps $\rho\leftrightarrow b$ in the formula.) We are specifically interested in the case $\alpha=-j$, $\beta=j$, $\gamma=0$ (yielding $\alpha+\beta+\gamma+1=1$) when the expression reduces to

$$\int_0^\infty s^{-j}J_j(sb)J_0(s\rho)ds = \frac{b^{j-1}}{2^j}\,\frac{\Gamma\left(\frac{1}{2}\right)}{\Gamma\left(j+\frac{1}{2}\right)}\,{}_2F_1\left(-j+\frac{1}{2}, \frac{1}{2}; 1; \frac{\rho^2}{b^2}\right) = 2^j b^{j-1}\,\frac{\Gamma(j)}{\Gamma(2j)}\,{}_2F_1\left(-j+\frac{1}{2}, \frac{1}{2}; 1; \frac{\rho^2}{b^2}\right). \tag{38}$$

The potential due to the density terms given by *negative* powers of ρ' can be obtained by inversion (6). Under the inversion, our $(\rho')^{2l}$ density and the corresponding potential transform as

$$w(\rho') \equiv (\rho')^{2l} \quad\longrightarrow\quad \frac{b^3}{\rho'^3}\,w(b^2/\rho') = \frac{b^{3+4l}}{\rho'^{3+2l}}, \qquad\qquad \nu^{(2l)}(\rho,z) \quad\longrightarrow\quad \frac{b}{\sqrt{\rho^2+z^2}}\,\nu^{(2l)}\left(\frac{b^2\rho}{\rho^2+z^2}, \frac{b^2z}{\rho^2+z^2}\right), \tag{39}$$

hence the density–potential pair

$$w(\rho') = (\rho')^{-3-2l}, \qquad \nu^{(-3-2l)}_{\rm i}(\rho,z) = \frac{b^{-2-4l}}{\sqrt{\rho^2+z^2}}\,\nu^{(2l)}\left(\frac{b^2\rho}{\rho^2+z^2}, \frac{b^2z}{\rho^2+z^2}\right). \tag{40}$$

More explicitly, the inverted potentials read

$$\begin{aligned}b^{4l}\nu^{(-3-2l)}_{\rm i}(\rho,z) = {}& \frac{2\pi|z|\,\widetilde{\mathcal{P}}^{(2l)}_H}{(\rho^2+z^2)^{3/2}}\,H\left(b - \frac{b^2\rho}{\rho^2+z^2}\right) - \frac{4\sqrt{b\rho}}{bk}\,\frac{\widetilde{\mathcal{P}}^{(2l)}_E E(k)}{\rho^2+z^2} - \frac{k\,\widetilde{\mathcal{P}}^{(2l)}_K K(k)}{b^3\sqrt{b\rho}}\\ &- \frac{\rho^2-b\rho+z^2}{\rho^2+b\rho+z^2}\,\frac{bz^2k\,\widetilde{\mathcal{P}}^{(2l)}_\Pi}{(\rho^2+z^2)^2\sqrt{b\rho}}\,\Pi\left(\frac{4b\rho(\rho^2+z^2)}{(\rho^2+b\rho+z^2)^2}, k\right),\end{aligned} \tag{41}$$

where $\widetilde{\mathcal{P}}^{(2l)}$ denote the respective polynomials $\mathcal{P}^{(2l)}$ "inverted" according to (6); modulus k of the elliptic integrals is invariant under the inversion, so it keeps the same form (20). Note that we distinguish the inverted potentials by "i," as opposed to the density w whose character is apparent. Note also that the potentials do not yet have the correct dimension—rather than being dimensionless,

$\nu^{(2\,l)}$ has the dimension [length]$^{2l+1}$ while $\nu_{\rm i}^{(-3-2l)}$ has the dimension [length]$^{-2l-2}$.

4. Circular Disks with Generic Power-law Densities

Due to the linearity of the Laplace equation, one can now obtain disk solutions with various power-law radial profiles of density $w(\rho')$ by superposition of elementary terms discussed above. Consider a circular thin disk extending from the center to some finite radius $\rho' = b$, with surface density given by an even polynomial in the radial coordinate,

$$w^{(m,2l)}(\rho') = W\left(1 - \frac{\rho'^{2l}}{b^{2l}}\right)^m, \qquad W = \begin{pmatrix} m + \frac{1}{l} \\ m \end{pmatrix} \frac{\mathcal{M}}{\pi b^2}, \tag{42}$$

where l and m are natural numbers and W is a normalization factor ensuring that the disk has the prescribed total mass $\mathcal{M}$. The radial integration in (10) can, for such a density, be performed using binomial expansion (similarly as Conway 2000 did for $l = 1$), to obtain

$$\begin{aligned}
\nu^{(m,2l)}(\rho, z) &= -2\pi W \int_0^\infty \int_0^b \rho' \left(1 - \frac{\rho'^{2l}}{b^{2l}}\right)^m J_0(s\rho') J_0(s\rho) e^{-s|z|}\, d\rho'\, ds \\
&= -2\pi W \sum_{q=0}^{m} \binom{m}{q} \frac{(-1)^q}{b^{2lq}} \int_0^\infty \int_0^b (\rho')^{2lq+1} J_0(s\rho') J_0(s\rho) e^{-s|z|}\, d\rho'\, ds \;\equiv\; W \sum_{q=0}^{m} \binom{m}{q} \frac{(-1)^q}{b^{2lq}}\, \nu^{(2lq)}(\rho, z) \\
&= -\pi W b^2 \sum_{q=0}^{m} \binom{m}{q} \frac{(-1)^q}{1 + lq} \int_0^\infty {}_1F_2\left(1 + lq;\, 2 + lq,\, 1;\, -\frac{b^2 s^2}{4}\right) J_0(s\rho) e^{-s|z|}\, ds \\
&\equiv \pi W b^2 \sum_{q=0}^{m} \binom{m}{q} (-1)^q (lq)! \sum_{j=1}^{lq+1} \frac{(-2)^j}{b^j (lq + 1 - j)!}\, \mathcal{I}_{(-j,j,0)} \\
&= \frac{W}{b^{2lm}} \left[2\pi |z| \mathcal{P}_H^{(m,2l)} H(b - \rho) - \frac{4\sqrt{b\rho}}{k}\, \mathcal{P}_E^{(m,2l)} E(k) - \frac{k}{\sqrt{b\rho}}\, \mathcal{P}_K^{(m,2l)} K(k) - \frac{b - \rho}{b + \rho}\, \frac{z^2 k}{\sqrt{b\rho}}\, \mathcal{P}_\Pi^{(m,2l)} \Pi\left(\frac{4b\rho}{(b + \rho)^2}, k\right) \right],
\end{aligned} \tag{43}$$

where $\mathcal{P}_{H,E,\Pi}^{(m,2l)}$ are polynomials (in ρ and z) of the order $2lm$ while $\mathcal{P}_K^{(m,2l)}$ are polynomials of the order $2lm + 2$. They are simply related to those obtained for the $(\rho')^{2l}$ density terms in (28)–(36),

$$\mathcal{P}_{H,\Pi}^{(1,2)} = b^2 - \mathcal{P}_{H,\Pi}^{(2)}, \qquad \mathcal{P}_E^{(1,2)} = b^2 - \mathcal{P}_E^{(2)}, \qquad \mathcal{P}_K^{(1,2)} = b^2(b^2 - \rho^2) - \mathcal{P}_K^{(2)}, \tag{44}$$

$$\mathcal{P}_{H,\Pi}^{(1,4)} = b^4 - \mathcal{P}_{H,\Pi}^{(4)}, \qquad \mathcal{P}_E^{(1,4)} = b^4 - \mathcal{P}_E^{(4)}, \qquad \mathcal{P}_K^{(1,4)} = b^4(b^2 - \rho^2) - \mathcal{P}_K^{(4)}, \tag{45}$$

$$\mathcal{P}_{H,\Pi}^{(1,6)} = b^6 - \mathcal{P}_{H,\Pi}^{(6)}, \qquad \mathcal{P}_E^{(1,6)} = b^6 - \mathcal{P}_E^{(6)}, \qquad \mathcal{P}_K^{(1,6)} = b^6(b^2 - \rho^2) - \mathcal{P}_K^{(6)}, \tag{46}$$

$$\mathcal{P}_{H,\Pi}^{(2,2)} = b^4 + \mathcal{P}_{H,\Pi}^{(4)} - 2b^2 \mathcal{P}_{H,\Pi}^{(2)}, \qquad \mathcal{P}_E^{(2,2)} = b^4 + \mathcal{P}_E^{(4)} - 2b^2 \mathcal{P}_E^{(2)}, \qquad \mathcal{P}_K^{(2,2)} = b^4(b^2 - \rho^2) + \mathcal{P}_K^{(4)} - 2b^2 \mathcal{P}_K^{(2)}, \tag{47}$$

$$\mathcal{P}_{H,\Pi}^{(3,2)} = b^6 - \mathcal{P}_{H,\Pi}^{(6)} + 3b^2 \mathcal{P}_{H,\Pi}^{(4)} - 3b^4 \mathcal{P}_{H,\Pi}^{(2)}, \tag{48}$$

$$\mathcal{P}_E^{(3,2)} = b^6 - \mathcal{P}_E^{(6)} + 3b^2 \mathcal{P}_E^{(4)} - 3b^4 \mathcal{P}_E^{(2)}, \tag{49}$$

$$\mathcal{P}_K^{(3,2)} = b^6(b^2 - \rho^2) - \mathcal{P}_K^{(6)} + 3b^2 \mathcal{P}_K^{(4)} - 3b^4 \mathcal{P}_K^{(2)}. \tag{50}$$

Actually, from the expression $\nu^{(m,2l)}(\rho, z) = W \sum_{q=0}^{m} \binom{m}{q} \frac{(-1)^q}{b^{2lq}}\, \nu^{(2lq)}(\rho, z)$, we can summarize the above relations as

$$\mathcal{P}_{H,\Pi,E}^{(m,2l)} = b^{2ml} + \sum_{q=1}^{m} (-1)^q \binom{m}{q} b^{2l(m-q)} \mathcal{P}_{H,\Pi,E}^{(2lq)}, \qquad \mathcal{P}_K^{(m,2l)} = b^{2ml}(b^2 - \rho^2) + \sum_{q=1}^{m} (-1)^q \binom{m}{q} b^{2l(m-q)} \mathcal{P}_K^{(2lq)}. \tag{51}$$

4.1. The Case of Annular Disks

Annular circular disks are again obtained by inversion (39). Substituting the inverted density

$$w_{\rm i}^{(m,2l)}(\rho') = \frac{b^3}{\rho'^3}\, w^{(m,2l)}(b^2/\rho') = W\, \frac{b^3}{\rho'^3} \left(1 - \frac{b^{2l}}{\rho'^{2l}}\right)^m$$

with W set at

$$W = \begin{pmatrix} m + \frac{1}{2l} \\ m \end{pmatrix} \frac{\mathcal{M}}{2\pi b^2}$$

in order for the total mass of the disk to come out $\mathcal{M}$ (i.e., in the same manner as in (8)),

$$2\pi\int_b^\infty \rho' w_{\rm i}^{(m,2l)}(\rho')d\rho' = \binom{m+\frac{1}{2l}}{m}\mathcal{M}b\int_b^\infty \frac{1}{\rho'^2}\left(1-\frac{b^{2l}}{\rho'^{2l}}\right)^m d\rho' = \mathcal{M},$$

we obtain the potential

$$\nu_{\rm i}^{(m,2l)}(\rho,z) = -\binom{m+\frac{1}{2l}}{m}\frac{m!\,\mathcal{M}b}{\sqrt{\rho^2+z^2}}\sum_{q=0}^{m}\frac{(lq)!}{(m-q)!\,q!}\sum_{j=1}^{lq+1}\frac{(-1)^{q+j+1}2^{j-1}}{b^j(lq+1-j)!}\,\widetilde{\mathcal{I}}_{(-j,j,0)}, \tag{52}$$

which, for l, $m \geqslant 1$, reads more explicitly

$$\nu_{\rm i}^{(m,2l)}(\rho,z) = \binom{m+\frac{1}{2l}}{m}\frac{\mathcal{M}}{2\pi b^{2ml}}\left[\frac{2\pi b|z|}{(\rho^2+z^2)^{3/2}}\widetilde{\mathcal{P}}_H^{(m,2l)}H\left(b-\frac{b^2\rho}{\rho^2+z^2}\right) - \frac{4\sqrt{b\rho}}{k(\rho^2+z^2)}\widetilde{\mathcal{P}}_E^{(m,2l)}E(k) - \frac{k}{b^2\sqrt{b\rho}}\widetilde{\mathcal{P}}_K^{(m,2l)}K(k)\right.$$
$$\left. - \frac{\rho^2-b\rho+z^2}{\rho^2+b\rho+z^2}\frac{b^2z^2k}{(\rho^2+z^2)^2\sqrt{b\rho}}\widetilde{\mathcal{P}}_\Pi^{(m,2l)}\Pi\left(\frac{4b\rho(\rho^2+z^2)}{(\rho^2+b\rho+z^2)^2},k\right)\right]. \tag{53}$$

We have denoted by $\widetilde{\mathcal{I}}_{(-j,j,0)}$ and $\widetilde{\mathcal{P}}^{(m,2l)}$ the respective integrals $\mathcal{I}_{(-j,j,0)}$ and polynomials $\mathcal{P}^{(m,2l)}$ "inverted" according to (6); modulus k of the elliptic integrals is invariant under the inversion, so it keeps the same form (20). The above potential already is dimensionless, as it should be.

Below, we illustrate that the solution is the same as the one given, in the form of multipole expansion, in Semerák (2004), for even $n(\equiv 2l)$.

4.2. Behavior of the Potential at Significant Locations

On the axis ($\rho = 0$), we have $k = 0$, so all the elliptic integrals reduce to $\pi/2$, and $H(b) = 1$, which yields

$$\nu_{\rm i}^{(m,2l)}(z) = \binom{m+\frac{1}{2l}}{m}\frac{\mathcal{M}}{2b^{2ml}z^2}\left[2b\,\widetilde{\mathcal{P}}_H^{(m,2l)} - \sqrt{b^2+z^2}\,\widetilde{\mathcal{P}}_E^{(m,2l)} - \frac{z^2}{b^2\sqrt{b^2+z^2}}\widetilde{\mathcal{P}}_K^{(m,2l)} - \frac{b^2}{\sqrt{b^2+z^2}}\widetilde{\mathcal{P}}_\Pi^{(m,2l)}\right]. \tag{54}$$

An explicit result is obtained by substituting for $\widetilde{\mathcal{P}}$s, which means computing the respective polynomials $\mathcal{P}^{(m,2l)}(\rho=0)$ and performing their inversion, which for $\rho = 0$ reduces to the change of $z \to b^2/z$. Using computer algebra, one checks that it really equals the formula

$$\nu_{\rm i}^{(m,n)}(z) = -\binom{m+\frac{1}{n}}{m}\frac{\mathcal{M}}{\sqrt{b^2+z^2}}\sum_{q=0}^{m}\frac{(-1)^q}{qn+2}\binom{m}{q}\,{}_2F_1\left(\frac{1}{2},1;2+\frac{qn}{2};\frac{1}{1+b^2/z^2}\right) \tag{55}$$

given by Semerák (2004). Especially at the very center, ($\rho = 0$, $z = 0$), the potential amounts to

$$\nu_{\rm i}^{(m,n)}(0,0) = -\frac{\mathcal{M}}{b}\frac{\Gamma(m+1+1/n)\Gamma(2/n)}{\Gamma(m+1+2/n)\Gamma(1/n)}.$$

This increases with m, whereas it decreases with n.

In the plane of the disk ($z = 0$), we were only able in Semerák (2004) to give the potential as an infinite series at $\rho > b$ (i.e., "within" the disk), while in the empty region in the disk center, we wrote

$$\nu_{\rm i}^{(m,n)}(\rho<b) = -\binom{m+\frac{1}{n}}{m}\frac{\mathcal{M}}{b}\sum_{q=0}^{m}\frac{(-1)^q}{qn+2}\binom{m}{q}\,{}_3F_2\left(\frac{1}{2},\frac{1}{2},1+\frac{qn}{2};1,2+\frac{qn}{2};\frac{\rho^2}{b^2}\right),$$

where ${}_3F_2$ is the generalized hypergeometric function. Now we newly obtain, from (53), the equatorial expression

$$\nu_{\rm i}^{(m,2l)}(\rho) = -\binom{m+\frac{1}{2l}}{m}\frac{\mathcal{M}}{\pi b^{2ml}}\left[\frac{\rho+b}{\rho^2}\widetilde{\mathcal{P}}_E^{(m,2l)}E(k) + \frac{\widetilde{\mathcal{P}}_K^{(m,2l)}K(k)}{b^2(\rho+b)}\right]$$

valid both above and below the disk rim. At the very rim, $\rho = b$, both formulae simplify in an obvious manner. In particular, the first one then involves the unity-argument ${}_3F_2$ function, ${}_3F_2\left(\frac{1}{2},\frac{1}{2},1+\frac{qn}{2};1,2+\frac{qn}{2};1\right)$, which is commonly discussed in the special-function literature. It may be worth noting that, in the even-n case, $n = 2l$, it can be expressed in the closed form (called Ramanujan's

formula)

$$ {}_3F_2\left(\frac{1}{2},\,\frac{1}{2},\,1+ql;\,1,\,2+ql;\,1\right)=\frac{4}{\pi}\,\frac{1+ql}{(1+2ql)^2}\,\frac{16^{ql}}{\binom{2ql}{ql}^2}\sum_{j=0}^{ql}\frac{\binom{2j}{j}^2}{16^j}. $$

In the second, elliptic-integral formula, one has (at the disk rim) $k=1$, which is the singularity of $K(k)$, but since the respective polynomial $\widetilde{\mathcal{P}}_K^{(m,2l)}$ always contains the factor $(\rho^2-b^2)^2$ in the equatorial plane, the K-term is actually eliminated at the rim and one is left there with

$$ \nu_{\rm i}^{(m,2l)}(\rho=b,\,z=0)=-\binom{m+\frac{1}{2l}}{m}\frac{2\mathcal{M}}{\pi b^{2ml+1}}\,\widetilde{\mathcal{P}}_E^{(m,2l)}. $$

Several first values read, at the rim ($\rho=b$, $z=0$),

$$ \nu_{\rm i}^{(1,2)}=-\frac{4}{3}\,\frac{\mathcal{M}}{\pi b},\quad \nu_{\rm i}^{(2,2)}=-\frac{16}{15}\,\frac{\mathcal{M}}{\pi b},\quad \nu_{\rm i}^{(3,2)}=-\frac{32}{35}\,\frac{\mathcal{M}}{\pi b},\quad \nu_{\rm i}^{(1,4)}=-\frac{68}{45}\,\frac{\mathcal{M}}{\pi b},\quad \nu_{\rm i}^{(1,6)}=-\frac{844}{525}\,\frac{\mathcal{M}}{\pi b}. $$

At radial infinity, the potential falls off as $-\mathcal{M}/\sqrt{\rho^2+z^2}$, which just confirms the meaning of $\mathcal{M}$.

5. Numerical Check of the Closed-form Formulae against Series Expansion

A closed-form solution has clear advantages over the series expansion, the more that the Legendre-type series do not tend to converge safely. It is natural to compare the two solutions now, in order to support the reliability of both.

In Tables 1–3, we numerically compare several examples of the annular-disk potential (53) with the solution expressed in term of the multipole expansion in Semerák (2004) (Equations (10) and (11) there). The main message of the tables is that the solutions are really identical. The second observation is that the series expansion converges quite well even at radii close to that of the disk rim, mainly for higher m and lower $2l$, for which the density falls off (or rises) less steeply at the disk edge, making the field more regular.

6. Trouble with Odd Powers of Radius in Density

Up to now, we have been able to employ Conway's method and reach the closed-form solution for even $n(=2l)$ in the density prescription (8). However, the odd-exponent case, $n=2l+1$, is more difficult, as already noticed in Semerák (2004) (the presence of logarithmic terms hindered the standard way of extending the axial result to a generic location). The integration over the source (43) in that case yields

$$ \begin{aligned}\int_0^b \rho'\left(1-\frac{\rho'^{2l+1}}{b^{2l+1}}\right)^m J_0(s\rho')d\rho' &= \sum_{q=0}^{m}\binom{m}{q}\frac{(-1)^q}{b^{(2l+1)q}}\int_0^b \rho'^{(2l+1)q+1}J_0(s\rho')d\rho' \\ &= \sum_{q=0}^{m}\binom{m}{q}\frac{(-1)^q\,b^2}{2+(2l+1)q}\,{}_1F_2\left(1+lq+\frac{q}{2};\,2+lq+\frac{q}{2},\,1;\,-\frac{b^2s^2}{4}\right). \end{aligned} \tag{56}$$

Here, the contiguous relation (12) does not always work, because the difference between the first and the third parameter of the above ${}_1F_2$ is only an integer for an even q, which means that for odd q the counterpart of (14) would generally be an *infinite* sum.

7. Finite Disks with Bump-type Density Profiles

Finally, we derive, in a closed form as well, the potential of a *finite* annular disk. The respective density profile can be composed, within a selected radial range ($\rho_{\rm in}$, $\rho_{\rm out}$), of the constant-density case plus the $l=0,\,1,\,2,\ldots,L$ (with $L\geqslant 1$) sum of the (40) terms. Let us illustrate the recipe on the simplest, $L=1$ case. Consider, for $\rho_{\rm in}\leqslant\rho'\leqslant\rho_{\rm out}$, the density

$$ w(\rho')=-W_0+\frac{W_{-3}}{\rho'^3}-\frac{W_{-5}}{\rho'^5},\qquad \text{with}\quad W_{-3}=W_0\,\frac{\rho_{\rm out}^5-\rho_{\rm in}^5}{\rho_{\rm out}^2-\rho_{\rm in}^2},\quad W_{-5}=W_0\,\rho_{\rm in}^2\rho_{\rm out}^2\,\frac{\rho_{\rm out}^3-\rho_{\rm in}^3}{\rho_{\rm out}^2-\rho_{\rm in}^2}. \tag{57}$$

Table 1
Comparison between the Annular-disk Potential Computed in Closed Form ("Exact" Column) and in Multipole Expansion in the Vicinity of the Disk Rim

$m=1,\ 2l=2$		Number of Summed Terms					
ρ	z	5	10	20	30	50	exact
4.80	−0.10	−0.0817932	−0.0831299	−0.0836179	−0.0837455	−0.0836892	−0.0834522
4.88		−0.0826293	−0.0836648	−0.0839682	−0.0840259	−0.0840193	−0.0839459
4.96		−0.0834771	−0.0842840	−0.0844754	−0.0845019	−0.0845023	−0.0844883
5.04		−0.0843199	−0.0849521	−0.0850746	−0.0850870	−0.0850877	−0.0850859
5.12		−0.0851449	−0.0856429	−0.0857223	−0.0857282	−0.0857285	−0.0857283
5.20		−0.0859424	−0.0863368	−0.0863888	−0.0863916	−0.0863918	−0.0863917
4.80	−0.05	−0.0815217	−0.0829155	−0.0834898	−0.0837177	−0.0840046	−0.0834822
4.88		−0.0824742	−0.0835518	−0.0839048	−0.0840036	−0.0840816	−0.0839843
4.96		−0.0834240	−0.0842621	−0.0844825	−0.0845263	−0.0845487	−0.0845434
5.04		−0.0843561	−0.0850117	−0.0851513	−0.0851712	−0.0851779	−0.0851784
5.12		−0.0852591	−0.0857746	−0.0858644	−0.0858735	−0.0858756	−0.0858758
5.20		−0.0861245	−0.0865321	−0.0865905	−0.0865948	−0.0865955	−0.0865955
4.80	0	−0.0812375	−0.0826507	−0.0832549	−0.0835202	−0.0839615	−0.0834923
4.88		−0.0823142	−0.0834060	−0.0837762	−0.0838902	−0.0840054	−0.0839975
4.96		−0.0833721	−0.0842207	−0.0844512	−0.0845013	−0.0845332	−0.0845639
5.04		−0.0843981	−0.0850615	−0.0852072	−0.0852297	−0.0852390	−0.0852417
5.12		−0.0853826	−0.0859041	−0.0859974	−0.0860077	−0.0860106	−0.0860109
5.20		−0.0863186	−0.0867307	−0.0867912	−0.0867961	−0.0867970	−0.0867970
4.80	0.05	−0.0815217	−0.0829155	−0.0834898	−0.0837177	−0.0840046	−0.0834822
4.88		−0.0824742	−0.0835518	−0.0839048	−0.0840036	−0.0840816	−0.0839843
4.96		−0.0834240	−0.0842621	−0.0844825	−0.0845263	−0.0845487	−0.0845434
5.04		−0.0843561	−0.0850117	−0.0851513	−0.0851712	−0.0851779	−0.0851784
5.12		−0.0852591	−0.0857746	−0.0858644	−0.0858735	−0.0858756	−0.0858758
5.20		−0.0861245	−0.0865321	−0.0865905	−0.0865948	−0.0865955	−0.0865955
4.80	0.10	−0.0817932	−0.0831299	−0.0836179	−0.0837455	−0.0836892	−0.0834522
4.88		−0.0826293	−0.0836648	−0.0839682	−0.0840259	−0.0840193	−0.0839459
4.96		−0.0834771	−0.0842840	−0.0844754	−0.0845019	−0.0845023	−0.0844883
5.04		−0.0843199	−0.0849521	−0.0850746	−0.0850870	−0.0850877	−0.0850859
5.12		−0.0851449	−0.0856429	−0.0857223	−0.0857282	−0.0857285	−0.0857283
5.20		−0.0859424	−0.0863368	−0.0863888	−0.0863916	−0.0863918	−0.0863917

Note. The disk parameters are $z=0$, $b=5\mathcal{M}$, $2l=2$, and $m=1$. Coordinates ρ and z are given in units of $\mathcal{M}$, while the potential values are dimensionless.

Such a combination of powers together yields a fairly reasonable "bump"-type profile. Since the total mass comes out

$$\mathcal{M} \equiv 2\pi \int_{\rho_{\rm in}}^{\rho_{\rm out}} \rho' w(\rho') d\rho' = 2\pi W_0 \int_{\rho_{\rm in}}^{\rho_{\rm out}} \left(-\rho' + \frac{1}{\rho'^2} \frac{\rho_{\rm out}^5 - \rho_{\rm in}^5}{\rho_{\rm out}^2 - \rho_{\rm in}^2} - \frac{\rho_{\rm in}^2 \rho_{\rm out}^2}{\rho'^4} \frac{\rho_{\rm out}^3 - \rho_{\rm in}^3}{\rho_{\rm out}^2 - \rho_{\rm in}^2} \right) d\rho'$$
$$= \pi W_0 \frac{(\rho_{\rm out} - \rho_{\rm in})^3 (4\rho_{\rm in}^2 + 7\rho_{\rm in}\rho_{\rm out} + 4\rho_{\rm out}^2)}{3\,\rho_{\rm in}\rho_{\rm out}(\rho_{\rm in} + \rho_{\rm out})},$$

the absolute factor W_0 should be chosen as

$$W_0 = \frac{3\mathcal{M}\,\rho_{\rm in}\rho_{\rm out}(\rho_{\rm in} + \rho_{\rm out})}{\pi(\rho_{\rm out} - \rho_{\rm in})^3 (4\rho_{\rm in}^2 + 7\rho_{\rm in}\rho_{\rm out} + 4\rho_{\rm out}^2)}.$$

The potential of the disk follows by subtraction

$$\nu(\rho, z; b = \rho_{\rm out}) - \nu(\rho, z; b = \rho_{\rm in}), \qquad \text{with} \quad \nu(\rho, z) = -W_0 \nu^{(0)} + W_{-3} \nu_{\rm i}^{(-3)} - W_{-5} \nu_{\rm i}^{(-5)}, \tag{58}$$

where $\nu^{(0)}$ is given by (26) and $\nu_{\rm i}^{(-3)}$, $\nu_{\rm i}^{(-5)}$ are given by (41) for $l=0$, 1. The density and potential of this type of disk are illustrated in Figure 1.

Higher bump-type disks can be constructed in a similar way. In general, one takes certain $L \geqslant 1$ and $\rho_{\rm out} > \rho_{\rm in} > 0$, considers (within the interval $\rho_{\rm in} \leqslant \rho' \leqslant \rho_{\rm out}$) the density

$$w(\rho') = -W_0 + \sum_{l=0}^{L} (-1)^l \frac{W_{-3-2l}}{(\rho')^{3+2l}},$$

Table 2
The Same Comparison as in Table 1, but for the Disk with $2l = 2$, $m = 2$ (Top Table) and $2l = 2$, $m = 3$ (Bottom Table)

$m = 2$, $2l = 2$		Number of Summed Terms					
ρ	z	5	10	20	30	50	Exact
4.80	−0.10	−0.0681220	−0.0673768	−0.0672671	−0.0672524	−0.0672551	−0.0672715
4.88		−0.0681614	−0.0675781	−0.0675086	−0.0675019	−0.0675021	−0.0675059
4.96		−0.0682612	−0.0678022	−0.0677576	−0.0677545	−0.0677544	−0.0677550
5.04		−0.0684146	−0.0680515	−0.0680225	−0.0680211	−0.0680210	−0.0680211
5.12		−0.0686144	−0.0683259	−0.0683068	−0.0683061	−0.0683061	−0.0683061
5.20		−0.0688538	−0.0686233	−0.0686107	−0.0686103	−0.0686103	−0.0686103
4.80	−0.05	−0.0682020	−0.0674278	−0.0673005	−0.0672748	−0.0672552	−0.0672815
4.88		−0.0682156	−0.0676106	−0.0675308	−0.0675195	−0.0675140	−0.0675172
4.96		−0.0683011	−0.0678258	−0.0677751	−0.0677700	−0.0677684	−0.0677684
5.04		−0.0684493	−0.0680739	−0.0680412	−0.0680389	−0.0680384	−0.0680384
5.12		−0.0686508	−0.0683529	−0.0683315	−0.0683305	−0.0683303	−0.0683303
5.20		−0.0688970	−0.0686594	−0.0686453	−0.0686448	−0.0686448	−0.0686448
4.80	0	−0.0682504	−0.0674663	−0.0673330	−0.0673033	−0.0672737	−0.0672848
4.88		−0.0682413	−0.0676290	−0.0675456	−0.0675327	−0.0675247	−0.0675211
4.96		−0.0683159	−0.0678351	−0.0677822	−0.0677765	−0.0677742	−0.0677730
5.04		−0.0684620	−0.0680825	−0.0680485	−0.0680459	−0.0680452	−0.0680451
5.12		−0.0686684	−0.0683673	−0.0683452	−0.0683439	−0.0683437	−0.0683437
5.20		−0.0689244	−0.0686844	−0.0686698	−0.0686693	−0.0686692	−0.0686692
4.80	0.05	−0.0682020	−0.0674278	−0.0673005	−0.0672748	−0.0672552	−0.0672815
4.88		−0.0682156	−0.0676106	−0.0675308	−0.0675195	−0.0675140	−0.0675172
4.96		−0.0683011	−0.0678258	−0.0677751	−0.0677700	−0.0677684	−0.0677684
5.04		−0.0684493	−0.0680739	−0.0680412	−0.0680389	−0.0680384	−0.0680384
5.12		−0.0686508	−0.0683529	−0.0683315	−0.0683305	−0.0683303	−0.0683303
5.20		−0.0688970	−0.0686594	−0.0686453	−0.0686448	−0.0686448	−0.0686448
4.80	0.10	−0.0681220	−0.0673768	−0.0672671	−0.0672524	−0.0672551	−0.0672715
4.88		−0.0681614	−0.0675781	−0.0675086	−0.0675019	−0.0675021	−0.0675059
4.96		−0.0682612	−0.0678022	−0.0677576	−0.0677545	−0.0677544	−0.0677550
5.04		−0.0684146	−0.0680515	−0.0680225	−0.0680211	−0.0680210	−0.0680211
5.12		−0.0686144	−0.0683259	−0.0683068	−0.0683061	−0.0683061	−0.0683061
5.20		−0.0688538	−0.0686233	−0.0686107	−0.0686103	−0.0686103	−0.0686103

$m = 3$, $2l = 2$		Number of Summed Terms					
ρ	z	5	10	20	30	50	Exact
4.80	−0.10	−0.0569667	−0.0577922	−0.0578323	−0.0578348	−0.0578347	−0.0578333
4.88		−0.0572943	−0.0579470	−0.0579729	−0.0579741	−0.0579741	−0.0579738
4.96		−0.0575848	−0.0581035	−0.0581204	−0.0581209	−0.0581209	−0.0581209
5.04		−0.0578497	−0.0582638	−0.0582749	−0.0582752	−0.0582752	−0.0582752
5.12		−0.0580979	−0.0584299	−0.0584373	−0.0584375	−0.0584375	−0.0584375
5.20		−0.0583363	−0.0586036	−0.0586086	−0.0586086	−0.0586086	−0.0586086
4.80	−0.05	−0.0569329	−0.0577875	−0.0578335	−0.0578378	−0.0578398	−0.0578382
4.88		−0.0572725	−0.0579474	−0.0579767	−0.0579787	−0.0579792	−0.0579791
4.96		−0.0575711	−0.0581066	−0.0581256	−0.0581265	−0.0581267	−0.0581267
5.04		−0.0578418	−0.0582688	−0.0582812	−0.0582816	−0.0582817	−0.0582817
5.12		−0.0580948	−0.0584367	−0.0584449	−0.0584451	−0.0584451	−0.0584451
5.20		−0.0583376	−0.0586125	−0.0586180	−0.0586181	−0.0586181	−0.0586181
4.80	0	−0.0569192	−0.0577836	−0.0578316	−0.0578365	−0.0578395	−0.0578398
4.88		−0.0572647	−0.0579469	−0.0579775	−0.0579797	−0.0579805	−0.0579809
4.96		−0.0575664	−0.0581076	−0.0581273	−0.0581283	−0.0581286	−0.0581286
5.04		−0.0578392	−0.0582705	−0.0582834	−0.0582838	−0.0582839	−0.0582839
5.12		−0.0580941	−0.0584393	−0.0584478	−0.0584480	−0.0584480	−0.0584480
5.20		−0.0583392	−0.0586167	−0.0586224	−0.0586225	−0.0586225	−0.0586225
4.80	0.05	−0.0569329	−0.0577875	−0.0578335	−0.0578378	−0.0578398	−0.0578382
4.88		−0.0572725	−0.0579474	−0.0579767	−0.0579787	−0.0579792	−0.0579791
4.96		−0.0575711	−0.0581066	−0.0581256	−0.0581265	−0.0581267	−0.0581267
5.04		−0.0578418	−0.0582688	−0.0582812	−0.0582816	−0.0582817	−0.0582817
5.12		−0.0580948	−0.0584367	−0.0584449	−0.0584451	−0.0584451	−0.0584451
5.20		−0.0583376	−0.0586125	−0.0586180	−0.0586181	−0.0586181	−0.0586181
4.80	0.10	−0.0569667	−0.0577922	−0.0578323	−0.0578348	−0.0578347	−0.0578333
4.88		−0.0572943	−0.0579470	−0.0579729	−0.0579741	−0.0579741	−0.0579738
4.96		−0.0575848	−0.0581035	−0.0581204	−0.0581209	−0.0581209	−0.0581209
5.04		−0.0578497	−0.0582638	−0.0582749	−0.0582752	−0.0582752	−0.0582752
5.12		−0.0580979	−0.0584299	−0.0584373	−0.0584375	−0.0584375	−0.0584375
5.20		−0.0583363	−0.0586036	−0.0586086	−0.0586086	−0.0586086	−0.0586086

Table 3
The Same Comparison as in Tables 1 and 2, but for the Disk with $2l = 4$, $m = 1$ (Top Table) and $2l = 6$, $m = 1$ (Bottom Table)

$m = 1$, $2l = 4$		Number of Summed Terms					
ρ	z	5	10	20	30	50	Exact
4.80	−0.10	−0.0909074	−0.0936320	−0.0945185	−0.0947409	−0.0946453	−0.0942394
4.88		−0.0922746	−0.0943892	−0.0949413	−0.0950419	−0.0950309	−0.0949059
4.96		−0.0936211	−0.0952718	−0.0956207	−0.0956669	−0.0956675	−0.0956439
5.04		−0.0949235	−0.0962192	−0.0964426	−0.0964643	−0.0964654	−0.0964624
5.12		−0.0961652	−0.0971877	−0.0973326	−0.0973429	−0.0973435	−0.0973431
5.20		−0.0973348	−0.0981457	−0.0982408	−0.0982458	−0.0982461	−0.0982460
4.80	−0.05	−0.0904014	−0.0932407	−0.0942827	−0.0946795	−0.0951708	−0.0942827
4.88		−0.0919799	−0.0941792	−0.0948207	−0.0949929	−0.0951267	−0.0949623
4.96		−0.0935060	−0.0952196	−0.0956208	−0.0956972	−0.0957356	−0.0957267
5.04		−0.0949607	−0.0963035	−0.0965581	−0.0965927	−0.0966042	−0.0966051
5.12		−0.0963312	−0.0973892	−0.0975529	−0.0975689	−0.0975725	−0.0975727
5.20		−0.0976094	−0.0984472	−0.0985539	−0.0985614	−0.0985626	−0.0985627
4.80	0	−0.0898955	−0.0927735	−0.0938696	−0.0943315	−0.0950867	−0.0942974
4.88		−0.0916961	−0.0939239	−0.0945965	−0.0947952	−0.0949925	−0.0949818
4.96		−0.0934096	−0.0951445	−0.0955638	−0.0956512	−0.0957058	−0.0957578
5.04		−0.0950222	−0.0963809	−0.0966463	−0.0966855	−0.0967015	−0.0967061
5.12		−0.0965254	−0.0975953	−0.0977655	−0.0977836	−0.0977884	−0.0977890
5.20		−0.0979147	−0.0987615	−0.0988722	−0.0988806	−0.0988822	−0.0988823
4.80	0.05	−0.0904014	−0.0932407	−0.0942827	−0.0946795	−0.0951708	−0.0942827
4.88		−0.0919799	−0.0941792	−0.0948207	−0.0949929	−0.0951267	−0.0949623
4.96		−0.0935060	−0.0952196	−0.0956208	−0.0956972	−0.0957356	−0.0957267
5.04		−0.0949607	−0.0963035	−0.0965581	−0.0965927	−0.0966042	−0.0966051
5.12		−0.0963312	−0.0973892	−0.0975529	−0.0975689	−0.0975725	−0.0975727
5.20		−0.0976094	−0.0984472	−0.0985539	−0.0985614	−0.0985626	−0.0985627
4.80	0.10	−0.0909074	−0.0936320	−0.0945185	−0.0947409	−0.0946453	−0.0942394
4.88		−0.0922746	−0.0943892	−0.0949413	−0.0950419	−0.0950309	−0.0949059
4.96		−0.0936211	−0.0952718	−0.0956207	−0.0956669	−0.0956675	−0.0956439
5.04		−0.0949235	−0.0962192	−0.0964426	−0.0964643	−0.0964654	−0.0964624
5.12		−0.0961652	−0.0971877	−0.0973326	−0.0973429	−0.0973435	−0.0973431
5.20		−0.0973348	−0.0981457	−0.0982408	−0.0982458	−0.0982461	−0.0982460

$m = 1$, $2l = 6$		Number of Summed Terms					
ρ	z	5	10	20	30	50	Exact
4.80	−0.10	−0.0940721	−0.0990223	−0.1003870	−0.1007140	−0.1005770	−0.0999929
4.88		−0.0961241	−0.0999771	−0.1008290	−0.1009760	−0.1009610	−0.1007820
4.96		−0.0980710	−0.1010870	−0.1016260	−0.1016940	−0.1016950	−0.1016610
5.04		−0.0998925	−0.1022660	−0.1026120	−0.1026440	−0.1026450	−0.1026410
5.12		−0.1015770	−0.1034550	−0.1036790	−0.1036940	−0.1036950	−0.1036950
5.20		−0.1031180	−0.1046110	−0.1047580	−0.1047660	−0.1047660	−0.1047660
4.80	−0.05	−0.0932709	−0.0984244	−0.1000260	−0.1006080	−0.1013160	−0.1000470
4.88		−0.0956494	−0.0996529	−0.1006410	−0.1008940	−0.1010870	−0.1008530
4.96		−0.0978652	−0.1009940	−0.1016130	−0.1017250	−0.1017800	−0.1017680
5.04		−0.0999080	−0.1023660	−0.1027600	−0.1028100	−0.1028270	−0.1028280
5.12		−0.1017740	−0.1037150	−0.1039690	−0.1039920	−0.1039970	−0.1039980
5.20		−0.1034630	−0.1050040	−0.1051690	−0.1051810	−0.1051820	−0.1051820
4.80	0	−0.0925102	−0.0977323	−0.0994168	−0.1000940	−0.1011800	−0.1000650
4.88		−0.0952238	−0.0992782	−0.1003140	−0.1006050	−0.1008890	−0.1008780
4.96		−0.0977140	−0.1008800	−0.1015270	−0.1016550	−0.1017340	−0.1018080
5.04		−0.0999807	−0.1024670	−0.1028770	−0.1029350	−0.1029580	−0.1029640
5.12		−0.1020290	−0.1039910	−0.1042550	−0.1042820	−0.1042890	−0.1042890
5.20		−0.1038650	−0.1054230	−0.1055950	−0.1056070	−0.1056090	−0.1056090
4.80	0.05	−0.0932709	−0.0984244	−0.1000260	−0.1006080	−0.1013160	−0.1000470
4.88		−0.0956494	−0.0996529	−0.1006410	−0.1008940	−0.1010870	−0.1008530
4.96		−0.0978652	−0.1009940	−0.1016130	−0.1017250	−0.1017800	−0.1017680
5.04		−0.0999080	−0.1023660	−0.1027600	−0.1028100	−0.1028270	−0.1028280
5.12		−0.1017740	−0.1037150	−0.1039690	−0.1039920	−0.1039970	−0.1039980
5.20		−0.1034630	−0.1050040	−0.1051690	−0.1051810	−0.1051820	−0.1051820
4.80	0.10	−0.0940721	−0.0990223	−0.1003870	−0.1007140	−0.1005770	−0.0999929
4.88		−0.0961241	−0.0999771	−0.1008290	−0.1009760	−0.1009610	−0.1007820
4.96		−0.0980710	−0.1010870	−0.1016260	−0.1016940	−0.1016950	−0.1016610
5.04		−0.0998925	−0.1022660	−0.1026120	−0.1026440	−0.1026450	−0.1026410
5.12		−0.1015770	−0.1034550	−0.1036790	−0.1036940	−0.1036950	−0.1036950
5.20		−0.1031180	−0.1046110	−0.1047580	−0.1047660	−0.1047660	−0.1047660

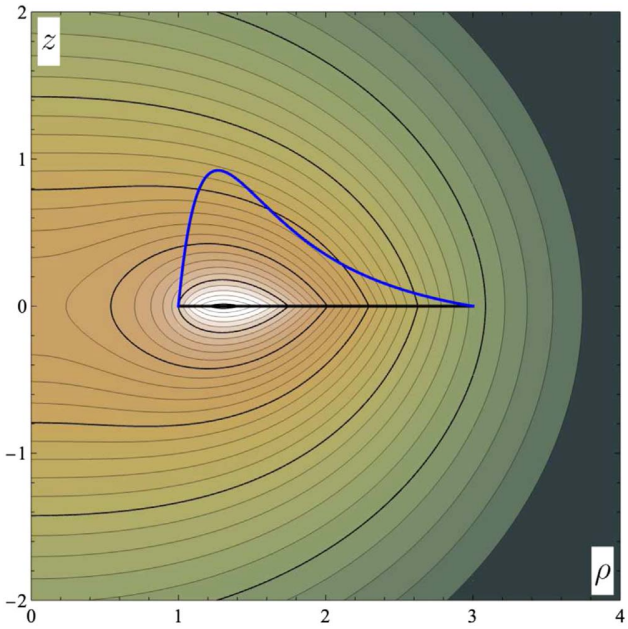

Figure 1. Meridional-plane contour plot of potential (58) of the disk with compact support at ($\rho_{\rm in} = \mathcal{M}$, $\rho_{\rm out} = 3\mathcal{M}$). The disk is indicated by the black line, and the corresponding density profile (57) is inserted into the plot by the thick blue line. The potential value ranges from −0.285 (dark green) to −0.846 (white). The values at the axes are in the units of $\mathcal{M}$.

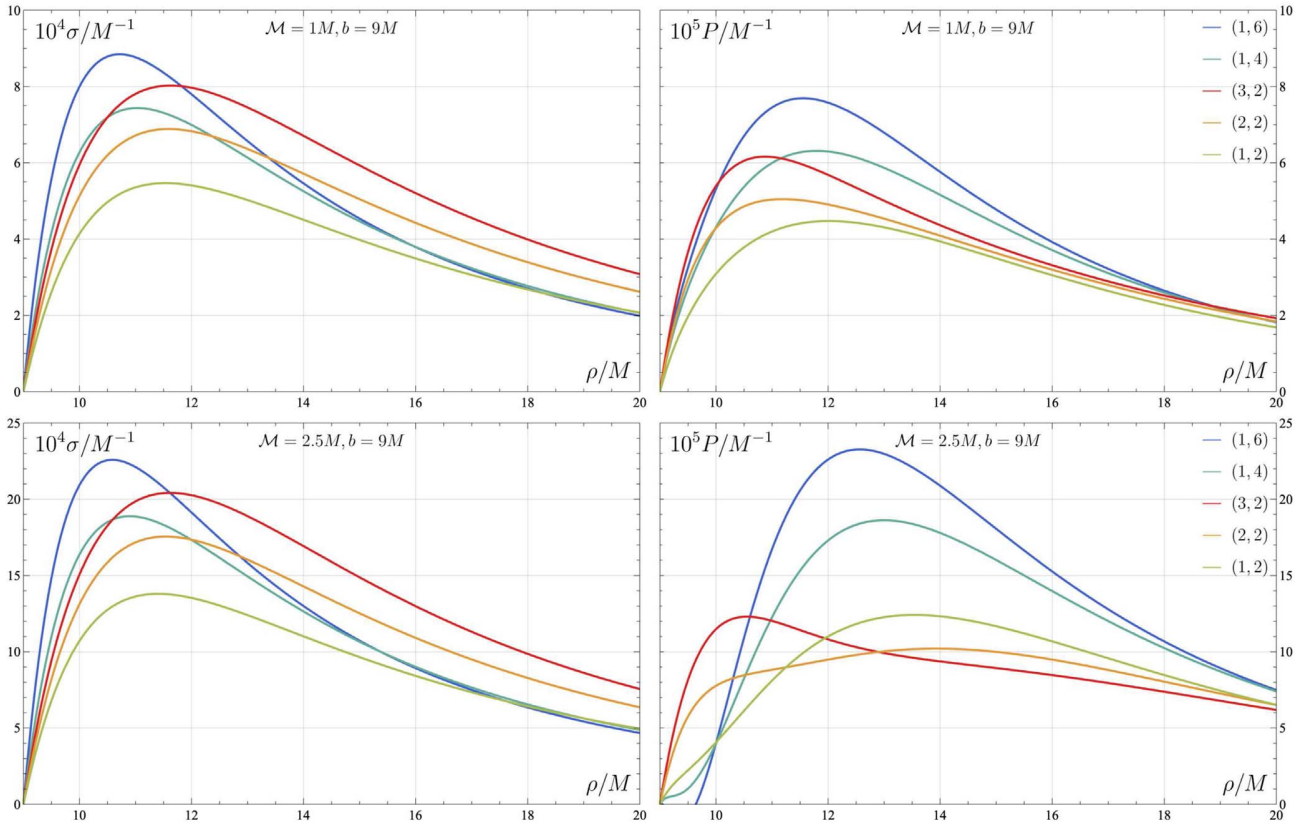

Figure 2. Radial profiles of the surface density σ (left column) and of azimuthal pressure P (right column), as measured by local static observers, are plotted for several disks of the infinite annular type ($\rho \geqslant b$)—i.e., those generating potentials (53)—encircling a Schwarzschild black hole (of mass M). Basic parameters are given in the plots, with different (m, $2l$) cases distinguished by color.

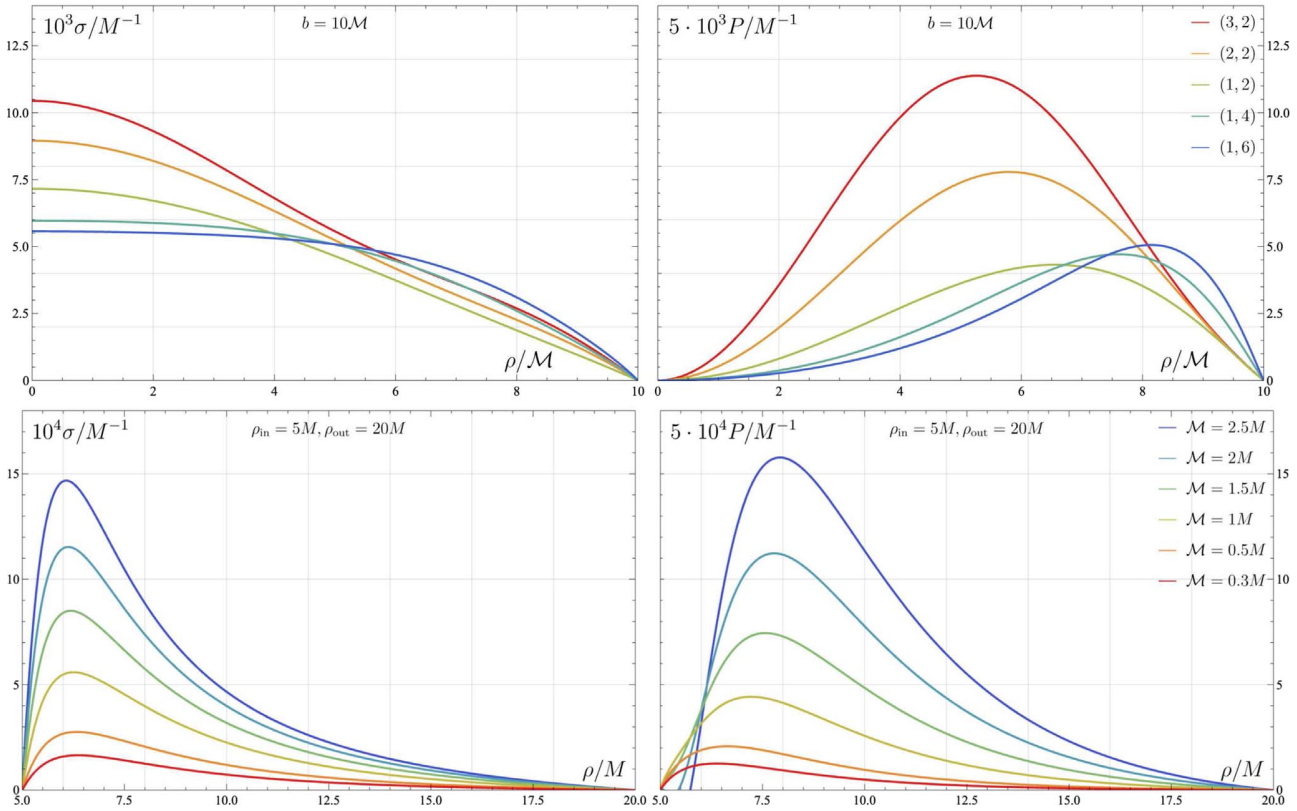

Figure 3. Radial profiles of the surface density σ (left column) and of azimuthal pressure P (right column), as measured by local static observers, are plotted for several solid disks ($\rho \leqslant b$) with potentials (43) (top row), and for several finite annular disks ($\rho_{\rm in} \leqslant \rho \leqslant \rho_{\rm out}$) with potentials (58) with a Schwarzschild black hole at their center (bottom row). Basic parameters are given in the plots, M is the black hole mass, and the different cases (m, $2l$) are distinguished by color.

and demands that

$$w(\rho' = \rho_{\rm in}) = 0, \quad w(\rho' = \rho_{\rm out}) = 0, \qquad \text{while} \quad w(\rho') > 0 \ \text{ for } \ \rho_{\rm in} < \rho' < \rho_{\rm out}.$$

For $L = 1$ (preceding paragraph), there are two parameters (W_{-3} and W_{-5}) and two constraints, so no parameters are left free (besides the overall scaling, as determined by $\mathcal{M}$ through W_0). For $L = 2$, the density contains three parameters (W_{-3}, W_{-5}, and W_{-7}), which again are bound by two constraints, so one of them effectively remains free. In general, $L - 1$ of the W parameters only remain restricted by condition that the density must not have any root *inside* the radial range of the disk.

8. Radial Profiles of Density and of Azimuthal Pressure

Two simple types of physical interpretation of the disk sources involve: (i) a single-component ideal fluid with a certain surface density (σ) and an azimuthal pressure (P), which keeps the orbits at their radius; or (ii) two identical counter-orbiting dust components with proper surface densities $\sigma_+ = \sigma_-$ following circular geodesics with equal but opposite velocities relative to static observers, $v_+ = -v_-$ (see, e.g., González & Espitia 2003). In Figure 2, we show the radial profiles of surface density σ and of azimuthal pressure P,[6]

$$\sigma = \frac{\nu_{,z}(z=0^+)}{2\pi}(1 - \rho\nu_{,\rho}), \qquad P = \frac{\nu_{,z}(z=0^+)}{2\pi}\,\rho\nu_{,\rho},$$

for several annular disks encircling a Schwarzschild black hole. Figure 3 illustrates the same parameters for several solid and several bump-type disks. Some curves are seen to fall below zero around the inner disk edge, which means such orbits (understood as hoops) would have to be in a state of tension in order to stay at their respective radii, i.e., they are attracted outward rather then downward, due to a "too large" mass of the disk at larger radii. Such a circumstance corresponds to when free circular motion is impossible (see the following section).

[6] Quantities defined in this way sum to $w \equiv \sigma + P = \nu_{,z}(z=0^+)/(2\pi)$, and exactly this sum satisfies the Poisson equation $\nabla^2\nu = 4\pi w(\rho)\delta(z)$, so it is the counterpart of Newtonian density.

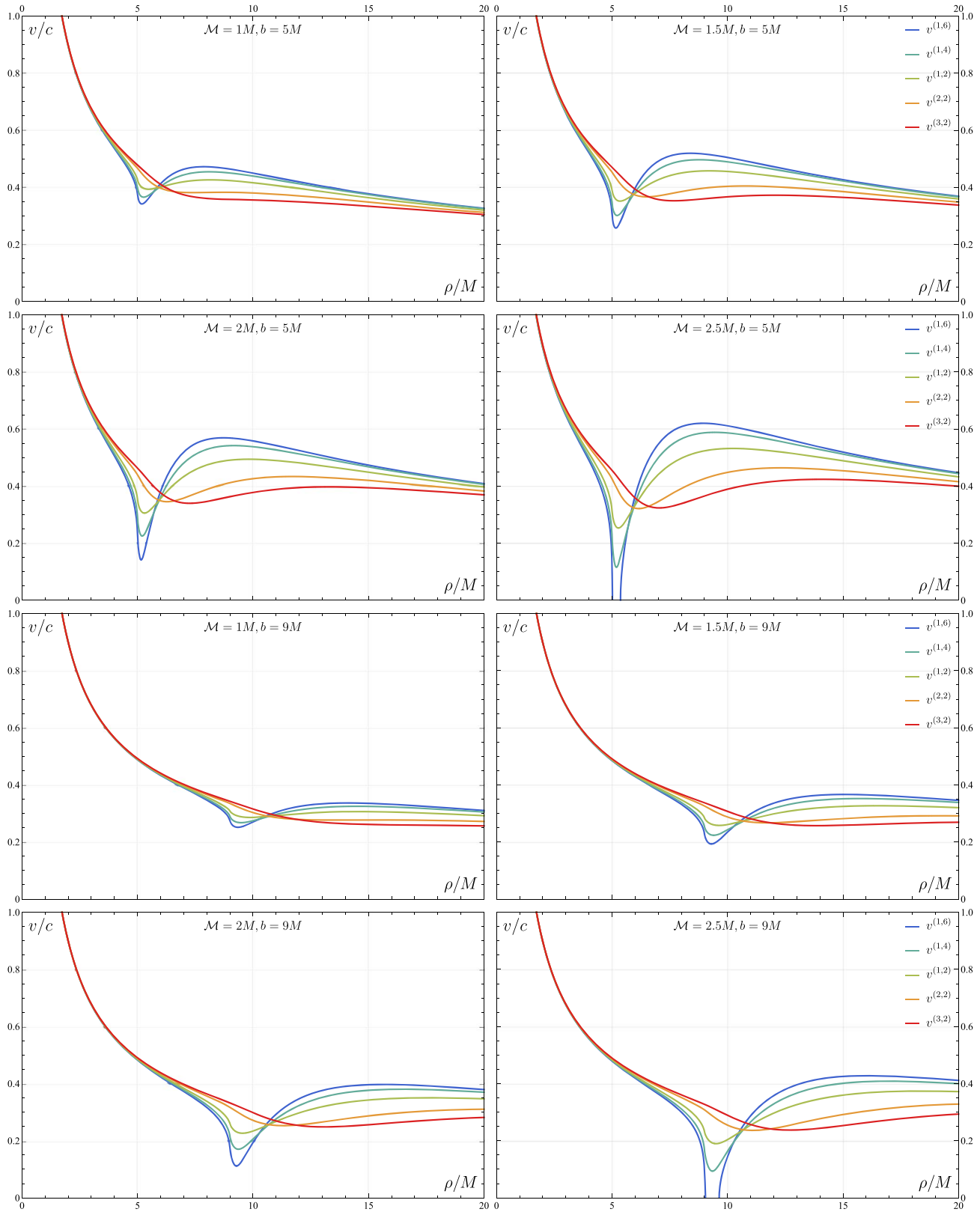

Figure 4. Radial profiles of circular-geodesic speeds as measured by local static observers, $v^{(m,2l)}$, plotted for a Schwarzschild black hole (of mass M) encircled by several disks of the annular type ($\rho \geqslant b$), i.e., those generating potentials (53). Basic parameters are given in the plots.

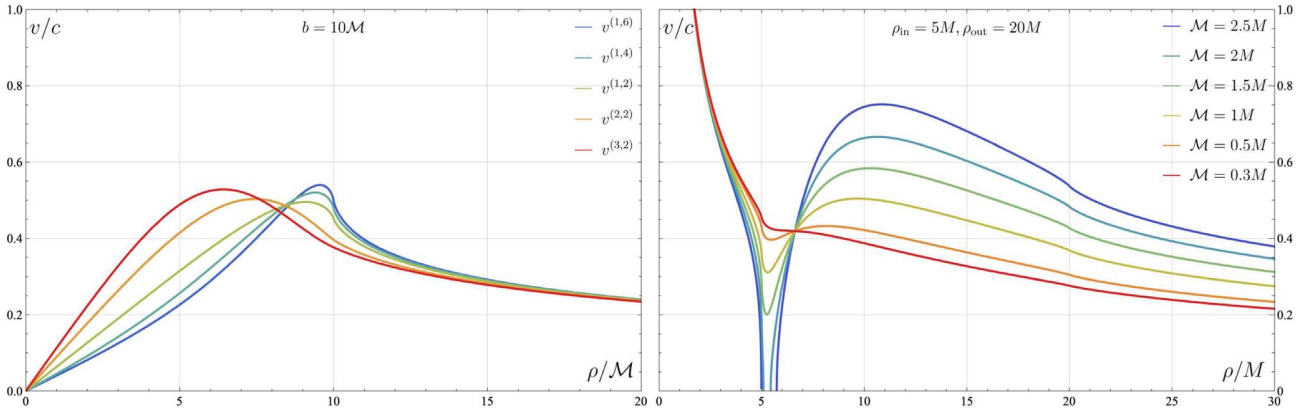

Figure 5. Radial profiles of circular-geodesic speeds relative to local static observers, plotted for several solid disks ($\rho \leqslant b$) with potentials (43) ($v^{(m,2\,l)}$, left), and for several finite annular disks ($\rho_{\rm in} \leqslant \rho \leqslant \rho_{\rm out}$) with potentials (58) with a Schwarzschild black hole at their center (right). Basic parameters are given in the plots, and M is the black hole mass.

9. Circular-velocity Profiles

One of useful illustrations of an axisymmetric-source field possessing a plane with respect to which it is reflection symmetric, at least locally (it is called the equatorial plane), is the radial profile of circular velocity, i.e., of the velocity corresponding to free circular orbits of test particles. In the Weyl-type spacetimes, such a (linear) velocity, measured by a static observer at the given radius, is given by

$$v_+^2 \equiv v_-^2 =: v^2 = \frac{P}{\sigma} = \frac{\rho\nu_{,\rho}}{1 - \rho\nu_{,\rho}}.$$

We show how the rotation profile appears for the above disk sources in Figures 4 (annular disks around a black hole) and 5 (solid disk without a black hole, and finite "bump"-type disk with a black hole). Since the equatorial plane in this case coincides with that of the disks, the profiles tell, at the same time, where it is possible to interpret the disk in terms of two identical counter-orbiting geodesic streams. In the figures, several occasions can be seen where the disk is so heavy that it is not possible to orbit freely below its maximum (even a particle at rest is attracted outward to the disk, despite the opposite effect of the black hole).

10. Concluding Remarks

We have computed in closed form the potential of static thin circular disks with density given by a power law in radius, employing the method suggested by Conway (2000). Starting with the contribution of the elementary density terms $(\rho')^{2l}$ (for solid disks) and $(\rho')^{-3-2l}$ (for annular disks reached by inversion), we wrote down the potential due to a generic static thin circular disk whose density involves even powers of density. The results are expressed in terms of elliptic integrals multiplied by polynomials, which can readily be found using Mathematica or a similar program.[7] All the results are exact solutions of Einstein field equations (belonging to the Weyl class of static and axisymmetric spacetimes). The annular disks resulting from inversion with respect to the rim are infinite (yet with finite mass), but finite disks can easily be obtained as well by suitable superposition of the basic density terms. We performed a numerical check of the results against Legendre-series expansion, which we used to solve the problem in the past (Semerák 2004). We also illustrated the results on the radial profiles of basic physical parameters of the disks.

Finally, let us mention several closely related results from the literature. In astrophysics, disk sources are constantly under study. This is particularly true in galactic dynamics, but also in relativistic astrophysics where accretion disks encircling compact objects are central to the physics of active galactic nuclei and of X-ray binaries. However, in the latter case, it is rather rare that the disk-source gravity is incorporated in an *exact* way. From the time we were interested in the problem in the 2000s, new exact analytical results on thin disks have been obtained by Huré and collaborators, in particular by employing their semi-analytical method of tackling the singularity of the Green function necessarily occurring inside the source (Huré & Pierens 2005)—see, e.g., Huré et al. (2007) for thus computed potentials of power-law thin disks. Schulz (2009) gave exact analytical solutions for the first three disks of what in general relativity is known as the counter-rotating Morgan–Morgan static thin disk family (Morgan & Morgan 1969), which we referred to in Section 2. He also (Schulz 2012) found the exact closed-form potential and field of the Mestel finite disk (it is the one for which the circular velocity is constant). Vogt & Letelier (2009) obtained new thin-disk solutions via special superpositions within the Kuzmin–Toomre disk family. A new family of thin disks was also presented by González et al. (2009), but Gleiser (2012) showed that the properties of these solutions are rather unsatisfactory. More physical results seem to have been obtained recently by Vieira (2020) via the "displace, cut, and reflect" method applied to multi-black-hole solutions (which appear as N collinear rods located on the symmetry axis in the Weyl coordinates).

[7] However, algorithms that we have found in the literature either aim at *numerical* evaluation of the integrals (16), or they involve *spherical* Bessel functions $j_j(x) = \sqrt{\frac{\pi}{2x}}\, J_{j+1/2}(x)$

We are thankful for support from grant GACR 21-11268S of the Czech Science Foundation (D.K., O.S.) and from grant schemes at Charles University, reg. No. CZ.02.2.69/0.0/0.0/19_073/0016935 (P.K.).

ORCID iDs

O. Semerák https://orcid.org/0000-0002-1272-6779

References

Bičák, J., Lynden-Bell, D., & Katz, J. 1993, PhRvD, 47, 4334
Conway, J. T. 2000, MNRAS, 316, 540
Conway, J. T. 2001, ITM, 37, 2977
Eason, G., Noble, B., & Sneddon, I. N. 1955, RSPTA, 247, 529
Gleiser, R. J. 2012, PhRvD, 85, 028501
González, G. A., & Espitia, O. A. 2003, PhRvD, 68, 104028
González, G. A., Gutiérrez-Piñeres, A. C., & Viña-Cervantes, V. M. 2009, PhRvD, 79, 124048
Hanson, M. T., & Puja, I. W. 1997, QApMa, 55, 505
Huré, J.-M., Pelat, D., & Pierens, A. 2007, A&A, 475, 401
Huré, J.-M., & Pierens, A. 2005, ApJ, 624, 289
Kausel, E., & Baig, M. M. I. 2012, QApMa, 70, 77
Lass, H., & Blitzer, L. 1983, CeMec, 30, 225
Lemos, J. P. S., & Letelier, P. S. 1994, PhRvD, 49, 5135
Morgan, T., & Morgan, L. 1969, PhRv, 183, 1097, (Errata: 1969, PhRv, 188, 2544; 1970, PhRvD, 1, 3522)
Schulz, E. 2009, ApJ, 693, 1310, (Erratum: 2018, ApJ, 857, 75)
Schulz, E. 2012, ApJ, 747, 106
Semerák, O. 2003, CQGra, 20, 1613
Semerák, O. 2004, CQGra, 21, 2203
Toomre, A. 1963, ApJ, 138, 385
Vieira, R. S. S. 2020, CQGra, 37, 205013
Vogt, D., & Letelier, P. S. 2009, MNRAS, 396, 1487

The Astrophysical Journal, 941:25 (11pp), 2022 December 10 https://doi.org/10.3847/1538-4357/ac9620

Black Hole Encircled by a Thin Disk: Fully Relativistic Solution*

Petr Kotlařík and David Kofroň
Institute of Theoretical Physics, Faculty of Mathematics and Physics, Charles University, Prague, Czech Republic
Received 2022 August 25; revised 2022 September 22; accepted 2022 September 27; published 2022 December 9

Abstract

We give a full metric describing the gravitational field of a static and axisymmetric thin disk without radial pressure encircling a Schwarzschild black hole. The disk density profiles are astrophysically realistic, stretching from the horizon to radial infinity, yet falling off quickly at both these locations. The metric functions are expressed as finite series of Legendre polynomials. The main advantages of the solution are that (i) the disks have no edges, so their fields are regular everywhere (outside the horizon), and (ii) *all* nontrivial metric functions are provided analytically and in closed forms. We examine and illustrate basic properties of the black hole−disk spacetimes.

Unified Astronomy Thesaurus concepts: Relativistic disks (1388); Black holes (162)

1. Introduction

Black holes are once again in the spotlight of astrophysical interest thanks to the unprecedented improvement of imaging techniques in the past couple of years. The key aspect in imaging a black hole shadow is the presence of accreting matter. Having nonvanishing angular momentum, such matter usually forms an accretion disk inspiraling into the black hole. The usual simplification of this model is neglecting the disk self-gravitation because the real accretion disks are supposed to be much lighter than the central black hole. However, in many situations, this is not necessarily true, and many disk properties, such as stability and positions of significant orbits, are sensible to the gravitational field. Thus, we should include also the disk's own gravity in our considerations.

Nevertheless, the complexity of Einstein's equations makes the treatment in the most general case almost impossible using just analytical methods. We have to simplify the problem at some point. A great source of difficulties is the presence of overall net rotation and the resulting dragging effects. But if the rotation can be neglected or if it is compensated by, e.g., two equal counterorbiting streams, the situation is much simpler. Namely, any static and axially symmetric vacuum spacetime (or any nonempty spacetime where the condition $T^{\rho}_{\rho} + T^{z}_{z} = 0$ for the stress–energy tensor holds) can always be described by a Weyl-type metric

$$\mathrm{d}s^2 = -e^{2\nu}\mathrm{d}t^2 + \rho^2 e^{-2\nu}\mathrm{d}\phi^2 + e^{2\lambda-2\nu}(\mathrm{d}\rho^2 + \mathrm{d}z^2), \qquad (1)$$

where t, ρ, ϕ, and z are Weyl coordinates and functions ν and λ depend solely on ρ and z. In vacuum, the function ν satisfies the three-dimensional Laplace equation (therefore ν is the counterpart of Newtonian gravitational potential), and for λ we have

$$\lambda_{,\rho} = \rho(\nu^2_{,\rho} - \nu^2_{,z}), \qquad \lambda_{,z} = 2\rho\nu_{,\rho}\nu_{,z}. \qquad (2)$$

Just like in electrostatics and Newtonian gravity, in order to find the external gravitational field in general relativity (GR), we have to solve the Laplace (or Poisson) equation. But that is only the (Newtonian) part of the whole story. The field is not fully determined only by the potential—there is also the second metric function λ, which influences the geometry in the meridional (ρ, z) plane. This feature can significantly deviate from the Newtonian picture. Moreover, while the linearity of the Laplace equation means a considerate simplification in obtaining the field generated by more than one individual source (the potentials simply add up), the nonlinear nature of Einstein's equations exhibits itself in the second metric function λ.

The first static superposition of a black hole and a thin disk (inverted solution of Morgan & Morgan 1969) was considered by Lemos & Letelier (1993) and further studied in, e.g., Semerák (2003). Later, Semerák (2004) found a potential of a disk with a general power-law density profile in terms of infinite series and studied its properties when superposed with a black hole. In a recent revision of this topic in Kotlařík et al. (2022), we provided this result in closed form. All these disks are thin and infinite and have an inner rim, where higher derivatives of curvature are singular. In addition, only the Newtonian part (i.e., gravitational potential) of the superposition is given analytically; the second metric function λ, if needed, has to be solved numerically using Equation (2). Here, we provide exact full relativistic solutions describing superposition of a black hole with a disk that extends from the horizon to infinity. The fields are everywhere regular, and both metric functions of the superposition are obtained in closed forms. It may seem inappropriate to consider disks that reach down to the horizon, since the stationary horizons cannot host any matter, and since quasi-stationary accretion disks are assumed to end somewhere about the innermost stable circular orbit. However, (i) our disk densities drop to zero toward the black hole, so there is really no matter at the very horizon, and (ii) the accretion disks around astrophysical black holes indeed continue toward the horizon (at least partially), though their matter is infalling there rather than orbiting in a quasi-circular regime. (Below the last stable orbit, the disk should not be interpreted in terms of stationary circular motion.) Hence, it is in fact more realistic to model the gravitational field of an accreting black hole employing a disk that does have a certain modest density going down to the horizon.

* Dedicated to our teacher, colleague, and friend, Professor Oldřich Semerák, on the occasion of his 60th orbit around the Sun. Oldřich's well-known lectures —famous not only among us (former) students of "math-phys" in Prague— were the first impulse that led us to devote our studies to general relativity.

Before we proceed further, let us also mention other *exact static* black hole–disk superposition, where both nontrivial metric functions have been obtained. González et al. (2009) found a family of infinite disks with an inner edge suitable for the superposition with a black hole. However, Gleiser (2012) showed that the disks have a problematic physical interpretation. A more realistic result was obtained by Vieira (2020) using the "displace, cut, and reflect" method applied to solutions of N black holes (singular rods in Weyl coordinates) arranged in a linear chain on the symmetry axis.

The paper is organized as follows. First, in Section 2, we review a family of thin infinite (in extent)—but of finite mass—disks due to Kuzmin (1956) and Toomre (1963), which were later studied in the context of GR by Bičák et al. (1993). Then, by inversion (Kelvin transformation) of the potential with respect to some Weyl radius, we find the potential describing, again, thin infinite disks of finite mass, but in this case their surface densities are zero at $\rho = 0$. The same potential has been found before, as a special case, by Vogt & Letelier (2009) via superposition within the Kuzmin–Toomre family. Here, we contribute to this result with the second metric function λ and thus obtain full relativistic solutions describing inverted Kuzmin–Toomre disks. Moreover, in Section 3, we also provide exact solutions of λ to all "single rings" found in Vogt & Letelier (2009)—disks similar to the inverted Kuzmin–Toomre ones, but their surface density falls faster. All these disks are suitable for the superposition with a central black hole, thanks to their "annular" character. This is done in Section 4, where, again, both metric functions of the black hole–disk superposition are derived. In the subsequent Sections 5 and 6 we study some properties of the resulting gravitational field, namely the disk's influence on the black hole horizon, radial profiles of densities, pressures, and circular speeds in the equatorial plane. Finally, in Section 7 we make several concluding remarks.

2. Kuzmin–Toomre Disks and Their Inversion

The n-order Kuzmin–Toomre disk, $n \geqslant 0$, is described by the potential (Kuzmin 1956; Toomre 1963; Evans & de Zeeuw 1992; Bičák et al. 1993)

$$\nu_n = -\frac{\mathcal{M}}{(2n-1)!!}\sum_{k=0}^{n}\frac{(2n-k)!}{2^{n-k}(n-k)!}\frac{b^k}{r_b^{k+1}}P_k(|\cos\theta_b|), \tag{3}$$

where we have denoted

$$r_b^2 \coloneqq \rho^2 + (|z|+b)^2, \qquad |\cos\theta_b| \coloneqq \frac{|z|+b}{r_b}, \tag{4}$$

$\mathcal{M}$ stands for the total mass of the disk, and P_k are Legendre polynomials. The corresponding Newtonian density[1] reads

$$w_n = \frac{(2n+1)b^{2n+1}}{2\pi}\frac{\mathcal{M}}{(\rho^2+b^2)^{n+3/2}}. \tag{5}$$

Such a potential can be constructed by considering some mass distribution along the negative half of the axis $z<0$, then cutting the solution along the equatorial plane $z=0$, and reflecting its upper part $z>0$ to the negative part $z<0$ of the axis—the so-called "displace, cut, and reflect" method (Kuzmin 1956; Vieira 2020). The resulting field is then symmetric with respect to the equatorial plane $z=0$ and given by

$$\nu = -\int_{-\infty}^{\infty}\frac{W(b')\,\mathrm{d}b'}{\sqrt{\rho^2+(|z|+b')^2)}}. \tag{6}$$

For the Kuzmin–Toomre solution, the weight function W is a distribution given by some combination of the derivatives of delta distribution (Bičák et al. 1993). Note that in Bičák et al. (1993) the weight function given in Equation (2.23) does not in fact correspond to the Kuzmin–Toomre disks, but rather to the solution obtained by inversion with respect to $\rho = b$, only with different normalization—see the explicit treatment below.

Inverted Kuzmin–Toomre disks are obtained by performing an inversion with respect to[2] b (Kelvin transformation), i.e., the coordinate transformation

$$\rho \longrightarrow \frac{b^2\rho}{\rho^2+z^2}, \qquad z \longrightarrow \frac{b^2 z}{\rho^2+z^2}, \tag{7}$$

and the respective potential and density transformation

$$\begin{aligned}&\nu_n(\rho,z) \longrightarrow \frac{b}{\sqrt{\rho^2+z^2}}\nu_n\left(\frac{b^2\rho}{\rho^2+z^2},\frac{b^2 z}{\rho^2+z^2}\right)\\ &\implies \quad w_n(\rho) \longrightarrow \frac{b^3}{\rho^3}w_n(b^2/\rho).\end{aligned} \tag{8}$$

The inversion of Equation (3), after a suitable rearrangement of the sum, is again separable in r_b and $\cos\theta_b$ and can be easily derived from Equation (3) by (i) replacing $b \to -b$, (ii) multiplying each term by the hypergeometric function ${}_2F_1(1+k, k-n; k-2n; 2)$, and (iii) fixing the normalization, so the total mass of the disk is still $\mathcal{M}$. The inverted potential reads[3]

$$\begin{aligned}\nu_n^{\mathrm{i}} = -\binom{n+1/2}{n}\frac{\mathcal{M}}{(1+2n)!!}\sum_{k=0}^{n}\frac{(2n-k)!}{2^{n-k}(n-k)!}\\ {}_2F_1(1+k,k-n;k-2n;2)\frac{(-b)^k}{r_b^{k+1}}P_k(|\cos\theta_b|),\end{aligned} \tag{9}$$

and the corresponding Newtonian density profile

$$w_n^{\mathrm{i}} = \binom{n+1/2}{n}\frac{\mathcal{M}b}{2\pi}\frac{\rho^{2n}}{(\rho^2+b^2)^{n+3/2}}. \tag{10}$$

Similarly to the original Kuzmin–Toomre disks (Equation (3)), the nth-order potential follows also from the recurrence relation

$$\nu_{n+1}^{\mathrm{i}} = \nu_n^{\mathrm{i}} + \frac{b}{2(n+1)}\frac{\partial}{\partial b}\nu_n^{\mathrm{i}}, \qquad \nu_0^{\mathrm{i}} = -\frac{\mathcal{M}}{r_b}. \tag{11}$$

The Newtonian surface densities are depicted in Figure 1. The shape of the disk potential along the equatorial plane and along the axis is illustrated in Figure 2.

The second metric function λ_n can be also obtained following the same steps as in Bičák et al. (1993). They consist of rewriting the derivatives in Equation (2) in terms of (r_b, θ_b) and integrating from r_b to infinity requiring $\lambda \to 0$ when

[1] ν is the solution of $\Delta\nu(\rho,z) = 4\pi w(\rho)\delta(z)$, where Δ is the standard Laplace operator in cylindrical coordinates and δ is the delta distribution.

[2] Performing the inversion around an arbitrary radius a leads to the same density profile but with different Weyl distance $b \longrightarrow a^2/b$.

[3] Note that $\frac{(2n-k)!}{2^{n-k}(n-k)!}{}_2F_1(1+k,k-n;k-2n;2) = \sum_{j=k}^{n}\binom{j}{k}\frac{(2n-j)!}{2^{n-j}(n-j)!}$.

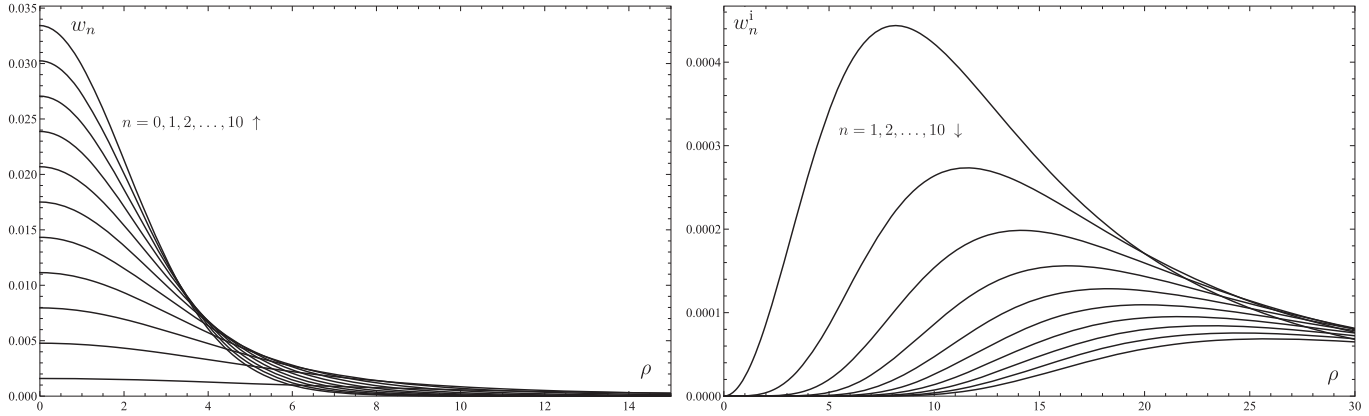

Figure 1. Radial (Newtonian) surface density profiles of the nth-order Kuzmin–Toomre disks (left) and their inversions (right) corresponding to $b = 10\mathcal{M}$ in both plots. The horizontal axes are in units of the disk masses $\mathcal{M}$, and the vertical axes are in units of $\mathcal{M}^{-2}$. In the left panel the maxima lie at $\rho_{\max} = \sqrt{2n/3}\, b$.

$r_b \to \infty$. Then,

$$\lambda_n^{\mathrm{i}} = -\binom{n + 1/2}{n}^2 \frac{\mathcal{M}^2 \sin^2\theta_b}{[(1+2n)!!]^2} \sum_{k,l=0}^{n} \mathcal{B}_{k,l} \frac{(-b)^{k+l}}{r_b^{k+l+2}} \mathcal{P}_{k,l}(\theta_b), \tag{12}$$

where

$$\mathcal{B}_{k,l} = \frac{(2n-k)!(2n-l)!}{2^{2n-k-l}(n-k)!(n-l)!(k+l+2)} \times {}_2F_1(1+k, k-n; k-2n; 2) \times {}_2F_1(1+l, l-n; l-2n; 2), \tag{13}$$

$$\mathcal{P}_{k,l} = (k+1)(l+1)P_k P_l + 2(k+1)|\cos\theta_b| P_k P_l' - \sin^2\theta_b P_k' P_l', \tag{14}$$

$$P_k' = \frac{\mathrm{d}}{\mathrm{d}|\cos\theta_b|} P_k(|\cos\theta_b|). \tag{15}$$

3. Vogt−Letelier Disks

Vogt & Letelier (2009) obtained a broader family of disks by a superposition within the original Kuzmin–Toomre disks. They took

$$\nu^{(m,n)} = W^{(m,n)} \sum_{k=0}^{n} (-1)^k \binom{n}{k} \frac{\nu_{m+k}}{2m+2k+1}, \tag{16}$$

where $W^{(m,n)}$ is a normalization factor dependent only on m, n. Resulting disks are again of infinite extent with the surface density

$$w^{(m,n)} = W^{(m,n)} \frac{\mathcal{M} b^{2m+1}}{2\pi} \frac{\rho^{2n}}{(\rho^2 + b^2)^{m+n+3/2}}, \tag{17}$$

which behaves as $\mathcal{O}(\rho^{-2m-3})$ at infinity; thus, the total mass of each disk is again finite. We fix $W^{(m,n)}$, so the total mass of the disk is still $\mathcal{M}$, more precisely

$$W^{(m,n)} = (2m+1)\binom{m+n+1/2}{n} \Longrightarrow 2\pi \int_0^\infty \rho w^{(m,n)} d\rho = \mathcal{M}\,. \tag{18}$$

For $m = 0$, we get the inverted Kuzmin–Toomre disks, which we discussed in the previous section. Disks of higher m can be obtained using a recurrence relation

$$\frac{(2m+1)(2n+3)}{2m+2n+3} \nu^{(m+1,n)} = \nu^{(m,n)} + \frac{4m(n+1)}{2m+2n+3} \nu^{(m,n+1)} - b\frac{\partial}{\partial b}\nu^{(m,n)}. \tag{19}$$

After substitution of the Kuzmin–Toomre potential into Equation (16), the double sum can be rearranged and performed over the k index. It leads to

$$\nu^{(m,n)} = -(2m+1)\mathcal{M}\binom{m+n+1/2}{n} \sum_{j=0}^{m+n} \mathcal{Q}_j^{(m,n)} \frac{b^j}{r_b^{j+1}} P_j(\cos\theta_b), \tag{20}$$

where we have already substituted $W^{(m,n)}$ from Equation (18) and

$$\mathcal{Q}_j^{(m,n)} = \begin{cases} \sum_{k=0}^{n} (-1)^k \binom{n}{k} \frac{2^{j-k-m}(2m+2k-j)!}{(m+k-j)!(2m+2k+1)!!} = \frac{2^{j-m}(2m-j)!}{(2m+1)!!(m-j)!} \, {}_3F_2\left(\frac{2m-j+1}{2}, \frac{2m-j+2}{2}, -n; \frac{2m+3}{2}, m-j+1; 1\right) & \text{if } j \leqslant m \\ \sum_{k=j}^{m+n} (-1)^{k-m} \binom{n}{k-m} \frac{2^{j-k}(2k-j)!}{(k-j)!(2k+1)!!} = \frac{(-1)^{j-m} j!}{(2j+1)!!} \binom{n}{j-m} \, {}_3F_2\left(\frac{j+1}{2}, \frac{j+2}{2}, j-m-n; \frac{2j+3}{2}, j-m+1; 1\right) & \text{if } j > m, \end{cases}$$

where ${}_3F_2$ is the generalized hypergeometric function.

The second metric function λ is again of the same structure (Equation (12)) as the original or inverted Kuzmin–Toomre

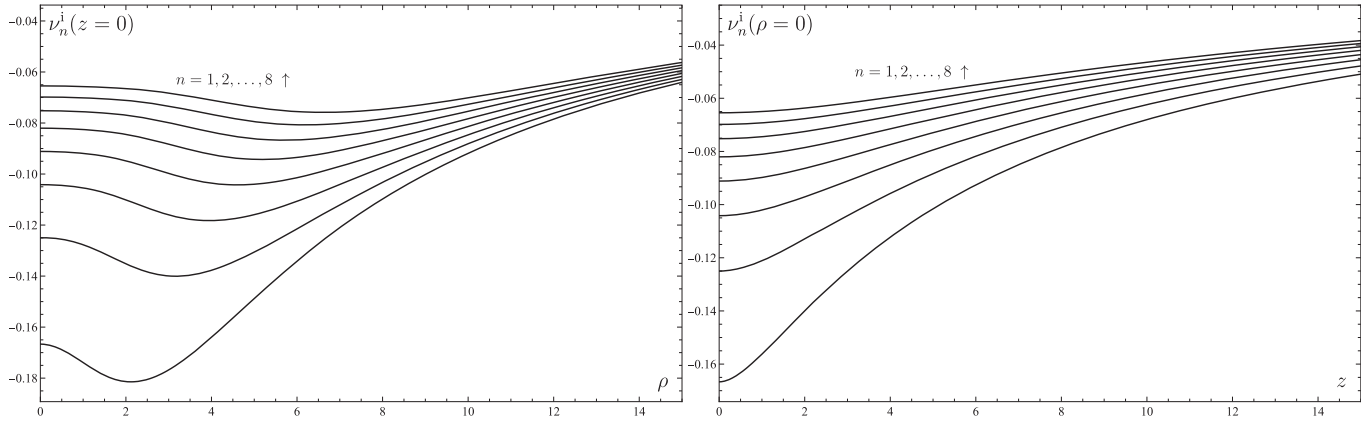

Figure 2. Coordinate plots of the inverted nth-order Kuzmin–Toomre disk potentials in the equatorial plane (left) and on the axis (right) corresponding to $b=3\mathcal{M}$. The horizontal axes are in units of the disk mass $\mathcal{M}$, while the vertical axes are dimensionless.

disks, but now

$$\lambda^{(m,n)}=-(2m+1)^2\binom{m+n+1/2}{n}^2\mathcal{M}^2\sin^2\theta_b \sum_{k,l=0}^{m+n}\mathcal{B}^{(m,n)}_{k,l}\frac{b^{k+l}}{r_b^{k+l+2}}\mathcal{P}_{k,l}(\theta_b), \tag{21}$$

$$\mathcal{B}^{(m,n)}_{k,l}=\frac{\mathcal{Q}^{(m,n)}_l\mathcal{Q}^{(m,n)}_k}{k+l+2}, \tag{22}$$

while the polynomials $\mathcal{P}_{k,l}$ are the same as in Equation (12). A shorter expression can be found by the off-diagonal resummation

$$\lambda^{(m,n)}=-(2m+1)^2\binom{m+n+1/2}{n}^2\mathcal{M}^2 \sum_{v=0}^{2(m+n)}\sum_{u=0}^{v}\frac{(1+u)(1+v-u)}{v+2}\frac{b^v}{r_b^{-2-v}}\mathcal{Q}^{(m,n)}_u\mathcal{Q}^{(m,n)}_{v-u} \times(P_uP_{v-u}-P_{1+u}P_{1+v-u}), \tag{23}$$

where $P_u\equiv P_u(|\cos\theta_b|)$ are the Legendre polynomials and we set $\mathcal{Q}^{(m,n)}_u=0$ for $u>m+n$. For the inverted Kuzmin–Toomre disks (i.e., $m=0$) the coefficients are reduced, $\mathcal{Q}^{(0,n)}_u=\frac{(-1)^u}{(2n+1)!!}\frac{(2n-u)!}{2^{n-u}(n-u)!}{}_2F_1(1+u,u-n;u-2n;2)$.

Newtonian density profiles of several Vogt–Letelier disks are plotted in Figure 3, and the behavior of disks' potentials in the equatorial plane and on the axis is illustrated in Figure 4.

4. Superposition with a Schwarzschild Black Hole

All Vogt–Letelier disks have a clear "annular" character—their densities are exactly zero in the center ($\rho=0$, $z=0$). Hence, it is physically reasonable to make a static superposition of such a disk with a black hole. In Weyl coordinates, the Schwarzschild black hole of the mass M is a singular rod placed on the axis ($\rho=0$, $|z|\leqslant M$) producing gravitational field described by

$$\nu_{\rm Schw}=\frac{1}{2}\ln\frac{d_1+d_2-2M}{d_1+d_2+2M}, \qquad \lambda_{\rm Schw}=\frac{1}{2}\ln\frac{(d_1+d_2)^2-4M^2}{4d_1d_2}, \tag{24}$$

where $d_{1,2}\equiv\sqrt{\rho^2+(|z|\mp M)^2}$. Then, the disk starts at the black hole horizon, but the density drops to zero sufficiently quickly there. Due to the linearity of the Laplace equation, the superposition of gravitational potentials is a simple sum of the individual sources, i.e., $\nu=\nu_{\rm Schw}+\nu_{\rm disk}$. The nonlinearity of the Einstein equations manifests itself in the second metric function λ, which does not superpose that simply. In fact, for two individual sources, a black hole and a disk, we can write $\lambda=\lambda_{\rm Schw}+\lambda_{\rm disk}+\lambda_{\rm int}$, where $\lambda_{\rm Schw}$ and $\lambda_{\rm disk}$ are contributions from the black hole and the disk alone (thus satisfying Equation (2) with just $\nu_{\rm Schw}$ and $\nu_{\rm disk}$, respectively) and $\lambda_{\rm int}$ is an "interaction" term for which

$$\lambda_{{\rm int},\rho}=2\rho(\nu_{{\rm Schw},\rho}\nu_{{\rm disk},\rho}-\nu_{{\rm Schw},z}\nu_{{\rm disk},z}), \tag{25}$$

$$\lambda_{{\rm int},z}=2\rho(\nu_{{\rm Schw},\rho}\nu_{{\rm disk},z}+\nu_{{\rm Schw},z}\nu_{{\rm disk},\rho}). \tag{26}$$

Notice that these conditions are already linear in $\nu_{\rm disk}$, i.e., if the potential of the disk is a sum of two components, then also λ must add in the same way. Hence, $\lambda_{\rm int}$ satisfies the same recurrence relations given by Equation (11) for the inverted Kuzmin–Toomre disks and Equation (19) for Vogt–Letelier disks of higher m, namely

$$\lambda^{(0,n+1)}_{\rm int}=\lambda^{(0,n)}_{\rm int}+\frac{b}{2(n+1)}\frac{\partial}{\partial b}\lambda^{(0,n)}_{\rm int}, \qquad \lambda^{(0,0)}_{\rm int}=-\frac{\mathcal{M}}{r_b}\left(\frac{d_1}{b+M}-\frac{d_2}{b-M}\right)-\frac{2\mathcal{M}M}{b^2-M^2}, \tag{27}$$

$$\frac{(2m+1)(2n+3)}{2m+2n+3}\lambda^{(m+1,n)}_{\rm int}=\lambda^{(m,n)}_{\rm int}+\frac{4m(n+1)}{2m+2n+3}\lambda^{(m,n+1)}_{\rm int}-b\frac{\partial}{\partial b}\lambda^{(m,n)}_{\rm int}. \tag{28}$$

Superposition with a black hole is best represented in Schwarzschild coordinates[4] (r,θ) introduced by

$$\rho=\sqrt{r(r-2M)}\sin\theta, \qquad z=(r-M)\cos\theta. \tag{29}$$

[4] Note that Schwarzschild coordinates (r,θ) are different from those coordinates with subscript b used in disks' potentials.

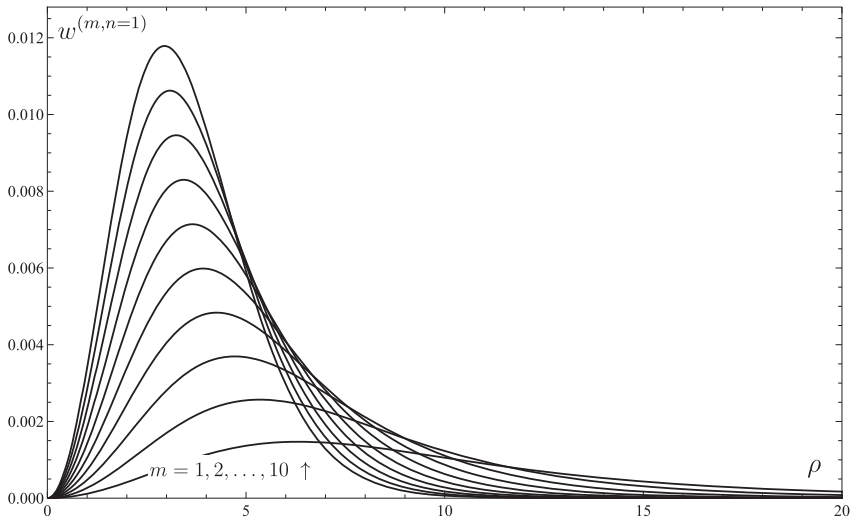

Figure 3. Newtonian surface densities of Vogt–Letelier disks for $n = 1$ and $b = 10\mathcal{M}$. Maxima lie at $\rho_{\max} = 2b\sqrt{\frac{n}{m+3/2}}$. The horizontal axis is in units of $\mathcal{M}$, while the vertical axis is in units of $\mathcal{M}^{-2}$.

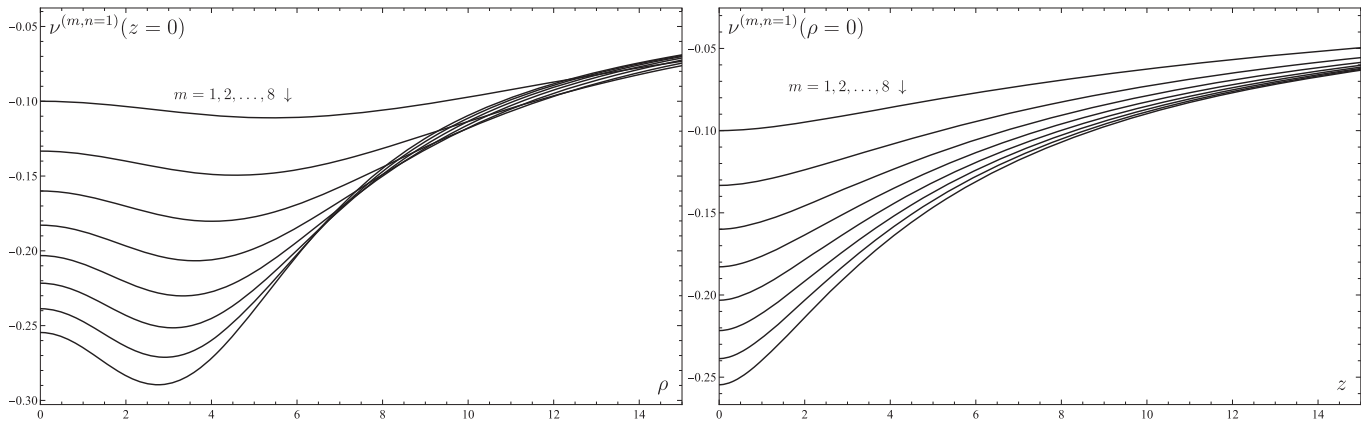

Figure 4. Coordinate plots of the Vogt–Letelier disks' potential ($n = 1$) in the equatorial plane (left) and on the axis (right). In both panels, $b = 10\mathcal{M}$, the horizontal axes are in units of $\mathcal{M}$, while the vertical axes are dimensionless.

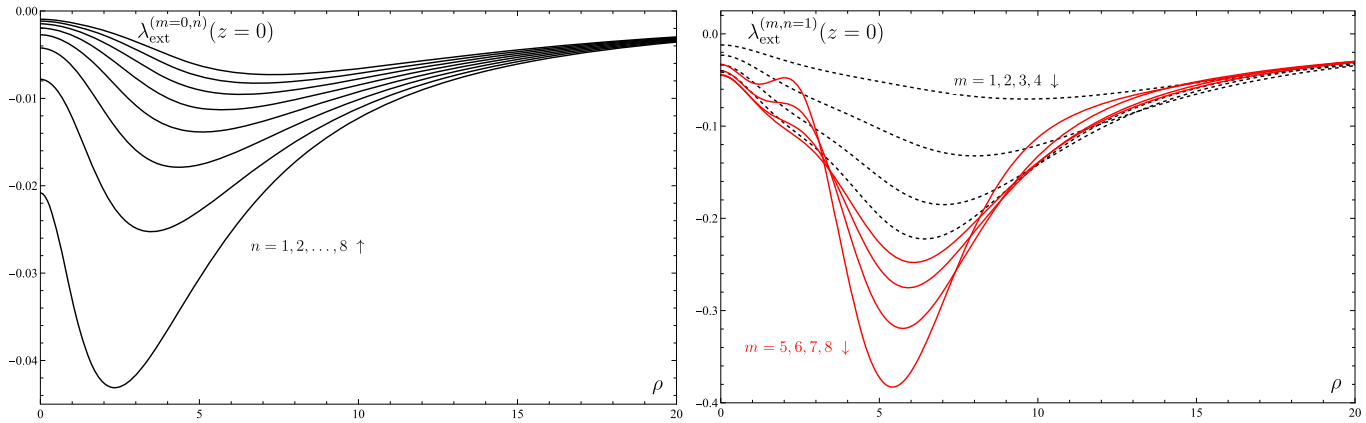

Figure 5. Equatorial plots (in Weyl radius) of $\lambda_{\text{ext}} = \lambda - \lambda_{\text{Schw}}$ of the superposition of a black hole and a disk (inverted Kuzmin–Toomre disks in the left panel; Vogt–Letelier disks in the right panel). Parameters of the disks are $\mathcal{M} = M$, $b = 3M$ in the left panel and $\mathcal{M} = 3.8M$, $b = 10M$ in the right panel. The horizontal axes are in units of M, while the vertical axes are dimensionless. In the right panel, the dashed black lines correspond to $m = 1, 2, 3, 4$, while the solid red lines correspond to $m = 5, 6, 7, 8$. The (color) line differentiation is chosen only for the sake of clarity.

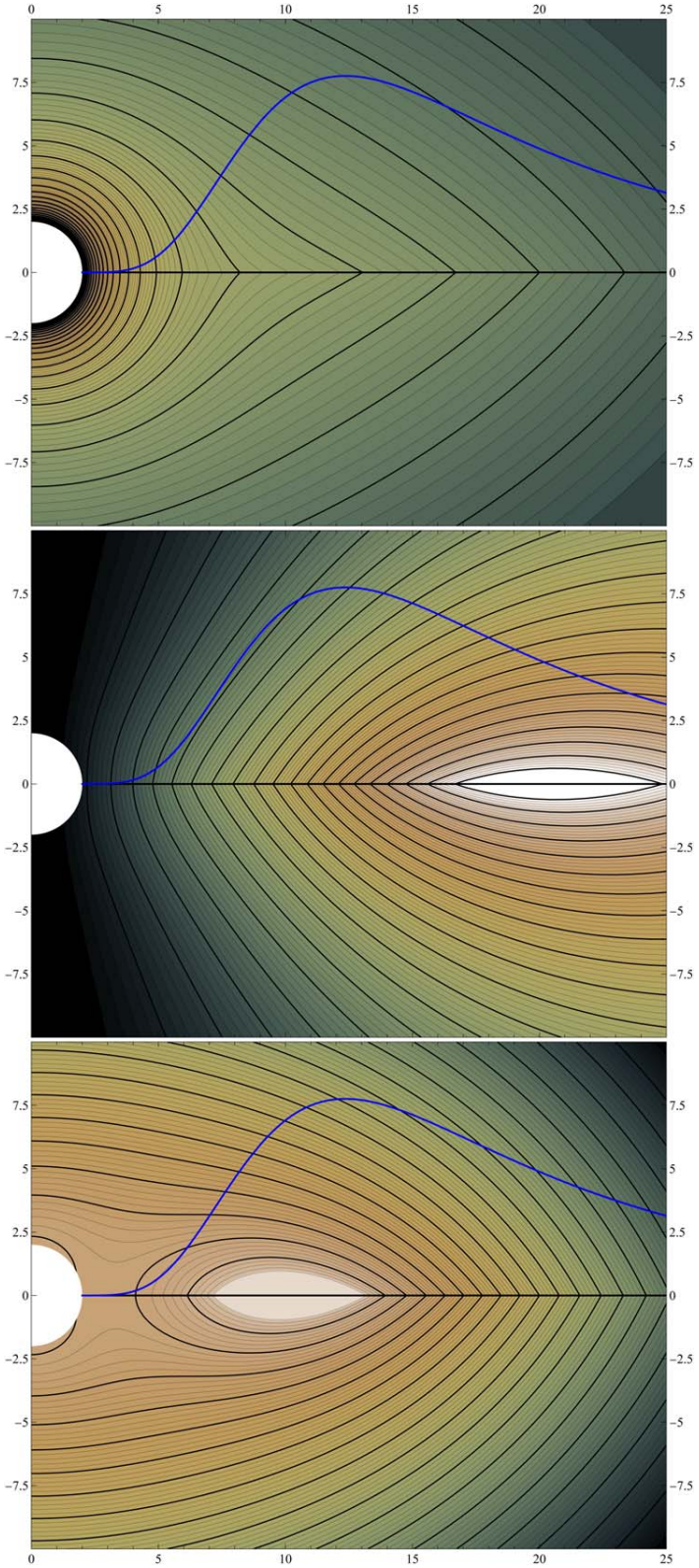

Figure 6. Meridional plane ($\phi = \text{const}$) contour plots of the superposition of the black hole and the inverted third-order Kuzmin–Toomre disk. Namely, the gravitational potential $\nu = \nu_{\text{Schw}} + \nu_{\text{disk}}$ (top), the second metric function $\lambda_{\text{ext}} = \lambda - \lambda_{\text{Schw}}$ (middle), and the difference $\lambda_{\text{ext}} - \nu_{\text{disk}}$ (bottom) are shown in Schwarzschild coordinates. The disk lies in the equatorial plane $z = 0$ and is highlighted by a thick black line. The thick blue line shows the Newtonian density profile of the disk; the white circle in the origin shows the black hole. To illustrate how the field of the black hole is distorted by the presence of the disk, rather extreme parameters are chosen in all plots—the mass of the disk $\mathcal{M} = 10M$ and $b = 8M$. Both axes are in units of the black hole mass M.

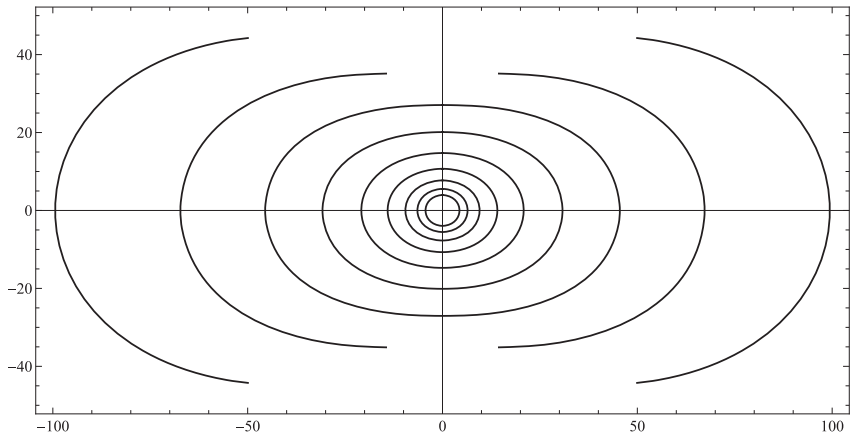

Figure 7. Meridional section ($\phi = \text{const}$) of the isometric embedding of the black hole horizon to Euclidean 3-space. The black hole is distorted owing to the inverted third-order Kuzmin–Toomre disk with $b = 2M$. The masses of the disk range as $\mathcal{M} = 5M$, $7.5M$, $10M$,... $25M$. The horizon becomes more and more flattened with increasing $\mathcal{M}$. For the last two cases, the horizon is not globally embeddable into Euclidean 3-space. Both axes are in units of M.

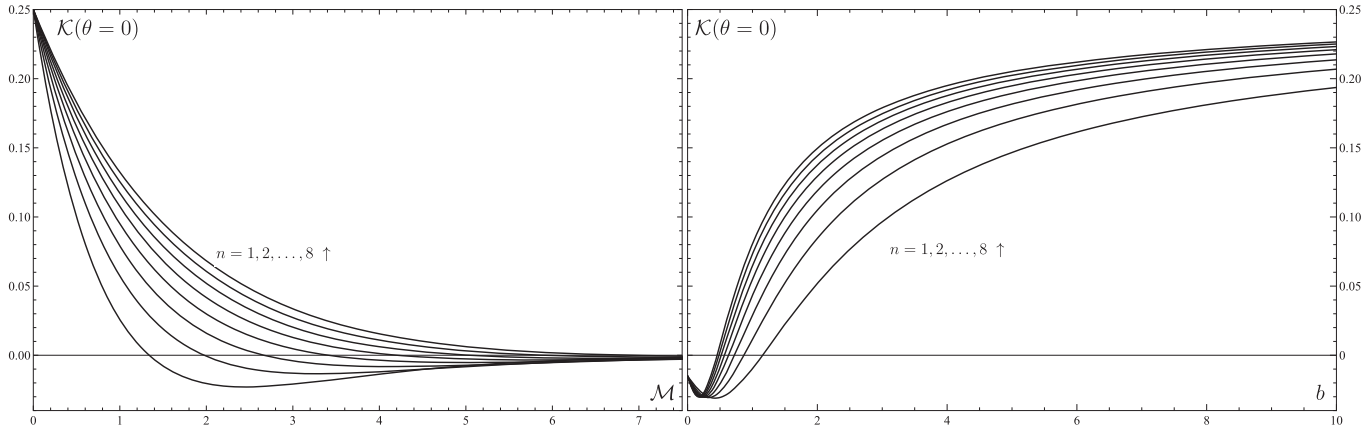

Figure 8. Gauss curvature at the horizon on the axis is plotted against the disk mass $\mathcal{M}$ (left) and b (right). The disks are inverted Kuzmin–Toomre of the third order. In the left panel $b = 0.75M$ is chosen, while in the right panel $\mathcal{M} = 3M$ is chosen. Gauss curvature turns negative if the disk is too massive or the density maximum is sufficiently close to the black hole. Both horizontal axes are in units of M, while the vertical axes are in units of M^{-2}.

In these coordinates the black hole horizon is rendered really spherical (at $r = 2M$), the Schwarzschild contribution becomes

$$\nu_{\text{Schw}} = \frac{1}{2}\ln\left(1 - \frac{2M}{r}\right),$$
$$\lambda_{\text{Schw}} = \frac{1}{2}\ln\frac{r^2 - 2Mr}{r^2 - 2Mr + M^2\sin^2\theta}, \tag{30}$$

and the metric of the superposition reads

$$ds^2 = -\left(1 - \frac{2M}{r}\right)e^{2\nu_{\text{disk}}}dt^2 + e^{2\lambda_{\text{ext}} - 2\nu_{\text{disk}}}\frac{dr^2}{1 - \frac{2M}{r}}$$
$$+ r^2 e^{-2\nu_{\text{disk}}}(e^{2\lambda_{\text{ext}}}d\theta^2 + \sin^2\theta d\phi^2)\,, \tag{31}$$

where $\lambda_{\text{ext}} \equiv \lambda - \lambda_{\text{Schw}} = \lambda_{\text{disk}} + \lambda_{\text{int}}$. In Figure 5, we show radial plots of λ_{ext} in the equatorial plane. The resulting field is illustrated in Figure 6 on several contour plots.

5. Isometric Embedding of the Horizon

Even though the horizon of the black hole always lies at the Schwarzschild radius $r = 2M$ and remains "spherical" in the Schwarzschild coordinates, its intrinsic geometry changes owing to the presence of the surrounding matter distribution. At any given (coordinate) time, the horizon is a 2D surface ($t = \text{const}$, $r = 2M$) with an induced metric

$$\mathrm{d}s^2_{\text{H}} = 4M^2 e^{-2\nu^{\text{H}}_{\text{disk}}(\theta)}[e^{4\nu^{\text{H}}_{\text{disk}}(\theta) - 4\nu^{\text{H}}_{\text{disk}}(\theta=0)}\mathrm{d}\theta^2 + \sin^2\theta\mathrm{d}\phi^2], \tag{32}$$

where $\nu^{\text{H}}_{\text{disk}}$ is the limit of the disk potential at the horizon ($r \to 2M$), and where we have already used solution $\lambda^{\text{H}}(\theta) = 2\nu^{\text{H}}(\theta) - 2\nu^{\text{H}}(\theta = 0)$ valid on the horizon (for any static or even stationary axially symmetric spacetime). For isometric embedding to Euclidean 3-space, we use the method by Smarr (1973). It consists in rewriting the 2-metric in terms of the coordinate $\mu = \cos\theta$, i.e.,

$$\mathrm{d}s^2 = \eta^2[f^{-1}(\mu)\mathrm{d}\mu^2 + f(\mu)\mathrm{d}\phi^2], \tag{33}$$

where

$$\eta = 2Me^{-\nu_{\text{disk}}(\mu=1)},$$
$$f = e^{2\nu_{\text{disk}}(\mu=1) - 2\nu_{\text{disk}}(\mu)}(1 - \mu^2). \tag{34}$$

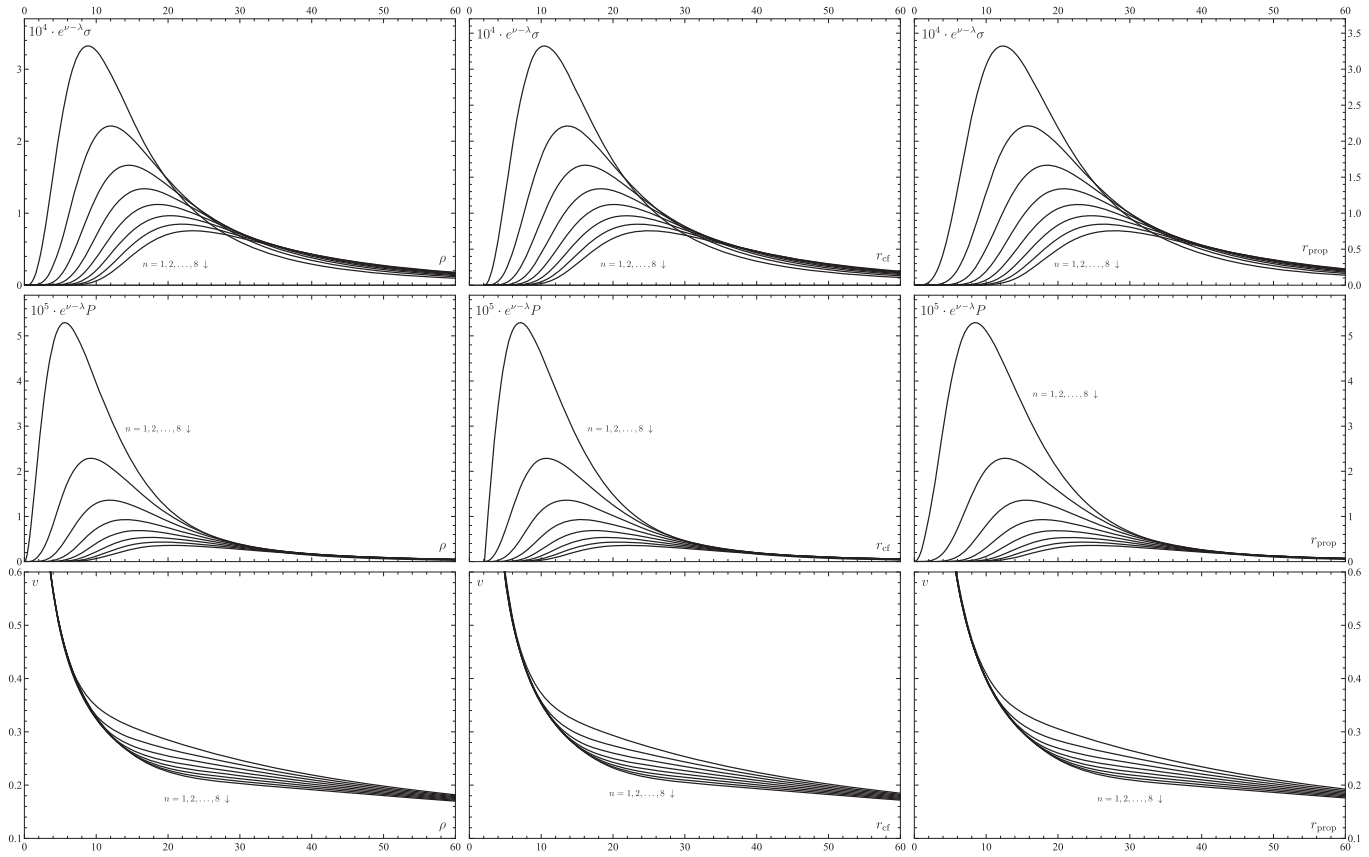

Figure 9. Profiles of disk densities (top row), azimuthal pressures (middle row), and circular velocities (bottom row) in terms of the radial coordinate ρ (left column), circumferential radius r_{cf} (middle column), and proper distance from the horizon r_{prop} (right column). Eight members of the inverted Kuzmin–Toomre family ($n = 1$, 2,...,8) are depicted in each panel. We chose the mass of the disks $\mathcal{M} = M$ and $b = 10M$, where M is the mass of the central black hole. The horizontal axes are in units of M, while the densities and pressures are in units of M^{-1} and the velocities in fractions of the speed of light.

Then, the isometric embedding of the horizon 2-surface in three-dimensional Euclidean space (x, y, z) is given by

$$x = \eta\sqrt{f}\cos\phi, \qquad y = \eta\sqrt{f}\sin\phi,$$
$$z = \eta\int_0^\mu \sqrt{\frac{1}{f}\left(1 - \frac{1}{4}f_{,\mu}^{\,2}\right)}\,\mathrm{d}\mu. \tag{35}$$

See Figure 7 for the numerical results. Another useful quantity for any 2D surface is its Gauss curvature $\mathcal{K} \equiv \frac{^{(2)}R}{2}$, where $^{(2)}R$ is the corresponding 2D scalar curvature. For the metric (32), we have

$$\mathcal{K}(\theta) = \left.\frac{1 + 3\nu_{\mathrm{disk},\theta}\cot\theta + \nu_{\mathrm{disk},\theta\theta} - 2\nu_{\mathrm{disk},\theta}^2}{4M^2 e^{2\nu_{\mathrm{disk}}(\theta) - 4\nu_{\mathrm{disk}}(0)}}\right|_{r=2M}. \tag{36}$$

The Gauss curvature is plotted against $\mathcal{M}$ and b in Figure 8. When the Gauss curvature turns negative, the horizon is not globally embeddable into Euclidean 3-space. Both the embedding and the Gauss curvature show flattened horizon in the direction of the disk.

6. Physical Properties of Disks

Two rather simple physical interpretations of *any* static thin disks are (i) a single-component ideal fluid with a certain surface density σ and an azimuthal pressure P, or (ii) two identical counterorbiting dust streams with proper surface densities $\sigma_+ = \sigma_- \equiv \frac{\sigma}{2}$ following circular geodesics. Both characteristics follow from the discontinuities of normal derivatives of the field over the equatorial plane

$$\sigma + P = \frac{\nu_{,z}(z = 0^+)}{2\pi} = w(\rho),$$
$$P = \frac{\lambda_{,z}(z = 0^+)}{4\pi} = \frac{\nu_{,z}(z = 0^+)}{2\pi}\rho\nu_{,\rho} = w(\rho)\rho\nu_{,\rho}, \tag{37}$$

where $w(\rho)$ is the Newtonian density (10), or Equation (17). The second interpretation is possible only when $\sigma, P \geqslant 0$.

6.1. Radial Profiles of Densities and Azimuthal Pressures

Density and pressure (Equation (37)) are not, yet, quantities measured by any physical observer. Actually, an observer at rest with respect to the disk would measure the density $e^{\nu-\lambda}\sigma$ and the pressure $e^{\nu-\lambda}P$ (Bičák et al. 1993). We show radial profiles of $e^{\nu-\lambda}\sigma$ and $e^{\nu-\lambda}P$ of the inverted Kuzmin–Toomre disks in Figures 9 and 10 and of Vogt–Letelier disks ($n = 1$) in Figures 11 and 12. The disk parameters in Figure 12 are rather extreme (especially for higher orders in m, because the mass of the disk is kept constant), but it shows the role of the multiplication factor $e^{\nu-\lambda}$, where also the second metric function λ is present. However, the circular velocities in the disk plane (see the section below) would be superluminal in some regions, so the double-stream interpretation of such disks would not be possible.

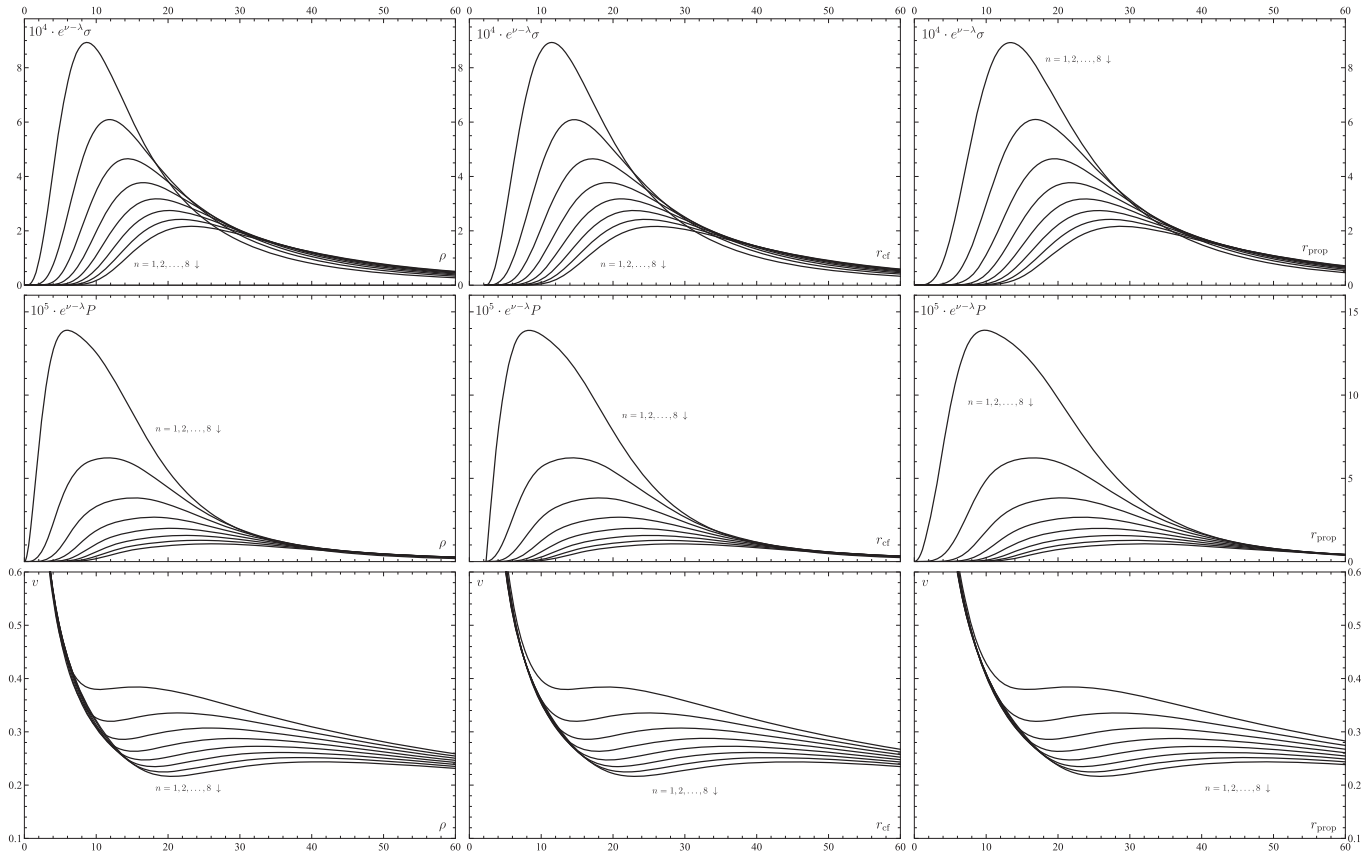

Figure 10. Same profiles as in Figure 9. The disks belong to the inverted Kuzmin–Toomre family; the disk mass is chosen to be $\mathcal{M} = 3M$, and $b = 10M$.

6.2. Circular-velocity Profiles

Another useful quantity is a physical speed v of circular geodesics in the equatorial plane measured locally by a static observer. Such a speed is given by

$$v^2 \equiv \frac{P}{\sigma} = \frac{\rho\nu_{,\rho}}{1 - \rho\nu_{,\rho}}, \tag{38}$$

and its time-like condition $0 \leqslant v^2 < 1$ covers both physical requirements for the disk—the energy conditions and non-negativity of azimuthal pressure. In Figures 9, 10, 11, and 13 we show velocity profiles for the inverted Kuzmin–Toomre disks and Vogt–Letelier disks ($n = 1$).

6.3. Coordinate and Geometrical Measures

Most of the statements about the spacetime are given in coordinate terms. Such statements have to be taken with some caution, although the Weyl (or Schwarzschild) coordinates represent some spacetime features adequately. In particular, we should also check the physical properties of disks by employing invariant measures like circumferential radius or proper radial distance. In our case, the proper circumference corresponding to a certain ρ (computed along constant t, ρ, and z) reads

$$\begin{aligned} &\int_0^{2\pi} \sqrt{g_{\phi\phi}}d\phi = 2\pi\sqrt{g_{\phi\phi}} = 2\pi\rho e^{-\nu} \\ &\Longrightarrow \qquad r_{\rm cf} \coloneqq \rho e^{-\nu}, \end{aligned} \tag{39}$$

where we have denoted the circumferential radius $r_{\rm cf}$ in such a way that the corresponding circumference is given as $2\pi r_{\rm cf}$. The proper radial distance from the black hole horizon to a certain ρ, calculated in the equatorial plane $z = 0$ for constant coordinates (t, ϕ), is given by

$$r_{\rm prop} \coloneqq \int_0^{\rho} \sqrt{g_{\rho\rho}}d\rho = \int_0^{\rho} e^{\lambda-\nu}d\rho. \tag{40}$$

The latter integral has to be solved numerically. All quantities in Figures 9–13 are depicted against the coordinate ρ, as well as both geometrical measures defined above. Note that the proper circumference is not zero at $(\rho = 0, z = 0)$; instead, it is the proper equatorial circumference of the black hole horizon. As illustrated in Section 5, this circumference must grow owing to the presence of the disk. Namely, the corresponding circumferential radius (for any black hole–Vogt–Letelier-disk spacetime) there reads

$$\begin{aligned} r_{\rm cf}(\rho = 0, z = 0) &= \lim_{\rho\to 0} \rho e^{-\nu(\rho, z=0)} \\ &= 2M \exp\left(\frac{(2m+1)\mathcal{M}}{b}\binom{m+n+1/2}{n}\sum_{j=0}^{m+n}\mathcal{Q}_j^{(m,n)}\right). \end{aligned} \tag{41}$$

7. Concluding Remarks

We have found a full metric describing *static* and axially symmetric superposition of a black hole and a thin disk. The disks we considered have finite mass, have no radial pressure, and extend from the black hole horizon to infinity. They also have no edges, so the field is regular everywhere outside the

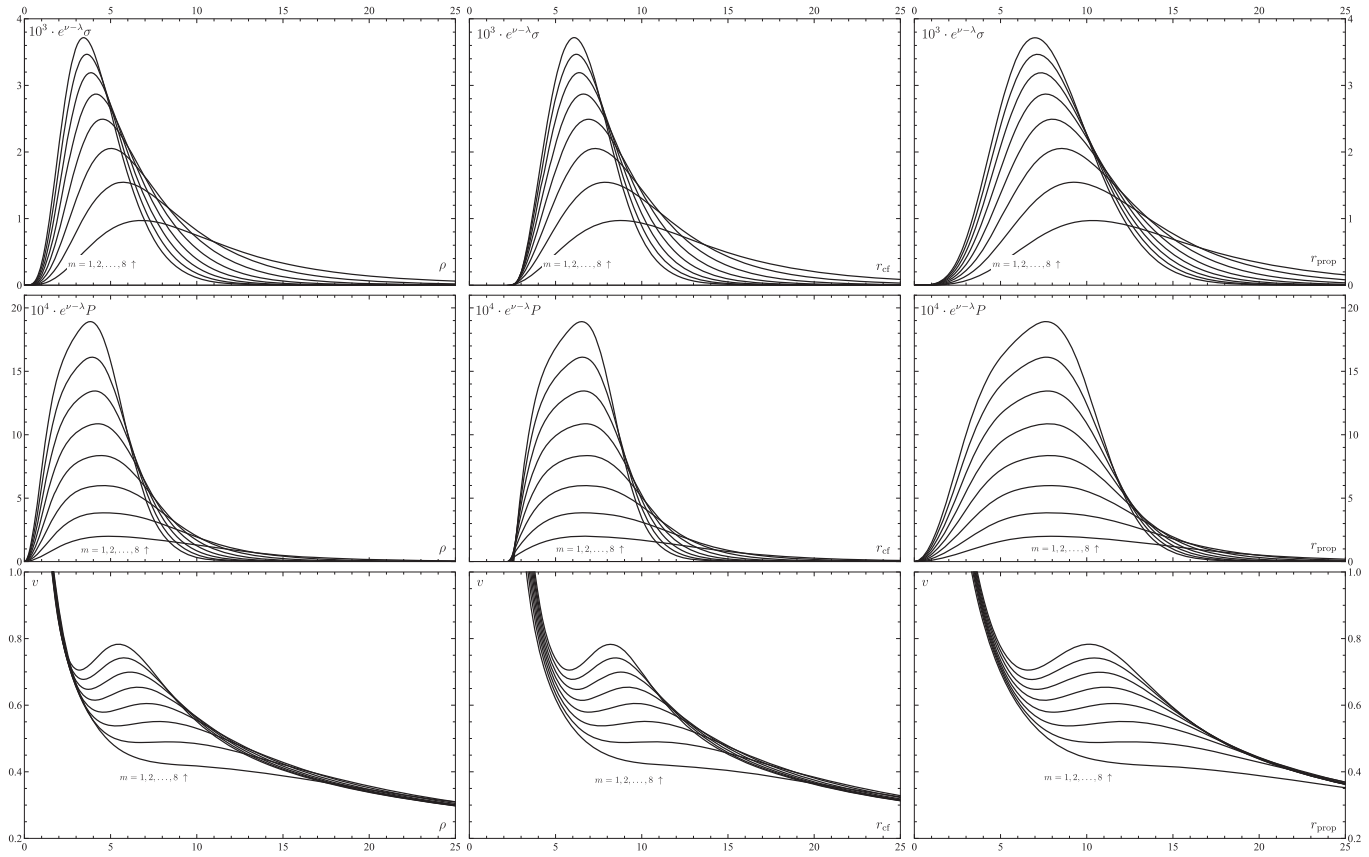

Figure 11. Same profiles as in Figure 9, but in this figure, eight members of Vogt–Letelier disks ($m = 1, 2,...,8$, $n = 1$) are depicted in each panel. The disks are of the same mass and b as in Figure 9, namely $\mathcal{M} = M$ and $b = 10M$.

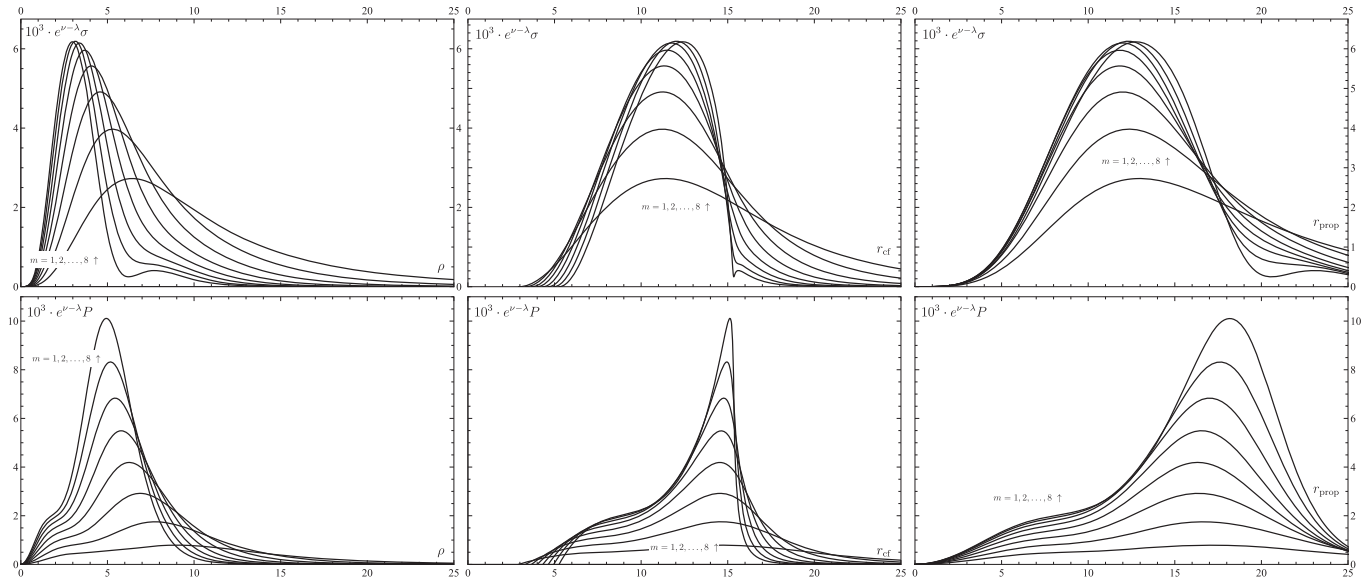

Figure 12. Profiles of disk densities (top row) and azimuthal pressures (bottom row) of the Vogt–Letelier disks ($m = 1, 2,...,8$, $n = 1$) in terms of radial distances, as in Figure 9. The rotational velocities are in separate figures, because rather extreme parameters have been chosen, namely $\mathcal{M} = 3.8M$ and $b = 10M$. Meanwhile, the densities and pressures are well behaving, the rotational velocities would be superluminal in some regions of the disks, and therefore the double-stream interpretation would not be possible.

horizon, yet the disks' surface densities fall off sufficiently quickly at both extremes $\rho = 0$ and $\rho \to \infty$. In particular, we have used disks resulting from the inversion (Kelvin transformation) of Kuzmin–Toomre solutions, as well as "simple" disks due to Vogt & Letelier (2009) (of which the inverted Kuzmin–Toomre disks are a distinct subclass). Both metric functions are given analytically and in closed forms. The gravitational field is illustrated in plots of the metric functions and profiles of densities, azimuthal pressures, and circular velocities. The black hole horizon was found to be distorted

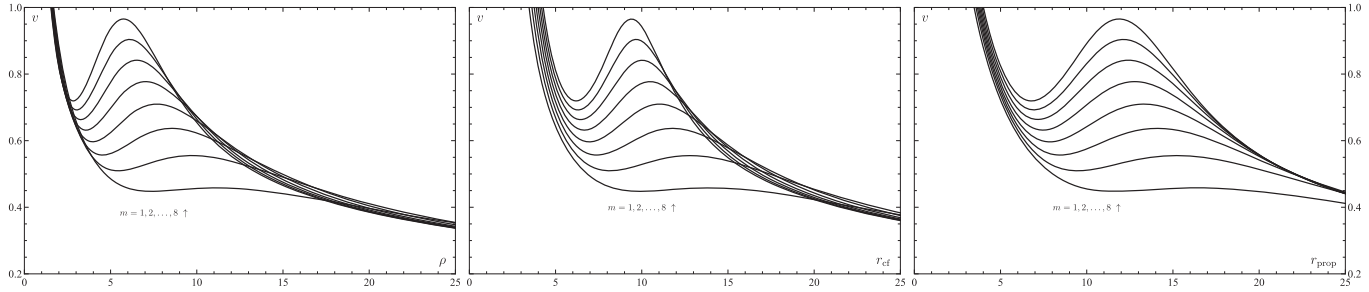

Figure 13. Profiles of circular velocities of the same disks as in Figure 12, just with different disk mass $\mathcal{M} = 1.5M$.

owing to the presence of the disk (flattened in the direction of the disk), which is in agreement with many previous results, e.g., Semerák (2004), Semerák (2003), and Semerák et al. (2001), or, in the stationary case, Kotlařík et al. (2018).

We acknowledge support from grant GACR 21-11268S of the Czech Science Foundation (D.K.) and from grant schemes at Charles University, reg. n. CZ.02.2.69/0.0/0.0/19_073/0016935 (P.K). We are also very grateful to Oldřich Semerák for the initial idea of inverting Kuzmin–Toomre disks and for helpful comments that improved the manuscript.

Software: Wolfram Mathematica 13.

ORCID iDs

Petr Kotlařík https://orcid.org/0000-0002-9228-0788
David Kofroň https://orcid.org/0000-0002-0278-7009

References

Bičák, J., Lynden-Bell, D., & Pichon, C. 1993, MNRAS, 265, 126
Evans, N. W., & de Zeeuw, P. T. 1992, MNRAS, 257, 152
Gleiser, R. J. 2012, PhRvD, 85, 028501
González, G. A., Gutiérrez-Piñeres, A. C., & Viña-Cervantes, V. M. 2009, PhRvD, 79, 124048
Kotlařík, P., Kofroň, D., & Semerák, O. 2022, ApJ, 931, 161
Kotlařík, P., Semerák, O., & Čížek, P. 2018, PhRvD, 97, 084006
Kuzmin, G. G. 1956, Astr. Zh., 33, 27
Lemos, J. P. S., & Letelier, P. S. 1993, CQGra, 10, L75
Morgan, T., & Morgan, L. 1969, PhRv, 183, 1097
Semerák, O. 2003, CQGra, 20, 1613
Semerák, O. 2004, CQGra, 21, 2203
Semerák, O., Zellerin, T., & Žáček, M. 2001, MNRAS, 322, 207
Smarr, L. 1973, PhRvD, 7, 289
Toomre, A. 1963, ApJ, 138, 385
Vieira, R. S. 2020, CQGra, 37, 205013
Vogt, D., & Letelier, P. S. 2009, MNRAS, 396, 1487

Relativistic disks by Appell-ring convolutions

D. Kofroň,* P. Kotlařík,† and O. Semerák‡
Institute of Theoretical Physics,
Faculty of Mathematics and Physics,
Charles University,
V Holešovičkách 2, 180 00 Prague 8, Czech Republic

We present a new method for generating the gravitational field of thin disks within the Weyl class of static and axially symmetric spacetimes. Such a gravitational field is described by two metric functions: one satisfies the Laplace equation and represents the gravitational potential, while the other is determined by line integration. We show how to obtain analytic thin-disk solutions by convolving a certain weight function – an Abel transformation of the physical surface-density profile – with the Appell-ring potential. We thus re-derive several known thin-disk solutions while, in some cases, completing the metric by explicitly computing the second metric function. Additionally, we obtain the total gravitational field of several superpositions of a disk with the Schwarzschild black hole. While the superposition problem is simple (linear) for the potential, it is mostly not such for the second metric function. However, in particular cases, both metric functions of the superposition can be found explicitly. Finally, we discuss a simpler procedure which yields the potentials of power-law-density disks we studied recently.

I. INTRODUCTION

When matter with modest energy has enough angular momentum, it often forms disk-like structures due to the mutual competition between gravitational and centrifugal forces. Such structures occur in many astrophysical phenomena from galaxy scales down to accretion disks around stellar-mass objects or even planets. Disks are crucial in high-energy processes which drive active galactic nuclei, X-ray binaries, and gamma-ray bursts. They are important in observations of black-hole silhouettes, and they may affect the future gravitational-wave images of compact objects.

In order to describe the disk gravitational field in general relativity (GR), one has to either impose some reasonable simplifications to tackle the problem analytically, or to solve the Einstein equations numerically. In this work, we follow the first approach – we propose a generic procedure which in some static and axially symmetric cases provides the full spacetime metric explicitly and in closed form.

For a physical system in a stationary equilibrium, if solenoidal-type motions are not important, it is natural to assume that its spacetime is circular, namely that it is stationary, axially symmetric, and orthogonally transitive (possessing global meridional planes). If the overall net rotation can be neglected, or if it is compensated due to counter-rotating mass currents, one can even consider the spacetime static. In such a case, if the condition $T^\rho_\rho + T^z_z = 0$ on the energy-momentum tensor holds (as e.g. in a vacuum or dust), the metric can be written in the Weyl form

$$\mathrm{d}s^2 = -e^{2\nu}\,\mathrm{d}t^2 + \rho^2 e^{-2\nu}\,\mathrm{d}\phi^2 + e^{2\lambda-2\nu}(\mathrm{d}\rho^2 + \mathrm{d}z^2)\,, \quad (1)$$

where the Weyl-type cylindrical coordinates (t, ρ, z, ϕ) are adapted to the symmetries – the metric is independent of the time t and of the azimuthal angle ϕ, while ρ and z cover the meridional planes in an isotropic way. In vacuum regions, the two metric functions $\nu(\rho, z)$ and $\lambda(\rho, z)$ satisfy the Einstein equations

$$\Delta\nu = 0\,, \quad (2)$$

$$\lambda_{,\rho} = \rho(\nu_{,\rho}^2 - \nu_{,z}^2)\,, \qquad \lambda_{,z} = 2\rho\nu_{,\rho}\nu_{,z}\,. \quad (3)$$

where Δ is the standard Laplace operator in cylindrical coordinates (ρ, z, ϕ) (with the ϕ term missing, however, thanks to the axial symmetry). Hence, just like in Newtonian gravity or in electrostatics, the field is described by solutions to the Laplace equation. However, in contrast to the former, in GR there also appears the second function λ which can deviate the result from the Newtonian expectations significantly. For instance, the Bach-Weyl ring is the natural analogue of the homogeneous thin ring from Newton's theory (they share the same form of the potential ν), but the meridional plane is very much deformed close to the ring – the space is not locally cylindrical around the ring, but rather strongly anisotropic [1].

We focus on infinitesimally thin disks here. Such a case finds applications where the typical cross thickness of the disk is negligible compared to other length scales. As relativists, we are mostly interested in disks formed in accretion in strong gravitational fields, e.g. that of a black hole or a neutron star. When the disk mass is much smaller than the mass of the central body, the accreting matter is usually treated as a test, non-gravitating one. Yet the field equations of Newton's as well as Einstein's theory involve mass *density*, so even if the total mass of the disk is not large, its gravity may still have a significant

* k.kofron@gmail.com
† kotlarik.petr@gmail.com
‡ oldrich.semerak@mff.cuni.cz

effect, including that on the disk's own structure, evolution and stability [2]. The disk gravitation has also been shown to induce subtle but possibly measurable effects on quasi-normal modes of black holes [3] or on extreme-mass-ratio inspirals [4], thus affecting the gravitational waves generated by the black-hole–disk systems; similarly, it can alter the appearance of the black-hole silhouettes [5]. Having an analytical model which includes the gravitational contribution of the disk may thus help to understand such phenomena.

Newtonian-density profiles[1] of static and axisymmetric razor-thin disks are proportional to the delta distribution in the z coordinate,

$$\sigma(\rho, z) \equiv \sigma(\rho)\delta(z)\,. \tag{4}$$

The spacetime is assumed to be reflection symmetric with respect to the disk plane ($z=0$), regular and asymptotically flat. The potential ν as well as the second metric function λ thus should be finite everywhere and vanish at spatial infinity ($\sqrt{\rho^2+z^2}\to\infty$).

The disk potential ν is given by the Poisson integral

$$\nu(\rho,z) = \\ -4\int_0^\infty \frac{\sigma(\rho')\rho'}{\sqrt{(\rho+\rho')^2+z^2}} K\left(\frac{2\sqrt{\rho\rho'}}{\sqrt{(\rho+\rho')^2+z^2}}\right)\mathrm{d}\rho'\,, \tag{5}$$

where $K(k)$ is the complete elliptic integral of the first kind, with k as its modulus. Since it is usually impossible to compute the integral (5) analytically, several other methods have been developed in the literature. Inspired by Kuzmin's trick (see Sec. II), we propose a new way to solve the problem by integrating, over the Abel transformation of the source density profile, the "Green function" given by the potential due to the Appell ring. We illustrate the procedure on several known thin-disk solutions while completing them by also finding the second metric function λ explicitly in some cases.

The plan of the paper is as follows. In Sec. II we review some techniques for solving the Weyl-Einstein equations (2), (3). In Sec. III, we list several explicit disk solutions, specifically the Morgan-Morgan disks and their inverted counterparts, the disks with polynomial and power-law densities, the Kuzmin-Toomre and the Vogt-Letelier disks; we mention in particular the case of the Appell disk/ring which will serve as an elementary solution in our method. The method itself is introduced in Sec. IV. Then in Sec. V we demonstrate the applicability of the approach on the above particular disk solutions. In addition, we generalize the Morgan-Morgan disks and superpose them with a Schwarzschild black hole, while also deriving the second metric function λ for the complete field. Finally, we revisit the case of power-law-density disks [6] and describe a simpler procedure for generating their potential. Concluding remarks are added in Sec. VI.

We use geometrized units in which the speed of light c and the gravitational constant G equal unity. The metric signature is $(-+++)$. The mass of the black hole is everywhere denoted by M and the mass of the disk by $\mathcal{M}$.

[1] The quantity σ satisfies the Poisson equation $\Delta\nu = 4\pi\sigma(\rho,z)$, so it is the analogue of the Newtonian matter density.

II. THIN-DISK SOLUTIONS TO EINSTEIN EQUATIONS

Let us outline some techniques for solving the equations (2), or (5), and (3) for a thin-disk distribution of matter. We focus on those which provide the solutions considered in the next section.

A. The potential of thin disks

One way to tackle the axisymmetric problem is to perform the integration (5) along the symmetry axis $\rho=0$ where $K(k)$ reduces to $\pi/2$. If the result can be expanded in a power series in z, the solution at the generic location is given by a similar series supplemented by Legendre polynomials [7]. Such a series typically does not converge very well [8], though, in the case of the Morgan-Morgan family of disks, it performs better (see Sec. III A for more details).

A different approach was used by Conway [9] and we have applied it in [6] recently. The trick is to rewrite the integral (5) in terms of the Laplace transform of a product of the zero-order Bessel functions,

$$\nu(\rho,z) = -2\pi\int_0^\infty\int_0^\infty \rho'\sigma(\rho')J_0(s\rho')J_0(s\rho)e^{-s|z|}\,\mathrm{d}s\,\mathrm{d}\rho'\,, \tag{6}$$

where s is an auxiliary real parameter of the dimension of inverse length. The double integration may look complicated, but it has proved quite efficient, specifically in the case of the polynomial and power-law density disks where it even yields closed-form formulae [6] (see Sec. III C).

Yet another useful approach is due to Kuzmin [10], later elaborated extensively by Evans & de Zeeuw [11] in the Newtonian context and by Bičák et al. [12, 13] in GR. It involves considering a line mass distribution along the negative-z half of the symmetry axis, cutting the resulting gravitational field along the $z=0$ plane, and copying (reflecting) the result obtained for the positive-z half-space below that plane. The resulting potential reads

$$\nu(\rho,z) = -\int_0^\infty \frac{W(b)\,\mathrm{d}b}{\sqrt{\rho^2+(|z|+b)^2}}\,, \tag{7}$$

with the "weight function" $W(b)$ describing the mass distribution, and the surface density induced by the metric-

gradient jump in the equatorial plane reads

$$\sigma(\rho) = \frac{1}{2\pi}\int_0^\infty \frac{W(b)b}{(\rho^2+b^2)^{3/2}}\,\mathrm{d}b\,. \tag{8}$$

Note that Vieira [14] employed a similar procedure in order to compute the potential of a black hole surrounded by a disk. His mass distribution was a chain of Schwarzschild black holes (rods) located on the axis, and he performed the cut and reflection in the middle of the positive-z one. The Kuzmin procedure can also be generalized to a stationary case if glueing along suitable hypersurfaces [15].

The potentials found by any of the above methods can be further extended by superpositions thanks to the linearity of the Laplace equation and by inversion with respect to a sphere of a certain prescribed radius (this so-called Kelvin transformation again yields a solution). The inversion with respect to the radius b changes the position as

$$\rho \longrightarrow \frac{b^2\rho}{\rho^2+z^2}\,, \quad z \longrightarrow \frac{b^2 z}{\rho^2+z^2}\,, \tag{9}$$

and the original potential $\nu(\rho,z)$ transforms to

$$\mathcal{K}\nu(\rho,z) \equiv \frac{b}{\sqrt{\rho^2+z^2}}\,\nu\left(\frac{b^2\rho}{\rho^2+z^2}, \frac{b^2 z}{\rho^2+z^2}\right). \tag{10}$$

It corresponds to a different ("inverted") density profile, which in the case of a thin disk reads

$$\sigma(\rho) \longrightarrow \frac{b^3}{\rho^3}\sigma(b^2/\rho)\,. \tag{11}$$

Besides the Weyl coordinates, we will also use the oblate ones, $\zeta \in (0,\infty)$ and $\xi \in (-1,+1)$, defined by

$$\rho^2 = b^2(1+\zeta^2)(1-\xi^2)\,, \qquad z = b\zeta\xi\,. \tag{12}$$

The inverse relations read

$$\zeta = \frac{\sqrt{2}|z|}{\sqrt{\sqrt{(\rho^2-b^2+z^2)^2+4b^2z^2}-(\rho^2-b^2+z^2)}}\,, \tag{13}$$

$$\xi = \frac{z}{b\zeta}\,, \tag{14}$$

and the Kelvin transformation works as

$$\zeta \longrightarrow \frac{\xi}{\sqrt{\zeta^2+1-\xi^2}}\,, \qquad \xi \longrightarrow \frac{\zeta}{\sqrt{\zeta^2+1-\xi^2}}\,. \tag{15}$$

$$\mathcal{K}\nu(\zeta,\xi) = \frac{1}{\sqrt{\zeta^2+1-\xi^2}}\,\nu\left(\frac{\xi}{\sqrt{\zeta^2+1-\xi^2}}, \frac{\zeta}{\sqrt{\zeta^2+1-\xi^2}}\right). \tag{16}$$

B. The function λ and superposition of multiple sources

For λ, there is no other option usually than to integrate equation (3) directly, although the reflecting method works for the whole metric, thus also for λ. In a vacuum, the main requirement on λ is to vanish on the axis (the "elementary flatness" requirement), plus we assume $\lambda=0$ at spatial infinity (asymptotic flatness).

Thanks to the linearity of the Laplace equation, the potentials of multiple sources just add, e.g. $\nu = \nu_1 + \nu_2$, yet still, the non-linearity of the Einstein equations shows itself in the second metric function λ. Denoting the pure individual contributions as λ_1 and λ_2 (they satisfy (3) with ν_1 and ν_2 respectively), the total λ (satisfying (3) with $\nu_1+\nu_2$) comes out as

$$\lambda = \lambda_1 + \lambda_2 + \lambda_{\mathrm{int}}\,, \tag{17}$$

where the "interaction" part λ_{int} has gradient

$$\lambda_{\mathrm{int},\rho} = 2\rho(\nu_{1,\rho}\nu_{2,\rho} - \nu_{1,z}\nu_{2,z})\,, \tag{18}$$

$$\lambda_{\mathrm{int},z} = 2\rho(\nu_{1,\rho}\nu_{2,z} + \nu_{1,z}\nu_{2,\rho})\,. \tag{19}$$

In particular, if "the first" of the sources is the Schwarzschild black hole (of mass M), the corresponding metric functions read

$$\nu_1 \equiv \nu_{\mathrm{Schw}} = \frac{1}{2}\ln\left(\frac{R_+ + R_- - 2M}{R_+ + R_- + 2M}\right), \tag{20}$$

$$\lambda_1 \equiv \lambda_{\mathrm{Schw}} = \frac{1}{2}\ln\left(\frac{(R_+ + R_-)^2 - 4M^2}{4R_+R_-}\right), \tag{21}$$

where

$$R_\pm = \sqrt{\rho^2 + (z \mp M)^2}\,. \tag{22}$$

III. SPECIFIC THIN DISKS

In this section, we review several solutions for thin disks which are empty in the central region (or which can be made such by inversion), being thus suitable for the superposition with a central source.

A. Morgan-Morgan disks and their inversion

A class of general relativistic thin disks with the Newtonian density profile

$$\sigma^{(n)}_{\mathrm{MM}}(\rho \le b) = \frac{(2n+1)\mathcal{M}}{2\pi b^2}\left(1-\frac{\rho^2}{b^2}\right)^{n-1/2} \tag{23}$$

was proposed by Morgan & Morgan already in 1969 [16]. These disks are finite, stretching between $\rho \in [0,b]$ and

having a finite total mass $\mathcal{M}$. Their field is described by the potential [17]

$$\nu^{(n)}_{\rm MM} = -\frac{\mathcal{M}}{b}(2n+1)!\sum_{j=0}^{n} C^{(n)}_{2j} iQ_{2j}(i\zeta)P_{2j}(\xi)\,, \qquad (24)$$

where P_{2j} and Q_{2j} are the Legendre functions of the first and second kind and the coefficients read

$$C^{(n)}_{2j} = \frac{(-1)^j(4j+1)(2j)!(n+j)!}{(j!)^2(n-j)!(2n+2j+1)!}\,. \qquad (25)$$

It is also possible to obtain the second metric function λ case by case integrating the Einstein equations (3) in the oblate spherical coordinates (see Sec. V A).

If interested in infinite disks with a central empty region, an inversion with respect to the outer rim b, i.e. the Kelvin transformation (10), can be applied. The resulting field corresponds to the disks with the Newtonian density profiles

$$\sigma^{(n)}_{\rm iMM}(\rho \geq b) = \frac{2^{2n}(n!)^2\mathcal{M}b}{(2n)!\pi^2\rho^3}\left(1-\frac{b^2}{\rho^2}\right)^{n-1/2}\,. \qquad (26)$$

They stretch from $\rho = b$ to radial infinity, yet their total mass $\mathcal{M}$ remains finite. There is no explicit result for λ in the literature. The inverted Morgan-Morgan disks were first considered and superposed with the Schwarzschild black hole by Lemos & Letelier [18].

B. Kuzmin-Toomre and Vogt-Letelier disks

When the weight function $W(b)$ in (7) is proportional to a certain sum of delta distributions and their derivatives, the associated potential describes the gravitational field of a particular family of thin disks studied by Kuzmin [10] and Toomre [19],

$$\nu^{(n)}_{\rm KT} = -\frac{\mathcal{M}}{(2n-1)!!}\sum_{k=0}^{n}\frac{(2n-k)!}{2^{n-k}(n-k)!}\frac{b^k}{r_b^{k+1}}P_k\left(|\cos\theta_b|\right)\,, \qquad (27)$$

where we have denoted

$$r_b^2 \equiv \rho^2 + (|z|+b)^2\,, \qquad |\cos\theta_b| \equiv \frac{|z|+b}{r_b}\,, \qquad (28)$$

and P_k are Legendre polynomials. The corresponding Newtonian density profiles read

$$\sigma^{(n)}_{\rm KT} = \frac{(2n+1)b^{2n+1}}{2\pi}\frac{\mathcal{M}}{(\rho^2+b^2)^{n+3/2}}\,. \qquad (29)$$

The second metric function λ was found by Bičák et al. in [12].

Taking a special superposition of expressions (27), Vogt & Letelier [20] obtained another potential-density pairs

$$\nu^{(m,n)}_{\rm VL} = W^{(m,n)}\sum_{k=0}^{n}(-1)^k\binom{n}{k}\frac{\nu^{(m+k)}_{\rm KT}}{2m+2k+1}\,, \qquad (30)$$

$$\sigma^{(m,n)}_{\rm VL} = W^{(m,n)}\frac{\mathcal{M}b^{2m+1}}{2\pi}\frac{\rho^{2n}}{(\rho^2+b^2)^{m+n+3/2}}\,, \qquad (31)$$

where $W^{(m,n)}$ is a normalization factor ensuring that $\mathcal{M}$ remains the total mass of the disk. Recently, in [21], we derived the second metric function λ and, using the fact that these disks are empty on the axis, we superposed them with the Schwarzschild black hole and provided both metric functions explicitly for the total spacetime.

C. Polynomial and power-law density disks

In [6], we presented solid finite disks of polynomial density profiles, infinite annular disks of power-law density and finite annular disks with a bump-like density,

$$\sigma^{(m,2l)}_{\rm pol}(\rho \leq b) = \binom{m+\frac{1}{l}}{m}\frac{\mathcal{M}}{\pi b^2}\left(1-\frac{\rho^{2l}}{b^{2l}}\right)^m\,, \qquad (32)$$

$$\sigma^{(m,2l)}_{\rm pl}(\rho \geq b) = \binom{m+\frac{1}{2l}}{m}\frac{\mathcal{M}b}{2\pi\rho^3}\left(1-\frac{b^{2l}}{\rho^{2l}}\right)^m\,, \qquad (33)$$

$$\sigma^{(L)}_{\rm bump}(b_{\rm in} \leq \rho \leq b_{\rm out}) = -W_0 + \sum_{j=0}^{L}(-1)^j\frac{W_{-3-2j}}{\rho^{3+2j}}\,, \qquad (34)$$

where W_i are constant coefficients. The construction employed the special properties of the Laplace equation, i.e., we integrated (6) for elementary density terms $\sigma^{(2l)}_{\rm pol} = \rho^{2l}$, applied Kelvin transformation (9) and (10) to get the negative powers ρ^{-3-2l}, and finally superposed the corresponding elementary potentials with appropriate weights. The resulting potentials were given in closed form in terms of complete elliptic integrals. The second metric function λ has not been found explicitly.

D. Appell ring

Already in 1887, Appell [22] obtained, within electrostatics, a ring-like solution to the Laplace equation by putting a charged point particle (massive particle in our case, $\mathcal{M}$) on the complex extension of the z axis. The corresponding complex potential reads

$$\nu_{\rm App} = -\frac{\mathcal{M}}{\sqrt{\rho^2+(z-{\rm i}b)^2}}\,, \qquad (35)$$

with a point mass located at $(\rho = 0, z = {\rm i}b)$, where b is real and of the dimension of length. Taking the real part,

we have

$$\nu_{\rm App} = -\frac{\mathcal{M}}{\sqrt{2}\,\Xi}\sqrt{\Xi+\rho^2+z^2-b^2}\,, \tag{36}$$

$$\lambda_{\rm App} = \frac{\mathcal{M}^2}{8b^2}\left[1-\frac{\rho^2+z^2+b^2}{\Xi}-\frac{2b^2\rho^2(\Xi^2-8z^2b^2)}{\Xi^4}\right], \tag{37}$$

where

$$\Xi = \sqrt{(\rho^2-b^2+z^2)^2+4b^2z^2}\,. \tag{38}$$

A thorough investigation of the whole broader family of Appell rings in GR was performed by Gleisler & Pullin [23]. Two interpretations of the simplest solution are at hand. It is either a disk of negative surface mass density diverging towards $-\infty$ at the rim ($\rho = b, z = 0$), jumping to $+\infty$ there, so that the total mass $\mathcal{M}$ is positive and finite, or, it is a singular ring of mass $\mathcal{M}$, through which the spacetime is analytically extended to a second asymptotically flat region. Semerák et al. [24] pointed out that the gravitational field is somewhat similar to the Kerr solution, although no dragging effects are present as the spacetime is static, and there is also no horizon. Independently of the interpretation, we use the Appell potential to generate physical thin-disk solutions similarly as Kuzmin did in [10] for the point mass on the (real) axis.

IV. CONVOLUTION OF APPELL RINGS

A. The potential ν

Let us combine the Kuzmin-inspired approach (7) and Appell's trick (36), i.e., integrate a line matter distribution on the complex extension of the z axis described by the real *weight function* $f(w)$ and mirror the positive half of the z axis to the negative half. The respective potential thus reads

$$\nu_f(\rho,z) = -\int_0^\infty \frac{f(w)\,{\rm d}w}{\sqrt{\rho^2+(|z|+{\rm i}w)^2}}\,, \tag{39}$$

Note that ν_f is a complex function at this moment. Its real part corresponds to some matter distribution in the equatorial plane, while its imaginary part corresponds to a dipole. Indeed, in the oblate spheroidal coordinates (12), for $\zeta \gg 1$, we have

$$\frac{f(w)\,{\rm d}w}{\sqrt{\rho^2+(|z|+{\rm i}w)^2}} \approx -\frac{f(w)}{b\zeta}+\frac{{\rm i}w\xi f(w)}{b^2\zeta^2}+\mathcal{O}(\zeta^{-3}), \tag{40}$$

so $\int_0^\infty f(w)\,{\rm d}w$ may be interpreted as the total mass. The imaginary part of (39) we will not consider any further, because it brings the non-physical dipole term.

The integral (39) can be rewritten as

$$\nu_f(\rho,z) = -{\rm i}\int_\gamma f\left(\frac{1}{2{\rm i}}\frac{\rho^2+z^2-t^2}{t-z}\right)\frac{{\rm d}t}{t-z} \tag{41}$$

if holomorphically extending the function f to a complex plane, with the integration contour

$$\gamma(w):\ t = \sqrt{\rho^2+(z+{\rm i}w)^2}-{\rm i}w\,, \qquad w\in[0,\infty)\,. \tag{42}$$

The integrand is holomorphic in the neighbourhood of the contour γ, so there exists an antiderivative F to (41) such that

$$\nu_f = F\left[\gamma(w=\infty)\right] - F\left[\gamma(w=0)\right]\,. \tag{43}$$

The corresponding (yet complex) Newtonian density profile reads

$$\sigma_f(\rho) = \frac{1}{2\pi}\lim_{z\to0^+}\frac{\partial\nu_f}{\partial z} \tag{44}$$

$$= \frac{1}{2\pi}\lim_{z\to0^+}\int_0^\infty \frac{(z+{\rm i}w)}{\left[\rho^2+(z+{\rm i}w)^2\right]^{3/2}}f(w)\,{\rm d}w\,. \tag{45}$$

Assuming that $f(w)$ is continuous, bounded, and vanishes on the boundary, integration by parts yields

$$\sigma_f(\rho) = -\frac{\rm i}{2\pi}\lim_{z\to0^+}\int_0^\infty \frac{\partial f}{\partial w}\frac{{\rm d}w}{\sqrt{(z+{\rm i}w)^2+\rho^2}} \tag{46}$$

$$= -\frac{\rm i}{2\pi}\int_0^\rho \frac{\partial f}{\partial w}\frac{{\rm d}w}{\sqrt{\rho^2-w^2}} - \frac{1}{2\pi}\int_\rho^\infty \frac{\partial f}{\partial w}\frac{{\rm d}w}{\sqrt{w^2-\rho^2}}\,, \tag{47}$$

where we took the limit $z\to0^+$ and split the integral into two parts. The principal branch of natural logarithm is used, i.e. $\log(-1) = {\rm i}\pi$, so $\sqrt{-1} \equiv e^{1/2\log(-1)} = {\rm i}$. Both integrands are real, thus only the second part contributes to the actual (physical) part of the Newtonian density,

$$\sigma_f(\rho) = -\frac{1}{2\pi}\int_\rho^\infty \frac{\partial f}{\partial w}\frac{{\rm d}w}{\sqrt{w^2-\rho^2}}\,, \tag{48}$$

which is the Abel transformation of the weight function $f(w)$. Its inverse reads

$$f(w) = 4\int_w^\infty \frac{\sigma_f(\rho)}{\sqrt{\rho^2-w^2}}\rho\,{\rm d}\rho\,. \tag{49}$$

Hence, rather than solving the challenging integral (5), we can find the weight function $f(w)$ of the desired Newtonian density using (49) and evaluate a simpler integration (39) to obtain the gravitational potential.

B. The second metric function λ

With the potential (39) at hand, we can look for λ. Equations (3) are quadratic in ν, thus working with the complex potential (39) and taking the real part later would not yield the correct λ-counterpart of the real part

of (39): one has to solve (3) for the real part of (39) directly. Similarly to [13], we can express λ as an integral over the individual ν pairs

$$\lambda_f = \int_0^\infty \int_0^\infty f(w_1) f(w_2) \mathcal{F}(w_1, w_2)\, \mathrm{d}w_1\, \mathrm{d}w_2\,, \quad (50)$$

where $\mathcal{F}$ is the cross term between the individual real parts of the Appell potentials

$$\nu_j = \frac{1}{2}\left[\nu_{\mathrm{App}}(w_j) + \overline{\nu}_{\mathrm{App}}(w_j)\right] \quad (j = 1, 2)\,, \quad (51)$$

satisfying the same equations as the interaction part of λ, (18) and (19), with ν_j. One finds that in general

$$\mathcal{F}(w_1, w_2) = 2\frac{(w_1^2 + w_2^2)}{(w_1^2 - w_2^2)^2} - \frac{1}{2}\left[\mathcal{H}(w_1, w_2) + \overline{\mathcal{H}}(w_1, w_2)\right]\,, \quad (52)$$

with

$$\mathcal{H}(w_1, w_2) \equiv h(w_1, w_2) + h(w_1, -w_2)\,,$$
$$h(w_1, w_2) \equiv \frac{\rho^2 + (z + \mathrm{i}w_1)(z + \mathrm{i}w_2)}{(w_1 - w_2)^2} \frac{1}{\mathscr{R}_1 \mathscr{R}_2}\,, \quad (53)$$

and with the notation

$$\mathscr{R}_j^2 = \rho^2 + (z + \mathrm{i}w_j)^2\,. \quad (54)$$

The constant term $2(w_1^2 + w_2^2)/(w_1^2 - w_2^2)^2$ appears due to the regularity condition on the axis, where we require $\lim_{\rho \to 0^+} \lambda = 0$.

We can now repeat the procedure for the Kelvin-inverted potential $\mathcal{K}\nu_f$. Introducing

$$\mathcal{K}\mathcal{H}(w_1, w_2) \equiv \frac{w_1 w_2}{b^4}\left[-\mathcal{K}h(w_1, w_2) + \mathcal{K}h(w_1, -w_2)\right]\,, \quad (55)$$

the cross term in this case reads

$$\mathcal{F}(w_1, w_2) = -\frac{4 w_1^2 w_2^2}{b^4 (w_1^2 - w_2^2)^2} - \frac{1}{2}\left[\mathcal{K}\mathcal{H}(w_1, w_2) + \mathcal{K}\overline{\mathcal{H}}(w_1, w_2)\right]\,. \quad (56)$$

The term $\mathcal{K}h$ is the h from (53) Kelvin-transformed according to (9).

The procedure works generally, yet in specific situations, it may be easier to solve the equations (3) directly, usually after transforming to some appropriate coordinates. For instance, in the oblate spheroidal coordinates (ζ, ξ), the equations for λ read

$$\frac{\zeta^2 + \xi^2}{\xi^2 - 1}\lambda_{,\zeta} = -\zeta(\xi^2 - 1)\nu_{,\xi}^2 - \zeta(\zeta^2 + 1)\nu_{,\zeta}^2 + 2\xi(\zeta^2 + 1)\nu_{,\zeta}\nu_{,\xi}\,, \quad (57)$$

$$\frac{\zeta^2 + \xi^2}{\zeta^2 + 1}\lambda_{,\xi} = \xi(\zeta^2 + 1)\nu_{,\zeta}^2 + \xi(\xi^2 - 1)\nu_{,\xi}^2 - 2\zeta(\xi^2 - 1)\nu_{,\zeta}\nu_{,\xi}\,. \quad (58)$$

C. Superposition with a black hole

When interested in a superposition of the disk with a black hole of mass M, the interaction part λ_{int} is also necessary. Note that the equations (18) and (19) for $\nu_1 = \nu_{\mathrm{Schw}}$ and $\nu_2 = \nu_f$ are linear in the disk contribution. Thus, the situation is in fact simpler since we can work with the complex potential ν_f and take the real part only at the end. One finds

$$\lambda_{\mathrm{int}} = \int_0^\infty \left\{ \frac{2Mf(w)}{w^2 + M^2} - \left[\frac{R_+(\rho, z)}{M + \mathrm{i}w} + \frac{R_-(\rho, z)}{M - \mathrm{i}w}\right] \frac{f(w)}{\sqrt{\rho^2 + (z + \mathrm{i}w)^2}} \right\} \mathrm{d}w\,, \quad (59)$$

where the first term again ensures the flatness condition on the axis.

In the case of the Kelvin-inverted disks, i.e. with $\nu_1 = \mathcal{K}\nu_f$ in (18) and (19), the interaction part reads

$$\lambda_{\mathrm{int}} = -\int_0^\infty \left[\frac{R_+(\rho, z)}{Mw - \mathrm{i}b^2} + \frac{R_-(\rho, z)}{Mw + \mathrm{i}b^2}\right] \frac{w f(w)\, \mathrm{d}w}{\sqrt{(b^2 + \mathrm{i}wz)^2 - w^2\rho^2}}\,. \quad (60)$$

V. PARTICULAR DISK SOLUTIONS

In this section, we rederive the disk solutions from Sec. III and complete their metrics by also finding the metric function λ in some cases. Suitable disks are superposed with the Schwarzschild black hole and the respective interaction part λ_{int} is computed. Finally, we also show a simpler procedure to generate the polynomial and power-law disks discussed in [6].

A. Generalized (inverted) Morgan-Morgan disks

1. The disks

The weight function which corresponds to the Morgan-Morgan counter-rotating family of disks reads

$$f_{\mathrm{MM}}^{(n)}(w \le b) = \frac{(2n+1)!}{2^{2n}(n!)^2}\frac{\mathcal{M}}{b}\left(1 - \frac{w^2}{b^2}\right)^n \quad (61)$$

(and zero elsewhere). Using this, we recover the potential (24) by taking the real part of the integral (39).

New disks can easily be found by considering higher exponents in (61), i.e. $\frac{w^l}{b^l}$ for l integers. From (48) it follows that such disks represent a certain superposition of the Morgan-Morgan disks plus a logarithmic term in density if l is odd.

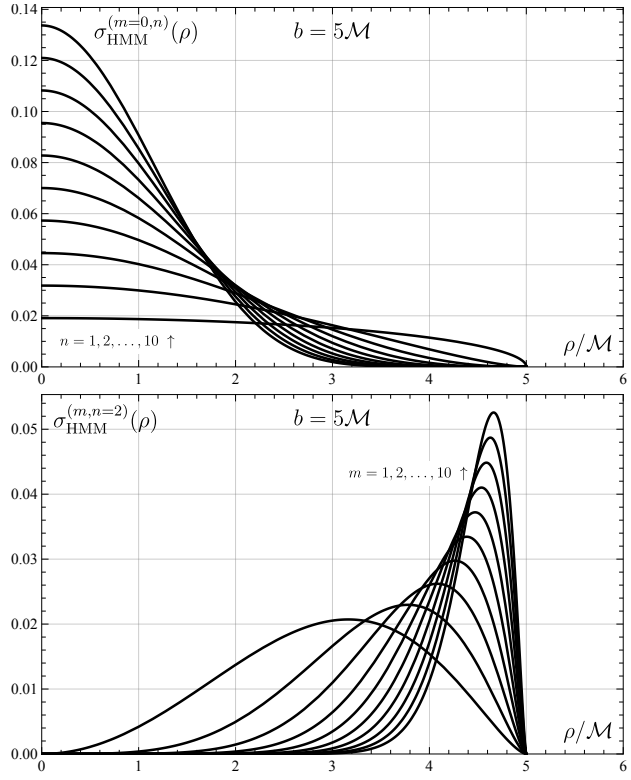

FIG. 1. The first ten Newtonian-density profiles of the original Morgan-Morgan disks (*top plot*) and the first ten profiles of the wider family of holey Morgan-Morgan disks (*bottom plot*) with fixed $n = 2$. The edge of the disk is located at $b = 5\mathcal{M}$ in both plots. Increasing the parameter n makes the density decrease more smoothly at the edge while increasing the parameter m makes the density peak narrower and closer to the edge, finally resembling a ring rather than a disk for high values of m. The vertical axis is in the units of $\mathcal{M}^{-1}$.

Nonetheless, there exists a more interesting and simpler generalization – the holey Morgan-Morgan disks proposed by Letelier [25]. These have densities

$$\sigma^{(m,n)}_{\mathrm{hMM}}(\rho \le b) = \frac{\mathcal{M}}{2\pi b^{2+2m}} \frac{\left(\frac{3}{2}\right)_{m+n}}{m!\left(\frac{1}{2}\right)_n} \rho^{2m} \left(1 - \frac{\rho^2}{b^2}\right)^{n-1/2}, \tag{62}$$

where $(a)_j = \Gamma(a+j)/\Gamma(a)$ is the Pochhammer symbol. As illustrated in Fig. 1, contrary to the original Morgan-Morgan family, the disks with non-zero parameter m have a hole in the center with the surface density exactly vanishing at $\rho = 0$. The associated weight function (49) reads

$$f^{(m,n)}_{\mathrm{hMM}}(w \le b) = \frac{(2m)!\left(\frac{3}{2}\right)_{m+n}}{2^{2m}(m!)^2(m+n)!} \frac{\mathcal{M}}{b} \sum_{j=0}^{m+n} \binom{m+n}{j} \frac{\left(\frac{1}{2}\right)_j}{\left(\frac{1}{2}-m\right)_j} \left(-\frac{w^2}{b^2}\right)^j. \tag{63}$$

The holey potential can again be obtained by integrating (39) and taking the real part, or, by a straightforward superposition of the original Morgan-Morgan disks

$$\nu^{(m,n)}_{\mathrm{hMM}} = N^{(m,n)} \sum_{k=0}^{m} (-1)^k \binom{m}{k} \frac{\nu^{(k+n)}_{\mathrm{MM}}}{2k+2n+1}, \tag{64}$$

with $N^{(m,n)}$ a normalization constant. The potential can be re-expressed in the basis of Legendre polynomials,

$$\nu^{(m,n)}_{\mathrm{hMM}} = \frac{\left(\frac{3}{2}\right)_{m+n}}{m!\left(\frac{1}{2}\right)_n} \frac{\mathcal{M}}{b} \sum_{k=0}^{m+n} C^{(m,n)}_{2k}\, iQ_{2k}(i\zeta) P_{2k}(\xi), \tag{65}$$

where the coefficients have a slightly more complicated form

$$C^{(m,n)}_{2k} = \begin{cases} \dfrac{(-1)^{k+1}4^{-n}(4k+1)(2n)!\left(\frac{1}{2}\right)_k}{k!(n-k)!\left(\frac{3}{2}\right)_{k+n}} {}_3F_2\left(\begin{matrix} -m, n+\frac{1}{2}, n+1 \\ n-k+1, n+k+\frac{3}{2} \end{matrix}; 1\right), & k \le n \\ \dfrac{(-1)^{n+1}\left[\left(\frac{1}{2}\right)_k\right]^2 (m+n-k+1)_{k-n}}{\left(\frac{1}{2}\right)_{2k}(k-n)!} {}_3F_2\left(\begin{matrix} k+\frac{1}{2}, k+1, k-m-n \\ 2k+\frac{3}{2}, k-n+1 \end{matrix}; 1\right), & k > n \end{cases}$$

involving the generalized hypergeometric function ${}_3F_2\left(\begin{smallmatrix} a,b,c \\ d,e \end{smallmatrix}; x\right)$ with integer and half-integer parameters evaluated at the point $x = 1$.

For the metric function λ, we can either solve the double integration (50), or tackle the equations for λ directly. In the Morgan-Morgan case, the latter approach is simpler as the potential is separated in the spheroidal coordinates ζ and ξ. A straightforward integration of (58) from the axis $\xi = 1$ (where $\lambda = 0$) to some general ξ yields

$$\lambda^{(m,n)}_{\mathrm{hMM}} = \mathcal{C}^{(m,n)}_{\mathrm{hMM}} \left[\frac{\left(\frac{3}{2}\right)_{m+n}}{m!\left(\frac{1}{2}\right)_n}\right]^2 \frac{\mathcal{M}^2}{b^2}(\xi^2-1)\Big[\mathcal{P}^{(m,n)}_{0,\mathrm{hMM}} + 2\zeta\mathcal{P}^{(m,n)}_{1,\mathrm{hMM}} \operatorname{arccot}(\zeta) + (\zeta^2+1)\mathcal{P}^{(m,n)}_{2,\mathrm{hMM}} \operatorname{arccot}^2(\zeta)\Big], \tag{66}$$

where $\mathcal{P}^{(m,n)}_{j,\mathrm{hMM}}$ are polynomials in (ζ, ξ), and $\mathcal{C}^{(m,n)}_{\mathrm{hMM}}$ is

a constant – the explicit expressions are given in Appendix A. Because the Laplace equation $\Delta\nu = 0$ is also the integrability condition for λ, integrating over ζ would give the same result.

Similarly to [17, 18, 25], we can make the inversion (16) of the potential (65) and obtain infinite (yet finite-mass) disks stretching from the radius $\rho = b$ to infinity while leaving the central region below b empty. The associated Newtonian density profiles read

$$\sigma_{\text{ihMM}}(\rho \geq b) = \frac{b^{2m+1}(m+n)!}{\pi^2 \left(\frac{1}{2}\right)_m \left(\frac{1}{2}\right)_n} \frac{\mathcal{M}}{\rho^{3+2m}} \left(1 - \frac{b^2}{\rho^2}\right)^{n-1/2}, \tag{67}$$

where we again fix the normalization so that $\mathcal{M}$ stands for the total disk mass. Clearly, when $m = 0$, we obtain the inverted Morgan-Morgan disks treated in [18] or [17]. The function λ again follows by direct integration of the Einstein equation (58). The result is similar to (66) if we apply the Kelvin transformation (15) on it, although the polynomials are different (since λ does not transform according to (16)). Specifically, the metric functions appear as

$$\nu_{\text{ihMM}} = \frac{2(m+n)!}{\pi \left(\frac{1}{2}\right)_m \left(\frac{1}{2}\right)_n} \frac{\mathcal{M}}{b\sqrt{\zeta^2+1-\xi^2}} \sum_{k=0}^{m+n} C_{2k}^{(m,n)} i Q_{2k}\left(\frac{i\xi}{\sqrt{\zeta^2+1-\xi^2}}\right) P_{2k}\left(\frac{\zeta}{\sqrt{\zeta^2+1-\xi^2}}\right), \tag{68}$$

$$\lambda_{\text{ihMM}}^{(m,n)} = \mathcal{C}_{\text{ihMM}}^{(m,n)} \left[\frac{2(m+n)!}{\pi \left(\frac{1}{2}\right)_m \left(\frac{1}{2}\right)_n}\right]^2 \frac{\mathcal{M}^2}{b^2} \mathcal{K}\left\{(\xi^2-1)\left[\mathcal{P}_{0,\text{ihMM}}^{(m,n)} + 2\zeta \mathcal{P}_{1,\text{ihMM}}^{(m,n)} \operatorname{arccot}(\zeta) + (\zeta^2+1)\mathcal{P}_{2,\text{ihMM}}^{(m,n)} \operatorname{arccot}^2(\zeta)\right]\right\}. \tag{69}$$

2. *Superposition with a black hole*

The holey Morgan-Morgan disks with $m \geq 1$ and their inverted versions with an arbitrary $m \geq 0$ are empty in the centre. Therefore, we can superpose them with a black hole of mass M placed at the origin – see the superposition scheme in Fig. 3. Already in Sec. II B we discussed how to superpose sources within the Weyl class. We provided all the necessary expressions in the previous sections, yet the last piece is still missing – the interaction part λ_{int}.

We will derive λ_{int} from (59) or (60), by performing the integration over the weight function (63) with the normalization adapted appropriately to the total mass $\mathcal{M}$. The general form reads

$$\begin{aligned}\lambda_{\text{hMM,int}}^{(m,n)} = {} & \mathscr{K}_{0,\text{hMM}}^{(m,n)} + \mathscr{K}_{1,\text{hMM}}^{(m,n)} \left\{\operatorname{atan2}\begin{bmatrix} b\xi - M\zeta \\ R_-(\zeta,\xi)\end{bmatrix} - \operatorname{atan2}\begin{bmatrix} b\xi + M\zeta \\ R_+(\zeta,\xi)\end{bmatrix}\right\} + \\ & + \mathscr{K}_{2,\text{hMM}}^{(m,n)} \sum_{\mp} R_{\mp}(\zeta,\xi)\left[\pm \mathscr{P}_{0,\text{hMM}}^{(m,n)}(\pm\zeta,\xi) + \mathscr{P}_{1,\text{hMM}}^{(m,n)}(\pm\zeta,\xi)\operatorname{arccot}(\zeta)\right],\end{aligned} \tag{70}$$

$$\begin{aligned}\lambda_{\text{ihMM,int}}^{(m,n)} = {} & \mathscr{K}_{1,\text{ihMM}}^{(m,n)} \left\{\operatorname{atan2}\begin{bmatrix} b\xi - M\zeta \\ R_-(\zeta,\xi)\end{bmatrix} + \operatorname{atan2}\begin{bmatrix} b\xi + M\zeta \\ R_+(\zeta,\xi)\end{bmatrix}\right\} + \\ & + \mathscr{K}_{2,\text{ihMM}}^{(m,n)} \sum_{\mp} R_{\mp}(\zeta,\xi)\,\mathcal{K}\left\{\sqrt{1+\zeta^2-\xi^2}\left[\pm \mathscr{P}_{0,\text{ihMM}}^{(m,n)}(\pm\zeta,\xi) + \mathscr{P}_{1,\text{ihMM}}^{(m,n)}(\pm\zeta,\xi)\operatorname{arccot}(\zeta)\right]\right\},\end{aligned} \tag{71}$$

where $\operatorname{atan2}(\frac{y}{x}) \equiv \operatorname{atan2}(y,x)$ denotes a 2-argument arcus tangent, $R_\pm(\zeta,\xi)$ are defined in (22) and transformed to the oblate spheroidal coordinates (12), $\mathscr{K}_{j,(\text{i})\text{hMM}}^{(m,n)}$ stand for constants which depends on the disk parameters, and $\mathscr{P}_{j,(\text{i})\text{hMM}}^{(m,n)}$ are polynomials in ζ and ξ. As in (69), we use the Kelvin transformation (15). Explicit expressions are given in Appendix A.

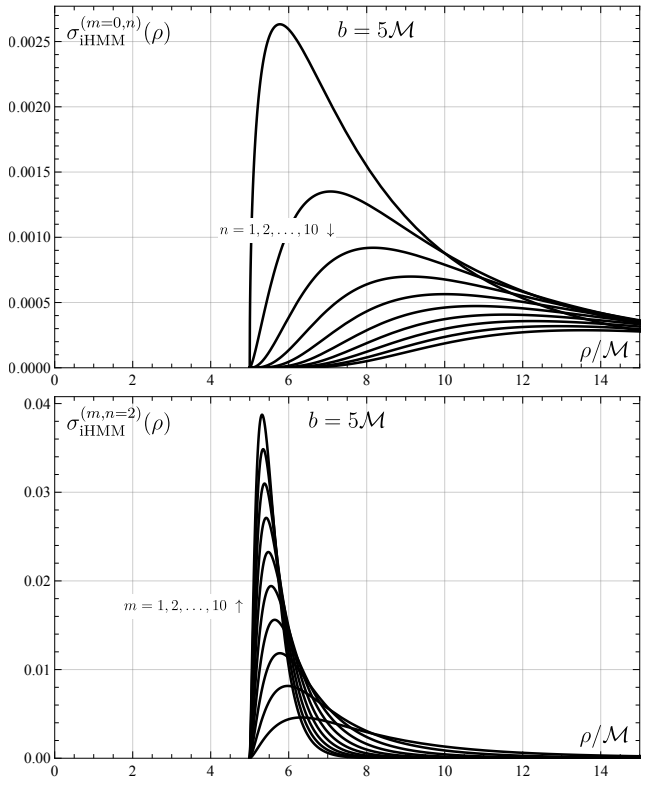

FIG. 2. The first ten Newtonian-density profiles of the inverted Morgan-Morgan disks (*top plot*) and the first ten profiles of the inverted holey Morgan-Morgan disks (*bottom plot*) with the fixed $n = 2$. As in Fig. 1, the edge of the disk is located at $b = 5\mathcal{M}$ in both plots, but the disks stretch from this edge to infinity and are empty bellow b. Again, increasing the parameter n makes the density decrease more smoothly at the edge while increasing the parameter m makes the density peak narrower and closer to the edge. The vertical axis is in the units of $\mathcal{M}^{-1}$.

B. Kuzmin-Toomre & Vogt-Letelier disks

The suggested method is general in the sense that most of the known disk solutions can be reformulated in terms of the weight function and integration (39). From (48), we easily obtain the weight function associated with the Kuzmin-Toomre disks (29),

$$f^{(n)}_{\rm KT}(w) = \frac{2^{2n+1}(n!)^2}{\pi(2n)!}\frac{\mathcal{M}b^{2n+1}}{(w^2+b^2)^{1+n}}\,, \qquad n \in \mathbb{N}_0\,. \quad (72)$$

Note that these disks are infinite, thus w ranges through the full interval $[0, \infty)$, with b just a length parameter not directly indicating the location of the disk edge. A simple generalization to half-integer exponents is possible as well,

$$f^{(n)}_{\rm gKT}(w) = \frac{n\,b^{2n}(2n)!}{2^{2n-1}(n!)^2}\frac{\mathcal{M}}{(w^2+b^2)^{n+1/2}}\,, \quad (73)$$

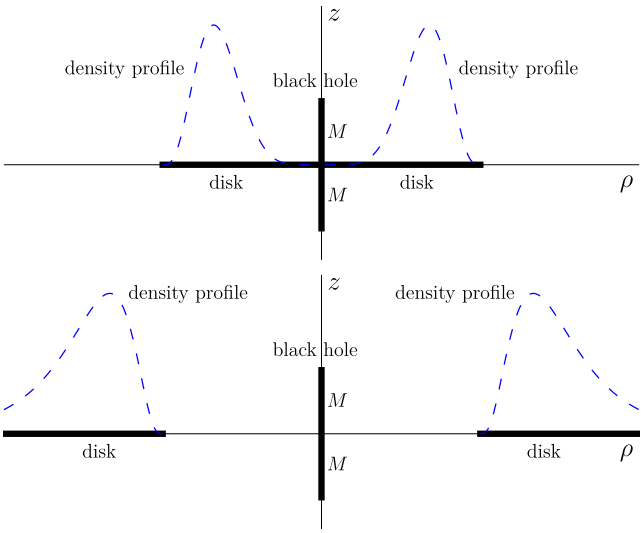

FIG. 3. Schematic plot of the meridional section of the superposition of the holey Morgan-Morgan disk (*top plot*) and of its inverted counterpart (*bottom plot*) with a central black hole. The black hole of the mass M is indicated by the thick black line placed symmetrically on the z axis. The thick black lines in the equatorial plane represent the disk. The density profile is depicted by the blue dashed lines. The edge of the disk is located at $(\rho = 2.5M, z = 0)$ in both plots.

resulting in Newtonian surface densities

$$\sigma^{(n)}_{\rm gKT}(\rho) = \frac{n\,b^{2n}}{\pi}\frac{\mathcal{M}}{(\rho^2+b^2)^{1+n}}\,. \quad (74)$$

However, the potential (39) is then given in terms of complete elliptic integrals, which we do not list here.

The weight function of the Vogt-Letelier disk family (31),

$$f^{(m,n)}_{\rm VL}(w) = \frac{2}{\pi(2m+1)}\frac{m!}{n!}\frac{\left(\frac{3}{2}\right)_{m+n}}{\left[\left(\frac{1}{2}\right)_m\right]^2}\frac{\mathcal{M}}{b}\left(\frac{b}{w}\right)^{2m+2}\times$$
$$\times\, {}_2F_1\left(\begin{matrix}1+m,\ \frac{3+2m+2n}{2}\\ \frac{3+2m}{2}\end{matrix};-\frac{b^2}{w^2}\right)\,, \quad (75)$$

can be reduced to

$$f^{(m,n)}_{\rm VL}(w) \propto \frac{\mathscr{P}^{(m,n)}_{\rm VL}(w)}{(w^2+b^2)^{m+n+1}}\,, \quad (76)$$

where $\mathscr{P}^{(m,n)}_{\rm VL}(w)$ is an even polynomial of the order $2n$ in w. Again, one can also consider half-integer exponents of $(w^2+b^2)^{-m-n-1/2}$ in (76) and compute the respective potential from (39). The result corresponds to the Newtonian surface densities (31), wherein the denominator there appears $(\rho^2+b^2)^{m+n+1}$ rather than a half-integer exponent. It again involves complete elliptic integrals.

In order to find the second metric function λ, one may use the approach presented above, including the interaction part $\lambda_{\rm int}$ necessary in superpositions with a black

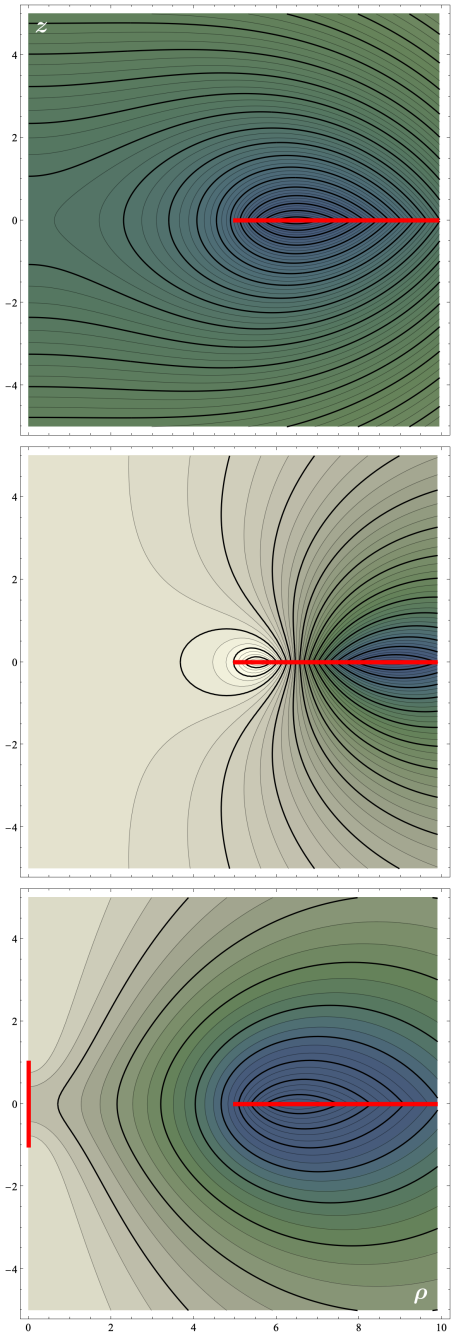

FIG. 4. Meridional-section contour plots in Weyl coordinates of the potential $\nu^{(1,2)}_{\mathrm{ihMM}}$ (*top plot*), the second metric function $\lambda^{(1,2)}_{\mathrm{ihMM}}$ (*middle plot*), and the interaction part $\lambda^{(1,2)}_{\mathrm{int,ihMM}}$ (*bottom plot*) of the inverted holey Morgan-Morgan disk with $(m = 1, n = 2)$ superposed with the Schwarzschild black hole of mass M. The disk's inner edge is located at $(\rho = 5M, z = 0)$ and its mass is $\mathcal{M} = 2M$. The disk is indicated by the thick horizontal red line, while the black hole is indicated by the thick vertical red line. In the middle plot, the largest negative values are coloured deep blue; they increase through green to light brown (indicating zero value) up to positive values indicated by white. The values range from about -0.32 to -0.17 in the top plot, from about -0.030 to 0.0066 in the middle plot, and from about -0.044 to 0 in the bottom plot. Both axes are in the units of M.

hole, yet it is easier to follow the direct approach like in [12, 21].

C. Polynomial and power-law disks

1. *The weight function*

The polynomial, power-law and bump disks derived in [6] can also be recast in the present formalism. In particular, the elementary density terms $\sigma^{(2l)}_{\mathrm{elem}}(\rho \le b) = \rho^{2l}$, $l \in \mathbb{N}_0$, translate to the weight function

$$f^{(2l)}_{\mathrm{elem}}(w \le b) = -2w^{2l+1} B_{\frac{w^2}{b^2}}\left(-\frac{1}{2} - l, \frac{1}{2}\right) \tag{77}$$

$$= \frac{b^{2l}\sqrt{b^2 - w^2}}{\pi^2(2l+1)} \sum_{k=0}^{l} \frac{(-l)_k}{\left(\frac{1}{2} - l\right)_k} \left(\frac{w}{b}\right)^{2k}, \tag{78}$$

where $B_x(c, d)$ is the incomplete Beta function. By evaluating the integral (39) and taking the real part, we reproduce the results of [6] obtained by direct integration of the axially symmetric Green function (6). Although the computation of λ is still beyond our reach, for the power-law disks superposed with a black hole the computation of the interaction part λ_{int} is feasible actually.

2. *Simpler recurrence relation for the potentials in [6]*

Before finishing this section, let us add a more straightforward way how to derive the potential-density pairs in [6]. In that paper, we used the approach proposed by [9] and explicitly integrated the axially symmetric Green function (6). Considering the elementary density terms $\sigma(\rho) = \rho^{2l}$, the problem reduces to the computation of the Bessel-Laplace integrals

$$\mathcal{I}_{(\alpha,\beta,\gamma)} = \int_0^\infty s^\alpha J_\beta(sb) J_\gamma(s\rho) e^{-s|z|}\, \mathrm{d}s\,. \tag{79}$$

Various recurrence relations can be used to explicitly calculate $\mathcal{I}_{(\alpha,\beta,\gamma)}$. In what follows, we show that it is not necessary to use the lengthy recurrence relations from [6]. Actually, we have found a simpler recipe inferred from relations between solutions to the generalized $2s+1$ dimensional Laplace (Poisson) equations.

The key observation is that if ν is an axially symmetric solution to the Laplace equation, then $\frac{\mathrm{d}^n \nu}{\mathrm{d}z^n}$ for $n \in \mathbb{N}$ is also a solution. Let us consider the equation for the generalized axially symmetric Laplace (Poisson) equation in a flat space of the dimension $(2s + 3)$ (for integer and half-integer spin values $s \ge -1/2$),

$$\frac{\partial^2 \nu_{(s)}}{\partial z^2} + \frac{\partial^2 \nu_{(s)}}{\partial \rho^2} + \frac{1 + 2s}{\rho} \frac{\partial \nu_{(s)}}{\partial \rho} \equiv \Delta_s \nu_{(s)} = \sigma(\rho, z)\,. \tag{80}$$

Now, the generalized Laplace equation can be also extended to spins $s < -1/2$, since it holds

$$\Delta_{-s}\nu_{(-s)} = \rho^{2s}\,\Delta_s\left[\rho^{-2s}\nu_{(-s)}\right]. \tag{81}$$

The Kelvin transformation can be extended to work for arbitrary s as well, because

$$\mathcal{K}\nu_{(s)}(\rho,z) \equiv \left(\frac{b}{\rho^2+z^2}\right)^{2s+1}\nu_{(s)}\left(\frac{b^2\rho}{\rho^2+z^2},\frac{b^2 z}{\rho^2+z^2}\right) \tag{82}$$

solves (80) if $\nu_{(s)}$ is a solution (with the density adjusted appropriately).

One can find identities between the different-s solutions of (80). If $\nu_{(s)}$ satisfies

$$\Delta_s\nu_{(s)} = \sigma(\rho,z)\,, \tag{83}$$

then it holds

$$\Delta_{s+1}\left[\frac{1}{\rho}\frac{\partial\nu_{(s)}}{\partial\rho}\right] = \frac{1}{\rho}\frac{\partial}{\partial\rho}\,\Delta_s\nu_{(s)} = \frac{1}{\rho}\frac{\partial\sigma(\rho,z)}{\partial\rho} \tag{84}$$

and

$$\Delta_{s-1}\left[\frac{1}{\rho^{2s-1}}\frac{\partial\rho^{2s}\nu_{(s)}}{\partial\rho}\right] = \frac{1}{\rho^{2s-1}}\frac{\partial}{\partial\rho}\,\rho^{2s}\Delta_s\nu_{(s)} = \frac{1}{\rho^{2s-1}}\frac{\partial}{\partial\rho}\,\rho^{2s}\sigma(\rho,z)\,. \tag{85}$$

Therefore, from known solutions $\nu_{(s)}$ of the Laplace equation, we can generate new solutions $\nu_{(s\pm1)}$ with the source density distributions given by (84) and (85).

It is then natural to introduce spin-raising and spin-lowering operators as follows,

$$\mathcal{S}^s_{s+1}\nu_{(s)} \equiv \frac{\kappa^2}{\rho}\frac{\partial\nu_{(s)}}{\partial\rho} \quad\text{and}\quad \mathcal{S}^s_{s-1}\nu_{(s)} \equiv \frac{1}{\rho^{2s-1}}\frac{\partial\rho^{2s}\nu_{(s)}}{\partial\rho}\,, \tag{86}$$

where κ is a constant of the dimension of length. As a seed potential-density pair we choose one of the solutions provided in [6], in particular the one which describes the field of a thin infinite annular disk extending from $\rho = b$ to $\rho = \infty$ lying in the $z = 0$ plane. Namely[2]

$$\nu^{(-3)}_{(0)}(\rho,z) = \frac{\sigma_c\,b^2}{2\pi}\left[\frac{2\pi b|z|}{(\rho^2+z^2)^{3/2}}H\left(b-\frac{\rho\,b^2}{\rho^2+z^2}\right) - \frac{4\sqrt{\rho b}}{k(\rho^2+z^2)}E(k) - \frac{(\rho^2+\rho b+z^2)(\rho^2-\rho b+z^2)k}{\sqrt{\rho b}\,(\rho^2+z^2)^2}K(k) - \right.$$
$$\left. - \frac{\rho^2-\rho b+z^2}{\rho^2+\rho b+z^2}\frac{b^2\,z^2\,k}{(\rho^2+z^2)^2\sqrt{\rho b}}\Pi\left(\frac{4b\rho(\rho^2+z^2)}{(\rho^2+b\rho+z^2)^2},k\right)\right] \tag{87}$$

$$\sigma^{(-3)}_{(0)}(\rho,z) = \frac{\sigma_c}{2\pi}\frac{b^3}{\rho^3}H(\rho-b)\delta(z)\,, \tag{88}$$

where σ_c is a constant with the dimension of surface density (inverse length), H is the Heaviside step function, and K, E, Π are the complete elliptic integrals of the first, the second, and the third kind with the modulus

$$k = \frac{2\sqrt{\rho b}}{\sqrt{(\rho+b)^2+z^2}}\,. \tag{89}$$

Applying the spin operators (86) to the potentials of the type $\nu^{(-3)}_{(0)}$ introduces derivatives of the Heaviside step function, which adds an artificial distributional source to the edge of the disk. To get rid of that, one has to subtract the potential of a ring with a uniform density, satisfying

$$\Delta_s\nu^{(\delta)}_{(s)} = \frac{1}{2\pi}\delta(\rho-b)\delta(z)\,. \tag{90}$$

The recurrence relations are thus obtained

$$\nu^{(-3-2l)}_{(0)} = -\frac{1}{2l+1}\left[\mathcal{S}^{-1}_0\nu^{(-1-2l)}_{(-1)} - \left(\frac{\kappa}{b}\right)^{2l+2}\nu^{(\delta)}_{(0)}\right], \tag{91}$$

$$\nu^{(-2l-1)}_{(-1)} = -\frac{1}{2l+1}\left[\mathcal{S}^{0}_{-1}\nu^{(-2l-1)}_{(0)} - \left(\frac{\kappa}{b}\right)^{2l+2}\nu^{(\delta)}_{(-1)}\right], \tag{92}$$

where $\kappa^2 = b^3\sigma_c$, and $\nu^{(\delta)}_{(0)}, \nu^{(\delta)}_{(-1)}$ are solutions of (90) with $s = 0, -1$, respectively, namely

$$\nu^{(\delta)}_{(0)} = -\frac{b}{\pi}\frac{K(k)}{\sqrt{(\rho-b)^2+z^2}}\,. \tag{93}$$

$$\nu^{(\delta)}_{(-1)} = \frac{1}{2\pi b}\left[\sqrt{(\rho-b)^2+z^2}E(k) - \right. \tag{94}$$

$$\left. - \frac{(\rho^2+b^2+z^2)K(k)}{\sqrt{(\rho-b)^2+z^2}}\right]. \tag{95}$$

[2] Note that normalization is different from [6].

In this way, we design disks with the surface density profile proportional to ρ^{-2l-3} from the seed solution $\nu^{(-3)}_{(0)}$. The Kelvin transformation then automatically provides $\nu^{(2l)}_{(0)}$, thus the densities proportional to ρ^{2l}. This construction works for any monotonous density profile, but a closed-form formula for the density ρ^{-2} is not yet known.

VI. CONCLUSIONS

We have revisited the topic of thin disks as sources of the Weyl class of spacetimes and proposed a new general method for obtaining their density and potential. The method can be understood in two ways: (*i*) Kuzmin's idea [10] and the Appell's trick [22] are combined in such way that the gravitational field is obtained from the field of a line distribution of matter described by the weight function $f(w)$ (an Abel transform of the Newtonian surface density) placed on the imaginary extension of the z axis, cut and mirrored with respect to the equatorial plane; (*ii*) a certain superposition (convolution) of Appell rings of radius w is made as weighted by the weight function $f(w)$. We showed on particular examples that the procedure is capable of reproducing various thin-disk solutions known from the literature. Moreover, it has proved useful in deriving the second metric function λ which is only rarely known explicitly. Indeed, we provided the whole metric in closed forms for the general holey Morgan-Morgan disks and their superposition with a Schwarzschild black hole. Finally, we also showed that the polynomial and power-law disks treated in [6] can be obtained by an easier procedure.

To conclude, let us acknowledge that Letelier & Oliveira [26] actually discovered the relation (39) for the zeroth member of the Morgan-Morgan family. Also, Klein [27] used a similar type of integration to construct inverted isochrone disks around Schwarzschild black holes, although he did not give the explicit form of the potential nor the second metric function λ. Anyway, the method presented here is completely general and can be applied to any thin-disk solution within the Weyl class of spacetimes.

ACKNOWLEDGMENTS

We are thankful for support from the grant GACR 21-11268S of the Czech Science Foundation.

Appendix A: The second metric function λ for the (inverted) generalized Morgan-Morgan disks

In the following, we list explicit results for the second metric function $\lambda_{\rm disk}$ for the (inverted) holey Morgan-Morgan disks, and the interaction part $\lambda_{\rm int}$ for their superposition with the black hole. We also provide a Mathematica notebook containing full expressions in the Supplement Material.

1. Holey Morgan-Morgan disks

a. Qudratic λ_{disk}: A general expression for the second metric function of the holey Morgan-Morgan disks (66) reads

$$\lambda^{(m,n)}_{\rm hMM} = \mathcal{C}^{(m,n)}_{\rm hMM}\left[\frac{\left(\frac{3}{2}\right)_{m+n}}{m!\left(\frac{1}{2}\right)_n}\right]^2 \frac{\mathcal{M}^2}{b^2}(\xi^2-1)\left[\mathcal{P}^{(m,n)}_{0,\rm hMM} + 2\zeta\mathcal{P}^{(m,n)}_{1,\rm hMM}\,\mathrm{arccot}(\zeta) + (\zeta^2+1)\mathcal{P}^{(m,n)}_{2,\rm hMM}\,\mathrm{arccot}^2(\zeta)\right], \tag{A1}$$

where $\mathcal{C}^{(m,n)}_{\rm hMM}$ are numerical constants and $\mathcal{P}^{(m,n)}_{j,\rm hMM}$ are polynomials in (ζ,ξ). The first few members read

$$\mathcal{C}^{(0,1)}_{\rm hMM} = \frac{1}{16} \tag{A2}$$

$$\mathcal{P}^{(0,1)}_{0,\rm hMM} = (9\zeta^2+4)\xi^2 - \zeta^2 + 4 \tag{A3}$$

$$\mathcal{P}^{(0,1)}_{1,\rm hMM} = -(9\zeta^2+7)\xi^2 + \zeta^2 - 1 \tag{A4}$$

$$\mathcal{P}^{(0,1)}_{2,\rm hMM} = \zeta^2(9\xi^2-1) + \xi^2 - 1 \tag{A5}$$

$$\mathcal{C}^{(0,2)}_{\rm hMM} = \frac{1}{2048} \tag{A6}$$

$$\begin{aligned}\mathcal{P}^{(0,2)}_{0,\rm hMM} = {} & 11025\zeta^6\xi^6 - 11475\zeta^6\xi^4 + 2835\zeta^6\xi^2 - 81\zeta^6 + 15150\zeta^4\xi^6 - 10890\zeta^4\xi^4 + 1098\zeta^4\xi^2 + 18\zeta^4 + 4945\zeta^2\xi^6 \\ & - 723\zeta^2\xi^4 - 45\zeta^2\xi^2 - 81\zeta^2 + 256\xi^6 + 256\xi^4 + 256\xi^2 + 256\end{aligned} \tag{A7}$$

$$\mathcal{P}^{(0,2)}_{1,\rm hMM} = -3(3675\zeta^6\xi^6 - 3825\zeta^6\xi^4 + 945\zeta^6\xi^2 - 27\zeta^6 + 6275\zeta^4\xi^6 - 4905\zeta^4\xi^4 + 681\zeta^4\xi^2 - 3\zeta^4 + 3005\zeta^2\xi^6 - 1111\zeta^2\xi^4$$

$$- 105\zeta^2\xi^2 + 3\zeta^2 + 357\xi^6 + 113\xi^4 + 15\xi^2 + 27) \tag{A8}$$

$$\mathcal{P}^{(0,2)}_{2,\mathrm{hMM}} = 9(1225\zeta^6\xi^6 - 1275\zeta^6\xi^4 + 315\zeta^6\xi^2 - 9\zeta^6 + 1275\zeta^4\xi^6 - 785\zeta^4\xi^4 + 17\zeta^4\xi^2 + 5\zeta^4 + 315\zeta^2\xi^6 - 17\zeta^2\xi^4 - 47\zeta^2\xi^2 + 5\zeta^2 + 9\xi^6 + 5\xi^4 - 5\xi^2 - 9) \tag{A9}$$

$$\mathcal{C}^{(1,1)}_{\mathrm{hMM}} = \frac{1}{6144} \tag{A10}$$

$$\mathcal{P}^{(1,1)}_{0,\mathrm{hMM}} = 33075\zeta^6\xi^6 - 34425\zeta^6\xi^4 + 8505\zeta^6\xi^2 - 243\zeta^6 + 45450\zeta^4\xi^6 - 52830\zeta^4\xi^4 + 14814\zeta^4\xi^2 - 522\zeta^4 + 14835\zeta^2\xi^6 - 20409\zeta^2\xi^4 + 5625\zeta^2\xi^2 - 51\zeta^2 + 768\xi^6 - 1280\xi^4 + 256\xi^2 + 256 \tag{A11}$$

$$\mathcal{P}^{(1,1)}_{1,\mathrm{hMM}} = -3(11025\zeta^6\xi^6 - 11475\zeta^6\xi^4 + 2835\zeta^6\xi^2 - 81\zeta^6 + 18825\zeta^4\xi^6 - 21435\zeta^4\xi^4 + 5883\zeta^4\xi^2 - 201\zeta^4 + 9015\zeta^2\xi^6 - 11653\zeta^2\xi^4 + 3525\zeta^2\xi^2 - 119\zeta^2 + 1071\xi^6 - 1645\xi^4 + 557\xi^2 + 17) \tag{A12}$$

$$\mathcal{P}^{(1,1)}_{2,\mathrm{hMM}} = 3(11025\zeta^6\xi^6 - 11475\zeta^6\xi^4 + 2835\zeta^6\xi^2 - 81\zeta^6 + 11475\zeta^4\xi^6 - 13785\zeta^4\xi^4 + 3993\zeta^4\xi^2 - 147\zeta^4 + 2835\zeta^2\xi^6 - 3993\zeta^2\xi^4 + 1497\zeta^2\xi^2 - 83\zeta^2 + 81\xi^6 - 147\xi^4 + 83\xi^2 - 17) \tag{A13}$$

$$\mathcal{C}^{(1,2)}_{\mathrm{hMM}} = \frac{1}{983040} \tag{A14}$$

$$\begin{aligned}\mathcal{P}^{(1,2)}_{0,\mathrm{hMM}} = {} & 60031125\zeta^{10}\xi^{10} - 121550625\zeta^{10}\xi^8 + 84341250\zeta^{10}\xi^6 - 23231250\zeta^{10}\xi^4 + 2165625\zeta^{10}\xi^2 - 28125\zeta^{10} \\ & + 141561000\zeta^8\xi^{10} - 278359200\zeta^8\xi^8 + 186202800\zeta^8\xi^6 - 48904800\zeta^8\xi^4 + 4276200\zeta^8\xi^2 - 52800\zeta^8 \\ & + 115519950\zeta^6\xi^{10} - 218461950\zeta^6\xi^8 + 137270700\zeta^6\xi^6 - 32294300\zeta^6\xi^4 + 2275750\zeta^6\xi^2 - 17030\zeta^6 \\ & + 37963800\zeta^4\xi^{10} - 68050080\zeta^4\xi^8 + 37925520\zeta^4\xi^6 - 6760800\zeta^4\xi^4 + 220440\zeta^4\xi^2 - 960\zeta^4 \\ & + 4282845\zeta^2\xi^{10} - 7093665\zeta^2\xi^8 + 2940690\zeta^2\xi^6 - 127890\zeta^2\xi^4 + 225\zeta^2\xi^2 - 2205\zeta^2 \\ & + 81920\xi^{10} - 114688\xi^8 + 8192\xi^6 + 8192\xi^4 + 8192\xi^2 + 8192\end{aligned} \tag{A15}$$

$$\begin{aligned}\mathcal{P}^{(1,2)}_{1,\mathrm{hMM}} = {} & -15(4002075\zeta^{10}\xi^{10} - 8103375\zeta^{10}\xi^8 + 5622750\zeta^{10}\xi^6 - 1548750\zeta^{10}\xi^4 + 144375\zeta^{10}\xi^2 - 1875\zeta^{10} \\ & + 10771425\zeta^8\xi^{10} - 21258405\zeta^8\xi^8 + 14287770\zeta^8\xi^6 - 3776570\zeta^8\xi^4 + 333205\zeta^8\xi^2 - 4145\zeta^8 + 10491390\zeta^6\xi^{10} \\ & - 20029590\zeta^6\xi^8 + 12789420\zeta^6\xi^6 - 3102060\zeta^6\xi^4 + 233910\zeta^6\xi^2 - 2142\zeta^6 + 4445490\zeta^4\xi^{10} - 8119146\zeta^4\xi^8 \\ & + 4737204\zeta^4\xi^6 - 941460\zeta^4\xi^4 + 40506\zeta^4\xi^2 + 222\zeta^4 + 763175\zeta^2\xi^{10} - 1309915\zeta^2\xi^8 + 635126\zeta^2\xi^6 - 63046\zeta^2\xi^4 \\ & - 5485\zeta^2\xi^2 + 113\zeta^2 + 36525\xi^{10} - 57009\xi^8 + 16434\xi^6 + 3918\xi^4 - 15\xi^2 + 147)\end{aligned} \tag{A16}$$

$$\begin{aligned}\mathcal{P}^{(1,2)}_{2,\mathrm{hMM}} = {} & 45(1334025\zeta^{10}\xi^{10} - 2701125\zeta^{10}\xi^8 + 1874250\zeta^{10}\xi^6 - 516250\zeta^{10}\xi^4 + 48125\zeta^{10}\xi^2 - 625\zeta^{10} + 2701125\zeta^8\xi^{10} \\ & - 5285385\zeta^8\xi^8 + 3513090\zeta^8\xi^6 - 914690\zeta^8\xi^4 + 78985\zeta^8\xi^2 - 965\zeta^8 + 1874250\zeta^6\xi^{10} - 3513090\zeta^6\xi^8 \\ & + 2170980\zeta^6\xi^6 - 493060\zeta^6\xi^4 + 31730\zeta^6\xi^2 - 154\zeta^6 + 516250\zeta^4\xi^{10} - 914690\zeta^4\xi^8 + 493060\zeta^4\xi^6 - 74500\zeta^4\xi^4 \\ & - 1918\zeta^4\xi^2 + 230\zeta^4 + 48125\zeta^2\xi^{10} - 78985\zeta^2\xi^8 + 31730\zeta^2\xi^6 + 1918\zeta^2\xi^4 - 1247\zeta^2\xi^2 - 5\zeta^2 + 625\xi^{10} - 965\xi^8 \\ & + 154\xi^6 + 230\xi^4 + 5\xi^2 - 49)\end{aligned} \tag{A17}$$

$$\mathcal{C}^{(2,1)}_{\mathrm{hMM}} = \frac{1}{983040} \tag{A18}$$

$$\begin{aligned}\mathcal{P}^{(2,1)}_{0,\mathrm{hMM}} = {} & 60031125\zeta^{10}\xi^{10} - 121550625\zeta^{10}\xi^8 + 84341250\zeta^{10}\xi^6 - 23231250\zeta^{10}\xi^4 + 2165625\zeta^{10}\xi^2 - 28125\zeta^{10} \\ & + 141561000\zeta^8\xi^{10} - 313286400\zeta^8\xi^8 + 239727600\zeta^8\xi^6 - 73701600\zeta^8\xi^4 + 7775400\zeta^8\xi^2 - 117600\zeta^8 \\ & + 115519950\zeta^6\xi^{10} - 283629150\zeta^6\xi^8 + 242657100\zeta^6\xi^6 - 84343100\zeta^6\xi^4 + 10217350\zeta^6\xi^2 - 184070\zeta^6 \\ & + 37963800\zeta^4\xi^{10} - 105255360\zeta^4\xi^8 + 102564240\zeta^4\xi^6 - 40778400\zeta^4\xi^4 + 5627160\zeta^4\xi^2 - 113760\zeta^4 \\ & + 4282845\zeta^2\xi^{10} - 13747905\zeta^2\xi^8 + 15665970\zeta^2\xi^6 - 7221810\zeta^2\xi^4 + 1024065\zeta^2\xi^2 - 3165\zeta^2 + 81920\xi^{10} \\ & - 311296\xi^8 + 425984\xi^6 - 229376\xi^4 + 16384\xi^2 + 16384\end{aligned} \tag{A19}$$

$$\begin{aligned}\mathcal{P}^{(2,1)}_{1,\mathrm{hMM}} = {} & -15(4002075\zeta^{10}\xi^{10} - 8103375\zeta^{10}\xi^8 + 5622750\zeta^{10}\xi^6 - 1548750\zeta^{10}\xi^4 + 144375\zeta^{10}\xi^2 - 1875\zeta^{10} \\ & + 10771425\zeta^8\xi^{10} - 23586885\zeta^8\xi^8 + 17856090\zeta^8\xi^6 - 5429690\zeta^8\xi^4 + 566485\zeta^8\xi^2 - 8465\zeta^8 \\ & + 10491390\zeta^6\xi^{10} - 25150230\zeta^6\xi^8 + 21004620\zeta^6\xi^6 - 7123020\zeta^6\xi^4 + 841110\zeta^6\xi^2 - 14718\zeta^6 + 4445490\zeta^4\xi^{10} \\ & - 11840682\zeta^4\xi^8 + 11071188\zeta^4\xi^6 - 4240500\zeta^4\xi^4 + 571034\zeta^4\xi^2 - 11650\zeta^4 + 763175\zeta^2\xi^{10} - 2302555\zeta^2\xi^8 \\ & + 2459990\zeta^2\xi^6 - 1083494\zeta^2\xi^4 + 165811\zeta^2\xi^2 - 3439\zeta^2 + 36525\xi^{10} - 127953\xi^8 + 160850\xi^6 - 83794\xi^4\end{aligned}$$

$$+ 14161\xi^2 + 211) \tag{A20}$$

$$\begin{aligned}\mathcal{P}^{(2,1)}_{2,\mathrm{hMM}} = 15(&4002075\zeta^{10}\xi^{10} - 8103375\zeta^{10}\xi^8 + 5622750\zeta^{10}\xi^6 - 1548750\zeta^{10}\xi^4 + 144375\zeta^{10}\xi^2 - 1875\zeta^{10} + 8103375\zeta^8\xi^{10} \\ &- 18184635\zeta^8\xi^8 + 14107590\zeta^8\xi^6 - 4397190\zeta^8\xi^4 + 470235\zeta^8\xi^2 - 7215\zeta^8 + 5622750\zeta^6\xi^{10} - 14107590\zeta^6\xi^8 \\ &+ 12349260\zeta^6\xi^6 - 4398060\zeta^6\xi^4 + 546870\zeta^6\xi^2 - 10158\zeta^6 + 1548750\zeta^4\xi^{10} - 4397190\zeta^4\xi^8 + 4398060\zeta^4\xi^6 \\ &- 1818540\zeta^4\xi^4 + 269094\zeta^4\xi^2 - 6318\zeta^4 + 144375\zeta^2\xi^{10} - 470235\zeta^2\xi^8 + 546870\zeta^2\xi^6 - 269094\zeta^2\xi^4 + 50307\zeta^2\xi^2 \\ &- 1711\zeta^2 + 1875\xi^{10} - 7215\xi^8 + 10158\xi^6 - 6318\xi^4 + 1711\xi^2 - 211)\end{aligned} \tag{A21}$$

$$\mathcal{C}^{(2,2)}_{\mathrm{hMM}} = \frac{1}{21139292160} \tag{A22}$$

$$\begin{aligned}\mathcal{P}^{(2,2)}_{0,\mathrm{hMM}} = &15978784696875\zeta^{14}\xi^{14} - 48220421374125\zeta^{14}\xi^{12} + 56556703578375\zeta^{14}\xi^{10} - 32478448550625\zeta^{14}\xi^8 \\ &+ 9431153510625\zeta^{14}\xi^6 - 1280535834375\zeta^{14}\xi^4 + 63814078125\zeta^{14}\xi^2 - 472696875\zeta^{14} + 53546682939750\zeta^{12}\xi^{14} \\ &- 163921910402250\zeta^{12}\xi^{12} + 195401453766750\zeta^{12}\xi^{10} - 114310631531250\zeta^{12}\xi^8 + 33912309611250\zeta^{12}\xi^6 \\ &- 4721464518750\zeta^{12}\xi^4 + 242354306250\zeta^{12}\xi^2 - 1878843750\zeta^{12} + 70144588639125\zeta^{10}\xi^{14} \\ &- 218331077008275\zeta^{10}\xi^{12} + 264573915831225\zeta^{10}\xi^{10} - 157245484449375\zeta^{10}\xi^8 + 47328582215775\zeta^{10}\xi^6 \\ &- 6667480157625\zeta^{10}\xi^4 + 344764777875\zeta^{10}\xi^2 - 2706591125\zeta^{10} + 45300791358900\zeta^8\xi^{14} \\ &- 143774916446700\zeta^8\xi^{12} + 177053751144900\zeta^8\xi^{10} - 106350197324700\zeta^8\xi^8 + 32049674367900\zeta^8\xi^6 \\ &- 4445363304900\zeta^8\xi^4 + 219341509100\zeta^8\xi^2 - 1563454900\zeta^8 + 14914843730325\zeta^6\xi^{14} - 48441884967315\zeta^6\xi^{12} \\ &+ 60540898489785\zeta^6\xi^{10} - 36386505134175\zeta^6\xi^8 + 10693987893855\zeta^6\xi^6 - 1374141802425\zeta^6\xi^4 \\ &+ 55823145875\zeta^6\xi^2 - 227556245\zeta^6 + 2318953337190\zeta^4\xi^{14} - 7743583874250\zeta^4\xi^{12} + 9790161391710\zeta^4\xi^{10} \\ &- 5770162221810\zeta^4\xi^8 + 1558297174770\zeta^4\xi^6 - 156345952350\zeta^4\xi^4 + 2730718410\zeta^4\xi^2 - 9285990\zeta^4 \\ &+ 133728684075\zeta^2\xi^{14} - 462058266285\zeta^2\xi^{12} + 586633472775\zeta^2\xi^{10} - 323550305505\zeta^2\xi^8 + 66781739745\zeta^2\xi^6 \\ &- 1531728135\zeta^2\xi^4 + 6065325\zeta^2\xi^2 - 9661995\zeta^2 + 1321205760\xi^{14} - 4718592000\xi^{12} + 5851054080\xi^{10} \\ &- 2604662784\xi^8 + 37748736\xi^6 + 37748736\xi^4 + 37748736\xi^2 + 37748736\end{aligned} \tag{A23}$$

$$\begin{aligned}\mathcal{P}^{(2,2)}_{1,\mathrm{hMM}} = -105(&152178901875\zeta^{14}\xi^{14} - 459242108325\zeta^{14}\xi^{12} + 538635272175\zeta^{14}\xi^{10} - 309318557625\zeta^{14}\xi^8 \\ &+ 89820509625\zeta^{14}\xi^6 - 12195579375\zeta^{14}\xi^4 + 607753125\zeta^{14}\xi^2 - 4501875\zeta^{14} + 560694709575\zeta^{12}\xi^{14} \\ &- 1714241754225\zeta^{12}\xi^{12} + 2040511317075\zeta^{12}\xi^{10} - 1191778867125\zeta^{12}\xi^8 + 352914547125\zeta^{12}\xi^6 \\ &- 49031521875\zeta^{12}\xi^4 + 2510720625\zeta^{12}\xi^2 - 19394375\zeta^{12} + 824506157475\zeta^{10}\xi^{14} - 2558909086965\zeta^{10}\xi^{12} \\ &+ 3092194963935\zeta^{10}\xi^{10} - 1832971953225\zeta^{10}\xi^8 + 550422482505\zeta^{10}\xi^6 - 77404535775\zeta^{10}\xi^4 \\ &+ 3998830325\zeta^{10}\xi^2 - 31341475\zeta^{10} + 615872395215\zeta^8\xi^{14} - 1945012278825\zeta^8\xi^{12} + 2385803488635\zeta^8\xi^{10} \\ &- 1429682265165\zeta^8\xi^8 + 430957746765\zeta^8\xi^6 - 60074226555\zeta^8\xi^4 + 3006587945\zeta^8\xi^2 - 22101455\zeta^8 \\ &+ 245626175025\zeta^6\xi^{14} - 791771672535\zeta^6\xi^{12} + 985062075525\zeta^6\xi^{10} - 592389903795\zeta^6\xi^8 + 175814410163\zeta^6\xi^6 \\ &- 23237084805\zeta^6\xi^4 + 1013428695\zeta^6\xi^2 - 5099569\zeta^6 + 50107809885\zeta^4\xi^{14} - 165506270475\zeta^4\xi^{12} \\ &+ 208418460705\zeta^4\xi^{10} - 124037312951\zeta^4\xi^8 + 34794346423\zeta^4\xi^6 - 3880100385\zeta^4\xi^4 + 92470027\zeta^4\xi^2 + 635299\zeta^4 \\ &+ 4487127225\zeta^2\xi^{14} - 15264485775\zeta^2\xi^{12} + 19370425773\zeta^2\xi^{10} - 11084212811\zeta^2\xi^8 + 2643918923\zeta^2\xi^6 \\ &- 142791597\zeta^2\xi^4 - 10494065\zeta^2\xi^2 + 119111\zeta^2 + 115920525\xi^{14} - 408771675\xi^{12} + 517889553\xi^{10} \\ &- 266212935\xi^8 + 34318407\xi^6 + 6821871\xi^4 - 57765\xi^2 + 92019)\end{aligned} \tag{A24}$$

$$\begin{aligned}\mathcal{P}^{(2,2)}_{2,\mathrm{hMM}} = 315(&50726300625\zeta^{14}\xi^{14} - 153080702775\zeta^{14}\xi^{12} + 179545090725\zeta^{14}\xi^{10} - 103106185875\zeta^{14}\xi^8 \\ &+ 29940169875\zeta^{14}\xi^6 - 4065193125\zeta^{14}\xi^4 + 202584375\zeta^{14}\xi^2 - 1500625\zeta^{14} + 153080702775\zeta^{12}\xi^{14} \\ &- 469360116225\zeta^{12}\xi^{12} + 560473711875\zeta^{12}\xi^{10} - 328522165125\zeta^{12}\xi^8 + 97678069125\zeta^{12}\xi^6 \\ &- 13633711875\zeta^{12}\xi^4 + 701850625\zeta^{12}\xi^2 - 5464375\zeta^{12} + 179545090725\zeta^{10}\xi^{14} - 560473711875\zeta^{10}\xi^{12} \\ &+ 681021858825\zeta^{10}\xi^{10} - 405723365775\zeta^{10}\xi^8 + 122347470735\zeta^{10}\xi^6 - 17254396425\zeta^{10}\xi^4 + 892054275\zeta^{10}\xi^2 \\ &- 7004325\zeta^{10} + 103106185875\zeta^8\xi^{14} - 328522165125\zeta^8\xi^{12} + 405723365775\zeta^8\xi^{10} - 243989684505\zeta^8\xi^8\end{aligned}$$

$$+ 73400477465\zeta^8\xi^6 - 10107342735\zeta^8\xi^4 + 489496965\zeta^8\xi^2 - 3340435\zeta^8 + 29940169875\zeta^6\xi^{14}$$
$$- 97678069125\zeta^6\xi^{12} + 122347470735\zeta^6\xi^{10} - 73400477465\zeta^6\xi^8 + 21340529945\zeta^6\xi^6 - 2643619215\zeta^6\xi^4$$
$$+ 92812165\zeta^6\xi^2 + 3437\zeta^6 + 4065193125\zeta^4\xi^{14} - 13633711875\zeta^4\xi^{12} + 17254396425\zeta^4\xi^{10} - 10107342735\zeta^4\xi^8$$
$$+ 2643619215\zeta^4\xi^6 - 219088905\zeta^4\xi^4 - 5739261\zeta^4\xi^2 + 314715\zeta^4 + 202584375\zeta^2\xi^{14} - 701850625\zeta^2\xi^{12}$$
$$+ 892054275\zeta^2\xi^{10} - 489496965\zeta^2\xi^8 + 92812165\zeta^2\xi^6 + 5739261\zeta^2\xi^4 - 1692159\zeta^2\xi^2 - 19255\zeta^2 + 1500625\xi^{14}$$
$$- 5464375\xi^{12} + 7004325\xi^{10} - 3340435\xi^8 - 3437\xi^6 + 314715\xi^4 + 19255\xi^2 - 30673) \tag{A25}$$

b. Interaction part λ_{int}: When a holey Morgan-Morgan disk is superposed with the Schwarzschild black hole, a general expression for the interaction part reads

$$\lambda^{(m,n)}_{\mathrm{hMM,int}} = \mathscr{K}^{(m,n)}_{0,\mathrm{hMM}} + \mathscr{K}^{(m,n)}_{1,\mathrm{hMM}} \left\{ \operatorname{atan2} \begin{bmatrix} b\xi - M\zeta \\ R_-(\zeta,\xi) \end{bmatrix} - \operatorname{atan2} \begin{bmatrix} b\xi + M\zeta \\ R_+(\zeta,\xi) \end{bmatrix} \right\} +$$
$$+ \mathscr{K}^{(m,n)}_{2,\mathrm{hMM}} \sum_{\mp} R_{\mp}(\zeta,\xi) \left[\pm \mathscr{P}^{(m,n)}_{0,\mathrm{hMM}}(\pm\zeta,\xi) + \mathscr{P}^{(m,n)}_{1,\mathrm{hMM}}(\pm\zeta,\xi) \operatorname{arccot}(\zeta) \right], \tag{A26}$$

where $\operatorname{atan2}(\frac{y}{x}) \equiv \operatorname{atan2}(y,x)$ denotes 2-argument arcus tangent, $R_\pm(\zeta,\xi)$ comes from the Schwarzschild potential (22) transformed to the oblate spheroidal coordinates (12), $\mathscr{K}^{(m,n)}_{j,\mathrm{hMM}}$ stands for constants which depend on the disk parameters, and $\mathscr{P}^{(m,n)}_{j,\mathrm{hMM}}$ are polynomials in ζ and ξ. A few first members read

$$\mathscr{K}^{(1,1)}_{0,\mathrm{hMM}} = \frac{15\mathcal{M}}{16b^5} \left[-\pi b^4 + 2b^3 M + 2\pi b^2 M^2 + 2(b^2 - 3M^2)(b^2 + M^2) \arctan\left(\frac{b}{M}\right) + 6bM^3 + 3\pi M^4 \right] \tag{A27}$$

$$\mathscr{K}^{(1,1)}_{1,\mathrm{hMM}} = \frac{15\mathcal{M}}{16b^5}(b^2 - 3M^2)(b^2 + M^2) \tag{A28}$$

$$\mathscr{K}^{(1,1)}_{2,\mathrm{hMM}} = -\frac{15\mathcal{M}}{32b^5} \tag{A29}$$

$$\mathscr{P}^{(1,1)}_{0,\mathrm{hMM}} = b(15b^2\zeta^2\xi^3 - 9b^2\zeta^2\xi + 4b^2\xi^3 - 2b^2\xi - 9b\zeta M\xi^2 + 3b\zeta M + 6M^2\xi) \tag{A30}$$

$$\mathscr{P}^{(1,1)}_{1,\mathrm{hMM}} = -15b^3\zeta^3\xi^3 + 9b^3\zeta^3\xi - 9b^3\zeta\xi^3 + 5b^3\zeta\xi + 9b^2\zeta^2 M\xi^2 - 3b^2\zeta^2 M + 3b^2 M\xi^2 + b^2 M - 6b\zeta M^2\xi + 6M^3 \tag{A31}$$

$$\mathscr{K}^{(1,2)}_{0,\mathrm{hMM}} = \frac{35\mathcal{M}}{96b^7} \left[6b^5 M + 44b^3 M^3 - 3\pi(b^2 - 5M^2)(b^2 + M^2)^2 + 6(b^2 - 5M^2)(b^2 + M^2)^2 \arctan\left(\frac{b}{M}\right) + 30bM^5 \right] \tag{A32}$$

$$\mathscr{K}^{(1,2)}_{1,\mathrm{hMM}} = (b^2 - 5M^2)(b^2 + M^2)^2 \tag{A33}$$

$$\mathscr{K}^{(1,2)}_{2,\mathrm{hMM}} = -\frac{35\mathcal{M}}{768b^7} \tag{A34}$$

$$\mathscr{P}^{(1,2)}_{0,\mathrm{hMM}} = b(945b^4\zeta^4\xi^5 - 1050b^4\zeta^4\xi^3 + 225b^4\zeta^4\xi + 735b^4\zeta^2\xi^5 - 610b^4\zeta^2\xi^3 + 51b^4\zeta^2\xi + 64b^4\xi^5 - 16b^4\xi^3 - 24b^4\xi$$
$$- 525b^3\zeta^3 M\xi^4 + 450b^3\zeta^3 M\xi^2 - 45b^3\zeta^3 M - 275b^3\zeta M\xi^4 + 66b^3\zeta M\xi^2 + 33b^3\zeta M + 300b^2\zeta^2 M^2\xi^3$$
$$- 180b^2\zeta^2 M^2\xi + 80b^2 M^2\xi^3 + 96b^2 M^2\xi - 180b\zeta M^3\xi^2 + 60b\zeta M^3 + 120M^4\xi) \tag{A35}$$

$$\mathscr{P}^{(1,2)}_{1,\mathrm{hMM}} = -3(315b^5\zeta^5\xi^5 - 350b^5\zeta^5\xi^3 + 75b^5\zeta^5\xi + 350b^5\zeta^3\xi^5 - 320b^5\zeta^3\xi^3 + 42b^5\zeta^3\xi + 75b^5\zeta\xi^5 - 42b^5\zeta\xi^3 - 9b^5\zeta\xi$$
$$- 175b^4\zeta^4 M\xi^4 + 150b^4\zeta^4 M\xi^2 - 15b^4\zeta^4 M - 150b^4\zeta^2 M\xi^4 + 72b^4\zeta^2 M\xi^2 + 6b^4\zeta^2 M - 15b^4 M\xi^4 - 6b^4 M\xi^2$$
$$- 3b^4 M + 100b^3\zeta^3 M^2\xi^3 - 60b^3\zeta^3 M^2\xi + 60b^3\zeta M^2\xi^3 + 12b^3\zeta M^2\xi - 60b^2\zeta^2 M^3\xi^2 + 20b^2\zeta^2 M^3$$
$$- 20b^2 M^3\xi^2 - 52b^2 M^3 + 40b\zeta M^4\xi - 40M^5) \tag{A36}$$

$$\mathscr{K}^{(2,1)}_{0,\mathrm{hMM}} = \frac{35\mathcal{M}}{128b^7} \left[6b^5 M - 8b^3 M^3 - 3\pi(b^2 + M^2)(b^4 - 2b^2 M^2 + 5M^4) - 30bM^5 + \right.$$
$$\left. + 6(b^2 + M^2)(b^4 - 2b^2 M^2 + 5M^4) \arctan\left(\frac{b}{M}\right) \right] \tag{A37}$$

$$\mathscr{K}^{(2,1)}_{1,\mathrm{hMM}} = \frac{105\mathcal{M}}{128b^7}(b^2 + M^2)(b^4 - 2b^2 M^2 + 5M^4) \tag{A38}$$

$$\mathscr{K}^{(2,1)}_{2,\mathrm{hMM}} = \frac{35\mathcal{M}}{1024b^7} \tag{A39}$$

$$\mathscr{P}^{(2,1)}_{0,\mathrm{hMM}} = b(945b^4\zeta^4\xi^5 - 1050b^4\zeta^4\xi^3 + 225b^4\zeta^4\xi + 735b^4\zeta^2\xi^5 - 970b^4\zeta^2\xi^3 + 267b^4\zeta^2\xi + 64b^4\xi^5 - 112b^4\xi^3 + 24b^4\xi$$
$$- 525b^3\zeta^3M\xi^4 + 450b^3\zeta^3M\xi^2 - 45b^3\zeta^3M - 275b^3\zeta M\xi^4 + 282b^3\zeta M\xi^2 - 39b^3\zeta M + 300b^2\zeta^2M^2\xi^3$$
$$- 180b^2\zeta^2M^2\xi + 80b^2M^2\xi^3 - 48b^2M^2\xi - 180b\zeta M^3\xi^2 + 60b\zeta M^3 + 120M^4\xi) \tag{A40}$$

$$\mathscr{P}^{(2,1)}_{1,\mathrm{hMM}} = -3(315b^5\zeta^5\xi^5 - 350b^5\zeta^5\xi^3 + 75b^5\zeta^5\xi + 350b^5\zeta^3\xi^5 - 440b^5\zeta^3\xi^3 + 114b^5\zeta^3\xi + 75b^5\zeta\xi^5 - 114b^5\zeta\xi^3$$
$$+ 31b^5\zeta\xi - 175b^4\zeta^4M\xi^4 + 150b^4\zeta^4M\xi^2 - 15b^4\zeta^4M - 150b^4\zeta^2M\xi^4 + 144b^4\zeta^2M\xi^2 - 18b^4\zeta^2M$$
$$- 15b^4M\xi^4 + 18b^4M\xi^2 + 5b^4M + 100b^3\zeta^3M^2\xi^3 - 60b^3\zeta^3M^2\xi + 60b^3\zeta M^2\xi^3 - 36b^3\zeta M^2\xi - 60b^2\zeta^2M^3\xi^2$$
$$+ 20b^2\zeta^2M^3 - 20b^2M^3\xi^2 - 4b^2M^3 + 40b\zeta M^4\xi - 40M^5) \tag{A41}$$

$$\mathscr{K}^{(2,2)}_{0,\mathrm{hMM}} = \frac{105\mathcal{M}}{1024b^9}\Big[18b^7M - 30b^5M^3 - 290b^3M^5 - 3\pi(b^2+M^2)^2(3b^4 - 10b^2M^2 + 35M^4) +$$
$$+6(b^2+M^2)^2(3b^4 - 10b^2M^2 + 35M^4)\arctan\left(\frac{b}{M}\right) - 210bM^7\Big] \tag{A42}$$

$$\mathscr{K}^{(2,2)}_{1,\mathrm{hMM}} = \frac{105\mathcal{M}}{1024b^9}(b^2+M^2)^2(3b^4 - 10b^2M^2 + 35M^4) \tag{A43}$$

$$\mathscr{K}^{(2,2)}_{2,\mathrm{hMM}} = \frac{105\mathcal{M}}{16384b^9} \tag{A44}$$

$$\mathscr{P}^{(2,2)}_{0,\mathrm{hMM}} = b(45045b^6\zeta^6\xi^7 - 72765b^6\zeta^6\xi^5 + 33075b^6\zeta^6\xi^3 - 3675b^6\zeta^6\xi + 57750b^6\zeta^4\xi^7 - 91980b^6\zeta^4\xi^5 + 40950b^6\zeta^4\xi^3$$
$$- 4400b^6\zeta^4\xi + 17829b^6\zeta^2\xi^7 - 27783b^6\zeta^2\xi^5 + 10575b^6\zeta^2\xi^3 - 381b^6\zeta^2\xi + 768b^6\xi^7 - 1152b^6\xi^5 + 96b^6\xi^3$$
$$+ 144b^6\xi - 24255b^5\zeta^5M\xi^6 + 33075b^5\zeta^5M\xi^4 - 11025b^5\zeta^5M\xi^2 + 525b^5\zeta^5M - 24990b^5\zeta^3M\xi^6$$
$$+ 31500b^5\zeta^3M\xi^4 - 9150b^5\zeta^3M\xi^2 + 320b^5\zeta^3M - 4851b^5\zeta M\xi^6 + 5265b^5\zeta M\xi^4 - 441b^5\zeta M\xi^2 - 213b^5\zeta M$$
$$+ 13230b^4\zeta^4M^2\xi^5 - 14700b^4\zeta^4M^2\xi^3 + 3150b^4\zeta^4M^2\xi + 10290b^4\zeta^2M^2\xi^5 - 8900b^4\zeta^2M^2\xi^3 + 930b^4\zeta^2M^2\xi$$
$$+ 896b^4M^2\xi^5 - 320b^4M^2\xi^3 - 336b^4M^2\xi - 7350b^3\zeta^3M^3\xi^4 + 6300b^3\zeta^3M^3\xi^2 - 630b^3\zeta^3M^3$$
$$- 3850b^3\zeta M^3\xi^4 + 1140b^3\zeta M^3\xi^2 + 390b^3\zeta M^3 + 4200b^2\zeta^2M^4\xi^3 - 2520b^2\zeta^2M^4\xi + 1120b^2M^4\xi^3$$
$$+ 1200b^2M^4\xi - 2520b\zeta M^5\xi^2 + 840b\zeta M^5 + 1680M^6\xi) \tag{A45}$$

$$\mathscr{P}^{(2,2)}_{1,\mathrm{hMM}} = -3(15015b^7\zeta^7\xi^7 - 24255b^7\zeta^7\xi^5 + 11025b^7\zeta^7\xi^3 - 1225b^7\zeta^7\xi + 24255b^7\zeta^5\xi^7 - 38745b^7\zeta^5\xi^5 + 17325b^7\zeta^5\xi^3$$
$$- 1875b^7\zeta^5\xi + 11025b^7\zeta^3\xi^7 - 17325b^7\zeta^3\xi^5 + 7095b^7\zeta^3\xi^3 - 507b^7\zeta^3\xi + 1225b^7\zeta\xi^7 - 1875b^7\zeta\xi^5 + 507b^7\zeta\xi^3$$
$$+ 79b^7\zeta\xi - 8085b^6\zeta^6M\xi^6 + 11025b^6\zeta^6M\xi^4 - 3675b^6\zeta^6M\xi^2 + 175b^6\zeta^6M - 11025b^6\zeta^4M\xi^6$$
$$+ 14175b^6\zeta^4M\xi^4 - 4275b^6\zeta^4M\xi^2 + 165b^6\zeta^4M - 3675b^6\zeta^2M\xi^6 + 4275b^6\zeta^2M\xi^4 - 837b^6\zeta^2M\xi^2$$
$$- 51b^6\zeta^2M - 175b^6M\xi^6 + 165b^6M\xi^4 + 51b^6M\xi^2 + 23b^6M + 4410b^5\zeta^5M^2\xi^5 - 4900b^5\zeta^5M^2\xi^3$$
$$+ 1050b^5\zeta^5M^2\xi + 4900b^5\zeta^3M^2\xi^5 - 4600b^5\zeta^3M^2\xi^3 + 660b^5\zeta^3M^2\xi + 1050b^5\zeta M^2\xi^5 - 660b^5\zeta M^2\xi^3$$
$$- 102b^5\zeta M^2\xi - 2450b^4\zeta^4M^3\xi^4 + 2100b^4\zeta^4M^3\xi^2 - 210b^4\zeta^4M^3 - 2100b^4\zeta^2M^3\xi^4 + 1080b^4\zeta^2M^3\xi^2$$
$$+ 60b^4\zeta^2M^3 - 210b^4M^3\xi^4 - 60b^4M^3\xi^2 - 18b^4M^3 + 1400b^3\zeta^3M^4\xi^3 - 840b^3\zeta^3M^4\xi + 840b^3\zeta M^4\xi^3$$
$$+ 120b^3\zeta M^4\xi - 840b^2\zeta^2M^5\xi^2 + 280b^2\zeta^2M^5 - 280b^2M^5\xi^2 - 680b^2M^5 + 560b\zeta M^6\xi - 560M^7) \tag{A46}$$

2. Inverted holey Morgan-Morgan disks

a. Quadratic λ_{disk}: For the inverted holey Morgan-Morgan disks, a general expression for the second metric function (69) reads

$$\lambda^{(m,n)}_{\mathrm{ihMM}} = \mathcal{C}^{(m,n)}_{\mathrm{ihMM}}\left[\frac{2(m+n)!}{\pi\left(\frac{1}{2}\right)_m\left(\frac{1}{2}\right)_n}\right]^2\frac{\mathcal{M}^2}{b^2}\mathcal{K}\left\{(\xi^2-1)\left[\mathcal{P}^{(m,n)}_{0,\mathrm{ihMM}} + 2\zeta\mathcal{P}^{(m,n)}_{1,\mathrm{ihMM}}\operatorname{arccot}(\zeta) + (\zeta^2+1)\mathcal{P}^{(m,n)}_{2,\mathrm{ihMM}}\operatorname{arccot}^2(\zeta)\right]\right\}, \tag{A47}$$

where $\mathcal{P}^{(m,n)}_{j,\mathrm{ihMM}}$ are polynomials in (ζ,ξ), and $\mathcal{C}^{(m,n)}_{\mathrm{ihMM}}$ are numerical constants. For the first few members, we have explicitly

$$\mathcal{C}^{(0,1)}_{\mathrm{ihMM}} = \frac{1}{96} \tag{A48}$$

$$\mathcal{P}^{(0,1)}_{0,\mathrm{ihMM}} = 225\zeta^4\xi^4 - 126\zeta^4\xi^2 + 9\zeta^4 + 201\zeta^2\xi^4 - 96\zeta^2\xi^2 + 3\zeta^2 + 16\xi^4 - 8\xi^2 - 8 \tag{A49}$$

$$\mathcal{P}^{(0,1)}_{1,\mathrm{ihMM}} = -3(75\zeta^4\xi^4 - 42\zeta^4\xi^2 + 3\zeta^4 + 92\zeta^2\xi^4 - 46\zeta^2\xi^2 + 2\zeta^2 + 21\xi^4 - 8\xi^2 - 1) \tag{A50}$$

$$\mathcal{P}^{(0,1)}_{2,\mathrm{ihMM}} = 3(75\zeta^4\xi^4 - 42\zeta^4\xi^2 + 3\zeta^4 + 42\zeta^2\xi^4 - 18\zeta^2\xi^2 + 3\xi^4 + 1) \tag{A51}$$

$$\mathcal{C}^{(0,2)}_{\mathrm{ihMM}} = \frac{1}{40960} \tag{A52}$$

$$\begin{aligned}\mathcal{P}^{(0,2)}_{0,\mathrm{ihMM}} = {} & 893025\zeta^8\xi^8 - 1367100\zeta^8\xi^6 + 633150\zeta^8\xi^4 - 89100\zeta^8\xi^2 + 2025\zeta^8 + 1664775\zeta^6\xi^8 - 2238600\zeta^6\xi^6 \\ & + 856350\zeta^6\xi^4 - 86400\zeta^6\xi^2 + 675\zeta^6 + 949935\zeta^4\xi^8 - 1026940\zeta^4\xi^6 + 262410\zeta^4\xi^4 - 6300\zeta^4\xi^2 - 225\zeta^4 \\ & + 169705\zeta^2\xi^8 - 120320\zeta^2\xi^6 + 3930\zeta^2\xi^4 + 360\zeta^2\xi^2 + 405\zeta^2 + 4096\xi^8 - 1024\xi^6 - 1024\xi^4 - 1024\xi^2 \\ & - 1024\end{aligned} \tag{A53}$$

$$\begin{aligned}\mathcal{P}^{(0,2)}_{1,\mathrm{ihMM}} = {} & -15(59535\zeta^8\xi^8 - 91140\zeta^8\xi^6 + 42210\zeta^8\xi^4 - 5940\zeta^8\xi^2 + 135\zeta^8 + 130830\zeta^6\xi^8 - 179620\zeta^6\xi^6 + 71160\zeta^6\xi^4 \\ & - 7740\zeta^6\xi^2 + 90\zeta^6 + 95032\zeta^4\xi^8 - 110108\zeta^4\xi^6 + 32772\zeta^4\xi^4 - 1812\zeta^4\xi^2 - 12\zeta^4 + 25330\zeta^2\xi^8 - 21820\zeta^2\xi^6 \\ & + 3112\zeta^2\xi^4 + 156\zeta^2\xi^2 + 6\zeta^2 + 1785\xi^8 - 768\xi^6 - 134\xi^4 - 24\xi^2 - 27)\end{aligned} \tag{A54}$$

$$\begin{aligned}\mathcal{P}^{(0,2)}_{2,\mathrm{ihMM}} = {} & 45(19845\zeta^8\xi^8 - 30380\zeta^8\xi^6 + 14070\zeta^8\xi^4 - 1980\zeta^8\xi^2 + 45\zeta^8 + 30380\zeta^6\xi^8 - 39620\zeta^6\xi^6 + 14340\zeta^6\xi^4 \\ & - 1260\zeta^6\xi^2 + 14070\zeta^4\xi^8 - 14340\zeta^4\xi^6 + 3240\zeta^4\xi^4 - 28\zeta^4\xi^2 + 2\zeta^4 + 1980\zeta^2\xi^8 - 1260\zeta^2\xi^6 \\ & + 28\zeta^2\xi^4 + 28\zeta^2\xi^2 - 8\zeta^2 + 45\xi^8 + 2\xi^4 + 8\xi^2 + 9)\end{aligned} \tag{A55}$$

$$\mathcal{C}^{(1,1)}_{\mathrm{ihMM}} = \frac{1}{40960} \tag{A56}$$

$$\begin{aligned}\mathcal{P}^{(1,1)}_{0,\mathrm{ihMM}} = {} & 893025\zeta^8\xi^8 - 1367100\zeta^8\xi^6 + 633150\zeta^8\xi^4 - 89100\zeta^8\xi^2 + 2025\zeta^8 + 1664775\zeta^6\xi^8 - 2805600\zeta^6\xi^6 \\ & + 1448550\zeta^6\xi^4 - 232200\zeta^6\xi^2 + 6075\zeta^6 + 949935\zeta^4\xi^8 - 1808140\zeta^4\xi^6 + 1050810\zeta^4\xi^4 - 187980\zeta^4\xi^2 \\ & + 5295\zeta^4 + 169705\zeta^2\xi^8 - 375320\zeta^2\xi^6 + 250850\zeta^2\xi^4 - 45280\zeta^2\xi^2 + 365\zeta^2 + 4096\xi^8 - 11264\xi^6 + 9216\xi^4 \\ & - 1024\xi^2 - 1024\end{aligned} \tag{A57}$$

$$\begin{aligned}\mathcal{P}^{(1,1)}_{1,\mathrm{ihMM}} = {} & -5(178605\zeta^8\xi^8 - 273420\zeta^8\xi^6 + 126630\zeta^8\xi^4 - 17820\zeta^8\xi^2 + 405\zeta^8 + 392490\zeta^6\xi^8 - 652260\zeta^6\xi^6 \\ & + 331920\zeta^6\xi^4 - 52380\zeta^6\xi^2 + 1350\zeta^6 + 285096\zeta^4\xi^8 - 524364\zeta^4\xi^6 + 295476\zeta^4\xi^4 - 51492\zeta^4\xi^2 + 1428\zeta^4 \\ & + 75990\zeta^2\xi^8 - 158460\zeta^2\xi^6 + 99856\zeta^2\xi^4 - 18436\zeta^2\xi^2 + 410\zeta^2 + 5355\xi^8 - 13128\xi^6 + 9350\xi^4 - 1568\xi^2 - 73)\end{aligned} \tag{A58}$$

$$\begin{aligned}\mathcal{P}^{(1,1)}_{2,\mathrm{ihMM}} = {} & 5(178605\zeta^8\xi^8 - 273420\zeta^8\xi^6 + 126630\zeta^8\xi^4 - 17820\zeta^8\xi^2 + 405\zeta^8 + 273420\zeta^6\xi^8 - 469980\zeta^6\xi^6 \\ & + 247500\zeta^6\xi^4 - 40500\zeta^6\xi^2 + 1080\zeta^6 + 126630\zeta^4\xi^8 - 247500\zeta^4\xi^6 + 147360\zeta^4\xi^4 - 26868\zeta^4\xi^2 + 762\zeta^4 \\ & + 17820\zeta^2\xi^8 - 40500\zeta^2\xi^6 + 26868\zeta^2\xi^4 - 5052\zeta^2\xi^2 + 96\zeta^2 + 405\xi^8 - 1080\xi^6 + 762\xi^4 - 96\xi^2 + 73)\end{aligned} \tag{A59}$$

$$\mathcal{C}^{(1,2)}_{\mathrm{ihMM}} = \frac{1}{41287680} \tag{A60}$$

$$\begin{aligned}\mathcal{P}^{(1,2)}_{0,\mathrm{ihMM}} = {} & 10145260125\zeta^{12}\xi^{12} - 25573259250\zeta^{12}\xi^{10} + 23821441875\zeta^{12}\xi^8 - 10044877500\zeta^{12}\xi^6 + 1872871875\zeta^{12}\xi^4 \\ & - 124031250\zeta^{12}\xi^2 + 1378125\zeta^{12} + 28955012625\zeta^{10}\xi^{12} - 72801382500\zeta^{10}\xi^{10} + 67610426625\zeta^{10}\xi^8 \\ & - 28406574000\zeta^{10}\xi^6 + 5272981875\zeta^{10}\xi^4 - 347287500\zeta^{10}\xi^2 + 3766875\zeta^{10} + 30767710050\zeta^8\xi^{12} \\ & - 77117537700\zeta^8\xi^{10} + 70975576350\zeta^8\xi^8 - 29263495800\zeta^8\xi^6 + 5239763550\zeta^8\xi^4 - 321545700\zeta^8\xi^2 \\ & + 2934050\zeta^8 + 14941303650\zeta^6\xi^{12} - 37303988400\zeta^6\xi^{10} + 33648082650\zeta^6\xi^8 - 13213628400\zeta^6\xi^6 \\ & + 2130600150\zeta^6\xi^4 - 102093600\zeta^6\xi^2 + 344750\zeta^6 + 3245151105\zeta^4\xi^{12} - 8062033770\zeta^4\xi^{10} \\ & + 6975883215\zeta^4\xi^8 - 2440446540\zeta^4\xi^6 + 290714655\zeta^4\xi^4 - 3789450\zeta^4\xi^2 - 22575\zeta^4 + 254587725\zeta^2\xi^{12} \\ & - 628428780\zeta^2\xi^{10} + 500078565\zeta^2\xi^8 - 128429280\zeta^2\xi^6 + 2173815\zeta^2\xi^4 + 41580\zeta^2\xi^2 + 57015\zeta^2 \\ & + 2949120\xi^{12} - 7372800\xi^{10} + 5013504\xi^8 - 147456\xi^6 - 147456\xi^4 - 147456\xi^2 - 147456\end{aligned} \tag{A61}$$

$$\begin{aligned}\mathcal{P}^{(1,2)}_{1,\mathrm{ihMM}} = {} & -105(96621525\zeta^{12}\xi^{12} - 243554850\zeta^{12}\xi^{10} + 226870875\zeta^{12}\xi^8 - 95665500\zeta^{12}\xi^6 + 17836875\zeta^{12}\xi^4 \\ & - 1181250\zeta^{12}\xi^2 + 13125\zeta^{12} + 307969200\zeta^{10}\xi^{12} - 774531450\zeta^{10}\xi^{10} + 719532450\zeta^{10}\xi^8 - 302427300\zeta^{10}\xi^6 \\ & + 56164500\zeta^{10}\xi^4 - 3701250\zeta^{10}\xi^2 + 40250\zeta^{10} + 376357905\zeta^8\xi^{12} - 943918920\zeta^8\xi^{10} + 870427845\zeta^8\xi^8\end{aligned}$$

$$
\begin{aligned}
&- 360375960\zeta^8\xi^6 + 65056635\zeta^8\xi^4 - 4059840\zeta^8\xi^2 + 38735\zeta^8 + 219960000\zeta^6\xi^{12} - 549802980\zeta^6\xi^{10} \\
&+ 499104180\zeta^6\xi^8 - 199150440\zeta^6\xi^6 + 33292200\zeta^6\xi^4 - 1754100\zeta^6\xi^2 + 10020\zeta^6 + 62214495\zeta^4\xi^{12} \\
&- 154850850\zeta^4\xi^{10} + 136301949\zeta^4\xi^8 - 50147564\zeta^4\xi^6 + 6902553\zeta^4\xi^4 - 200178\zeta^4\xi^2 - 1013\zeta^4 \\
&+ 7501200\zeta^2\xi^{12} - 18569250\zeta^2\xi^{10} + 15388458\zeta^2\xi^8 - 4689140\zeta^2\xi^6 + 334788\zeta^2\xi^4 + 14454\zeta^2\xi^2 + 34\zeta^2 \\
&+ 255675\xi^{12} - 628980\xi^{10} + 459747\xi^8 - 76320\xi^6 - 9951\xi^4 - 396\xi^2 - 543) \qquad \text{(A62)}
\end{aligned}
$$

$$
\begin{aligned}
\mathcal{P}^{(1,2)}_{2,\text{ihMM}} = 315(&32207175\zeta^{12}\xi^{12} - 81184950\zeta^{12}\xi^{10} + 75623625\zeta^{12}\xi^8 - 31888500\zeta^{12}\xi^6 + 5945625\zeta^{12}\xi^4 - 393750\zeta^{12}\xi^2 \\
&+ 4375\zeta^{12} + 81184950\zeta^{10}\xi^{12} - 204053850\zeta^{10}\xi^{10} + 189428400\zeta^{10}\xi^8 - 79550100\zeta^{10}\xi^6 + 14757750\zeta^{10}\xi^4 \\
&- 971250\zeta^{10}\xi^2 + 10500\zeta^{10} + 75623625\zeta^8\xi^{12} - 189428400\zeta^8\xi^{10} + 173940165\zeta^8\xi^8 - 71343720\zeta^8\xi^6 \\
&+ 12639795\zeta^8\xi^4 - 758280\zeta^8\xi^2 + 6495\zeta^8 + 31888500\zeta^6\xi^{12} - 79550100\zeta^6\xi^{10} + 71343720\zeta^6\xi^8 \\
&- 27605480\zeta^6\xi^6 + 4298820\zeta^6\xi^4 - 186180\zeta^6\xi^2 + 160\zeta^6 + 5945625\zeta^4\xi^{12} - 14757750\zeta^4\xi^{10} + 12639795\zeta^4\xi^8 \\
&- 4298820\zeta^4\xi^6 + 467775\zeta^4\xi^4 + 1338\zeta^4\xi^2 - 267\zeta^4 + 393750\zeta^2\xi^{12} - 971250\zeta^2\xi^{10} + 758280\zeta^2\xi^8 \\
&- 186180\zeta^2\xi^6 - 1338\zeta^2\xi^4 + 2262\zeta^2\xi^2 - 132\zeta^2 + 4375\xi^{12} - 10500\xi^{10} + 6495\xi^8 - 160\xi^6 - 267\xi^4 + 132\xi^2 \\
&+ 181) \qquad \text{(A63)}
\end{aligned}
$$

b. Interaction part λ_{int}: A general expression for the interaction part of λ for the superposition of the inverted holey Morgan-Morgan disks with the Schwarzschild black hole (71) is

$$
\begin{aligned}
\lambda^{(m,n)}_{\text{ihMM,int}} = \mathscr{K}^{(m,n)}_{1,\text{ihMM}} &\left\{ \text{atan2}\begin{bmatrix} b\xi - M\zeta \\ R_-(\zeta,\xi) \end{bmatrix} + \text{atan2}\begin{bmatrix} b\xi + M\zeta \\ R_+(\zeta,\xi) \end{bmatrix} \right\} + \\
&+ \mathscr{K}^{(m,n)}_{2,\text{ihMM}} \sum_{\mp} R_{\mp}(\zeta,\xi)\, \mathcal{K}\left\{ \sqrt{1+\zeta^2-\xi^2} \left[\pm \mathscr{P}^{(m,n)}_{0,\text{ihMM}}(\pm\zeta,\xi) + \mathscr{P}^{(m,n)}_{1,\text{ihMM}}(\pm\zeta,\xi)\,\text{arccot}(\zeta) \right] \right\}, \qquad \text{(A64)}
\end{aligned}
$$

with the same notation conventions as in (A1), namely $\mathscr{K}^{(m,n)}_{j,\text{ihMM}}$ are constants and $\mathscr{P}^{(m,n)}_{j,\text{ihMM}}$ are polynomials in ζ and ξ. A few first members read explicitly

$$
\mathscr{K}^{(0,1)}_{1,\text{ihMM}} = \frac{2\mathcal{M}\left(b^2+M^2\right)}{\pi M^3} \qquad \text{(A65)}
$$

$$
\mathscr{K}^{(0,1)}_{2,\text{ihMM}} = \frac{\mathcal{M}}{\pi b M^2} \qquad \text{(A66)}
$$

$$
\mathscr{P}^{(0,1)}_{0,\text{ihMM}} = -2b\xi + 3\zeta M\xi^2 - \zeta M \qquad \text{(A67)}
$$

$$
\mathscr{P}^{(0,1)}_{1,\text{ihMM}} = \frac{1}{M}(-2b^2 + 2b\zeta M\xi - 3\zeta^2 M^2\xi^2 + \zeta^2 M^2 - M^2\xi^2 - M^2) \qquad \text{(A68)}
$$

$$
\mathscr{K}^{(0,2)}_{1,\text{ihMM}} = \frac{2\mathcal{M}\left(b^2+M^2\right)^2}{\pi M^5} \qquad \text{(A69)}
$$

$$
\mathscr{K}^{(0,2)}_{2,\text{ihMM}} = \frac{\mathcal{M}}{12\pi b M^4} \qquad \text{(A70)}
$$

$$
\begin{aligned}
\mathscr{P}^{(0,2)}_{0,\text{ihMM}} = &-24b^3\xi + 36b^2\zeta M\xi^2 - 12b^2\zeta M - 60b\zeta^2 M^2\xi^3 + 36b\zeta^2 M^2\xi - 16bM^2\xi^3 - 24bM^2\xi + 105\zeta^3 M^3\xi^4 \\
&- 90\zeta^3 M^3\xi^2 + 9\zeta^3 M^3 + 55\zeta M^3\xi^4 - 6\zeta M^3\xi^2 - 9\zeta M^3 \qquad \text{(A71)}
\end{aligned}
$$

$$
\begin{aligned}
\mathscr{P}^{(0,2)}_{1,\text{ihMM}} = \frac{-3}{M}(&8b^4 - 8b^3\zeta M\xi + 12b^2\zeta^2 M^2\xi^2 - 4b^2\zeta^2 M^2 + 4b^2 M^2\xi^2 + 12b^2 M^2 - 20b\zeta^3 M^3\xi^3 + 12b\zeta^3 M^3\xi \\
&- 12b\zeta M^3\xi^3 - 4b\zeta M^3\xi + 35\zeta^4 M^4\xi^4 - 30\zeta^4 M^4\xi^2 + 3\zeta^4 M^4 + 30\zeta^2 M^4\xi^4 - 12\zeta^2 M^4\xi^2 - 2\zeta^2 M^4 + 3M^4\xi^4 \\
&+ 2M^4\xi^2 + 3M^4) \qquad \text{(A72)}
\end{aligned}
$$

$$
\mathscr{K}^{(1,1)}_{1,\text{ihMM}} = \frac{2\mathcal{M}\left(-3b^4 - 2b^2M^2 + M^4\right)}{\pi M^5} \qquad \text{(A73)}
$$

$$
\mathscr{K}^{(1,1)}_{2,\text{ihMM}} = \frac{\mathcal{M}}{4\pi b M^4} \qquad \text{(A74)}
$$

$$
\begin{aligned}
\mathscr{P}^{(1,1)}_{0,\text{ihMM}} = &24b^3\xi - 36b^2\zeta M\xi^2 + 12b^2\zeta M + 60b\zeta^2 M^2\xi^3 - 36b\zeta^2 M^2\xi + 16bM^2\xi^3 - 8bM^2\xi - 105\zeta^3 M^3\xi^4 + 90\zeta^3 M^3\xi^2 \\
&- 9\zeta^3 M^3 - 55\zeta M^3\xi^4 + 54\zeta M^3\xi^2 - 7\zeta M^3 \qquad \text{(A75)}
\end{aligned}
$$

$$\mathscr{P}^{(1,1)}_{1,\mathrm{ihMM}} = \frac{1}{M}(24b^4 - 24b^3\zeta M\xi + 36b^2\zeta^2M^2\xi^2 - 12b^2\zeta^2M^2 + 12b^2M^2\xi^2 + 4b^2M^2 - 60b\zeta^3M^3\xi^3 + 36b\zeta^3M^3\xi$$
$$- 36b\zeta M^3\xi^3 + 20b\zeta M^3\xi + 105\zeta^4M^4\xi^4 - 90\zeta^4M^4\xi^2 + 9\zeta^4M^4 + 90\zeta^2M^4\xi^4 - 84\zeta^2M^4\xi^2 + 10\zeta^2M^4$$
$$+ 9M^4\xi^4 - 10M^4\xi^2 - 7M^4) \tag{A76}$$

$$\mathscr{K}^{(1,2)}_{1,\mathrm{ihMM}} = \frac{2\mathcal{M}\left(M^2 - 5b^2\right)\left(b^2 + M^2\right)^2}{\pi M^7} \tag{A77}$$

$$\mathscr{K}^{(1,2)}_{2,\mathrm{ihMM}} = \frac{\mathcal{M}}{24\pi bM^6} \tag{A78}$$

$$\mathscr{P}^{(1,2)}_{0,\mathrm{ihMM}} = 240b^5\xi - 360b^4\zeta M\xi^2 + 120b^4\zeta M + 600b^3\zeta^2M^2\xi^3 - 360b^3\zeta^2M^2\xi + 160b^3M^2\xi^3 + 192b^3M^2\xi$$
$$- 1050b^2\zeta^3M^3\xi^4 + 900b^2\zeta^3M^3\xi^2 - 90b^2\zeta^3M^3 - 550b^2\zeta M^3\xi^4 + 132b^2\zeta M^3\xi^2 + 66b^2\zeta M^3 + 1890b\zeta^4M^4\xi^5$$
$$- 2100b\zeta^4M^4\xi^3 + 450b\zeta^4M^4\xi + 1470b\zeta^2M^4\xi^5 - 1220b\zeta^2M^4\xi^3 + 102b\zeta^2M^4\xi + 128bM^4\xi^5 - 32bM^4\xi^3$$
$$- 48bM^4\xi - 3465\zeta^5M^5\xi^6 + 4725\zeta^5M^5\xi^4 - 1575\zeta^5M^5\xi^2 + 75\zeta^5M^5 - 3570\zeta^3M^5\xi^6 + 4410\zeta^3M^5\xi^4$$
$$- 1230\zeta^3M^5\xi^2 + 38\zeta^3M^5 - 693\zeta M^5\xi^6 + 705\zeta M^5\xi^4 - 27\zeta M^5\xi^2 - 33\zeta M^5 \tag{A79}$$

$$\mathscr{P}^{(1,2)}_{1,\mathrm{ihMM}} = \frac{3}{M}(80b^6 - 80b^5\zeta M\xi + 120b^4\zeta^2M^2\xi^2 - 40b^4\zeta^2M^2 + 40b^4M^2\xi^2 + 104b^4M^2 - 200b^3\zeta^3M^3\xi^3 + 120b^3\zeta^3M^3\xi$$
$$- 120b^3\zeta M^3\xi^3 - 24b^3\zeta M^3\xi + 350b^2\zeta^4M^4\xi^4 - 300b^2\zeta^4M^4\xi^2 + 30b^2\zeta^4M^4 + 300b^2\zeta^2M^4\xi^4 - 144b^2\zeta^2M^4\xi^2$$
$$- 12b^2\zeta^2M^4 + 30b^2M^4\xi^4 + 12b^2M^4\xi^2 + 6b^2M^4 - 630b\zeta^5M^5\xi^5 + 700b\zeta^5M^5\xi^3 - 150b\zeta^5M^5\xi$$
$$- 700b\zeta^3M^5\xi^5 + 640b\zeta^3M^5\xi^3 - 84b\zeta^3M^5\xi - 150b\zeta M^5\xi^5 + 84b\zeta M^5\xi^3 + 18b\zeta M^5\xi + 1155\zeta^6M^6\xi^6$$
$$- 1575\zeta^6M^6\xi^4 + 525\zeta^6M^6\xi^2 - 25\zeta^6M^6 + 1575\zeta^4M^6\xi^6 - 1995\zeta^4M^6\xi^4 + 585\zeta^4M^6\xi^2 - 21\zeta^4M^6$$
$$+ 525\zeta^2M^6\xi^6 - 585\zeta^2M^6\xi^4 + 99\zeta^2M^6\xi^2 + 9\zeta^2M^6 + 25M^6\xi^6 - 21M^6\xi^4 - 9M^6\xi^2 - 11M^6) \tag{A80}$$

[1] O. Semerák, Static axisymmetric rings in general relativity: How diverse they are, Phys. Rev. D **94**, 104021 (2016).

[2] V. Karas, J.-M. Hure, and O. Semerák, Gravitating discs around black holes, Class. Quantum Grav. **21**, R1 (2004).

[3] C.-Y. Chen and P. Kotlařík, Quasinormal modes of black holes encircled by a gravitating thin disk, Physical Review D **108**, 064052 (2023).

[4] L. Polcar, G. Lukes-Gerakopoulos, and V. Witzany, Extreme mass ratio inspirals into black holes surrounded by matter, Phys. Rev. D **106**, 044069 (2022).

[5] P. V. P. Cunha, N. A. Eiró, C. A. R. Herdeiro, and J. P. S. Lemos, Lensing and shadow of a black hole surrounded by a heavy accretion disk, JCAP **2020** (03), 035.

[6] P. Kotlařík, D. Kofroň, and O. Semerák, Static Thin Disks with Power-law Density Profiles, ApJ **931**, 161 (2022).

[7] J. D. Jackson, *Classical Electrodynamics*, 3rd ed. (Wiley, New York, 1999).

[8] O. Semerák, Exact power-law discs around static black holes, Class. Quantum Grav. **21**, 2203 (2004).

[9] J. T. Conway, Analytical solutions for the Newtonian gravitational field induced by matter within axisymmetric boundaries, MNRAS **316**, 540 (2000).

[10] G. G. Kuzmin, A stationary galaxy model admitting triaxial velocity distribution, Astr. Zh. **33**, 27 (1956).

[11] N. W. Evans and P. T. de Zeeuw, Potential-density pairs for flat galaxies, MNRAS **257**, 152 (1992).

[12] J. Bičák, D. Lynden-Bell, and C. Pichon, Relativistic Discs and Flat Galaxy Models, MNRAS **265**, 126 (1993).

[13] J. Bičák, D. Lynden-Bell, and J. Katz, Relativistic disks as sources of static vacuum spacetimes, Phys. Rev. D **47**, 4334 (1993).

[14] R. S. S. Vieira, Self-gravitating razor-thin discs around black holes via multi-hole seeds, Class. Quantum Grav. **37**, 205013 (2020).

[15] T. Ledvinka and J. Bičák, Disk sources of the Kerr and Tomimatsu-Sato spacetimes: Construction and physical properties, Phys. Rev. D **99**, 064046 (2019).

[16] T. Morgan and L. Morgan, The Gravitational Field of a Disk, Phys. Rev. **183**, 1097 (1969).

[17] O. Semerák, Gravitating discs around a Schwarzschild black hole: III, Class. Quantum Grav. **20**, 1613 (2003).

[18] J. P. S. Lemos and P. S. Letelier, Exact general relativistic thin disks around black holes, Phys. Rev. D **49**, 5135 (1994).

[19] A. Toomre, On the Distribution of Matter Within Highly Flattened Galaxies, ApJ **138**, 385 (1963).

[20] D. Vogt and P. S. Letelier, Analytical potential-density pairs for flat rings and toroidal structures, MNRAS **396**, 1487 (2009).

[21] P. Kotlařík and D. Kofroň, Black Hole Encircled by a Thin Disk: Fully Relativistic Solution, ApJ **941**, 25 (2022).

[22] P. Appell, Quelques remarques sur la théorie des potentiels multiformes, Math. Ann. **30**, 155 (1887).

[23] R. J. Gleiser and J. A. Pullin, Appell rings in general relativity, Class. Quantum Grav. **6**, 977 (1989).

[24] O. Semerák, T. Zellerin, and M. Zacek, The structure of superposed Weyl fields, MNRAS **308**, 691 (1999).

[25] P. S. Letelier, Simple potential–density pairs for flat rings, MNRAS **381**, 1031 (2007).
[26] P. S. Letelier and S. R. Oliveira, Exact self-gravitating disks and rings: A solitonic approach, JMP **28**, 165 (1987).
[27] C. Klein, Counter-rotating dust rings around a static black hole, Class. Quantum Grav. **14**, 2267 (1997).

CHAPTER

3

QUASINORMAL MODES (QNMS)

When a particle, e.g. a star, hits a black hole, two black holes merge, or a new black hole is formed from the gravitational collapse, the black hole rings and emits gravitational waves until it settles to a stationary equilibrium described by the Kerr(-Newman) solution. Because the whole system is "open" (asymptotically flat), the gravitational waves exponentially decay. Such a behaviour is described by *quasi-normal modes* – a sum of exponentially damped harmonic oscillations. For an isolated black hole, the quasi-normal modes are determined by its mass, spin, and, in the case of electrovacuum, electric charge. Thus, in the recent boom of new gravitational wave experiments, the quasi-normal modes of black holes may become very important for robust tests of GR.

The black-hole solutions, however, describe only isolated black holes. For any observable astrophysical black hole, this condition is not strictly satisfied. So far, the discussion of "dirty" black holes has been limited to situations where the spherical symmetry is preserved. Leung et al. (1997, 1999) showed that the spherical thin shell of matter surrounding the Schwarzschild black hole could significantly alter the QNMs spectrum. It was later clarified that the additional matter may actually induce the second barrier in the effective potential Barausse et al. (2015). This barrier triggers the pseudospectral instability (Jaramillo et al., 2021; Cheung et al., 2022), which can destroy the spectrum completely. However, the frequencies may still be extracted from the signal in the time domain Berti et al. (2022). The pseudospectral instability can be avoided if we consider just a moderate contribution from the surrounding matter Cardoso et al. (2022). We continue in the research of this problem by studying a more general case. We relax the spherical symmetry considering an axially symmetric accretion disc instead.

In this section, we briefly summarize some basic results regarding the QNMs of the Schwarzschild black hole and summarize our contribution in Chen & Kotlařík (2023).

3.1 Quasi-normal modes of the Schwarzschild black hole

Let's begin with a Schwarzschild black hole in the spherical (Schwarzschild) coordinates (1.34). We will denote $f(r) \equiv 1 - 2M/r$ and the metric

$$\mathrm{d}s^2 = g_{\alpha\beta}\,\mathrm{d}x^\alpha x^\beta \equiv -f(r)\,\mathrm{d}t^2 + \frac{\mathrm{d}r^2}{f(r)} + r^2(\mathrm{d}\theta^2 + \sin^2\theta\,\mathrm{d}\phi^2)\,. \tag{3.1}$$

Consider a linear perturbation of the background Schwarzschild metric,

$$g_{\mu\nu}^{\text{exact}} = g_{\mu\nu} + h_{\mu\nu}\,, \tag{3.2}$$

such that $|h_{\mu\nu}| \ll |g_{\mu\nu}|$. We now separate every component of the perturbation tensor $h_{\mu\nu}$ into the product of four functions, each depending on only one coordinate. Namely, we decompose the time dependence into frequencies $\exp(-\mathrm{i}kt)$, the angular part (θ, ϕ) into the spherical harmonics and the radial dependence will be described by an auxiliary function of r. Under rotations on the sphere, the components h_{tt}, h_{tr}, h_{rr} transform as scalars, the tuples $(h_{t\theta}, h_{t\phi})$ and $(h_{r\theta}, h_{r\phi})$ transform as components of two two-vectors, and $h_{\theta\theta}, h_{\theta\phi}, h_{\phi\phi}$ transform as components of a symmetric two-tensor. Thus, some vector and tensor generalization of the spherical harmonics is necessary. The perturbation problem was partially solved in the pioneering work by Regge & Wheeler (1957) and later completed by Zerilli (1970). They focused on the spherical harmonics with fixed parity with respect to the angular transformation $(\theta, \phi) \to (\pi - \theta, \phi + \pi)$. Since $Y_{\ell m_z}(\pi - \theta, \phi + \pi) = (-1)^\ell Y_{\ell m_z}(\theta, \phi)$, the perturbations may be expanded into the spherical harmonics with the same parity called "polar" (or "even"), or with the opposite parity called "axial" (or "odd").

Regge & Wheeler (1957) found a certain gauge in which the perturbation is described by two axial and four polar scalar functions, and they showed that the axial part decouples from the polar part. For the axial part, one of the unknown radial functions can further be expressed in terms of the other one, and a convenient redefinition of the quantities leads to the wave (Schrödinger-like) equation

$$\frac{\partial^2\Psi}{\partial r_*^2} + \Big[k^2 - V_{\text{eff}}(r)\Big]\,\Psi = 0\,, \tag{3.3}$$

where r_* is the tortoise coordinate, $\mathrm{d}r_* = (1 - 2M/r)^{-1}\,\mathrm{d}r$, and the effective potential reads

$$V_{\text{eff}}^{\text{ax}}(r) = \left(1 - \frac{2M}{r}\right)\left[\frac{\ell(\ell+1)}{r^2} - \frac{6M}{r^3}\right]. \tag{3.4}$$

Analogously, Zerilli (1970) showed that the polar problem reduces to the identical wave equation, although with a more complicated effective potential

$$V_{\text{eff}}^{\text{pol}} = \left(1 - \frac{2M}{r}\right)\frac{2n^2(n+1)r^3 + 6n^2Mr^2 + 18nM^2r + 18M^3}{r^3(nr+3M)^2}\,, \tag{3.5}$$

where $n = \frac{1}{2}(\ell - 1)(\ell + 2)$. Surprisingly, Chandrasekhar & Detweiler (1975) discovered a correspondence between the axial and polar parts. Both modes may

be encoded into a single radial function which satisfies the wave equation (3.3) for the same choice of $V_{\rm eff}(r)$ (different from the Reggee-Wheeler and Zerilli ones).

Thus, the analysis of the linear perturbation of the Schwarzschild black hole is closely connected to the problem of waves propagating in the black-hole spacetime.

3.2 Waves propagating in the perturbed black-hole spacetime

The Regge & Wheeler (1957) analysis was based on the fact that the background metric is vacuum, static and spherically symmetric. When the black hole is not isolated and the spherical symmetry is violated, the full analysis of linearized Einstein equations becomes a lot more difficult and is, at the moment, beyond our reach. However, a good starting point is to consider an analogous problem of massless-scalar-field perturbations propagating in the given background spacetime. Indeed, this is a great simplification, although already at this level, we can address some interesting issues, e.g. the stability of the system, without dealing with the complexity of the linearized gravitational equations.

The massless scalar field ψ is governed by the Klein-Gordon equation

$$\Box\psi = 0\,. \tag{3.6}$$

For the Schwarzschild spacetime, the wave equation (3.6) is separable. In particular, when we decompose the field into Fourier modes and expand the angular part into spherical harmonics,

$$\psi = \int_{-\infty}^{\infty} \sum_{m_z=-\infty}^{\infty} \sum_{\ell=|m_z|}^{\infty} \psi_{k\ell m_z}(r) Y_{\ell m_z}(\theta,\phi) e^{-ikt}\,{\rm d}k\,, \tag{3.7}$$

Eq. (3.6) reduces to the following radial equation for each mode

$$\frac{1}{r^2}\frac{\partial}{\partial r}\left(r^2 f(r)\,\frac{\partial\psi_{k\ell m_z}(r)}{\partial r}\right) + \left[f^{-1}(r)k^2 - \frac{\ell(\ell+1)}{r^2}\right]\psi_{k\ell m_z}(r) = 0\,. \tag{3.8}$$

Substituting $\hat{\psi}_{k\ell m_z}(r) = r\psi_{k\ell m_z}(r)$ and rewriting the equation in the tortoise coordinate ${\rm d}r_* = f^{-1}(r)\,{\rm d}r$, we obtain

$$\frac{\partial^2\hat{\psi}_{\ell m_z}}{\partial r_*^2} + \left[k^2 - V_{\rm eff}(r)\right]\hat{\psi}_{\ell m_z} = 0\,, \tag{3.9}$$

where the effective potential reads

$$V_{\rm eff}(r) = \frac{f(r)f'(r)}{r} + \frac{\ell(\ell+1)f}{r^2}\,, \quad f'(r) \equiv \frac{{\rm d}f}{{\rm d}r}\,. \tag{3.10}$$

However, even a slight perturbation of the original Schwarzschild spacetime breaks the separability of the wave equation. Yet, recently, Cano et al. (2020) proposed a projection method which can deal with "nearly" separable systems. These are the systems which depart from the Schwarzschild solution by a linear perturbation, so the zero-order wave equation is separable, while the non-separability

solely comes from the perturbative corrections. Let's denote a small parameter which parametrizes the deformations as ϵ and suppose that the perturbation preserves static metric, but it can slightly depart from the spherical symmetry. In frequencies, denote

$$\Box\psi \equiv \int_{-\infty}^{\infty} e^{-ikt}\mathcal{D}_k^2\psi_k(r,\theta,\phi)\,\mathrm{d}k = 0\,, \tag{3.11}$$

so that each mode satisfies

$$\mathcal{D}_k^2\psi_k(r,\theta,\phi) = 0\,. \tag{3.12}$$

Now, we can split the operator $\mathcal{D}_k^2$ into the separable part $\mathcal{D}_{(0)k}^2$ and the linear corrections $\mathcal{D}_{(1)k}^2$, i.e.

$$\mathcal{D}_k^2 = \mathcal{D}_{(0)k}^2 + \epsilon\mathcal{D}_{(1)k}^2\,, \tag{3.13}$$

where

$$\mathcal{D}_{(0)k}^2 = f^{-1}(r)k^2 + \frac{1}{r^2}\frac{\partial}{\partial r}\left(r^2 f(r)\,\frac{\partial}{\partial r}\right) + \frac{1}{r^2\sin\theta}\,\frac{\partial}{\partial\theta}\left(\sin\theta\,\frac{\partial}{\partial\theta}\right) + \frac{1}{r^2\sin^2\theta}\frac{\partial^2}{\partial\phi^2}\,. \tag{3.14}$$

Spherical harmonics form a complete set of functions on a sphere, thus the decomposition (3.7) is always possible. At the zeroth order, the equation $\mathcal{D}_{(0)k}^2\psi_k = 0$ can be factorized into a decoupled set of radial equations (3.8), each of which contains particular ℓ and m_z. Let us choose one of these particular solutions, say ℓ_0, m_{z0}. It is natural to assume that the other terms $\ell \neq \ell_0, m \neq m_0$ in the decomposition (3.7) arrive from the first perturbation order. Thus, we can consistently write

$$\psi_k(r,\theta,\phi) = \psi_{k\ell_0 m_{z0}}(r)Y_{\ell_0 m_{z0}}(\theta,\phi) + \epsilon\sum_{\substack{m_z=-\infty\\ m_z\neq m_{z0}}}^{\infty}\sum_{\substack{\ell=-|m_z|\\ \ell\neq\ell_0}}^{\infty}\psi_{k\ell m_z}(r)Y_{\ell m_z}(\theta,\phi)\,. \tag{3.15}$$

Using (3.13) and (3.15), we have

$$\begin{aligned}\mathcal{D}_k^2\psi_k(r,\theta,\phi) = \left[\mathcal{D}_{(0)k}^2 + \epsilon\mathcal{D}_{(1)k}^2\right]\psi_{k\ell_0 m_{z0}}(r)Y_{\ell_0 m_{z0}}(\theta,\phi) + \\ + \epsilon\sum_{\substack{m_z=-\infty\\ m_z\neq m_{z0}}}^{\infty}\sum_{\substack{\ell=-|m_z|\\ \ell\neq\ell_0}}^{\infty}\mathcal{D}_{(0)k}^2\psi_{k\ell m_z}(r)Y_{\ell m_z}(\theta,\phi) + \mathcal{O}(\epsilon^2)\,.\end{aligned} \tag{3.16}$$

Spherical harmonics are the eigenfunctions of the operator $\mathcal{D}_{(0)k}$, thus if we project (3.16) onto a certain $Y_{\ell_0 m_{z0}}$, the last term vanishes for an arbitrary m_{z0} due to the orthogonality of the spherical harmonics,

$$\begin{aligned}\int_0^{2\pi}\int_0^{\pi} Y_{\ell_0 m_{z0}}^*\mathcal{D}_k^2\psi_k(r,\theta,\phi)\sin\theta\,\mathrm{d}\theta\,\mathrm{d}\phi = \\ = \int_0^{2\pi}\int_0^{\pi} Y_{\ell_0 m_{z0}}^*\left[\mathcal{D}_{(0)k}^2 + \epsilon\mathcal{D}_{(1)k}^2\right]\psi_{k\ell m_z}(r)Y_{\ell m_z}(\theta,\phi)\sin\theta\,\mathrm{d}\theta\,\mathrm{d}\phi\,.\end{aligned} \tag{3.17}$$

From the zeroth order, we reproduce Eq. (3.8), while the first-order part brings linear corrections to the effective potential.

3.3 Quasi-normal modes of the Schwarzschild black hole in the presence of a thin disc

We can now use the recipe above and apply it to the spacetime of interest. In the paper Chen & Kotlařík (2023) we studied the influence of a gravitating disc on the spectrum of scalar field QNMs. We choose the solution of Kotlařík & Kofroň (2022), see also Sec. 2.6.2, describing a Schwarzschild black hole encircled by a static thin disc. Although the derived metric is exact, we considered that the mass of the disc is small compared to the mass of the black hole $\mathcal{M} \ll M$, thus setting $\epsilon = \mathcal{M}/M$. We found that the QNM frequencies are shifted due to the presence of the disc. In particular, both real and imaginary parts *decrease* with respect to the pure Schwarzschild value. Moreover, these shifts follow the same direction in the complex plane through a wide range of disc parameters. Similar behaviour was also observed in cases when the matter around the black hole respects spherical symmetry (Cardoso et al., 2022; Konoplya, 2021). This seems to be a universal relation. If held generically, it may help in distinguishing the environmental effects (such as gravitating accretion disc) from other effects predicted by alternative theories of gravity.

Quasinormal modes of black holes encircled by a gravitating thin disk

Che-Yu Chen*
RIKEN iTHEMS, Wako, Saitama 351-0198, Japan and
Institute of Physics, Academia Sinica, Taipei 11529, Taiwan

Petr Kotlařík†
Institute of Theoretical Physics, Faculty of Mathematics and Physics,
Charles University, V Holešovičkách 2, 180 00 Prague 8, Czech Republic

The ringdown phase of gravitational waves emitted by a perturbed black hole is described by a superposition of exponentially decaying sinusoidal modes, called quasinormal modes (QNMs), whose frequencies depend only on the property of the black hole geometry. The extraction of QNM frequencies of an isolated black hole would allow for testing how well the black hole is described by general relativity. However, astrophysical black holes are not isolated. It remains unclear whether the extra matter surrounding the black holes such as accretion disks would affect the validity of the black hole spectroscopy when the gravitational effects of the disks are taken into account. In this paper, we study the QNMs of a Schwarzschild black hole superposed with a gravitating thin disk. Considering up to the first order of the mass ratio between the disk and the black hole, we find that the existence of the disk would decrease the oscillating frequency and the decay rate. In addition, within the parameter space where the disk model can be regarded as physical, there seems to be a universal relation that the QNM frequencies tend to obey. The relation, if it holds generically, would assist in disentangling the QNM shifts caused by the disk contributions from those induced by other putative effects beyond general relativity. The QNMs in the eikonal limit, as well as their correspondence with bound photon orbits in this model, are briefly discussed.

I. INTRODUCTION

Black holes ring when they are perturbed, with the ringing frequencies determined by the underlying spacetime geometry. The feature of the ringings of black holes is tightly related to the fact that the whole system is dissipative. For an asymptotically flat black-hole spacetime, the emitted gravitational waves propagate outward, escaping from the system to spatial infinity. In addition, the event horizon, i.e., a point beyond which no infalling matter can return, acts as the other boundary of dissipation of the system. Because of the dissipation, the ringings of black holes would decay. Such a "ringdown" phase can be described by a superposition of exponentially decaying sinusoidal oscillations, called quasinormal modes (QNMs) [1–3]. The QNM frequencies are complex-valued, with the real part describing the oscillations, and the imaginary part determining the decay of the amplitudes. Importantly, for an isolated black hole in general relativity (GR), the spacetime geometry dictates the QNM spectrum, and they both satisfy the no-hair theorem, i.e., they are purely determined by the mass and the spin of the black hole. Therefore, based on the current achievements [4, 5] and with the upcoming advancements in the gravitational wave detection of binary merger events [6, 7], the extraction of QNM frequencies from ringdown signals may be accessible, helping us to identify the black hole parameters and even to test GR.

However, astrophysical black holes are generally not isolated. They may be surrounded by dark matter halos, or be encircled by accretion disks. The validity of using black hole QNMs to extract parameters describing the black hole spacetime requires a sufficient understanding of how the surrounding matter would alter the QNMs. One has to ensure that the contributions from the environments can be disentangled from those induced by the black hole geometry itself, at least under suitable approximations.

The QNM spectra of black holes surrounded by matter – the dirty black holes – have been explored in the literature. In Refs. [8, 9], the surrounding matter was modeled by a spherical dust thin-shell. It was shown, both numerically and analytically, that the QNM spectrum could deviate significantly from the vacuum case, especially when the shell is far away from the black hole. It was later clearly elucidated in Refs. [10, 11], assuming again spherically symmetric matter configurations, that this large amount of frequency shifts could be actually due to the existence of the double-barrier structure on the effective potential in the QNM master equations. The surrounding matter induces an additional barrier in the effective potential, which could induce pseudospectral instability of black hole QNMs [12]. Even an additional tiny bump on the effective potential would already trigger the instability and excite additional modes. The instability could happen even to the fundamental modes – the longest-lived modes [13], but their frequencies may still be extracted robustly from the prompt ringdown signals in time-domain [14] (see also [15]). The pseudospectral instability can be avoided when the contributions of the surrounding matter on the effective potential are suffi-

* b97202056@gmail.com
† kotlarik.petr@gmail.com

ciently mild in the sense that, in the case of nonrotating black holes, the effective potential retains its single-peak structure. This can be achieved as shown by the model of Ref. [16], in which the authors, assuming spherical symmetry, proposed an effective metric that can describe the spacetime geometry of a whole galaxy harboring a supermassive black hole. In this case, the frequencies of fundamental modes are shifted mildly by the environmental effects. The highly damped QNMs of spherically symmetric dirty black holes were also studied [17].

Apparently, the discussion of the QNM spectrum for dirty black holes so far is still quite confined to the assumption that the overall spacetime remains spherically symmetric. However, in a more realistic scenario, such as a black hole encircled by a gravitating accretion disk, the spherical symmetry is no longer preserved. But, the complicated structure of the Einstein equations makes obtaining the common gravitational field of the black hole with the disk a rather difficult task, at least for analytical work. Some reasonable simplifications (symmetries) are still needed. The simplest viable option is to consider an axially symmetric disk and neglect (or compensate) the total rotation present in the spacetime, so the spacetime is also static, and the black hole is described by the Schwarzschild metric. Another assumption that can be made is that the typical thickness of the disk is much smaller than the black hole radius, thus it is effectively infinitesimally thin. Then the Einstein equations are simplified considerably. Nevertheless, not many models of the Schwarzschild black hole encircled by a thin disk (SBH-disk models) are known in the literature. The first "superposition" was made in Ref. [18] (further studied in Ref. [19]) using inverted Morgan-Morgan disk [20]. It was also used to calculate the influence of a heavy accretion disk on the black-hole shadow in the more recent work [21]. Another class of disk solutions was proposed in Ref. [22], revisited recently in Ref. [23]. Both of these models have a slight disadvantage in that only a part of the metric was obtained explicitly, the rest being left to numerical treatments when needed. Yet recently, new solutions have been found [24, 25], where the whole metric of the entire superposition was derived explicitly and in closed-forms. In this paper, we consider the SBH-disk model proposed in Ref. [25].

From the astrophysical point of view, the SBH-disk model [25] may not properly describe any realistic scenario of accretion processes. In addition, being static, it does not include the spin of the central black hole nor the rotation of the disk. However, the disk possesses physically reasonable properties, and it can demonstrate the effects that may actually occur in the real astrophysical setup where the gravitation from the disk cannot be totally neglected.

In the presence of the gravitating disk, the calculations of the QNMs for the SBH-disk model become substantially challenging because the master equations in general are nontrivial partial differential equations. This is true even for the calculations of the QNMs of massless scalar fields. To proceed, we assume that the mass of the disk is much smaller than the black hole one. Up to the first order of the mass ratio, we adopt the projection method, which was proposed in Ref. [26] then applied in Refs. [27–30], to derive the master equation and investigate how the QNM frequencies of a massless scalar field are shifted by the gravitating disk. To ensure the validity of the projection method and the stability of the disk, we can fairly consider the parameter space of the model in which the aforementioned pseudospectral instability of fundamental modes does not happen. This can be achieved by focusing only on the effective potential, which can be defined in our treatment, with a single-peak structure. Furthermore, adopting the geometric optics approximations, we consider the frequencies of eikonal QNMs and identify their correspondence with bound photon orbits in the SBH-disk model.

The rest of this paper is organized as follows. In sec. II, we briefly review the SBH-disk model proposed in Ref. [25]. In order to analyze the QNMs of the SBH-disk model, in sec. III we consider a deformed Schwarzschild black hole, and demonstrate how to recast the master equation for scalar field perturbations in a Schrödinger-like form. This section is based on the results of Ref. [27]. The main results of our paper are presented in sec. IV, in which we show how the effective potentials of the master equation (sec. IV A) and the QNM frequencies (sec. IV B) vary with respect to the parameters in the SBH-disk model. Then, in sec. V, we comment on the eikonal correspondence between QNMs and bound photon orbits in the SBH-disk model. Finally, we conclude in sec. VI.

II. THE SBH-DISK MODEL

Due to the inherent non-linearity of Einstein equations, it is difficult to "superpose" multiple sources in GR. However, in the static and axially symmetric case, the situation is much simpler. In fact, in Weyl cylindrical coordinates (t, ρ, z, φ) Einstein equations outside of sources (i.e. in vacuum) are reduced to the Laplace equation and a line integration

$$\Delta\nu = 0\,, \tag{1}$$

$$\lambda_{,\rho} = \rho(\nu_{,\rho}^2 - \nu_{,z}^2)\,, \qquad \lambda_{,z} = 2\rho\nu_{,\rho}\nu_{,z}\,, \tag{2}$$

where the $\nu(\rho, z)$ and $\lambda(\rho, z)$ are the only nontrivial components of the Weyl-type metric

$$ds^2 = -e^{2\nu}dt^2 + \rho^2 e^{-2\nu}d\varphi^2 + e^{2\lambda-2\nu}(d\rho^2 + dz^2)\,. \tag{3}$$

Thus any axially symmetric gravitational field with its potential ν known from Newton's theory has its GR counterpart. However, the potential ν does not tell the whole story. The presence of the second metric function λ may significantly depart from the pure Newtonian picture. Moreover, while the Laplace equation (1) is linear, and thus makes the superposition problem for the potential ν

trivial, it is not the case for λ as Eqs. (2) are quadratic in ν.

Here, we wish to study the QNMs of a black hole that is surrounded by some matter in a physically appealing configuration. Namely, we take a recently derived solution [25] describing a Schwarzschild black hole encircled by a thin disk (SBH-disk model). Such a structure is of clear astrophysical importance as disk-like sources often result from an accretion of matter onto a compact central body. While the total potential is a simple sum $\nu = \nu_{\rm Schw} + \nu_{\rm disk}$, for the second metric function we write $\lambda = \lambda_{\rm Schw} + \lambda_{\rm disk} + \lambda_{\rm int}$, where $\lambda_{\rm Schw}$ and $\lambda_{\rm disk}$ denote contributions from the Schwarzschild black hole and the disk (thus each satisfying (2) with their corresponding $\nu_{\rm Schw}$, or, $\nu_{\rm disk}$ respectively). The non-linear "interaction" part $\lambda_{\rm int}$ satisfies

$$\lambda_{{\rm int},\rho} = 2\rho(\nu_{{\rm Schw},\rho}\nu_{{\rm disk},\rho} - \nu_{{\rm Schw},z}\nu_{{\rm disk},z})\,, \qquad (4)$$

$$\lambda_{{\rm int},z} = 2\rho(\nu_{{\rm Schw},\rho}\nu_{{\rm disk},z} + \nu_{{\rm Schw},z}\nu_{{\rm disk},\rho})\,. \qquad (5)$$

Notice that when we treat the existence of the disk as a small perturbation of the black hole, i.e. $|\nu_{\rm disk}| \ll |\nu_{\rm Schw}|$, and consider its contributions up to the first order, only the interaction part $\lambda_{\rm int}$ is relevant because $\lambda_{\rm disk}$ is of second order.

In Weyl coordinates, the Schwarzschild black hole is a singular rod of length $2M$ – twice the black-hole mass M – placed symmetrically on the z axis described by

$$\nu_{\rm Schw} = \frac{1}{2}\ln\left(\frac{R_+ + R_- - 2M}{R_+ + R_- + 2M}\right)\,, \qquad (6)$$

$$\lambda_{\rm Schw} = \frac{1}{2}\ln\left[\frac{(R_+ + R_-)^2 - 4M^2}{4R_+R_-}\right]\,, \qquad (7)$$

where

$$R_\pm = \sqrt{\rho^2 + (|z| \mp M)^2}\,. \qquad (8)$$

The disks considered in Ref. [25] are infinitesimally thin and spatially infinite (with a finite total mass) extending from the horizon. The disk density falls off quickly enough both at the horizon and at infinity – see the schematic Fig. 1. The Newtonian surface density profiles[1] read

$$w^{(m,n)} = W^{(m,n)}\frac{b^{2m+1}\rho^{2n}}{2\pi(\rho^2+b^2)^{m+n+3/2}}\,, \quad m,n \in \mathrm{N}_0 \quad (9)$$

where b is a parameter of the dimension of length and the normalization $W^{(m,n)}$ is chosen in such a way that the total mass of the disk $2\pi\int_0^\infty w^{(m,n)}(\rho)\rho\,d\rho = \mathcal{M}$. In particular,

$$W^{(m,n)} = (2m+1)\binom{m+n+1/2}{n}\mathcal{M}\,. \qquad (10)$$

[1] The quantity $w(\rho)$ satisfies exactly the Poisson equation $\Delta\nu = 4\pi w(\rho)\delta(z)$, where $\delta(z)$ is the delta distribution, so it is the precise counterpart of the Newtonian surface density.

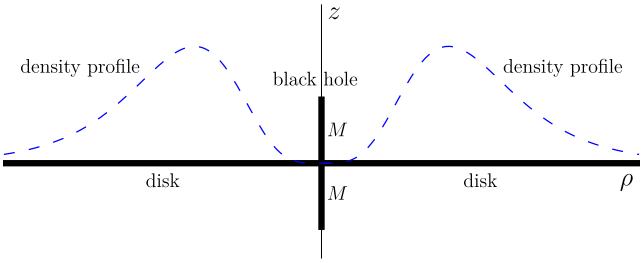

FIG. 1. The schematic plot in Weyl coordinates of a Schwarzschild black hole (thick black vertical line) encircled by a thin disk [25] (thick black horizontal line). The disk lies in the equatorial plane stretching from the horizon to infinity. The disk surface density profile (9) is indicated by the dashed blue line.

The densities (9) have a single maximum located at $\rho_{\rm max} = b\sqrt{\frac{2n}{3+2m}}$. Thus, increasing b (or n) when m,n (or m,b) are fixed means shifting the maximum further from the central region, as well as expanding the width of the peak. Whereas increasing m when n,b fixed corresponds to shifting the maximum towards the central region while shrinking the width of the peak. When keeping the total disk mass $\mathcal{M}$ constant, the maximum density decreases when increasing b (or n) while it increases when increasing m.

If we denote

$$r_b^2 := \rho^2 + (|z|+b)^2\,, \qquad |\cos\theta_b| := \frac{|z|+b}{r_b}\,, \qquad (11)$$

the potential is given by

$$\nu^{(m,n)} = -W^{(m,n)}\sum_{j=0}^{m+n}\mathcal{Q}_j^{(m,n)}\frac{b^j}{r_b^{j+1}}P_j(|\cos\theta_b|)\,, \qquad (12)$$

where P_j are the Legendre polynomials and the coefficients

$$\mathcal{Q}_j^{(m,n)} = \begin{cases} \sum_{k=0}^{n}(-1)^k\binom{n}{k}\frac{2^{j-k-m}(2m+2k-j)!}{(m+k-j)!(2m+2k+1)!!} & \text{if } j \le m \\ \sum_{k=j}^{m+n}(-1)^{k-m}\binom{n}{k-m}\frac{2^{j-k}(2k-j)!}{(k-j)!(2k+1)!!} & \text{if } j > m\,. \end{cases}$$

The potential (12) was first obtained by Vogt & Letelier [31] by taking a specific superposition of the Kuzmin-Toomre family of discs [32].

The second metric function $\lambda_{\rm disk}$ was also found explicitly (see [25] Eq. (21)), but we will not repeat it here as we shall not need it. The interaction part $\lambda_{\rm int}$ satisfies following recurrence relations

$$\lambda_{\rm int}^{(0,0)} = -\frac{\mathcal{M}}{r_b}\left(\frac{R_+}{b+M} - \frac{R_-}{b-M}\right) - \frac{2\mathcal{M}M}{b^2-M^2}\,, \qquad (13)$$

$$\lambda_{\rm int}^{(0,n+1)} = \lambda_{\rm int}^{(0,n)} + \frac{b}{2(n+1)}\frac{\partial}{\partial b}\lambda_{\rm int}^{(0,n)}\,, \qquad (14)$$

$$\frac{(2m+1)(2n+3)}{2m+2n+3}\lambda_{\rm int}^{(m+1,n)} = \lambda_{\rm int}^{(m,n)} + \frac{4m(n+1)}{2m+2n+3}\lambda_{\rm int}^{(m,n+1)} - b\frac{\partial}{\partial b}\lambda_{\rm int}^{(m,n)}\,. \qquad (15)$$

Thus the whole metric (both metric functions) of the SBH-disk model is known explicitly and in closed-form. From now on, to simplify the expression, the notation (m, n) that indicates the explicit dependence of the disk functions on the indices m and n will be dropped. One should keep in mind that ν and λ explicitly depend on $\mathcal{M}$, b, m, and n.

Two physical interpretations of these disks are possible: a) a single component ideal fluid with density σ and azimuthal pressure P (a set of solid rings with internal azimuthal stress), or, b) two equally counter-rotating pressureless dust streams with the densities $\sigma_\pm = \sigma/2$ following circular geodesics. Both characteristics follow from the metric

$$\sigma + P = e^{\nu-\lambda}\frac{\nu_{,z}(z=0^+)}{2\pi} = e^{\nu-\lambda}w(\rho)\,, \tag{16}$$

$$P = e^{\nu-\lambda}\frac{\nu_{,z}(z=0^+)}{2\pi}\rho\nu_{,\rho} = e^{\nu-\lambda}w(\rho)\rho\nu_{,\rho}\,, \tag{17}$$

where $w(\rho)$ is the Newtonian surface density (9). See Appendix A for the derivation in more details.

Clearly $\sigma + P \geq 0$, so the strong energy condition is satisfied automatically for any disk. The dominant energy condition is generally satisfied everywhere (for a broad range of parameters) except close to the black-hole horizon, where $\sigma < P$. In fact, the accretion disks are usually assumed to end around the innermost stable circular orbit (ISCO). However, we argue that (i) our disk density drops to zero toward the horizon, so there is really no matter on the horizon itself, and, (ii) accretion disks around realistic black holes would indeed stretch toward the horizon, although the matter will infall there rather than orbiting on circular trajectories. Thus, in this sense, it is more realistic to model the gravitational field with some modest density going down to the horizon. By choosing appropriate parameters (m, n) and b, the density can be made arbitrarily small below a chosen radius, e.g., the ISCO orbit.

For the double-stream interpretation, both energy conditions considered above require $\sigma_\pm \geq 0$, which also implies $P \geq 0$ for the single component interpretation. Finally, the energy conditions are satisfied for both interpretations if the speed of a particle on a circular geodesic in the equatorial plane

$$v^2 = \frac{P}{\sigma} = \frac{\rho\nu_{,\rho}}{1-\rho\nu_{,\rho}} \tag{18}$$

acquire timelike values $0 \leq |v| < 1$.

While superposition can be carried out very straightforwardly in Weyl coordinates, it will be convenient to work in Schwarzschild coordinates (t, r, θ, φ) from now on. The two sets of coordinates are related as follows[2]

$$\rho = \sqrt{r(r-2M)}\sin\theta\,, \quad z = (r-M)\cos\theta\,, \tag{19}$$

and the metric of the SBH-disk model in Schwarzschild coordinates then reads

$$\begin{aligned} ds^2 =& -f(r)\mathrm{e}^{2\nu_{\rm disk}}dt^2 + \mathrm{e}^{2\lambda_{\rm ext}-2\nu_{\rm disk}}\frac{dr^2}{f(r)} \\ &+ r^2\mathrm{e}^{-2\nu_{\rm disk}}\left(\mathrm{e}^{2\lambda_{\rm ext}}d\theta^2 + \sin^2\theta d\varphi^2\right)\,, \end{aligned} \tag{20}$$

where $\lambda_{\rm ext} = \lambda_{\rm disk} + \lambda_{\rm int}$ and $f(r) \equiv \nu_{\rm Schw} = 1 - 2M/r$ after the transformation into Schwarzschild coordinates.

III. DEFORMED SCHWARZSCHILD BLACK HOLES – MASTER EQUATION

The SBH-disk metric of Eq. (20) describes the spacetime of a Schwarzschild black hole encircled by a gravitating thin disk. The main goal of this work is to investigate the QNMs propagating in this superposed spacetime. However, due to the general (r, θ) dependence appearing in the metric functions through $\nu_{\rm disk}$ and $\lambda_{\rm ext}$, the radial and the latitudinal sectors of the wave equation are not separable. In order to proceed, we assume that the disk mass $\mathcal{M}$ is much smaller than the black hole mass M and consider the contributions up to $O(\mathcal{M}/M)$. Besides having its astrophysical applicability, this assumption, as mentioned in the previous section, allows us to simplify the calculations by omitting $\lambda_{\rm disk}$ term because it is of second order in $\mathcal{M}/M$. Then, we focus on the QNMs of scalar field perturbations. Adopting the projection method [26] to the master equation up to $O(\mathcal{M}/M)$, one can separate the radial component of the master equation from the latitudinal one. This has been shown explicitly in Ref. [27] for a very general class of deformed Schwarzschild spacetimes. In this section, we briefly review the results in Ref. [27], based on which one can compute the scalar field QNMs of the SBH-disk model.

We consider a deformed Schwarzschild spacetime and assume that the spacetime remains static and axially symmetric in the presence of deformations. The nonzero metric components of the deformed spacetime can be expressed as [27]

$$\begin{aligned} g_{tt}(r,\theta) &= -f(r)\left(1+\epsilon A_j(r)|\cos^j\theta|\right)\,, \\ g_{rr}(r,\theta) &= \frac{1}{f(r)}\left(1+\epsilon B_j(r)|\cos^j\theta|\right)\,, \\ g_{\theta\theta}(r,\theta) &= r^2\left(1+\epsilon C_j(r)|\cos^j\theta|\right)\,, \\ g_{\varphi\varphi}(r,\theta) &= r^2\sin^2\theta\left(1+\epsilon D_j(r)|\cos^j\theta|\right)\,, \end{aligned} \tag{21}$$

where ϵ is a dimensionless parameter that quantifies the amount of deformations. In general, the spacetime deformations are functions of r and θ. In Eqs. (21), we expand the latitudinal part of the deformation functions as a Taylor series in terms of $\cos\theta$. Each term in the series is weighted by a function of r, i.e., the functions $A_j(r)$, $B_j(r)$, $C_j(r)$, and $D_j(r)$ that appear in the expansion. The dummy index j stands for summations

[2] Note the difference between r_b and θ_b with the subscript b defined in (11) and the Schwarzschild coordinates r, θ.

running upward from $j = 0$. The absolute value in each term in the expansion is to preserve the equatorial reflection symmetry, with the possibility of having a nonzero surface density at the equatorial plane. When the deformations are small, i.e., $|\epsilon| \ll 1$, we can consider terms up to $O(\epsilon)$. As we will show later, the radial sector of the Klein-Gordon equation can then be separated from the latitudinal one, and it can be further recast into the Schrödinger-like form.

A. Massless scalar field: Effective potential

In this work, we will focus on the massless scalar field perturbations, whose QNMs are governed by the Klein-Gordon equation

$$\Box\psi = 0\,. \tag{22}$$

Indeed, the investigation of the ringdown phase in real gravitational wave emission has to be based on the computations of linearized gravitational equations rather than Eq. (22). However, as the simplest scenario, the consideration of scalar field perturbations already allows us to address interesting issues, such as the (in)stability of the system, without suffering the computational complexity in linearized gravitational equations of deformed background spacetimes. In addition, according to the geometric optics approximations, the behaviors of scalar field QNMs should be able to capture those of the gravitational perturbations at least in the eikonal regimes, that is, when the multipole number l is large. This will be discussed later in sec. V.

For the master equation of scalar fields in the Schwarzschild spacetime, one can use the associated Legendre functions $P_l^{m_z}(x)$, where $x \equiv \cos\theta$ and m_z is the azimuthal number, as the angular basis to separate the radial and latitudinal sectors of the wave equation. The radial equation is labeled by the multipole number l and determines the evolution of the mode of l. The azimuthal number m_z degenerates because of the spherical symmetry of the spacetime. In the presence of deformations of $O(\epsilon)$, there would appear off-diagonal terms that correspond to the modes with multipole numbers l different from that of the zeroth-order one. These off-diagonal terms in the wave equations are $O(\epsilon)$. Therefore, by taking advantage of the orthogonality of $P_l^{m_z}$ among multipole numbers, one can project out the off-diagonal terms and focus only on the corrections on the zeroth-order equation. In the following, we will only show the main results of the calculations and refer the readers to sec. IV of Ref. [27] for more details.

Essentially, the projection method allows us to separate the radial and the latitudinal sectors of the wave equation. To further recast the radial equation into the Schrödinger-like form, we find it convenient to define the following coefficients:

$$a^j_{lm_z} = \frac{2{m_z}^2}{\mathcal{N}_{lm_z}}\int_0^1 \frac{x^j\left(P_l^{m_z}\right)^2}{1-x^2}dx\,, \tag{23}$$

$$b^j_{lm_z} = \frac{2}{\mathcal{N}_{lm_z}}\int_0^1 x^j\left(P_l^{m_z}\right)^2 dx\,, \tag{24}$$

$$c^j_{lm_z} = \frac{2}{\mathcal{N}_{lm_z}}\int_0^1 x^j P_l^{m_z}\left[\left(1-x^2\right)\partial_x^2 - 2x\partial_x\right]P_l^{m_z}dx\,, \tag{25}$$

$$d^j_{lm_z} = \frac{2}{\mathcal{N}_{lm_z}}\int_0^1 P_l^{m_z}\left(1-x^2\right)\left(\partial_x x^j\right)\left(\partial_x P_l^{m_z}\right)dx\,, \tag{26}$$

where the normalization constant $\mathcal{N}_{lm_z} \equiv 2(l+m_z)!/[(2l+1)(l-m_z)!]$ is determined by the orthogonality condition

$$\int_{-1}^1 dx P_l^{m_z}(x)P_k^{m_z}(x) = \mathcal{N}_{lm_z}\delta_{lk}\,. \tag{27}$$

Note that the coefficients given by Eqs. (23)-(26) depend on l and m_z, but they are invariant under $m_z \leftrightarrow -m_z$.

After Fourier transformations, we denote the radial part of the Fourier modes of the scalar field as $\Psi_{l,m_z}(r)$. By using the projection method, the radial wave function is found to satisfy the following Schrödinger-like equation [27]

$$\partial^2_{r_*}\Psi_{l,m_z}(r) + \omega^2\Psi_{l,m_z}(r) = V_{\rm eff}(r)\Psi_{l,m_z}(r)\,, \tag{28}$$

where ω is the mode frequency. The effective potential $V_{\rm eff}(r)$ can be expressed as

$$\begin{aligned}V_{\rm eff}(r) = {}& l(l+1)\frac{f(r)}{r^2} + \frac{f(r)}{r}\frac{df}{dr}\left[1+\epsilon b^j_{lm_z}\left(A_j(r)-B_j(r)\right)\right]\\ &+\epsilon\Bigg\{\frac{f(r)}{r^2}\left[a^j_{lm_z}\left(A_j(r)-D_j(r)\right) - c^j_{lm_z}\left(A_j(r)-C_j(r)\right) - \frac{d^j_{lm_z}}{2}\left(A_j(r)+B_j(r)-C_j(r)+D_j(r)\right)\right]\\ &-\frac{b^j_{lm_z}}{4}\frac{d^2}{dr_*^2}\left[A_j(r)-B_j(r)\right] + \frac{1}{4r^2}\frac{d}{dr_*}\left[b^j_{lm_z}r^2\frac{d}{dr_*}\left(A_j(r)-B_j(r)+C_j(r)+D_j(r)\right)\right]\Bigg\}\,,\end{aligned} \tag{29}$$

which explicitly contains the coefficients given by Eqs. (23)-(26). The tortoise radius r_* is defined as follows

$$\frac{dr}{dr_*} = f(r)\left\{1+\frac{\epsilon}{2}b^j_{lm_z}\left[A_j(r)-B_j(r)\right]\right\}\,. \tag{30}$$

On the above equations (29) and (30), the summations over j are implicitly assumed. It can be seen that when $\epsilon = 0$, the effective potential and the whole master equation reduce to those of the Schwarzschild spacetime. In this case, as we have mentioned, the azimuthal numbers m_z degenerate, and Eq. (28) is labeled only by l. However, in the presence of deformations, the spacetime is no longer spherically symmetric, hence the degeneracy among m_z splits. Different values of $|m_z|$ in the range of $0 \leq |m_z| \leq l$ give distinctive QNM frequencies.

IV. QNMS OF SBH-DISK MODEL

Having discussed the master equation of the scalar field perturbations in a general deformed Schwarzschild spacetime, we then consider the SBH-disk model whose metric is given by Eq. (20). The SBH-disk model can also be treated as a deformed Schwarzschild spacetime whose deformations are caused by the thin disk. Typical mass M of the astrophysical black hole is usually expected to dominate over the mass of the accretion disk $\mathcal{M}$. Therefore, it is natural to set $\epsilon = \mathcal{M}/M$ and consider terms up to $O(\mathcal{M}/M)$. As we have mentioned, in this linear approximation, we have $\lambda_{\rm ext} \approx \lambda_{\rm int}$ because $\lambda_{\rm disk}$ is quadratic in ϵ. The metric components of the SBH-disk model can then be approximated as

$$\begin{aligned} g_{tt}(r,\theta) &\approx -f(r)\left(1+2\nu_{\rm disk}\right) , \\ g_{rr}(r,\theta) &\approx \frac{1}{f(r)}\left(1+2\lambda_{\rm int}-2\nu_{\rm disk}\right) , \\ g_{\theta\theta}(r,\theta) &\approx r^2\left(1+2\lambda_{\rm int}-2\nu_{\rm disk}\right) , \\ g_{\varphi\varphi}(r,\theta) &\approx r^2\sin^2\theta\left(1-2\nu_{\rm disk}\right) . \end{aligned} \tag{31}$$

The approximated metric (31) belongs to the class of deformed Schwarzschild metrics of Eq. (21), as will be shown more explicitly below.

A. Effective potential

The identification between the metrics (21) and (31) is made by first expanding $\nu_{\rm disk}$ and $\lambda_{\rm int}$ in terms of $|x|$ as follows:

$$\nu_{\rm disk} = \epsilon\mathcal{V}_j(r)|x^j| , \quad \lambda_{\rm int} = \epsilon\mathcal{L}_j(r)|x^j| , \tag{32}$$

where $\mathcal{V}_j(r)$ and $\mathcal{L}_j(r)$ depend on m, n, and b, but are independent of ϵ. Again, the summations over j are implicitly imposed as before. One then identifies the weighting functions in Eq. (21) as follows

$$\begin{aligned} A_k(r) &= -D_k(r) = 2\mathcal{V}_k(r) , \\ B_k(r) &= C_k(r) = 2\mathcal{L}_k(r) - 2\mathcal{V}_k(r) , \end{aligned}$$

for all k. With these mappings, one sees that the approximated metric (31) does belong to the class of metrics (21). As a result, the effective potential (29) can be written as

$$\begin{aligned} V_{\rm eff}(r) = l(l+1)\frac{f(r)}{r^2} &+ \frac{f(r)}{r}\frac{df}{dr}\left[1+\epsilon b^j_{lm_z}\left(4\mathcal{V}_j(r)-2\mathcal{L}_j(r)\right)\right] \\ &+ \epsilon\left\{\frac{f}{r^2}\left[4a^j_{lm_z}\mathcal{V}_j(r) - c^j_{lm_z}\left(4\mathcal{V}_j(r)-2\mathcal{L}_j(r)\right)\right] - \frac{b^j_{lm_z}}{2}\frac{d^2}{dr_*^2}\left[2\mathcal{V}_j(r)-\mathcal{L}_j(r)\right]\right\} , \end{aligned} \tag{33}$$

and the definition of the tortoise radius r_*, which is given by Eq. (30), becomes

$$\frac{dr}{dr_*} = f(r)\left\{1+\epsilon b^j_{lm_z}\left[2\mathcal{V}_j(r)-\mathcal{L}_j(r)\right]\right\} . \tag{34}$$

Note that when $\epsilon = 0$, the spacetime recovers a pure Schwarzschild one and the effective potential is given by

$$V^{\rm Sch}_{\rm eff}(r) \equiv l(l+1)\frac{f(r)}{r^2} + \frac{f(r)}{r}\frac{df}{dr} . \tag{35}$$

With the master equation (28) and the effective potential (33), we can calculate the QNM frequencies of the scalar field perturbations of the SBH-disk model.

We first check that the effective potential, which is ideally defined as an infinite sum in j, has a sufficiently fast rate of convergence when increasing the summation order j. In Fig. 2, we consider the effective potential $V_{\rm eff}(r)$ of the SBH-disk model with $m = 0$, $n = 1$, $b = 10M$, $l = |m_z| = 2$, and $\mathcal{M} = 0.02M$, then calculate the radius of its peak r_m with various truncation values of j, which we defined as j_t. We find that when $j_t \geq 4$, the results of r_m already converge very well. Therefore, in the rest of this paper, the effective potential of the SBH-disk model will be calculated with the summation truncated at $j_t = 4$.

In Fig. 3, we set $m = 0$, $n = 2$, $b = 10M$, and

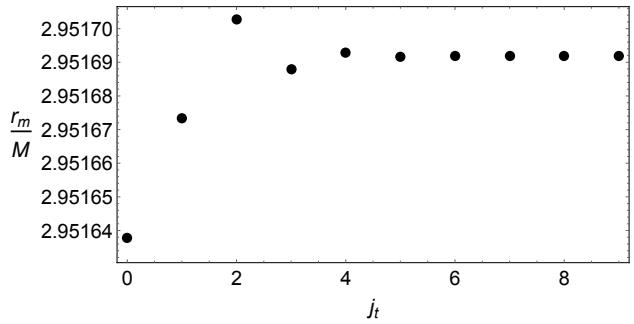

FIG. 2. The radius of potential peak r_m calculated with various j_t at which the summation is truncated. In this figure we choose $m = 0$, $n = 1$, $b = 10M$, $l = |m_z| = 2$, $\mathcal{M} = 0.02M$. The results converge very well already at $j_t = 4$.

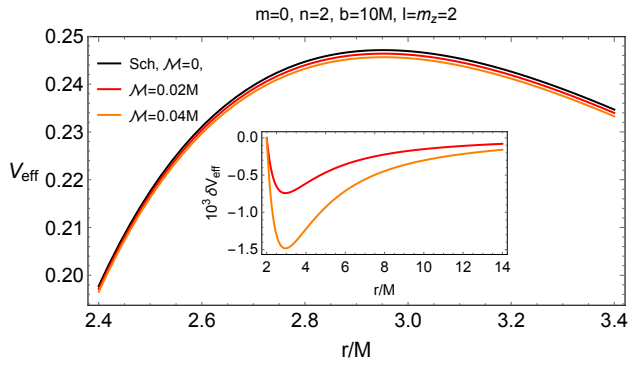

FIG. 3. The effective potentials $V_{\rm eff}(r)$ of the SBH-disk model are shown with various $\mathcal{M}/M$. The presence of the disk flattens the effective potential.

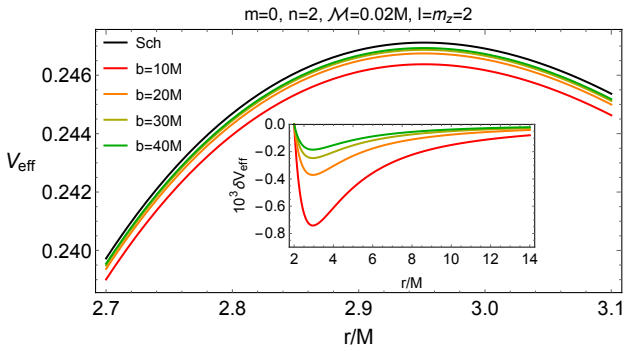

FIG. 4. The effective potentials $V_{\rm eff}(r)$ of the SBH-disk model are shown with various b/M. When b/M increases, the effective potential converges to that of the pure Schwarzschild black hole.

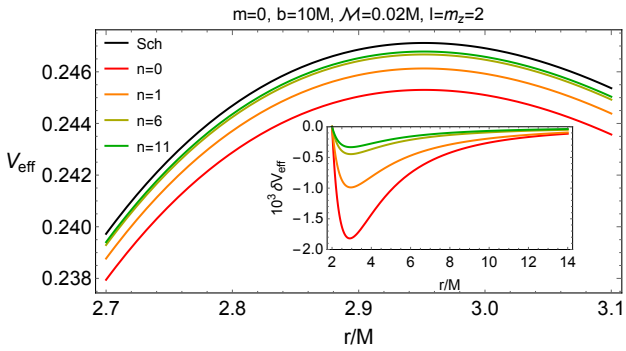

FIG. 5. The effective potentials $V_{\rm eff}(r)$ of the SBH-disk model are shown with different n. As n increases, the effective potential slowly converges to the Schwarzschild one.

$l = |m_z| = 2$. The effective potentials of SBH-disk models are shown with respect to different values of the disk mass $\mathcal{M}$. The black curve corresponds to the pure Schwarzschild black hole, i.e., $\mathcal{M} = 0$, whose effective potential is given by $V_{\rm eff}^{\rm Sch}(r)$. The inset shows the deviation of the effective potentials in the presence of the disk with respect to the pure Schwarzschild one ($\delta V_{\rm eff} \equiv V_{\rm eff} - V_{\rm eff}^{\rm Sch}$). One can see that the effective potential is flattened in the presence of the disk. This is consistent with the findings in Ref. [25] that the disk provides additional gravitational attractions and makes the horizon, as well as the effective potential as a whole, more flattened. Also, from the inset, one finds that the effective potential reduces to $V_{\rm eff}^{\rm Sch}(r)$ both near the horizon and at the spatial infinity. This is also expected as the surface density of the disk drops to zero there, as one can see in Fig. 1. In fact, the inset of Fig. 3 also indicates that the effective potential in the presence of the disk acquires the largest deviation from the pure Schwarzschild one near the peak r_m.

Then, we explore the shape of the effective potential within the parameter space of the disk model itself, i.e., m, n, and b. In Figs. 4, 5, and 6, we focus on how the effective potentials vary with respect to the changes of b, n, and m, respectively. We find that the effective potentials gradually reduce to $V_{\rm eff}^{\rm Sch}$ when increasing b or n. On the other hand, increasing the index m would further flatten the effective potential, as can be seen from Fig. 6. As we have mentioned in sec. II, when keeping $\mathcal{M}/M$ constant and increasing either n, b, or $1/m$, the density peak of the disk would get lower and move further away from the black hole. Therefore, the net effects due to the disk become weaker. It is also worth remarking that in the presence of the disk, $|\delta V_{\rm eff}|$ seems to always get its largest value near the potential peak r_m.

B. Scalar field QNMs

The QNM frequencies of the scalar field perturbations in the SBH-disk model can be calculated by solving Eq. (28) with the effective potential (33) after imposing proper boundary conditions. Typical boundary conditions for black hole QNMs require that there are purely outgoing waves at spatial infinity and purely ingoing waves at the event horizon. The system can be treated as a wave-scattering problem through the peak

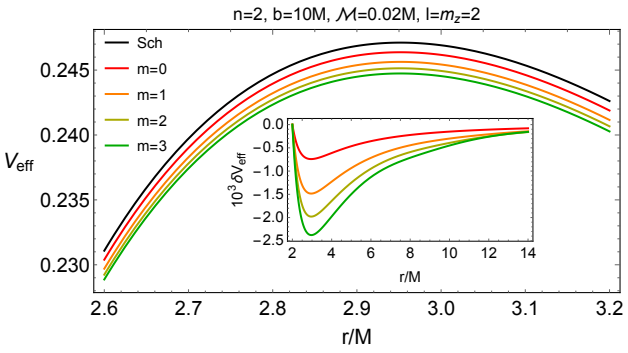

FIG. 6. The effective potentials $V_{\rm eff}(r)$ of the SBH-disk model are shown with different m. Increasing m makes the peak of the surface density of the disk higher, narrower, and closer to the black hole, thus altering the effective potential more significantly.

of the effective potential. The whole system is dissipative because of the boundary conditions. Therefore, the QNM frequencies in general would acquire an imaginary part that quantifies the decay of the modes.

In this section, we focus on the cases where the effective potential retains its single-peak structure. This can be easily achieved when only orders of $O(\epsilon)$ are considered. The single-peak structure of the effective potential allows us to calculate the QNM frequencies using the third-order Wentze-Kramers-Brillouin (WKB) method [33, 34][3]. We also make use of the asymptotic iteration method (AIM) [40, 41] to check the consistency of the results. In this section, we shall focus on the fundamental modes with $l = |m_z|$ because the fundamental modes have the longest decay time and hence are more astrophysically relevant. In addition, our numerical results suggest that changing $|m_z|$ only shifts the frequencies very weakly as compared to the frequency shifts generated by other model parameters.

The complex planes of QNM frequencies within some parameter space are shown in Fig. 7. In each panel, the three branches correspond to the complex QNM frequencies with multipole numbers $l = 2$, $l = 4$, and $l = 6$, from left to right, respectively. For each branch in the top panel, we fix the set of parameters $\{m, n, b\}$ as that in Fig. 3 and use the third-order WKB method to calculate the QNM frequencies with respect to the disk mass, which is chosen to be $\mathcal{M} = 0$, $0.02M$, $0.04M$, $0.06M$, $0.08M$, and $0.1M$ (black points from top to bottom). The green (magenta) points are the results calculated using AIM, with disk mass $\mathcal{M} = 0$ ($\mathcal{M} = 0.1M$). In this case, the topmost points in each branch correspond to the QNM frequencies of a pure Schwarzschild black

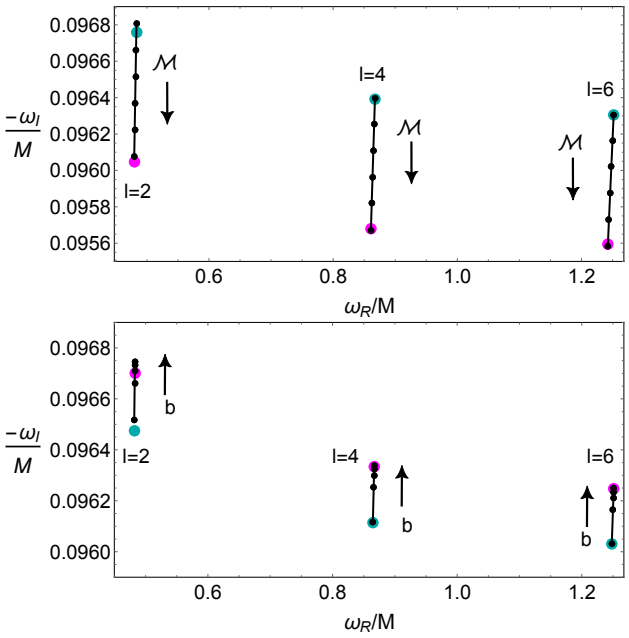

FIG. 7. The QNM frequencies of the SBH-disk model with different choices of the parameters. The frequencies are calculated using the third-order WKB method (black points) and AIM (colored points). (Top) $\mathcal{M}$ varies from 0 to $0.1M$ (from top to bottom in each branch) with other parameters $\{m, n, b\}$ fixed as those in Fig. 3. The green and magenta points correspond to $\mathcal{M}/M = 0$ and 0.1, respectively. (Bottom) b/M varies from 5 to 25 (from bottom to top in each branch) with other parameters $\{m, n, \mathcal{M}\}$ fixed as those in Fig. 4. The green and magenta points correspond to $b/M = 5$ and 25, respectively. The arrows indicate the direction along which the referred parameters increase.

hole. In the bottom panel of Fig. 7, we fix the set of parameters $\{m, n, \mathcal{M}\}$ as that in Fig. 4, and vary only $b = 25M$, $20M$, $15M$, $10M$, and $5M$ (black points from top to bottom) for each branch. The green (magenta) points are the results calculated using AIM, with $b = 5M$ ($b = 25M$).

From Fig. 7, one first sees that the WKB method and AIM give quite consistent results, particularly in the regime of large l where the WKB method is expected to be accurate. Second, increasing the disk mass $\mathcal{M}$ would reduce the values of ω_R and $|\omega_I|$ [4]. In addition, given a non-zero $\mathcal{M}$, the pure Schwarzschild results can be recovered when $b \to \infty$. Reducing the value of b decreases the values of ω_R and $|\omega_I|$, as compared with the pure Schwarzschild case. This is consistent with our previous finding that when b increases, the effective potential gradually reduces to $V_{\rm eff}^{\rm Sch}$.

In fact, after a careful examination of the parameter space, we find that the presence of a thin disk would al-

[3] The WKB method for calculating black hole QNMs has been extended to higher orders [35–38]. We refer the readers to Ref. [39] for the review of the method and, in particular, its range of applicability.

[4] The change of ω_R in each branch may not be easily seen in Fig. 7. See Fig. 8 for more details.

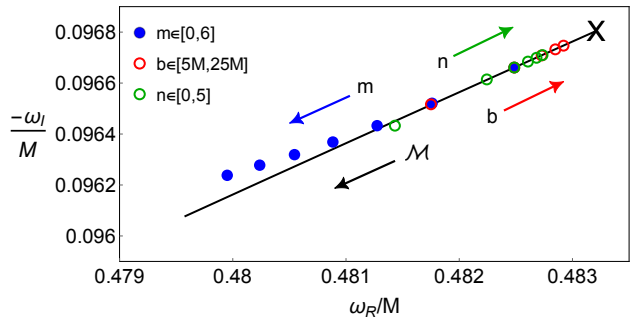

FIG. 8. The $l = 2$ QNM frequencies of the SBH-disk model. The solid curve shows the results of fixing $\{m, n, b\}$ as in Fig. 3, while varying $\mathcal{M}/M$ from 0 to 0.1 (right to left). The cross corresponds to the pure Schwarzschild results ($\mathcal{M} = 0$). The colored points show the results of fixing $\mathcal{M}/M = 0.02$ and other parameters except for the one indicated in the legend. The arrows indicate the direction along which the referred parameters change.

ways reduce the values of ω_R and $|\omega_I|$, as long as $\mathcal{M}/M$ stays reasonably small and the index m remains $O(1)$. In such cases, the validity of the first-order approximation used to derive the effective potential (33) is ensured. Moreover, the effective potential has a single-peak structure, whose shape monotonically deviates from the pure Schwarzschild one. In Fig. 8, we focus on $l = 2$ and investigate the QNM frequencies in the parameter space $\{m, n, b, \mathcal{M}\}$. The solid curve shows the results of fixing $m = 0$, $n = 2$, $b = 10M$, and varying $\mathcal{M}/M$ from 0 to 0.1. The cross indicates the pure Schwarzschild frequency $\mathcal{M} = 0$. The colored points and open circles show the results of fixing $\mathcal{M}/M = 0.02$ and other parameters except for those indicated in the legend. From Fig. 8, we find that the larger the parameters b (red circle) or n (green circle) are, the closer the QNM frequencies are to the Schwarzschild one. On the other hand, increasing m would reduce ω_R and $|\omega_I|$.

Another important observation from Fig. 8 is that almost all the colored points are nicely lined along the black curve. Although the SBH-disk model has a large parameter space $\{m, n, b, \mathcal{M}, l, m_z\}$, there seems to be a universal relation that the QNM frequencies of the model have to obey. We also consider other multipole numbers l and a universal relation seems to exist among the modes, as can be seen in Fig. 9. A similar trend of QNM shifts also appears in the model in which the black hole spacetime is superposed with a spherically symmetric matter distribution [16, 42], indicating that the relation may be really universal in the sense that it is insensitive to the matter configuration in the distribution. In general, the universal relation inevitably implies a strong degeneracy among intrinsic disk parameters. However, the relation could be helpful to distinguish the disk effects from those contributed by other putative external parameters not belonging to the disk model. For example, if the black hole QNM frequencies are found to be away from this universal relation, e.g, they are not lined along the black curve in Fig. 9, such a frequency shift must be induced by effects other than the disk contributions. In fact, several quantum-corrected black hole models predict larger values of ω_R [43–49], hence the QNMs of the models would not be lined on the black curve. The quantum parameters in these models are thus robustly disentangled from the disk effects, hence enhancing the possibility of testing these quantum-corrected black hole models through black hole spectroscopy.

Having said that, if there does exist a universal relation, one should still be careful with the range of its validity. In particular, from Fig. 9, the relation seems not valid anymore when one keeps increasing m or $\mathcal{M}$. Indeed, disk models with sufficiently large m and $\mathcal{M}$ could acquire a very dense and narrow peak in the density profile outside the black hole, resembling a flattened torus or ring rather than a disk. This extreme density profile could largely alter the shape of the effective potential, including the possibility of generating extra peaks outside the original one (see Fig. 10 for an example). If this happens, pseudospectral instability may be triggered, which would totally destroy the QNM spectrum [13] and the universal relation would not be valid anymore. In fact, when the second peak appears in the effective potential, gravitational echoes following the main sinusoidal-decaying phase may appear in the time domain signals. These echoes correspond to the long-lived modes which are trapped between the potential barriers before they slowly leak through the outer one. However, we would like to emphasize that the possibility of having multiple peaks in the effective potential has to be treated with great care. This is because increasing the disk mass $\mathcal{M}$ would, at some point, violate the validity of the first-order approximations from which we derive the effective potential (33). In addition, although all energy conditions discussed at the end of sec. II hold for the disk parameters considered in Fig. 10, for high m the density peak is located around the Schwarzschild value of the ISCO radius. Thus, for the most part, those disks would not be stable. Therefore, the double-peak structure in the effective potential demonstrated in Fig. 10 may have issues regarding its theoretical and physical viability. Therefore, we will not discuss it more in the present paper.

V. QNMS IN EIKONAL LIMITS

Consider a test field propagating in curved spacetimes. In the geometric optics approximation, the wavelength of the field is assumed to be much smaller than any other length scale in the system. In the leading order of this approximation, sometimes also called eikonal approximation, the equations of motion of the propagating field share the same form as those of the freely moving photons. When adopting the approximation to black hole spacetimes, it is well-known that the eikonal black hole

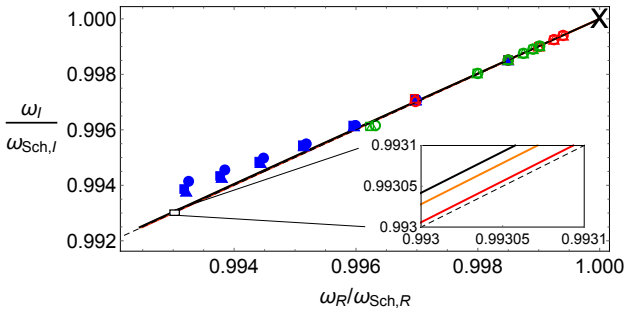

FIG. 9. The ratio of the QNM frequencies of the SBH-disk model with various parameter choices, with respect to the Schwarzschild QNM frequencies ω_{Sch}. The black ($l = 2$), orange ($l = 4$), and red ($l = 6$) continuous curves show the results of varying $\mathcal{M}/M$ from 0 to 0.1. The cross located at the coordinate $(1, 1)$ corresponds to the pure Schwarzschild results ($\mathcal{M} = 0$). The circular, rectangular, and triangular points correspond to $l = 2$, $l = 4$, and $l = 6$, respectively. The parameter sets chosen for the points are referred to by the colors as those in Fig. 8. The thin dashed line with a slope equal to one is shown for reference.

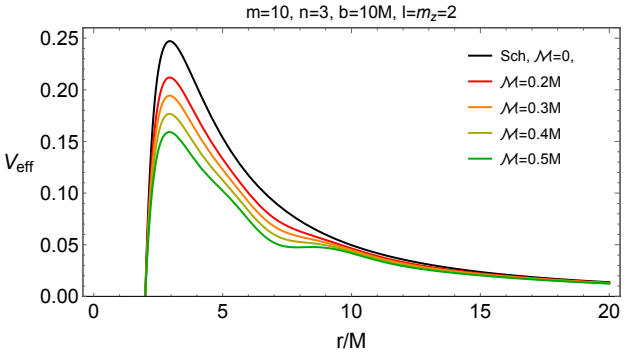

FIG. 10. The effective potential $V_{\mathrm{eff}}(r)$ of the SBH-disk model with $b = 10M$, $n = 3$, $m = 10$, $l = |m_z| = 2$. In some cases, the disk density is huge enough to induce multiple peaks in the effective potential (green).

QNMs have some properties that can be directly linked to the photon orbits in such a spacetime. More explicitly, one can identify the so-called eikonal correspondence between the eikonal QNMs and the bound photon orbits around the black hole.

In a static and spherically symmetric black hole spacetime, the QNMs are determined up to their multipole number l because the azimuthal numbers m_z degenerate. As for the bound photon orbits, it turns out that all the bound photon orbits in this case are circular orbits and have a single radius, called the photon sphere [50]. In this simple spacetime configuration, the eikonal correspondence can be identified straightforwardly through the fact that the peak of the effective potential of QNMs of $l \gg 1$ is precisely at the photon sphere. Based on this identification, the real and the imaginary parts of the large-l QNMs would correspond to the orbital frequency and the Lyapunov exponent of photons on the photon sphere, respectively [51]. The eikonal correspondence can be extended to rotating black hole spacetimes [52, 53], black holes with multiple photon spheres [54], and even deformed black hole spacetimes [27]. The possibility of testing eikonal correspondence through black hole observations has been proposed in Ref. [55].

When the black hole is slightly deformed, as the SBH-disk model considered in this paper, the QNM equations depend on both l and m_z. Therefore, the identification of the eikonal correspondence has to be carried out with care. In fact, for the SBH-disk model, circular orbits only exist at the equatorial plane. Any inclined bound photon orbits would acquire θ-dependent deformations such that they do not have a constant radius. In Ref. [27], it has been demonstrated that the eikonal correspondence of deformed Schwarzschild black hole spacetimes can be identified by defining the averaged radius of the bound photon orbits along one complete period. More explicitly, the averaged radius would correspond to the peak of the effective potentials of QNMs with $l \gg 1$ and arbitrary m_z.

In this section, we will investigate the eikonal correspondence for the SBH-disk model. Specifically, we will consider the equatorial eikonal modes ($l = |m_z| \gg 1$) and the polar eikonal modes ($m_z = 0$ and $l \gg 1$). The results obtained in this section can be treated as a consistency check with those exhibited in Ref. [27].

A. The equatorial modes $l = |m_z|$

When $l = |m_z|$, the coefficients (23)-(26) can be expressed as

$$
\begin{aligned}
a_{ll}^{2k} &= a_{l-l}^{2k} = \frac{l(2l+1)}{2} X_{\mathrm{even}}(l,k)\,, \\
b_{ll}^{2k} &= b_{l-l}^{2k} = \frac{2l+1}{2l+2k+1} X_{\mathrm{even}}(l,k)\,, \\
c_{ll}^{2k} &= c_{l-l}^{2k} = \frac{l(2l+1)(2k-1)}{2(2l+2k+1)} X_{\mathrm{even}}(l,k)\,, \\
d_{ll}^{2k} &= d_{l-l}^{2k} = -\frac{2kl(2l+1)}{2l+2k+1} X_{\mathrm{even}}(l,k)\,, \\
a_{ll}^{2k+1} &= a_{l-l}^{2k+1} = \frac{l(2l+1)}{2} X_{\mathrm{odd}}(l,k)\,, \\
b_{ll}^{2k+1} &= b_{l-l}^{2k+1} = \frac{2l+1}{2l+2k+1} X_{\mathrm{odd}}(l,k)\,, \\
c_{ll}^{2k+1} &= c_{l-l}^{2k+1} = \frac{l(2l+1)(2k-1)}{2(2l+2k+1)} X_{\mathrm{odd}}(l,k)\,, \\
d_{ll}^{2k+1} &= d_{l-l}^{2k+1} = -\frac{2kl(2l+1)}{2l+2k+1} X_{\mathrm{odd}}(l,k)\,,
\end{aligned}
\tag{36}
$$

where k are non-negative integers, and

$$
X_{\mathrm{even}}(l,k) \equiv \frac{C_k^{l+k}}{C_{2k}^{2l+2k}}\,, \quad X_{\mathrm{odd}}(l,k) \equiv \frac{C_l^{2l}}{4^l C_k^{l+k}}\,, \tag{37}
$$

where C^i_j are the binomial coefficients. Therefore, in the eikonal limit $l \gg 1$, only the coefficients a^0_{ll} and a^0_{l-l} dominate and read

$$a^0_{ll} = a^0_{l-l} \approx l^2 \,. \tag{38}$$

The effective potential (33) of the SBH-disk model can thus be approximated as

$$V_{\rm eff}(r) \approx l^2 \frac{f(r)}{r^2} \left[1 + 4\epsilon \mathcal{V}_0(r)\right] \,. \tag{39}$$

In this case, the eikonal QNMs with $l = |m_z| \gg 1$ correspond to the photons that undergo bound circular motion on the equatorial plane. According to Ref. [27], the radius of these orbits is determined by the root of $\partial_r (g_{tt}/g_{\varphi\varphi})_{x=0} = 0$. For the SBH-disk model with approximated metric (31), this equation can be written as

$$\partial_r \left[\frac{f(r)}{r^2}\left(1 + 4\nu_{\rm disk}\right)\right]_{x=0} = 0 \,, \tag{40}$$

which is precisely the equation that determines the peak of the effective potential (39) for $l = |m_z| \gg 1$ because $\nu_{\rm disk}|_{x=0} = \epsilon \mathcal{V}_0$.

B. The polar modes $m_z = 0$

When $m_z = 0$, the dominant coefficients in the eikonal limit $l \gg 1$ are

$$c^j_{l0} \approx \begin{cases} -\dfrac{1}{4^k} C^{2k}_k l^2 \,, & \text{if } j = 2k \\ -\dfrac{4^{k+1} l^2}{\pi (k+1) C^{2k+2}_{k+1}} \,, & \text{if } j = 2k+1 \,. \end{cases}$$

The effective potential (33) is then approximated as

$$V_{\rm eff}(r) \approx l^2 \frac{f(r)}{r^2} \Bigg\{ 1 + \epsilon \sum_{k=0}^{\infty} \Bigg[\frac{C^{2k}_k}{4^k} \left(4\mathcal{V}_{2k} - 2\mathcal{L}_{2k}\right) + \frac{4^{k+1}}{\pi (k+1) C^{2k+2}_{k+1}} \left(4\mathcal{V}_{2k+1} - 2\mathcal{L}_{2k+1}\right) \Bigg] \Bigg\} \,. \tag{41}$$

Note that the last term on the right-hand side comes from the terms with odd j.

The peak of the effective potential (41) can also be obtained through the calculations of photon geodesic equations. Consider the polar photon orbits on the photon sphere around the Schwarzschild black hole. Those orbits have zero azimuthal angular momentum L_z and repeatedly reach the poles $x = \pm 1$. When the spacetime is deformed, i.e., $\epsilon \neq 0$, these polar orbits would also be deformed such that $\dot{r} = O(\epsilon)$ and $L_z = O(\epsilon)$, where the dot denotes the derivative along the geodesic with respect to the affine parameter λ. Up to the first-order of ϵ, the radial component of the geodesic equations

$$\frac{d}{d\lambda}\left(g_{\mu\nu}\dot{x}^\nu\right) = \frac{1}{2}\left(\partial_\mu g_{\alpha\beta}\right)\dot{x}^\alpha \dot{x}^\beta \tag{42}$$

can be written as

$$\frac{d}{d\lambda}\left(g_{rr}\dot{r}\right) = \frac{1}{2}\frac{E^2}{g_{tt}} \partial_r \ln \left|\frac{g_{tt}}{g_{\theta\theta}}\right| + O\left(\epsilon^2\right) \,, \tag{43}$$

where E is the energy of photons. Following Ref. [27], we assume that the deformed orbits remain periodic and form a class of limit cycles in the phase space. We can then integrate Eq. (43) along a closed loop along λ. We then obtain

$$\begin{aligned} o(\epsilon) &\propto \int_0^{2\pi} d\theta \partial_r \left(\frac{g_{tt}}{g_{\theta\theta}}\right) \\ &\propto \int_0^{2\pi} d\theta \partial_r \left\{ \frac{f(r)}{r^2} \left[1 + \left(4\mathcal{V}_j(r) - 2\mathcal{L}_j(r)\right) \left|\cos^j \theta\right|\right] \right\} \,, \end{aligned} \tag{44}$$

with j a dummy index standing for summations over all non-negative integers. Because of the absolute value of $\cos^j \theta$, both even and odd powers of j contribute to the integration[5]. One can eventually get

$$\partial_r \Bigg\{ \frac{f(r)}{r^2} \Bigg[1 + \epsilon \sum_{k=0}^{\infty} \Bigg(\frac{C^{2k}_k}{4^k} \left(4\mathcal{V}_{2k} - 2\mathcal{L}_{2k}\right) + \frac{4^{k+1}}{\pi (k+1) C^{2k+2}_{k+1}} \left(4\mathcal{V}_{2k+1} - 2\mathcal{L}_{2k+1}\right) \Bigg) \Bigg] \Bigg\} = o(\epsilon) \,, \tag{45}$$

and then see that the root of Eq. (45) coincides with the peak of the effective potential (41). In Ref. [27], it has been proved that the root of Eq. (45) is precisely the averaged radius of the polar photon orbits along full periods. The averaged radius of bound photon orbits, both in the cases of equatorial orbits (40) and polar orbits (45), can be captured by their corresponding effective potentials of QNMs in the eikonal limit, i.e., Eqs. (39) and (41), respectively. This is the manifestation of eikonal correspondence between bound photon orbits and high-frequency QNMs. Here, we show explicitly that even in the presence of spacetime deformations induced by a gravitating thin disk, as long as the disk mass is much smaller than the black hole mass, i.e., $\epsilon \ll 1$, the eikonal correspondence can be identified through the definition of the averaged radius of bound photon orbits. This is consistent with the results of Ref. [27].

VI. CONCLUSIONS

In this paper, we consider a recently obtained solution of deformed Schwarzschild black holes (SBH-disk model)

[5] In Ref. [27], the metric functions are expressed in series of $\cos\theta$ without absolute values. Therefore, in that case, only even powers of j would contribute.

[25] and investigate the QNMs of a massless scalar field of this spacetime. The SBH-disk model describes the spacetime geometry of a Schwarzschild black hole encircled by a gravitating thin accretion disk. The superposed spacetime is an exact solution to GR and the gravitational field is regular everywhere outside the event horizon. In particular, the presence of the gravitating thin disk breaks the spherical symmetry, which is usually assumed in the literature when considering the gravitating fluid in the environment around astrophysical black holes.

The lack of spherical symmetry of the SBH-disk model inevitably leads to the computational complexity of QNM frequencies because the angular and radial sectors of the QNM master equation are highly coupled. We overcome this difficulty by assuming that the disk mass $\mathcal{M}$ is much smaller than the black hole mass M. Up to the first order of $\mathcal{M}/M$, one can obtain the master equation that allows us to investigate the frequency shifts of QNMs in the presence of the disk. In particular, the radial sector of the master equation can be recast in a Schrödinger-like form in which the effective potential $V_{\rm eff}(r)$ can be defined unambiguously and it reduces to the Schwarzschild one $V_{\rm eff}^{\rm Sch}(r)$ in proper limits.

Besides the black hole mass M, the SBH-disk model contains four additional parameters, which essentially control the shape of the surface density profile for the disk. Taking a physically reasonable density profile, we find that the disk gravity would flatten the effective potential $V_{\rm eff}(r)$ as compared with the Schwarzschild one. This behavior is robust among different choices of disk parameters. Furthermore, the presence of the gravitating disk would lower the real part of the QNM frequencies, while increase the damping time. In particular, the shifts of the real and imaginary parts with respect to their Schwarzschild counterparts, seem to follow a universal relation in the sense that they are shifted toward the same direction on the complex plane by the same amount in the presence of the disk (Fig. 9). Similar results also appear when the matter around the black hole is modeled based on the assumption of spherical symmetry [16, 42]. Although still far away from a rigorous proof, if such a universal relation is indeed robust against the changes of matter configuration around the black hole, it would aid the discrimination between the disk effects on the QNM spectrum and those contributed by other putative physics beyond GR. This line of research deserves further investigation.

In addition to QNM frequencies, we investigate two special kinds of bound photon orbits around the SBH-disk model. Since the equatorial symmetry is still preserved, the circular photon orbits on the equatorial plane exist, and the radius of the orbits is precisely at the peak of the effective potential of the eikonal equatorial QNMs. On the other hand, each polar orbit has a θ-dependent radius because of the spacetime deformations. Assuming periodicity of the orbits, we find that the averaged radius of the orbits along a full period would correspond to the peak of the effective potential of the eikonal polar modes. This result is consistent with that found in the literature.

In order to directly connect to the ringdown phase of gravitational waves, extending the present work to gravitational perturbations is necessary[6]. In addition, the physical properties of the SBH-disk model are not much explored so far. These include a detailed investigation of the geodesic dynamics of photons and massive particles. An extension towards a more realistic situation would be to include rotation of the black hole, the disk, or both in the black-hole–disk model and in the analysis of QNMs. We leave these interesting issues for future work.

ACKNOWLEDGMENTS

CYC is supported by the Institute of Physics of Academia Sinica and the Special Postdoctoral Researcher (SPDR) Program at RIKEN. PK acknowledges support from GACR 21-11268S of the Czech Science Foundation.

Appendix A: Physical properties of the disks

To describe the matter content of infinitesimally thin disks, we have to introduce the stress-energy tensor on a singular hypersurface. Using the formalism developed by Israel [57], the surface stress-energy tensor of a singular layer of matter located at $z = \text{const}$ reads [58]

$$S_{\alpha\beta} = -\frac{\sqrt{g_{\rho\rho}}}{8\pi}\left(\frac{g_{\alpha\beta}}{g_{\rho\rho}}\right)_{,z} . \tag{A1}$$

This expression holds for any axially symmetric and stationary spacetime in Weyl coordinates. If the spacetime is static described by a metric (3), the stress-energy tensor (A1) has only two non-trivial components which read

$$S_{tt} = \frac{1}{2\pi}e^{3\nu-\lambda}\nu_{,z}(1-\rho\nu_{,\rho}) , \tag{A2}$$

$$S_{\varphi\varphi} = \frac{1}{2\pi}e^{-\lambda-\nu}\rho^3\nu_{,z}\nu_{,\rho} , \tag{A3}$$

where the right-hand sides are evaluated in the singular hypersurface, i.e., in the equatorial plane $z = 0$ where our disk lies. Consider a static observer equipped with a tetrad

$$e^\alpha_{(t)} = \frac{1}{\sqrt{-g_{tt}}}\delta^\alpha_t , \qquad e^\alpha_{(\varphi)} = \frac{1}{\sqrt{g_{\varphi\varphi}}}\delta^\alpha_\varphi , \tag{A4}$$

$$e^\alpha_{(\rho)} = \frac{1}{\sqrt{g_{\rho\rho}}}\delta^\alpha_\rho , \qquad e^\alpha_{(z)} = \frac{1}{\sqrt{g_{zz}}}\delta^\alpha_z . \tag{A5}$$

[6] Similar analysis has been carried out in Ref. [56] in which the matter field around the black hole is assumed not to deform the black hole geometry at the background level, while interact gravitationally only at the perturbation level.

In this tetrad, we easily observe that the disk can be interpreted as ideal fluid with density and azimuthal pressure (measured by the static observer hovering above the disk)

$$\sigma \equiv S_{\alpha\beta} e^{\alpha}_{(t)} e^{\beta}_{(t)} = \frac{1}{2\pi} e^{\nu-\lambda} \nu_{,z} (1 - \rho \nu_{,\rho}) \,, \tag{A6}$$

$$P \equiv S_{\alpha\beta} e^{\alpha}_{(\varphi)} e^{\beta}_{(\varphi)} = \frac{1}{2\pi} e^{\nu-\lambda} \rho \nu_{,z} \nu_{,\rho} \,. \tag{A7}$$

The relation between the z derivative of the potential and the Newtonian surface density $w(\rho)$ can be obtained by integrating the Poisson equation $\Delta\nu = 4\pi w(\rho)\delta(z)$ over the z coordinate. Assuming that the spacetime is reflection symmetric with respect to the equatorial plane, only the term $\nu_{,zz}$ gives some non-zero contributions, thus

$$w(\rho) = \frac{1}{2\pi} \lim_{z \to 0^+} \nu_{,z} \,. \tag{A8}$$

Substituting this relation into (A7) we get precisely (17).

[1] K. D. Kokkotas and B. G. Schmidt, Living Rev. Rel. **2**, 2 (1999).
[2] E. Berti, V. Cardoso and A. O. Starinets, Class. Quant. Grav. **26**, 163001 (2009).
[3] R. A. Konoplya and A. Zhidenko, Rev. Mod. Phys. **83**, 793-836 (2011).
[4] B. P. Abbott *et al.* [LIGO Scientific and Virgo], Phys. Rev. Lett. **116**, no.6, 061102 (2016).
[5] R. Abbott *et al.* [LIGO Scientific, VIRGO and KAGRA], [arXiv:2111.03606 [gr-qc]].
[6] D. Reitze, R. X. Adhikari, S. Ballmer, B. Barish, L. Barsotti, G. Billingsley, D. A. Brown, Y. Chen, D. Coyne and R. Eisenstein, *et al.* Bull. Am. Astron. Soc. **51**, no.7, 035 (2019) [arXiv:1907.04833 [astro-ph.IM]].
[7] M. Maggiore, C. Van Den Broeck, N. Bartolo, E. Belgacem, D. Bertacca, M. A. Bizouard, M. Branchesi, S. Clesse, S. Foffa and J. García-Bellido, *et al.* JCAP **03**, 050 (2020).
[8] P. T. Leung, Y. T. Liu, W. M. Suen, C. Y. Tam and K. Young, Phys. Rev. Lett. **78**, 2894-2897 (1997).
[9] P. T. Leung, Y. T. Liu, W. M. Suen, C. Y. Tam and K. Young, Phys. Rev. D **59**, 044034 (1999).
[10] E. Barausse, V. Cardoso and P. Pani, Phys. Rev. D **89**, no.10, 104059 (2014).
[11] E. Barausse, V. Cardoso and P. Pani, J. Phys. Conf. Ser. **610**, no.1, 012044 (2015).
[12] J. L. Jaramillo, R. Panosso Macedo and L. Al Sheikh, Phys. Rev. X **11**, no.3, 031003 (2021).
[13] M. H. Y. Cheung, K. Destounis, R. P. Macedo, E. Berti and V. Cardoso, Phys. Rev. Lett. **128**, no.11, 111103 (2022).
[14] E. Berti, V. Cardoso, M. H. Y. Cheung, F. Di Filippo, F. Duque, P. Martens and S. Mukohyama, Phys. Rev. D **106**, no.8, 084011 (2022).
[15] K. Kyutoku, H. Motohashi and T. Tanaka, Phys. Rev. D **107**, no.4, 044012 (2023).
[16] V. Cardoso, K. Destounis, F. Duque, R. P. Macedo and A. Maselli, Phys. Rev. D **105**, no.6, L061501 (2022).
[17] A. J. M. Medved, D. Martin and M. Visser, Class. Quant. Grav. **21**, 1393-1406 (2004).
[18] J. P. S. Lemos and P. S. Letelier, Phys. Rev. D, **49**, no.10, 5135–5143 (1994).
[19] O. Semerák and M. Žáček, Class. Quantum Grav., **17**, no.7, 1613–1626 (2000).
[20] T. Morgan and L. Morgan, Phys. Rev., **183**, no.5, 1097–1101 (1969).
[21] P. V. P. Cunha, N. A. Eiró, C. A. R. Herdeiro, and J. P. S. Lemos, J. Cosmol. Astropart. Phys., **2020**, no.3, 035, (2020).
[22] O. Semerák, Class. Quantum Grav., **21**, no.8, 2203–2218 (2004).
[23] P. Kotlařík, D. Kofroň, and O. Semerák, ApJ, **931**, no.2, 161 (2022).
[24] R. S. S. Vieira, Class. Quantum Grav., **37**, no.20, 205013 (2020).
[25] P. Kotlařík and D. Kofroň, Astrophys. J. **941**, no.1, 25 (2022).
[26] P. A. Cano, K. Fransen and T. Hertog, Phys. Rev. D **102**, no.4, 044047 (2020).
[27] C. Y. Chen, H. W. Chiang and J. S. Tsao, Phys. Rev. D **106**, no.4, 044068 (2022).
[28] V. Cardoso and A. Foschi, Phys. Rev. D **104**, no.2, 024004 (2021).
[29] Y. Zhao, Y. Cai, S. Das, G. Lambiase, E. N. Saridakis and E. C. Vagenas, [arXiv:2301.09147 [gr-qc]].
[30] R. Ghosh, N. Franchini, S. H. Völkel and E. Barausse, [arXiv:2303.00088 [gr-qc]].
[31] D. Vogt and P. S. Letelier MNRAS **396**, no. 3, pp. 1487–1498 (2009).
[32] A. Toomre ApJ **138**, p. 385 (1963).
[33] B. F. Schutz and C. M. Will, Astrophys. J. Lett. **291**, L33-L36 (1985).
[34] S. Iyer and C. M. Will, Phys. Rev. D **35**, 3621 (1987).
[35] R. A. Konoplya, Phys. Rev. D **68**, 024018 (2003).
[36] J. Matyjasek and M. Opala, Phys. Rev. D **96**, no.2, 024011 (2017).
[37] J. Matyjasek and M. Telecka, Phys. Rev. D **100**, no.12, 124006 (2019).
[38] Y. Hatsuda, Phys. Rev. D **101**, no.2, 024008 (2020).
[39] R. A. Konoplya, A. Zhidenko and A. F. Zinhailo, Class. Quant. Grav. **36**, 155002 (2019).
[40] H. T. Cho, A. S. Cornell, J. Doukas and W. Naylor, Class. Quant. Grav. **27**, 155004 (2010).
[41] H. T. Cho, A. S. Cornell, J. Doukas, T. R. Huang and W. Naylor, Adv. Math. Phys. **2012**, 281705 (2012).
[42] R. A. Konoplya, Phys. Lett. B **823**, 136734 (2021).
[43] D. J. Liu, B. Yang, Y. J. Zhai and X. Z. Li, Class. Quant. Grav. **29**, 145009 (2012).
[44] S. Fernando and J. Correa, Phys. Rev. D **86**, 064039 (2012).
[45] A. Flachi and J. P. S. Lemos, Phys. Rev. D **87**, no.2, 024034 (2013).
[46] M. Bouhmadi-López, S. Brahma, C. Y. Chen, P. Chen and D. h. Yeom, JCAP **07**, 066 (2020).

[47] R. G. Daghigh, M. D. Green and G. Kunstatter, Phys. Rev. D **103**, no.8, 084031 (2021).
[48] K. Jafarzade, M. Kord Zangeneh and F. S. N. Lobo, Annals Phys. **446**, 169126 (2022).
[49] D. del-Corral and J. Olmedo, Phys. Rev. D **105**, no.6, 064053 (2022).
[50] C. M. Claudel, K. S. Virbhadra and G. F. R. Ellis, J. Math. Phys. **42**, 818-838 (2001).
[51] V. Cardoso, A. S. Miranda, E. Berti, H. Witek and V. T. Zanchin, Phys. Rev. D **79**, no.6, 064016 (2009).
[52] H. Yang, D. A. Nichols, F. Zhang, A. Zimmerman, Z. Zhang and Y. Chen, Phys. Rev. D **86**, 104006 (2012).
[53] P. C. Li, T. C. Lee, M. Guo and B. Chen, Phys. Rev. D **104**, no.8, 084044 (2021).
[54] G. Guo, P. Wang, H. Wu and H. Yang, JHEP **06**, 060 (2022).
[55] C. Y. Chen, Y. J. Chen, M. Y. Ho and Y. H. Tseng, [arXiv:2212.10028 [gr-qc]].
[56] A. Nagar, O. Zanotti, J. A. Font and L. Rezzolla, Phys. Rev. D **75**, 044016 (2007).
[57] W. Israel Nuovo Cim. B **44** p. 14, (1966).
[58] T. Ledvinka and J. Bičák Phys. Rev. D **99**, no. 6, p. 064046 (2019).

CHAPTER

4

TOWARDS STATIONARY PERTURBATIONS OF BLACK HOLES

Although the stationary and axially symmetric Einstein equations are fully integrable, thus in principle *all* solutions are known, only a few of them have been found in an explicit form and even fewer describe some astrophysical objects. In Chap. 2, we already studied the simplest subclass of such spacetimes where dragging effects associated with the rotation of matter fields were neglected. We showed that the static problem is partially linear, the Einstein equations reduce to the Laplace equation plus a quadrature for the only other non-trivial metric function. In the stationary case, even in a vacuum, we have to solve the full non-linear system of Einstein equations. That amounts to start with the choice of B satisfying (1.10), then solve the coupled equations (1.11), (1.12) for the gravitational potential ν and dragging angular velocity ω, and finally integrate (1.14) and (1.15) to get the last metric function λ. Up to this date, there is no physical exact solution describing the rotating black hole with some additional (rotating) matter fields. Even the powerful generation techniques like the inverse scattering method based on the Ernst potential formulation failed so far to produce any physically realistic explicit exact solution (Semerák, 2002a; Lenells, 2011), see also the topical review (Semerák, 2002b) and references therein. Hence, one has to typically resort to either numerical solutions of the Einstein equations, or some approximate methods, like perturbations. We are going to address the latter direction here.

Consider a known background solution $\nu_0, \omega_0, \lambda_0$ (we choose $B = 1$ for simplicity), then the linearized vacuum Einstein equations for the perturbations ν_1, ω_1

read

$$\nabla \cdot \nabla \nu_1 - \frac{1}{2}\rho^2 e^{-4\nu_0}\left[4\nu_1(\nabla\omega_0)^2 - \nabla\omega_0 \cdot \nabla\omega_1\right] = 0\,, \tag{4.1}$$

$$\nabla \cdot \left[\rho^2 e^{-4\nu_0}(\nabla\omega_1 - 4\nu_1\nabla\omega_0)\right] = 0\,, \tag{4.2}$$

where we already subtracted the background solution. If we assume that the background is static, in particular, if we look for a perturbation of the Schwarzschild black hole, the Eqs. (4.1) and (4.2) decouple! Moreover, the equation for ν_1 reduces to the Laplace equation. Thus, the static superpositions studied in Chap. 2 are also solutions of the stationary case, although they have to be supplemented by an appropriate solution for ω_1. The problem was considered already by Will (1974) where he obtained the Green function ω_1 in terms of a multipole expansion. More recently, Čížek & Semerák (2017) rederived the Green function in closed-form and provided the solution describing a light, thin and slowly rotating finite disc around the Schwarzschild black hole[1]. We then studied its basic physical properties in Kotlařík et al. (2018). However, this "minimal" approach has not led to a more general solution for the dragging ω_1 so far, nor it is convenient for the perturbations of the rotating Kerr black hole, since the equations for ν_1 and ω_1 do not decouple anymore.

Nevertheless, we might have more luck using techniques of the black hole perturbation theory. We already touched the basics in Chap. 3, where we studied quasinormal modes. After the groundbreaking works of Regge & Wheeler (1957) and Zerilli (1970), rapid development started in the 70s after Teukolsky (1973) succeeded in separating the perturbed equations for the Petrov-type-D spacetimes. Soon, Linet (1977) applied the Teukolsky results to the stationary and axially symmetric case and provided an expression for calculating the Green function of the Teukolsky equation. However, since then not many explicit solutions have been found. This last chapter aims to continue in the direction that Linet initiated. Yet, we start with a related simpler problem of the electromagnetic field first.

The topic of the electromagnetic (Maxwell) field on a background containing a black hole attracted a lot of attention already in the 1950s/1960s with significant progress following the derivation of separated equations for the Maxwell field in the previously mentioned work by Teukolsky (1973). We will revisit the problem of the electromagnetic field sourced by a massless ring on the Kerr background, a subject that has been extensively explored in numerous works (Petterson, 1974; Chitre & Vishveshwara, 1975; Petterson, 1975; Linet, 1976; Bičák & Dvořák, 1976; Bičák & Dvořák, 1977). Despite the variety of forms in which the results have been presented, they all share a common feature: they are expressed in terms of the multipole expansion, which exhibits rather suboptimal convergence properties in the vicinity of the ring source. We will show how to rederive the results in the framework of the Debye potential and present the solution in closed-form.

Both problems, the electromagnetic field on a curved background and gravitational perturbations, will be studied in a specific tetrad. Given the special algebraic properties of the Kerr geometry, the tetrad formalism developed by Newman & Penrose (1962) is ideal for the task. We will achieve even further

[1]Note that they choose $B \neq 1$ in the paper which, however, is merely a coordinate change (1.24) as we already know.

simplification of the equations using the refined version due to Geroch, Held, and Penrose (Geroch et al., 1973). In the following pages, we will introduce both tetrad formalisms, solve equations for the electromagnetic field on the Kerr background and, at the end of the chapter, discuss the gravitational perturbations providing an outline for a similar procedure in that case.

4.1 NP formalism

All quantities describing a certain spacetime can be expressed in terms of scalars constructed from the projections on some tetrad. In particular, Newman & Penrose (1962) introduced a set of four linearly independent null vectors l^μ, n^μ, m^μ, $\bar{m}^\mu$, where l^μ, n^μ are real and m^μ, $\bar{m}^\mu$ are complex conjugate, such that

$$g_{\alpha\beta} l^\alpha n^\beta = -1\,, \qquad g_{\alpha\beta} m^\alpha \bar{m}^\beta = 1\,, \qquad \text{and other products are zero}\,. \tag{4.3}$$

They form a tetrad $e_{\hat{a}}{}^{\mu} \equiv (l^\mu, n^\mu, m^\mu, \bar{m}^\mu)$ where the Latin indices with a hat represent components in the tetrad frame and go through $\hat{a} = \{l, n, m, \bar{m}\}$. We define an object

$$\eta_{\hat{a}\hat{b}} \equiv g_{\alpha\beta} e_{\hat{a}}{}^{\alpha} e_{\hat{b}}{}^{\beta} = \begin{pmatrix} 0 & -1 & 0 & 0 \\ -1 & 0 & 0 & 0 \\ 0 & 0 & 0 & 1 \\ 0 & 0 & 1 & 0 \end{pmatrix} = \eta^{\hat{a}\hat{b}}\,, \tag{4.4}$$

which will represent the metric in the tetrad frame. In particular, for the metric components it then follows[2]

$$g_{\mu\nu} = \eta^{\hat{a}\hat{b}} e_{\hat{a}\mu} e_{\hat{b}\nu} = -2 l_{(\mu} n_{\nu)} + 2 m_{(\mu} \bar{m}_{\nu)}\,. \tag{4.5}$$

The covariant derivative is determined by projections of the connection onto the tetrad,

$$\gamma_{\hat{a}\hat{b}\hat{c}} = e_{\hat{a}}{}^{\alpha} e_{\hat{b}}{}^{\beta} \nabla_\alpha e_{\hat{c}\beta}\,, \tag{4.6}$$

which are commonly called the *spin coefficients*. From the definition, we immediately see that

$$\gamma_{\hat{a}\hat{b}\hat{c}} = -\gamma_{\hat{a}\hat{c}\hat{b}}\,. \tag{4.7}$$

It is useful to introduce directional derivatives along the tetrad vectors,

$$D \equiv l^\alpha \nabla_\alpha\,, \qquad \Delta \equiv n^\alpha \nabla_\alpha\,, \qquad \delta \equiv m^\alpha \nabla_\alpha\,, \qquad \bar{\delta} \equiv \bar{m}^\alpha \nabla_\alpha\,. \tag{4.8}$$

There is a total number of 12 complex spin coefficients defined in Tab. 4.1. The table works as follows: e.g., the spin coefficient κ is defined as

$$\kappa \equiv -m^\alpha D l_\alpha = -m^\alpha l^\beta \nabla_\beta l_\alpha = -\gamma_{lml}\,, \qquad \text{etc.}$$

In terms of the spin coefficients, we cast the Einstein equations into a set of linear equations. We split the Riemann tensor into[3]

$$R_{\mu\nu\sigma\tau} = C_{\mu\nu\sigma\tau} + g_{\mu[\sigma} R_{\tau]\nu} - g_{\nu[\sigma} R_{\tau]\mu} - \frac{1}{3} R g_{\mu[\sigma} g_{\tau]\nu}\,, \tag{4.9}$$

[2]The round brackets denote symmetrization, e.g., $l_{(\mu} n_{\nu)} = \frac{1}{2}(l_\mu n_\nu + l_\nu n_\mu)$.

[3]Where antisymmetrization is denoted by square brackets, e.g., $A_{[\mu\nu]} = \frac{1}{2}(A_{\mu\nu} - A_{\nu\mu})$.

∇	$-m^\alpha \nabla l_\alpha$	$-\frac{1}{2}(n^\alpha \nabla l_\alpha - \bar{m}^\alpha \nabla m_\alpha)$	$\bar{m}^\alpha \nabla n_\alpha$
D	κ	ϵ	π
Δ	τ	γ	ν
δ	σ	β	μ
$\bar{\delta}$	ϱ	α	λ

Table 4.1: Spin coefficients

where $C_{\mu\nu\sigma\tau}$ denotes the Weyl tensor. Since the Ricci tensor $R_{\mu\nu}$ and Ricci scalar R are fixed by the sources via the Einstein equations, the Weyl tensor represents the degrees of freedom of pure gravitational field. In the NP tetrad formalism, the 10 independent components of the Weyl tensor are encoded in 5 complex scalars

$$\psi_0 = C_{\alpha\beta\gamma\delta} l^\alpha m^\beta l^\gamma m^\delta \,, \tag{4.10}$$
$$\psi_1 = C_{\alpha\beta\gamma\delta} l^\alpha n^\beta l^\gamma m^\delta \,, \tag{4.11}$$
$$\psi_2 = C_{\alpha\beta\gamma\delta} l^\alpha m^\beta \bar{m}^\gamma n^\delta \,, \tag{4.12}$$
$$\psi_3 = C_{\alpha\beta\gamma\delta} l^\alpha n^\beta \bar{m}^\gamma n^\delta \,, \tag{4.13}$$
$$\psi_4 = C_{\alpha\beta\gamma\delta} n^\alpha \bar{m}^\beta n^\gamma \bar{m}^\delta \,. \tag{4.14}$$

Information about the matter is in the components of the Ricci tensor

$$\Phi_{00} = \frac{1}{2} R_{\alpha\beta} l^\alpha l^\beta = \bar{\Phi}_{00} \,, \qquad \Phi_{11} = \frac{1}{4} R_{\alpha\beta} (l^\alpha n^\beta + m^\alpha \bar{m}^\beta) = \bar{\Phi}_{11} \,, \tag{4.15}$$
$$\Phi_{01} = \frac{1}{2} R_{\alpha\beta} l^\alpha m^\beta = \bar{\Phi}_{10} \,, \qquad \Phi_{12} = \frac{1}{2} R_{\alpha\beta} n^\alpha m^\beta = \bar{\Phi}_{21} \,, \tag{4.16}$$
$$\Phi_{02} = \frac{1}{2} R_{\alpha\beta} m^\alpha m^\beta = \bar{\Phi}_{20} \,, \qquad \Phi_{22} = \frac{1}{2} R_{\alpha\beta} n^\alpha n^\beta = \bar{\Phi}_{22} \,, \tag{4.17}$$

determined by the Einstein equations (1.9) according to

$$\Phi_{00} = \frac{1}{2} R_{\alpha\beta} l^\alpha l^\beta = 4\pi T_{\alpha\beta} l^\alpha l^\beta \equiv 4\pi T_{ll} \,, \qquad \text{etc.} \tag{4.18}$$

4.2 GHP formalism

By making some symmetries of the NP tetrad explicit, Geroch et al. (1973) refined the NP formalism introducing the concept of spin and boost weights. We first define a discrete transformation $'$ which swaps between the vectors of the NP tetrad,

$$(l^\mu)' \equiv n^\mu \,, \qquad (n^\mu)' \equiv l^\mu \,, \qquad (m^\mu)' \equiv \bar{m}^\mu \,, \qquad (\bar{m}^\mu)' \equiv m^\mu \,. \tag{4.19}$$

This can be used to reduce the amount of necessary spin coefficients by half with the other half following from the prime transformation. The common choice is to use $(\kappa, \sigma, \varrho, \tau, \beta, \epsilon)$ and their primed counterparts

$$\kappa' = -\nu \,, \quad \sigma' = -\lambda \,, \quad \varrho' = -\mu \,, \quad \tau' = -\pi \,, \quad \beta' = -\alpha \,, \quad \epsilon' = -\gamma \,. \tag{4.20}$$

Similarly, for the directional derivatives, we have

$$D' = \Delta\,, \quad \delta' = \bar{\delta}\,. \tag{4.21}$$

Locally, without any real physical changes, we are free to choose any tetrad vectors related by the Lorentz transformations. In geometries with some preferred null directions, it is useful to decompose the 6-dimensional group of Lorentz transformations into a two-parameter Abelian subgroup of boosts in nl-directions and spatial rotations in the $m\bar{m}$-plane. Explicitly,

$$l^\mu \to \chi\bar{\chi} l^\mu\,, \quad n^\mu \to \chi^{-1}\bar{\chi}^{-1} n^\mu\,, \quad m^\mu \to \chi\bar{\chi}^{-1} m^\mu\,, \quad \bar{m}^\mu \to \chi^{-1}\bar{\chi}\bar{m}^\mu\,, \tag{4.22}$$

for an arbitrary complex function χ. GHP weights are defined in the following way: any tensor field φ associated with the tetrad $e^\mu_{\hat{a}}$, which under the change (4.22) undergos the transformation

$$\varphi \to \chi^p \bar{\chi}^q \varphi\,, \tag{4.23}$$

has the weights $\{p, q\}$; we call the combination $\frac{1}{2}(p-q)$ the spin-weight while the combination $\frac{1}{2}(p+q)$ the boost-weight of φ. In particular, the NP tetrad vectors have weights

$$l^\mu : \{1,1\}\,, \quad n^\mu : \{-1,-1\}\,, \quad m^\mu : \{1,-1\}\,, \quad \bar{m}^\mu : \{-1,1\}\,. \tag{4.24}$$

The prime transformation and complex conjugation change the weights as

$$'\,:\ \{p,q\} \to \{-p,-q\}\,, \qquad\qquad {}^-\,:\ \{p,q\} \to \{q,p\}\,. \tag{4.25}$$

Some NP scalars $(\kappa, \sigma, \varrho, \tau)$ and their primed versions are GHP scalars of weights

$$\kappa : \{3,1\}\,, \qquad \sigma : \{3,-1\}\,, \qquad \varrho : \{1,1\}\,, \qquad \tau : \{1,-1\}\,. \tag{4.26}$$

However, the rest of the scalars are not GHP quantities. Similarly, the directional derivatives (4.8) do not produce well-defined GHP quantities as well. But, they can be incorporated into GHP derivatives defined as operators acting on a quantity of weights $\{p, q\}$ as follows

$$\text{Þ}\varphi = (D - p\epsilon - q\bar{\epsilon})\varphi\,, \qquad \eth\varphi = (\delta - p\beta + q\bar{\beta}')\varphi\,, \tag{4.27}$$

$$\text{Þ}'\varphi = (\Delta + p\epsilon' + q\bar{\epsilon}')\varphi\,, \qquad \eth'\varphi = (\bar{\delta} + p\beta' - q\bar{\beta})\varphi\,. \tag{4.28}$$

The operators Þ ("thorn") and ð ("edth") generate the following change of the weights

$$\text{Þ}\varphi : \{p+1, q+1\}\,, \qquad \eth\varphi : \{p+1, q-1\}\,, \tag{4.29}$$

$$\text{Þ}'\varphi : \{p-1, q-1\}\,, \qquad \eth'\varphi : \{p-1, q+1\}\,. \tag{4.30}$$

For completeness, we list the weights of the Weyl scalars

$$\psi_0 : \{4,0\}\,, \quad \psi_1 : \{2,0\}\,, \quad \psi_2 : \{0,0\}\,, \quad \psi_3 : \{-2,0\}\,, \quad \psi_4 : \{-4,0\}\,, \tag{4.31}$$

and the Ricci scalars

$$\Phi_{00} : \{2,2\}\,, \qquad \Phi_{01} : \{2,0\}\,, \qquad \Phi_{02} : \{2,-2\}\,, \tag{4.32}$$

$$\Phi_{11} : \{0,0\}\,, \qquad \Phi_{12} : \{0,-2\}\,, \qquad \Phi_{22} : \{-2,-2\}\,. \tag{4.33}$$

We give the full set of GHP equations in Appendix A. That includes 4 commutation relations, 9 Ricci equations and 4 Bianchi identities plus their counterparts following from the prime transformation and complex conjugation.

4.3 Type D spacetimes and the Kerr black hole

Any vector k^μ which satisfies the condition

$$k^\beta k^\gamma k_{[\epsilon} C_{\alpha]\beta\gamma[\delta} k_{\sigma]} = 0 \tag{4.34}$$

is called the *principal null vector*. For each spacetime, there are exactly four of them, but one or more of the principal null vectors can coincide meaning that some directions might be degenerate. By a number of unique principal null directions, Petrov (1954) grouped all spacetimes into six algebraic types. The stationary black-hole solutions belong to the Petrov type-D class, which is characterized by the existence of two distinct principal null vectors, both having degeneracy two. In the NP tetrad with l^μ and n^μ aligned with the principal null directions, ψ_2 is the only non-zero component of the Weyl tensor ($\psi_0 = \psi_1 = \psi_3 = \psi_4 = 0$). Also, some of the spin coefficients vanish $\kappa = \kappa' = \sigma = \sigma' = 0$ as well. The Ricci equations for all type-D spacetimes are reduced to

$$\text{Þ}\varrho = \varrho^2\,, \qquad \text{Þ}\tau = \varrho(\tau - \bar{\tau}')\,, \tag{4.35}$$

$$\eth\tau = \tau^2\,, \qquad \eth\varrho = \tau(\varrho - \bar{\varrho})\,, \tag{4.36}$$

$$\text{Þ}'\varrho = \eth'\tau + \varrho\bar{\varrho}' - \tau\bar{\tau} - \psi_2\,, \tag{4.37}$$

and the Bianchi identities read

$$\text{Þ}\psi_2 = 3\varrho\psi_2\,, \qquad \eth\psi_2 = 3\tau\psi_2\,, \tag{4.38}$$

plus there are equations which follow from the prime transformation and the complex conjugation. The commutators of the GHP operators acting on a quantity φ of the weights $\{p, q\}$ become

$$\left[\text{Þ}\text{Þ}' - \text{Þ}'\text{Þ}\right]\varphi = \left[(\bar{\tau} - \tau')\eth + (\tau - \bar{\tau}')\eth' - p(\psi_2 - \tau\tau') - q(\bar{\psi}_2 - \bar{\tau}\bar{\tau}')\right]\varphi\,, \tag{4.39}$$

$$\left[\text{Þ}\eth - \eth\text{Þ}\right]\varphi = \left[\bar{\varrho}\eth - \bar{\tau}'\text{Þ} + q\bar{\varrho}\bar{\tau}'\right]\varphi\,, \tag{4.40}$$

$$\left[\eth\eth' - \eth'\eth\right]\varphi = \left[(\bar{\varrho}' - \varrho')\text{Þ} + (\varrho - \bar{\varrho})\text{Þ}' + p(\psi_2 + \varrho\varrho') - q(\bar{\psi}_2 + \bar{\varrho}\bar{\varrho}')\right]\varphi\,, \tag{4.41}$$

and three more following from the complex conjugation and prime transformation of (4.40). Combining the commutation relations with Bianchi identities and Ricci equations leads to additional identities in general type-D spacetimes (Edgar et al., 2009)

$$\varrho\bar{\varrho}' = \bar{\varrho}\varrho'\,, \qquad \tau\bar{\tau} = \tau'\bar{\tau}'\,, \qquad \text{Þ}'\varrho = \text{Þ}\varrho'\,, \qquad \eth\tau' = \eth'\tau \tag{4.42}$$

and

$$\text{Þ}\tau' = \eth'\varrho = -\bar{\varrho}\tau' + 2\varrho\tau' - \varrho\bar{\tau}\,, \tag{4.43}$$

plus the primed counterpart of the last equation and the complex conjugate. In spacetimes which admit a Killing tensor we find extra identities between the spin coefficients (Demianski & Francaviglia, 1981)

$$\frac{\varrho}{\bar{\varrho}} = \frac{\varrho'}{\bar{\varrho}'} = -\frac{\tau'}{\bar{\tau}} = -\frac{\tau}{\bar{\tau}'}\,, \tag{4.44}$$

thus from (4.43) we get

$$\text{Þ}\tau' = \text{ð}'\varrho = 2\varrho\tau' \tag{4.45}$$

and from the commutator $\left[\text{Þ}\text{Þ}' - \text{Þ}'\text{Þ}\right]\varrho$ and the Ricci equation (4.37) we obtain

$$\text{Þ}'\varrho = \varrho\varrho' + \tau(\tau' - \bar{\tau}) - \frac{1}{2}\psi_2 - \frac{\varrho}{2\bar{\varrho}}\bar{\psi}_2\,, \tag{4.46}$$

$$\text{ð}'\tau = \tau\tau' + \varrho(\varrho' - \bar{\varrho}') + \frac{1}{2}\psi_2 - \frac{\varrho}{2\bar{\varrho}}\bar{\psi}_2\,. \tag{4.47}$$

Such a Killing tensor, i.e., the tensor $K_{\mu\nu}$ satisfying $K_{(\mu\nu;\alpha)} = 0$, exists in all non-accelerating type D spacetimes, often referred to as the Kerr-NUT subclass. For a more detailed survey of Killing symmetries of the black-hole related spacetimes, follow Andersson et al. (2015).

One of the most prominent member of the non-accelerating type-D spacetimes is the Kerr solution (1.47). The standard choice of the tetrad aligned with the principal null directions is the so-called Kinnersley tetrad[4] (Kinnersley, 1969). In the Boyer-Lindquist coordinates (t, r, θ, ϕ) the Kinnersley vectors read

$$l^\mu = \frac{1}{\sqrt{2}\Delta}\left(r^2 + a^2, \Delta, 0, a\right)\,, \tag{4.48}$$

$$n^\mu = \frac{1}{\sqrt{2}\Sigma}\left(r^2 + a^2, -\Delta, 0, a\right)\,, \tag{4.49}$$

$$m^\mu = \frac{1}{\sqrt{2}(r + \mathrm{i}\,a\cos\theta)}\left(\mathrm{i}\,a\sin\theta, 0, 1, \frac{\mathrm{i}}{\sin\theta}\right)\,, \tag{4.50}$$

where Δ and Σ are defined in (1.46). Spin coefficients of the Kerr geometry in Kinnersley tetrad are given as

$$\varrho = \frac{1}{\sqrt{2}}\frac{1}{r - \mathrm{i}\,a\cos\theta}\,, \qquad \mu = \frac{1}{\sqrt{2}}\frac{\Delta}{\Sigma}\frac{1}{r - \mathrm{i}\,a\cos\theta}\,, \tag{4.51}$$

$$\tau = \frac{\mathrm{i}}{\sqrt{2}}\frac{a\sin\theta}{\Sigma}\,, \qquad \pi = -\frac{\mathrm{i}}{\sqrt{2}}\frac{a\sin\theta}{(r - \mathrm{i}\,a\cos\theta)^2}\,, \tag{4.52}$$

$$\beta = -\frac{1}{2\sqrt{2}}\frac{\cot\theta}{r + \mathrm{i}\,a\cos\theta}\,, \qquad \alpha = \pi - \bar{\beta}\,, \tag{4.53}$$

$$\epsilon = 0\,, \qquad \gamma = 0\,, \tag{4.54}$$

and the only non-zero component of the Weyl tensor is

$$\psi_2 = -\frac{M}{(r - \mathrm{i}\,a\cos\theta)^3}\,. \tag{4.55}$$

4.4 Maxwell field

We begin with discussing the electromagnetic field on the Kerr background. In the NP formalism, the Maxwell field is completely described by three complex

[4]Note that we adopt a boost factor $\sqrt{2}$ as opposed to the standard Kinnersley tetrad.

scalars obtained from the projections of the antisymmetric electromagnetic tensor $F_{\mu\nu}$ onto the tetrad,

$$\varphi_0 = F_{\alpha\beta} l^\alpha m^\beta \,, \qquad \varphi_1 = \frac{1}{2} F_{\alpha\beta}(l^\alpha n^\beta - m^\alpha \bar{m}^\beta) \,, \qquad \varphi_2 = F_{\alpha\beta} \bar{m}^\alpha n^\beta \,. \tag{4.56}$$

Equivalently,

$$F_{\mu\nu} = 2\varphi_0 \bar{m}_{[\mu} n_{\nu]} + 2\varphi_1 (n_{[\mu} l_{\nu]} + m_{[\mu} \bar{m}_{\nu]}) + 2\varphi_2 l_{[\mu} m_{\nu]} + \text{c.c}\,, \tag{4.57}$$

where c.c. denotes complex conjugation. The scalars have the following GHP weights

$$\varphi_0 : \{2, 0\} \,, \quad \varphi_1 : \{0, 0\} \,, \quad \varphi_2 : \{-2, 0\} \,. \tag{4.58}$$

Note that by applying the prime transformation, φ_0 and φ_2 swap, while all three components change signs

$$\varphi_0' = -\varphi_2 \,, \qquad \varphi_1' = -\varphi_1 \,, \qquad \varphi_2' = -\varphi_0 \,. \tag{4.59}$$

The Maxwell equations,

$$F_{[\mu\nu;\alpha]} = 0 \,, \qquad F^{\mu\alpha}{}_{;\alpha} = 4\pi J^\mu \,, \tag{4.60}$$

where J_μ is the four-current characterizing sources, are on the type D background equivalent to

$$(\text{Þ} - 2\varrho)\varphi_1 - (\eth' - \tau')\varphi_0 = 2\pi J_l \,, \tag{4.61}$$

$$(\eth - 2\tau)\varphi_1 - (\text{Þ}' - \varrho')\varphi_0 = 2\pi J_m \,, \tag{4.62}$$

plus two primed counterparts. Teukolsky (1973) showed that the equations for φ_0 and φ_2 can be decoupled, in particular the component φ_0 satisfies

$$\left[(\text{Þ} - \bar{\varrho} - 2\varrho)(\text{Þ}' - \varrho') - (\eth - \bar{\tau}' - 2\tau)(\eth' - \tau')\right] \varphi_0 = 2\pi J_0 \,, \tag{4.63}$$

where the source term reads

$$J_0 = (\eth - 2\tau - \bar{\tau}')J_l - (\text{Þ} - 2\varrho - \bar{\varrho})J_m \,. \tag{4.64}$$

The scalar φ_2 satisfies the primed version of Eq. (4.63). Although φ_1 also decouples from the other two scalars, the equation is not separable on the Kerr background (Fackerell & Ipser, 1972). It is thus more complicated to obtain φ_1 by solving the GHP Maxwell equations directly. However, we will overcome the difficulties by finding the Debye potential of the field, see the following section.

4.4.1 Hertz and Debye potentials of the electromagnetic field

It has been known since the 19$^{\text{th}}$ century that in flat spacetime, we can introduce the so-called Hertz and Debye potentials for the Maxwell field. In the 1970s, Cohen & Kegeles (1974) developed a similar technique applicable to curved spacetimes. In this section, we will follow their construction. In the language of differential forms, the electromagnetic two-form

$$\boldsymbol{F} = \frac{1}{2} F_{\alpha\beta} \mathbf{d}x^\alpha \wedge \mathbf{d}x^\beta \tag{4.65}$$

satisfies the source-free Maxwell equations in a vacuum

$$\mathbf{d}\boldsymbol{F} = 0\,, \qquad\qquad \boldsymbol{\delta}\boldsymbol{F} = 0\,, \tag{4.66}$$

where $\mathbf{d}$ denotes the exterior derivative and $\boldsymbol{\delta} \equiv *\mathbf{d}*$ is the coderivative obtained from the Hodge dual operation $*$. Poincaré's lemma ensure the existence of a *vector potential* $\boldsymbol{A}$ such that $\boldsymbol{F} = \mathbf{d}\boldsymbol{A}$. The choice of $\boldsymbol{A}$ is not unique, the vector potential $\boldsymbol{A} + \mathbf{d}\chi$ for an arbitrary scalar field χ generate the same field. This gauge freedom can be restricted by imposing the Lorentz gauge

$$\boldsymbol{\delta}\boldsymbol{A} = 0\,. \tag{4.67}$$

From Poincaré's lemma, it follows that there exists a two-form $\boldsymbol{H}$ known as the *Hertz potential* such that $\boldsymbol{A} = \boldsymbol{\delta}\boldsymbol{H}$. If the second equation in (4.66) should remain satisfied, we have to require

$$\boldsymbol{\delta}\boldsymbol{F} = \boldsymbol{\delta}\mathbf{d}\boldsymbol{\delta}\boldsymbol{H} = -\boldsymbol{\delta}\boldsymbol{\delta}\mathbf{d}\boldsymbol{H} = 0\,, \tag{4.68}$$

in other words

$$\boldsymbol{\Delta}\boldsymbol{H} \equiv (\mathbf{d}\boldsymbol{\delta} + \boldsymbol{\delta}\mathbf{d})\boldsymbol{H} = 0\,, \tag{4.69}$$

where we have denoted the Beltrami-Laplace operator as $\boldsymbol{\Delta}$.

Let us introduce an arbitrary ("gauge") 1-form $\boldsymbol{G}$ and 3-form $\boldsymbol{W}$. If it holds for $\boldsymbol{H}$ that

$$\boldsymbol{\Delta}\boldsymbol{H} = \mathbf{d}\boldsymbol{G} + \boldsymbol{\delta}\boldsymbol{W}\,, \tag{4.70}$$

the two-form

$$\boldsymbol{F} = \mathbf{d}\boldsymbol{\delta}\boldsymbol{H} + \mathbf{d}\boldsymbol{G} = -\boldsymbol{\delta}\mathbf{d}\boldsymbol{H} + \boldsymbol{\delta}\boldsymbol{W} \tag{4.71}$$

satisfies the vacuum Maxwell equations (4.66). Note, however, that such a procedure does not yield the vector potential $\boldsymbol{A}$ in the Lorentz gauge. It is in the so-called *radiation gauge* instead.

So far, the construction works for all curved spacetimes. Since the electromagnetic field has only two degrees of freedom, we might hope for further reduction of the problem. This can be achieved in spacetimes with a preferred direction, in other words in spacetimes that are algebraically special. Then, we can use the gauge freedom to align the Hertz potential with the repeated principal null direction. As a result, we obtain only two non-zero components, which can be incorporated into a single complex scalar function, the so-called *Debye potential*.

To make the construction explicit, we need to translate the above equations into a tensorial form. The Hertz potential $H_{\mu\nu}$ is defined in such a way that the four-potential A_μ satisfying the standard relation $F_{\mu\nu} = A_{\nu;\mu} - A_{\mu;\nu}$ is given by

$$A_\mu = -H_{\alpha\mu}{}^{;\alpha}\,. \tag{4.72}$$

The source-free Maxwell equations are then satisfied provided that (4.70) holds. In the tensorial form it reads

$$-H_{\mu\nu}{}^{;\alpha}{}_{\alpha} + (H_{\alpha\nu}{}^{;\alpha}{}_{\mu} - H_{\alpha\nu;\mu}{}^{\alpha}) + (H_{\alpha\mu}{}^{;\alpha}{}_{\nu} - H_{\alpha\mu;\nu}{}^{\alpha}) = (G_{\nu;\mu} - G_{\mu;\nu}) - W_{\alpha\mu\nu}{}^{;\alpha}\,, \tag{4.73}$$

where G_μ is an arbitrary covector field and $W_{\alpha\mu\nu}$ is an arbitrary totally antisymmetric tensor. Cohen & Kegeles (1974) showed that the following choice of the Hertz potential with appropriate gauge tensors

$$H_{\mu\nu} = 2\, m_{[\mu} l_{\nu]} \Psi + \text{c.c.}\,, \tag{4.74}$$
$$G_\mu = 2(\varrho\, m_\mu - \tau\, l_\mu)\Psi + \text{c.c.}\,, \tag{4.75}$$
$$W_{\alpha\mu\nu} = 12(\tau\, m_{[\alpha} l_\mu \bar{m}_{\nu]} + \varrho\, n_{[\alpha} l_\mu m_{\nu]})\Psi + \text{c.c.}\,, \tag{4.76}$$

leads to a single wave equation for the complex scalar Debye potential Ψ,

$$\left[(\text{Þ}' - \varrho')(\text{Þ} + \bar{\varrho}) - (\eth - \tau)(\eth' + \bar{\tau})\right] \bar{\Psi} = 0\,. \tag{4.77}$$

Note that the weights of the Debye potential Ψ are $\{-2, 0\}$, thus its complex conjugate $\bar{\Psi}$ has the weights $\{0, -2\}$. We could have chosen a different component of the Hertz potential, $\Psi : \{0, 0\}$ for $H_{ln} \equiv \Psi$, or $\Psi : \{2, 0\}$ for $H_{lm} \equiv \Psi$ which would satisfy analogical Debye equations. The electromagnetic field then follows from a straightforward differentiation of the Debye potential,

$$\varphi_0 = -(\text{Þ} - \bar{\rho})(\text{Þ} + \bar{\rho})\bar{\Psi}\,, \tag{4.78}$$
$$\varphi_1 = \left[-\text{Þ}(\eth' + \bar{\tau}) + (\bar{\tau} - \tau')(\text{Þ} + \bar{\varrho})\right] \bar{\Psi}\,, \tag{4.79}$$
$$\varphi_2 = \left[-(\eth' - \bar{\tau})(\eth' + \bar{\tau}) + \lambda(\text{Þ} + \bar{\varrho})\right] \bar{\Psi}\,. \tag{4.80}$$

We remark that Stewart (1979) provided the same result more concisely based on the language of spinors. A much simpler and more formal method was proposed by Wald (1978) using the notion of adjoint operators. We will use Wald's approach when we discuss gravitational perturbations, see Sec. 4.5.2.

4.4.2 Axially symmetric Debye superpotential of the electromagnetic field

Consider the spacetime of a spinning black hole as the background and assume that the electromagnetic field respects the symmetries, i.e., it is stationary and axially symmetric as well. In the Kinnersley tetrad (4.48)-(4.50), the components of the electromagnetic field can be obtained just by twice differentiating the Debye potential Ψ. Explicitly,

$$\varphi_0 = \frac{1}{2}\frac{\partial^2 \bar{\Psi}}{\partial r^2}\,, \tag{4.81}$$
$$\varphi_1 = \frac{1}{2\sin\theta}\frac{\partial^2}{\partial r \partial\theta}\left(\frac{\sin\theta}{r - \mathrm{i}\, a\cos\theta}\bar{\Psi}\right) - \mathrm{i}\,\frac{a\sin\theta}{(r - \mathrm{i}\, a\cos\theta)^3}\bar{\Psi}\,, \tag{4.82}$$
$$\varphi_2 = -\frac{\Delta}{(r - \mathrm{i}\, a\cos\theta)^2}\varphi_0\,. \tag{4.83}$$

However, we will proceed in the opposite manner. We will solve the Teukolsky equation (4.63) for φ_0, which takes the following form

$$-\Delta^{-1}\frac{\partial}{\partial r}\left(\Delta^2\frac{\partial\varphi_0}{\partial r}\right) - \frac{1}{\sin\theta}\frac{\partial}{\partial\theta}\left(\sin\theta\,\frac{\partial\varphi_0}{\partial\theta}\right) + (\cot^2\theta - 1)\,\varphi_0 = 4\pi\Sigma J_0\,. \tag{4.84}$$

With φ_0 known, we can derive the Debye potential by twice integrating (4.81) and then obtain the two remaining components φ_1, φ_2 from the Debye potential. Let us look for the Debye potential, which after the differentiation of (4.81) gives the Green function of the Teukolsky equation (4.84), i.e., it leads to the solution of (4.84) with the source

$$J_0 = \frac{1}{4\pi\Sigma}\delta(r - r_0)\delta(\cos\theta - \cos\theta_0)\,, \tag{4.85}$$

where δ stands for the delta distribution. Linet (1979) showed that the problem leads to an axially symmetric Green function of the Laplace equation in an auxiliary flat 5-dimensional space. In particular, if we define the function $g(\rho, z)$ as

$$\varphi_0 \equiv g(\rho, z)\sin\theta \tag{4.86}$$

and transform the Teukolsky equation into the Weyl coordinates (ρ, z)[5], we obtain

$$\left(\frac{\partial^2}{\partial\rho^2} + \frac{3}{\rho}\frac{\partial}{\partial\rho} + \frac{\partial^2}{\partial z^2}\right) g(\rho, z) = \frac{1}{2\rho_0 \sin\theta_0}\delta(\rho - \rho_0)\delta(z - z_0)\,. \tag{4.87}$$

From the generalized axially symmetric potential theory (GASP) we learn that

$$g(\rho, z) = \frac{\rho_0^2}{4\pi\sin\theta_0}\int_0^\pi \frac{\sin^2\alpha}{(\rho^2 - 2\rho\rho_0\cos\alpha + \rho_0^2 + (z - z_0)^2)^{3/2}}\,\mathrm{d}\alpha = \tag{4.88}$$

$$= \frac{1}{4\pi\sin\theta_0}\frac{1}{\rho^2}\left[\frac{\rho^2 + \rho_0^2 + (z - z_0)^2}{\sqrt{(\rho + \rho_0)^2 + (z - z_0)^2}}K(k) - \right. \tag{4.89}$$

$$\left. - \sqrt{(\rho + \rho_0)^2 + (z - z_0)^2}E(k)\right]\,, \tag{4.90}$$

where $K(k)$ and $E(k)$ are the complete elliptic integrals of the first and second kinds with the modulus

$$k = \frac{2\sqrt{\rho\rho_0}}{\sqrt{(\rho + \rho_0)^2 + (z - z_0)^2}}\,. \tag{4.91}$$

For a particular source J_0 the field follows from the convolution

$$\varphi_0 = \int_0^\infty \int_0^\pi g(r, \theta; r', \theta')J_0(r', \theta')\Sigma(r', \theta')\sin\theta'\,\mathrm{d}\theta'\,\mathrm{d}r'\,. \tag{4.92}$$

The associated Debye potential, which generates the Green function of the Teukolsky equation for φ_0, is then given by integrating (4.81). We call it the *Debye superpotential* Ψ_g. Let us also introduce the rescaled superpotential Ξ_g as

$$\bar{\Psi}_g = \sin\theta\Delta(r)\Xi_g\,. \tag{4.93}$$

With such a substitution and transformation to the Weyl coordinates, the Debye equation is also reduced to the 5-dimensional Laplace equation for Ξ_g. However, we are not looking for the Green function of the Debye superpotential. Instead, we want to find the Debye superpotential which generates the Green function of

[5]Let us remind the relation between the Boyer-Lindquist coordinates (r, θ) and the Weyl coordinates: $\rho = \sqrt{\Delta(r)}\sin\theta$, and $z = (r - M)\cos\theta$.

the Teukolsky equation by (4.81). But since it satisfies the Laplace equation as well, it is sufficient to know the values only on the symmetry axis $\rho = 0$. The solution everywhere then follows from the integral

$$\Xi_g(\rho, z) = \frac{2}{\pi} \int_0^\pi \Xi_g(0, z + \mathrm{i}\rho\cos\alpha) \sin^2\alpha \, \mathrm{d}\alpha \,. \tag{4.94}$$

Since both the elliptic integrals reduce to just $\pi/2$ on the symmetry axis, the integration of (4.81) is simple and leads to the following expression in Weyl coordinates

$$\Xi_g(\rho = 0, z) = \frac{1}{4\sin\theta_0} \frac{\sqrt{(z - z_0)^2 + \rho_0^2}}{z^2 - M^2 + a^2} \,. \tag{4.95}$$

Hence, the Debye superpotential at general (ρ, z) reads

$$\Xi_g(\rho, z) = \frac{1}{2\pi\sin\theta_0} \int_0^\pi \frac{\sqrt{(z + \mathrm{i}\rho\cos\alpha - z_0)^2 + \rho_0^2}}{(z + \mathrm{i}\rho\cos\alpha)^2 - M^2 + a^2} \sin^2\alpha \, \mathrm{d}\alpha \,. \tag{4.96}$$

In Kofroň & Kotlařík (2022) we explicitly integrated (4.96) in closed-form, analyzed the structure of the superpotential and applied the result to ring sources on the Kerr background.

4.4.3 Ring sources on the Kerr background

With the Debye superpotential at hand, we can now derive the electromagnetic field of specific sources. The axially symmetric and stationary four-current reads

$$J^\mu = j_t \, \xi^\mu_{(t)} + j_\phi \, \xi^\mu_{(\phi)} \,, \tag{4.97}$$

where we remind the reader of the notation for the Killing vector fields $\xi^\mu_{(t,\phi)}$. We considered two types of sources in Kofroň & Kotlařík (2022):

- a static charged ring

$$j_t = \frac{\hat{j}_t(r_0, \theta_0)}{\Sigma(r_0, \theta_0)} \delta(r - r_0)\delta(\cos\theta - \cos\theta_0) \,, \qquad j_\phi = 0 \,, \tag{4.98}$$

- and an axial current loop

$$j_t = 0 \,, \qquad j_\phi = \frac{\hat{j}_\phi(r_0, \theta_0)}{\Sigma(r_0, \theta_0)} \delta(r - r_0)\delta(\cos\theta - \cos\theta_0) \,. \tag{4.99}$$

The source for the Teukolsky equation reads

$$\begin{aligned} J_0 = \frac{1}{2\Sigma} \frac{1}{r - ia\cos\theta} \Bigg\{ & - \frac{\partial}{\partial\theta} \left[j_t(r, \theta)(r - \mathrm{i}\, a\cos\theta)^2 \right] + \\ & + \mathrm{i}\, a \sin\theta \frac{\partial}{\partial r} \left[j_t(r, \theta)(r - \mathrm{i}\, a\cos\theta)^2 \right] + \\ & + \frac{\partial}{\partial\theta} \left[j_\phi(r, \theta)\, a \sin\theta \, (r - \mathrm{i}\, a\cos\theta)^2 \right] - \end{aligned}$$

$$- \mathrm{i}\,\frac{\partial}{\partial r}\left[j_\phi(r,\theta)(r^2+a^2)\sin\theta\,(r-\mathrm{i}\,a\cos\theta)^2\right]\Bigg\}\,, \tag{4.100}$$

from which we obtain the Debye potential by

$$\bar{\Psi} = \int_0^\pi \int_0^\infty \bar{\Psi}_g(r,\theta,r',\theta') J_0(r',\theta')\Sigma(r',\theta')\sin\theta'\,\mathrm{d}r'\,\mathrm{d}\theta'\,, \tag{4.101}$$

$$= \int_0^\pi \int_0^\infty \Xi_g(r,\theta,r',\theta') J_0(r',\theta')\Delta(r')\sin^2\theta'\,\mathrm{d}r'\,\mathrm{d}\theta'\,. \tag{4.102}$$

The components of the electromagnetic field follow from (4.81)-(4.83).

The results were checked against the infinite series expansion derived in Bičák & Dvořák (1976) and showed integral curves of the reconstructed electric and magnetic field from the point of view of the ZAMO observers.

4.5 Linearized gravitational perturbations

Now, we turn to the gravitational perturbations. Again, we will assume the Kerr black hole as the background spacetime with the tetrad vectors l^μ and n^μ aligned with the two double principal null directions of the unperturbed Weyl tensor. The perturbation will be controlled by a small parameter $\varepsilon \ll 1$. We expand the exact metric in the powers of ε as

$$g_{\mu\nu}^{\mathrm{exact}} = g_{\mu\nu} + \varepsilon h_{\mu\nu} + \mathcal{O}(\varepsilon^2)\,, \tag{4.103}$$

where $g_{\mu\nu}$ stands for the background spacetime and $h_{\mu\nu}$ encodes the linear contribution. This amounts to the perturbation of the tetrad vectors and all the NP quantities. Unperturbed quantities will not be denoted in any special way, while perturbed quantities will be indicated with a breve above them, e.g., $\breve{l}^\mu$, $\breve{\kappa}, \breve{\psi}_2$, etc. We will be interested in the first-order perturbation, thus only keeping the terms linear in ε.

By the direct computation of the Weyl scalars, we find the linear perturbation of scalars ψ_0 and ψ_4,

$$\begin{aligned} -2\breve{\psi}_0 = {} & (\eth - \bar{\tau}')(\eth - \bar{\tau}')h_{ll} + (\text{Þ} - \bar{\varrho})(\text{Þ} - \bar{\varrho})h_{mm} - \\ & - \left[(\text{Þ} - \bar{\varrho})(\eth - 2\bar{\tau}') + (\eth - \bar{\tau}')(\text{Þ} - 2\bar{\varrho})\right] h_{(lm)}\,, \end{aligned} \tag{4.104}$$

$$\begin{aligned} -2\breve{\psi}_4 = {} & (\eth' - \bar{\tau})(\eth' - \bar{\tau})h_{nn} + (\text{Þ}' - \bar{\varrho}')(\text{Þ}' - \bar{\varrho}')h_{\bar{m}\bar{m}} - \\ & - \left[(\text{Þ}' - \bar{\varrho}')(\eth' - 2\bar{\tau}) + (\eth' - \bar{\tau})(\text{Þ}' - 2\bar{\varrho}')\right] h_{(n\bar{m})}\,. \end{aligned} \tag{4.105}$$

Detailed computation and results for the remaining Weyl scalars are given in Appendix B.

Similarly to the Maxwell field, Teukolsky (1973) found decoupled equations for $\breve{\psi}_0$ and $\breve{\psi}_4$. By perturbing the Bianchi identity (A.10) and the primed counterpart of (A.13) we get

$$(\eth' - \tau')\breve{\psi}_0 - (\text{Þ} - 4\varrho)\breve{\psi}_1 - 3\breve{\kappa}\psi_2 = 4\pi\left[(\eth - \bar{\tau}')\breve{T}_{ll} - (\text{Þ} - 2\bar{\rho})\breve{T}_{lm}\right]\,, \tag{4.106}$$

$$(\text{Þ}' - \varrho')\breve{\psi}_0 - (\eth - 4\tau)\breve{\psi}_1 - 3\breve{\sigma}\psi_2 = 4\pi\left[(\eth - 2\bar{\tau}')\breve{T}_{lm} - (\text{Þ} - \bar{\varrho})\breve{T}_{mm}\right]\,. \tag{4.107}$$

Then, the perturbed Ricci equation (A.6)

$$(\text{Þ} - \varrho - \bar{\varrho})\breve{\sigma} - (\eth - \tau - \bar{\tau}')\breve{\kappa} - \breve{\psi}_0 = 0 \tag{4.108}$$

combined with the identity

$$\left[(\text{Þ} - 4\varrho - \bar{\varrho})(\eth - 4\tau) - (\eth - \tau' - 4\tau)(\text{Þ} - 4\varrho)\right]\varphi = 0\,, \tag{4.109}$$

valid for any GHP quantity φ of the weight $\{p, 0\}$, leads to the *Teukolsky master equation*

$$\left[(\text{Þ} - 4\varrho - \bar{\varrho})(\text{Þ}' - \rho') - (\eth - 4\tau - \bar{\tau}')(\eth' - \tau') - 3\,\psi_2\right]\breve{\psi}_0 = 4\pi T_0 \tag{4.110}$$

with the source term

$$\begin{aligned} T_0 = (\eth - \bar{\tau}' - 4\tau)\left[(\text{Þ} - 2\bar{\varrho})\breve{T}_{(lm)} - (\eth - \bar{\tau}')\breve{T}_{ll}\right] \\ + (\text{Þ} - 4\varrho - \bar{\varrho})\left[(\eth - 2\bar{\tau}')\breve{T}_{(lm)} - (\text{Þ} - \bar{\varrho})\breve{T}_{mm}\right]\,. \end{aligned} \tag{4.111}$$

The Teukolsky equation for $\breve{\psi}_4$ follows by the prime transformation. However, unlike the equation for $\breve{\psi}_0$, the Teukolsky equation for $\breve{\psi}_4$ is not separable in the Boyer-Lindquist coordinates. The separable equation is obtained after factoring out the term $\psi_2^{-4/3}$,

$$\left[(\text{Þ}' - \bar{\rho}')(\text{Þ} + 3\varrho) - (\eth' - \bar{\tau})(\eth + 3\tau) - 3\,\psi_2\right]\psi_2^{-\frac{3}{4}}\breve{\psi}_4 = 4\pi\,\psi_2^{-\frac{3}{4}}T_4\,, \tag{4.112}$$

where $T_4 = T_0'$.

4.5.1 Gauge freedom

In any tetrad formalism, we encounter two types of gauge freedom. We are free to change the tetrad vectors according to the Lorentz transformations, see Sec. 4.2, and we are free to choose any coordinates as well. However, in the perturbation theory, there is an additional complication. We deal with two kinds of spacetimes here, the (unperturbed) background spacetime and the physical one (including perturbations). The question which now arises is how to relate the quantities between them. This can be done by considering a one-parameter family of spacetimes $(\mathcal{M}_\varepsilon, g_\varepsilon)$ of which $(\mathcal{M}_0, g_0)$ denotes the background and ε ranges through some real interval starting from zero. Different spacetimes of such a family are identified by the gauge diffeomorphism $\gamma_\varepsilon : \mathcal{M}_0 \to \mathcal{M}_\varepsilon$, where γ_0 is the identity. Consider a quantity Q_0 on the background $\mathcal{M}_0$. Then we can define a family of quantities $\hat{Q}_\varepsilon$ living on the background associated with the perturbed one Q_ε by the pullback $\gamma_\varepsilon^*(Q_\varepsilon) \equiv \hat{Q}_\varepsilon$. The first order perturbation $\breve{Q}$ on $\mathcal{M}_0$ is then

$$\breve{Q} \equiv \left.\frac{\mathrm{d}\hat{Q}_\varepsilon}{\mathrm{d}\varepsilon}\right|_{\varepsilon=0}\,. \tag{4.113}$$

However, the choice of γ_ε is not unique. Consider another diffeomorphism defined on the background spacetime $\Gamma_\varepsilon : \mathcal{M}_0 \to \mathcal{M}_0$ (coordinate gauge transformation), and the associated gauge vector field on $\mathcal{M}_0$ given by

$$\Theta \equiv \left.\frac{\mathrm{d}\Gamma_\varepsilon}{\mathrm{d}\varepsilon}\right|_{\varepsilon=0}\,. \tag{4.114}$$

Then the new identification $\gamma_\varepsilon \circ \Gamma_\varepsilon$ gives a new family $\tilde{Q}_\varepsilon = \Gamma^*_\varepsilon(\hat{Q}_\varepsilon)$ on $\mathcal{M}_0$ and a new perturbation $\breve{\tilde{Q}}$ related to $\tilde{Q}$ by

$$\breve{\tilde{Q}} = \tilde{Q} + \mathcal{L}_\Theta Q_0 \,, \tag{4.115}$$

where $\mathcal{L}_\Theta$ denotes the Lie derivative along the gauge vector field Θ^μ.

Clearly, Q is identification gauge invariant if $\mathcal{L}_\Theta Q = 0$, that is if (i) Q_0 vanishes, or (ii) Q_0 is a constant scalar, or (iii) Q_0 is a linear combination of products of Kronecker deltas (Stewart et al., 1997). In particular, the metric perturbations $h \equiv \frac{\mathrm{d}\hat{g}_\varepsilon}{\mathrm{d}\varepsilon}|_{\varepsilon=0}$ are never gauge invariant in this sense.

But, we can always find some invariant quantities if we adopt the tetrad formalism and consider an algebraically special background. In the type-D spacetimes, the NP vectors l^μ and n^μ can always be chosen in the directions along the principal null vectors of the Weyl tensor. Hence, in particular, if the background ψ_0 and ψ_4 vanish, the linear perturbations $\breve{\psi}_0$ and $\breve{\psi}_4$ are identification gauge invariants. Moreover, $\breve{\psi}_0$ and $\breve{\psi}_4$ are also tetrad-gauge invariant as they remain unchanged under the local Lorentz transformations of the tetrad vectors (Stewart et al., 1997).

4.5.2 Debye (Hertz) potential

We described in Sec. 4.4.1 how to define the Hertz and Debye potentials of the electromagnetic field in curved spacetimes. Analogous potentials can also be introduced for gravitational perturbations. The whole business started with the work of Cohen & Kegeles (1975) immediately followed by Chrzanowski (1975) refining the approach in terms of factorized Green's functions. Later, Kegeles & Cohen (1979) provided a detailed description of their method as well. A more concise version was published by Stewart (1979), valid for any algebraically special spacetime. Finally, about the same time, Wald (1978) provided an elegant and formal way how to derive the results. His approach uses simple relations between adjoint operators. We will follow Wald's construction. For a linear differential operator $\mathcal{L}$, its adjoint $\mathcal{L}^\dagger$ is formally defined for arbitrary tensor fields ψ and φ in the following way

$$\langle \psi, \mathcal{L}\varphi \rangle \equiv \left\langle \mathcal{L}^\dagger \psi, \varphi \right\rangle \,, \tag{4.116}$$

with respect to the inner product

$$\langle \psi, \varphi \rangle = \int \psi_{\alpha\beta\ldots} \varphi^{\alpha\beta\ldots} \, \mathrm{d}\mathcal{V} \,, \tag{4.117}$$

where $\mathrm{d}\mathcal{V}$ is the volume element of the pertinent background spacetime. By definition, the GHP weights of tensor fields ψ and φ are such that the inner product has weights $\{0, 0\}$. We call the operator self-adjoint if $\mathcal{L} = \mathcal{L}^\dagger$. The adjoint of the product of two operators $\mathcal{L}_1$ and $\mathcal{L}_2$ is $(\mathcal{L}_1\mathcal{L}_2)^\dagger = \mathcal{L}_2^\dagger \mathcal{L}_1^\dagger$. Let us formally rewrite the Teukolsky equations into the language of operators. We consider four linear differential operators ($\mathcal{S}, \mathcal{E}, \mathcal{O}$, and $\mathcal{T}$) which will have the following meaning: the decoupling operator $\mathcal{S}$ maps the linearized Einstein equations $\mathcal{E}(h_{\mu\nu}) = 0$ into the set of decoupled equations $\mathcal{O}(\psi_{0,4})$ where the Weyl scalars are formally generated by the action of the operator $\mathcal{T}$ on the metric perturbation $\psi_{0,4} = \mathcal{T}(h_{\mu\nu})$. Hence, formally we have

$$\mathcal{S}\mathcal{E} = \mathcal{O}\mathcal{T} \,. \tag{4.118}$$

The Einstein equations $\mathcal{E}$ are self-adjoint, $\mathcal{E}^\dagger = \mathcal{E}$, therefore the adjoint of Eq. (4.118) reads

$$\mathcal{E}\mathcal{S}^\dagger = \mathcal{T}^\dagger\mathcal{O}^\dagger\,. \tag{4.119}$$

Clearly, if there exists Ψ satisfying $\mathcal{O}^\dagger\Psi = 0$, then $\mathcal{S}^\dagger\Psi$ is the solution to the Einstein equations. Such a Ψ is commonly known as the *Debye (or Hertz) potential*. There are two types of the Debye potential, one that starts from the Teukolsky equation for ψ_0, we will denote it as $\Psi^{\rm IRG}$, and the other that starts from the equation for ψ_4 which we will denote as $\Psi^{\rm ORG}$. The notation reflects that the resulting metric perturbation is in two different gauges – ingoing or outgoing radiation gauge, see the discussion in the next section.

The Teukolsky operator $\mathcal{O}$ can be read out from the homogeneous Teukolsky equation and the decoupling operator $\mathcal{S}$ from the source term. For the Weyl scalar ψ_0 we obtain, using (4.110) and (4.111),

$$\mathcal{O}_0 = (\text{Þ} - 4\varrho - \bar\varrho)(\text{Þ}' - \rho') - (\eth - 4\tau - \bar\tau')(\eth' - \tau') - 3\,\psi_2\,, \tag{4.120}$$

$$[\mathcal{S}_0]_{\mu\nu} = -l_\mu l_\nu(\eth - \bar\tau' - 4\tau)(\eth - \bar\tau') - m_\mu m_\nu(\text{Þ} - 4\varrho - \bar\varrho)(\text{Þ} - \bar\varrho) + \tag{4.121}$$

$$+\, l_\mu m_\nu\left[(\eth - \bar\tau' - 4\tau)(\text{Þ} - 2\bar\varrho) + (\text{Þ} - 4\varrho - \bar\varrho)(\eth - 2\bar\tau')\right]. \tag{4.122}$$

If we begin with the Teukolsky equation for ψ_4, the explicit form of both operators can be derived from the prime operation $\mathcal{O}_4 = \mathcal{O}_0'$ and $\mathcal{S}_4 = \mathcal{S}_0'$. In order to obtain an equation for the Debye potential, we need adjoints of these operators. The GHP scalars are all self-adjoint, but for the GHP derivatives we obtain

$$\text{Þ}^\dagger = -(\text{Þ} - \varrho - \bar\varrho)\,, \qquad \eth^\dagger = -(\eth - \tau - \bar\tau')\,, \tag{4.123}$$

$$\text{Þ}'^\dagger = -(\text{Þ}' - \varrho' - \bar\varrho')\,, \qquad \eth'^\dagger = -(\eth' - \tau' - \bar\tau)\,. \tag{4.124}$$

which follow from (4.116) using the definition of the derivatives, per partes under the integral and the covariant divergences of the NP tetrad,

$$\nabla_\alpha l^\alpha = \epsilon + \bar\epsilon - \varrho - \bar\varrho\,, \qquad \nabla_\alpha n^\alpha = \epsilon' + \bar\epsilon' - \varrho' - \bar\varrho'\,, \tag{4.125}$$

$$\nabla_\alpha m^\alpha = \beta + \bar\beta' - \tau - \bar\tau'\,, \qquad \nabla_\alpha \bar m^\alpha = \beta' + \bar\beta - \tau' - \bar\tau\,. \tag{4.126}$$

Thus, the Debye equation for the gravitational perturbations reads

$$\mathcal{O}_0^\dagger\Psi^{\rm IRG} = \left[(\text{Þ}' - \bar\rho')(\text{Þ} + 3\varrho) - (\eth' - \bar\tau)(\eth + 3\tau) - 3\,\psi_2\right]\Psi^{\rm IRG} = 0\,, \tag{4.127}$$

which is the same equation as the Teukolsky equation for $\psi_2^{-4/3}\psi_4$. The other Debye potential $\Psi^{\rm ORG}$ will satisfy the prime counterpart

$$\mathcal{O}_4^\dagger\Psi^{\rm ORG} = \left(\mathcal{O}_0^\dagger\right)'\Psi^{\rm ORG} = 0\,, \tag{4.128}$$

which is the same equation as the one to be satisfied by $\psi_2^{-4/3}\breve\psi_0$. Note that since ψ_0 and ψ_4 has GHP weights $\{4,0\}$ and $\{-4,0\}$ respectively, the Debye potentials $\Psi^{\rm IRG}$ and $\Psi^{\rm ORG}$ must have weights $\{-4,0\}$ and $\{4,0\}$, as required by the definition of the adjoint.

The metric perturbation reconstructed from the Debye potential then reads

$$h^{\rm IRG}_{\mu\nu} = \left[\mathcal{S}_0^\dagger\Psi^{\rm IRG}\right]_{\mu\nu} + \text{c.c.} =$$

$$
\begin{aligned}
&= \Big\{ l_\mu l_\nu (\eth - \tau)(\eth + 3\tau) - \\
&\quad - l_{(\mu} m_{\nu)} \Big[(\text{Þ} - \varrho + \bar{\varrho})(\eth + 3\tau) + (\eth - \tau + \bar{\tau}')(\text{Þ} + 3\rho) \Big] + \\
&\quad + m_\mu m_\nu (\text{Þ} - \varrho)(\text{Þ} + 3\varrho) \Big\} \, \Psi^{\text{IRG}} + \text{c.c.} \,, \qquad (4.129)
\end{aligned}
$$

while the metric in the outgoing radiation gauge follows from the prime transformation

$$
h^{\text{ORG}}_{\mu\nu} = \left[\mathcal{S}^\dagger_4 \Psi^{\text{IRG}} \right]_{\mu\nu} + \text{c.c.} = \left[\left(\mathcal{S}^\dagger_0 \right)' \Psi^{\text{IRG}} \right]_{\mu\nu} + \text{c.c.} \qquad (4.130)
$$

The complex conjugate is added, so the metric perturbation tensor is real.

Observe now that if Ψ satisfies $\mathcal{O}^\dagger \Psi = 0$, then $\mathcal{E}\mathcal{S}^\dagger \Psi = 0$, so the identity $\mathcal{S}(\mathcal{E}\mathcal{S}^\dagger \Psi) = \mathcal{O}(\mathcal{T}\mathcal{S}^\dagger \Psi)$ implies $\mathcal{O}(\mathcal{T}\mathcal{S}^\dagger \Psi) = 0$. In other words, the perturbed Weyl scalars reconstructed from the Debye potential are given by $\breve{\psi}_I = \mathcal{T}_I \left[\mathcal{S}^\dagger \Psi \right]_{\mu\nu} = \mathcal{T}_I(h_{\mu\nu})$, where $I = 0, 1, 2, 3, 4$. Using (4.129) and (4.104), (4.105) they read, explicitly,

$$
\breve{\psi}_0 = -\frac{1}{2} \text{Þ}^4 \bar{\Psi}^{\text{IRG}} \,, \qquad (4.131)
$$

$$
\breve{\psi}_1 = -\frac{1}{2} \left[\text{Þ}^3 \eth' + 3\tau' \text{Þ}^3 + 6\varrho \tau' \text{Þ}^2 + 6\varrho^2 \tau' \text{Þ} \right] \bar{\Psi}^{\text{IRG}} \,, \qquad (4.132)
$$

$$
\breve{\psi}_2 = -\frac{1}{2} \left[\text{Þ}^2 \eth'^2 + 4\tau' \text{Þ}^2 \eth' + 4\varrho \tau' \text{Þ} \eth' + 6\tau'^2 \text{Þ}^2 + 12 \varrho \tau'^2 \text{Þ} \right] \bar{\Psi}^{\text{IRG}} \,, \qquad (4.133)
$$

$$
\breve{\psi}_3 = -\frac{1}{2} \left[\text{Þ} \eth'^3 + 3\tau' \text{Þ} \eth'^2 + 6\tau'^2 \text{Þ} \eth' + 6\tau'^3 \text{Þ} \right] \bar{\Psi}^{\text{IRG}} \,, \qquad (4.134)
$$

$$
\breve{\psi}_4 = -\frac{1}{2} \eth'^4 \bar{\Psi}^{\text{IRG}} + \frac{3}{2} \psi_2 \left[\tau' \eth - \tau \eth' - \varrho' \text{Þ} + \varrho \text{Þ}' - 2\psi_2 \right] \Psi^{\text{IRG}} \,. \qquad (4.135)
$$

The Weyl scalars which would follow from Ψ^{ORG} are analogously can be determined by applying the prime transformation to the equations above, since

$$
\psi'_I = \psi_{4-I} \,, \qquad \text{i.e. } \psi'_0 = \psi_4 \qquad \text{etc.} \qquad (4.136)
$$

Notice that our results do not agree with Deadman & Stewart (2010). The authors computed the perturbations of the Weyl scalars arising solely from the perturbation of the Riemann tensor, missing the terms that follow from the perturbation of the NP tetrad and the metric – see Appendix B for more details.

Finally, let us remark that the same procedure also works for the Maxwell field (Wald, 1978). Recently, Aksteiner et al. (2021) showed how to proceed in any algebraically special spacetime.

4.5.3 Ingoing and outgoing radiation gauges

Observe that the metric perturbation satisfies

$$
l^\alpha h^{\text{IRG}}_{\alpha\beta} = 0 \,, \qquad g^{\alpha\beta} h^{\text{IRG}}_{\alpha\beta} = 0 \,, \qquad (4.137)
$$

$$
n^\alpha h^{\text{ORG}}_{\alpha\beta} = 0 \,, \qquad g^{\alpha\beta} h^{\text{ORG}}_{\alpha\beta} = 0 \,. \qquad (4.138)
$$

These conditions are known as *ingoing radiation gauge* (IRG) or *outgoing radiation gauge* (ORG). Note however that the perturbation in IRG is orthogonal to the vector field l^μ, thus there is only purely outgoing radiation present in this gauge and, vice versa for the ORG.

The IRG and ORG Hertz potentials are not independent. In a vacuum, the Weyl scalars ψ_0 and ψ_4 are related by the Teukolsky-Starobinsky identities (Teukolsky, 1972; Starobinskii & Churilov, 1974)

$$\text{Þ}^4(\psi_2^{-\frac{4}{3}}\breve{\psi}_4) = \text{ð}'^4(\psi_2^{-\frac{4}{3}}\breve{\psi}_0) - 3\mathcal{V}\breve{\bar{\psi}}_0\,, \tag{4.139}$$

$$\text{Þ}'^4(\psi_2^{-\frac{4}{3}}\breve{\psi}_0) = \text{ð}^4(\psi_2^{-\frac{4}{3}}\breve{\psi}_4) + 3\mathcal{V}\breve{\bar{\psi}}_4\,, \tag{4.140}$$

where the operator $\mathcal{V}$ is defined by its action on any GHP quantity of the weight $\{p, q\}$ as

$$\mathcal{V} = -\psi_2^{-\frac{1}{3}}\left[\tau'\text{ð} - \tau\text{ð}' + \varrho\text{Þ}' - \varrho'\text{Þ} + \frac{p}{2}\psi_2 + \frac{q}{2}\frac{\varrho\bar{\psi}_2}{\bar{\varrho}}\right]. \tag{4.141}$$

Since both gauges should produce the same perturbations of the Weyl scalars, analogous identities relate the Debye potentials

$$\text{Þ}^4\Psi^{\text{IRG}} = \text{ð}'^4\Psi^{\text{ORG}} + 3\bar{\psi}_2^{\frac{4}{3}}\bar{\mathcal{V}}\bar{\Psi}^{\text{ORG}}\,, \tag{4.142}$$

$$\text{Þ}'^4\Psi^{\text{ORG}} = \text{ð}^4\Psi^{\text{IRG}} - 3\bar{\mathcal{V}}\bar{\psi}_2^{\frac{4}{3}}\bar{\Psi}^{\text{IRG}}\,. \tag{4.143}$$

4.5.4 Towards the Debye superpotential of the gravitational perturbations

The recipe for the Debye potential is analogous to the Maxwell case (Linet, 1977). In the Kinnersley tetrad (4.48)-(4.50), the perturbed Weyl scalars $\breve{\psi}_0$ and $\breve{\psi}_4$ given by (4.131) and (4.135) reduce to

$$\breve{\psi}_0 = -\frac{1}{8}\frac{\partial^4\bar{\Psi}^{\text{IRG}}}{\partial r^4}\,, \tag{4.144}$$

$$\breve{\psi}_4 = \frac{\Delta^2}{(r - \mathrm{i}\,a\cos\theta)^4}\breve{\psi}_0\,. \tag{4.145}$$

Again, we are interested in the Debye potential which would generate the Green function of the axially symmetric Teukolsky equation (4.110)

$$\Delta^{-2}\frac{\partial}{\partial r}\left(\Delta^3\frac{\partial}{\partial r}\breve{\psi}_0\right) + \frac{1}{\sin\theta}\frac{\partial}{\partial\theta}\left(\sin\theta\frac{\partial}{\partial\theta}\breve{\psi}_0\right) + 2(2\cot^2\theta - 1)\breve{\psi}_0 = 8\pi\Sigma T_0\,, \tag{4.146}$$

where we substitute

$$T_0 = \frac{1}{8\pi\Sigma}\delta(r - r_0)\delta(\cos\theta - \cos\theta_0)\,. \tag{4.147}$$

With the substitution

$$\breve{\psi}_0 \equiv g(\rho, z)\sin^2\theta \tag{4.148}$$

and after transformation to the Weyl coordinates, the Teukolsky equation reduces to the Laplace equation in (auxiliary) flat 7-dimensional space

$$\left(\frac{\partial^2}{\partial\rho^2} + \frac{5}{\rho}\frac{\partial}{\partial\rho} + \frac{\partial^2}{\partial z^2}\right)g(\rho, z) = \frac{1}{\rho_0\sin^2\theta_0}\delta(\rho - \rho_0)\delta(z - z_0)\,. \tag{4.149}$$

The corresponding Green function is known to be

$$g(\rho,z) = \frac{\rho_0^4}{2\pi\sin^2\theta_0}\int_0^\pi \frac{\sin^4\alpha}{(\rho^2-2\rho\rho_0\cos\alpha+\rho_0^2+(z-z_0)^2)^{5/2}}\,\mathrm{d}\alpha = \tag{4.150}$$

$$= \frac{1}{6\pi\sin^2\theta_0}\frac{k}{\sqrt{\rho\rho_0}}\frac{1}{\rho^4}\left\{\left[(\rho^2+\rho_0^2+(z-z_0)^2)^2-\rho^2\rho_0^2\right]K(k^2)+\right.$$

$$\left. + \frac{4\rho\rho_0}{k^2}\left[\rho^2+\rho_0^2+(z-z_0)^2\right]E(k^2)\right\}. \tag{4.151}$$

Similarly, if we substitute

$$\bar{\Psi}_g^{\mathrm{IRG}} \equiv \Xi_g \Delta^2 \sin^2\theta\,, \tag{4.152}$$

the Debye equation (4.127) leads to the 7-dimensional Laplace equation for Ξ_g. Thus, just like in the Maxwell case, the superpotential can be determined from the values on the axis by integrating (4.144). We find that

$$\Xi_g(\rho=0,z) = \frac{1}{6\sin^2\theta_0}\frac{(\rho_0^2+(z-z_0)^2)^{\frac{3}{2}}}{(z^2-M^2+a^2)^2}\,, \tag{4.153}$$

thus the Debye superpotential at general (ρ,z) then follows by integration

$$\Xi_g(\rho,z) = \frac{2}{\pi}\int_0^\pi \Xi_g(0,z+\mathrm{i}\,\rho\cos\alpha)\sin^4\alpha\,\mathrm{d}\alpha\,. \tag{4.154}$$

It is again possible to find the solution of the above integration in closed-form in (many) terms of the complete elliptic integrals. However, we leave the analysis for the (near) future work.

Finally, let us add that the metric perturbation we reconstruct from the Debye potential is in IRG, which is not convenient for analyzing the obtained solution nor for comparing it with the results in the literature, e.g., Will (1974) or Čížek & Semerák (2017). The metric perturbation in some standard form would be rather preferable. Thus, we also should look for a specific gauge transformation which maps the perturbation obtained from the Debye potential to some standard form of circular metric such as (1.6), i.e. for a calibration field Θ^μ such that

$$h_{\mu\nu}^{\mathrm{circular}} = h_{\mu\nu}^{\mathrm{IRG}} + \mathcal{L}_\Theta g_{\mu\nu}\,. \tag{4.155}$$

Debye superpotential for charged rings or circular currents around Kerr black holes

David Kofroň* and Petr Kotlařík†
Institute of Theoretical Physics,
Faculty of Mathematics and Physics,
Charles University,
V Holešovičkách 2, 180 00 Prague 8, Czech Republic

We provide an explicit, closed and compact expression for the Debye superpotential of a circular source. This superpotential is obtained by integrating the Green function of Teukolsky Master Equation (TME). The Debye potential itself is then, for a particular configuration, calculated in the same manner as the φ_0 field component is calculated from the Green function of the TME — by convolution of the Green function with sources. This way we provide an exact field of charged ring and circular current on the Kerr background, finalizing thus the work of Linet.

I. INTRODUCTION

The test electromagnetic fields on a rotating black hole – a Kerr black hole [1] – background are of perpetual interest for their astrophysical importance; for an overview see [2]. Fields of stationary and axisymmetric charge/current configurations attract our attention for the fact that they can represent (simplified) models of electromagnetic fields generated by accretion discs.

Yet, the task to solve Maxwell's equations on a Kerr background is highly nontrivial.

The most fruitful approach is a special tetrad formulation based on null tetrad — Newman – Penrose (NP) formalism [3] and its refinement Geroch – Held – Penrose (GHP) formalism [4]. Then the Maxwell field equations (ME) are four coupled 1^{st} order PDEs for complex scalars φ_0, φ_1 and φ_2.

Due to the special algebraic properties of type D spacetimes — of which the Kerr solution is a prominent member — the Maxwell equations can be decoupled and cast in three 2^{nd} order partial differential equations for respective NP field components. Equations for φ_0 and φ_2 (so-called TMEs) were found in 1972 by Teukolsky [5, 6] while the equation for φ_1 (so-called FIE) was found by Fackerell and Ipser in 1971 [7] and elaborated recently in [8]. In fact, the TMEs are more general since they govern the behaviour of a test field of arbitrary spin and has been extensively studied.

The TMEs allow us to seek for solution by method of separation of variables and therefore are widely used. Whether or not are the NP scalars components of the same field (we have decoupled equations!) is answered by the Teukolsky – Starobinsky identities (TSI) [9–11].

The task of finding an electromagnetic field of charged ring or circular current has been pursued by many relativist during 60's and 70's in progressively more general setting [12–17]. The very first attempts started with a classical 4-potential formulation but soon the NP approach attracted more attention. TMEs are separable — thus it is easy to find a solution of φ_0, φ_2 corresponding to a given source in a form of infinite series. Then the remaining NP component φ_1 has to be solved from ME directly.

Yet another general approach for solving test fields of arbitrary spin on type D backgrounds is to introduce the Debye potentials. A single complex scalar function (the only independent component of Hertz potential in a particular gauge) is enough to describe the whole test field. This approach has been introduced in the realms of general relativity by Cohen and Kegeles [18, 19], later elaborated in [20, 21] and recently developed and explained in terms of fundamental spinor operators by Acksteiner, Andersson and Bäckdahl in [22, 23].

The Debye potentials were used by Linet in 1979 [24] for construction of the electromagnetic field of a stationary axisymmetric field on Kerr background — the theory was established 43 years ago, but no explicit results were given. One is not surprised because already the simplest possible textbook example — a current loop in flat spacetime — is nontrivial since it contains elliptic integrals. This is where we are going to proceed further.

The paper is organized as follows. We briefly introduce the Kerr metric and the Kinnersley tetrad in Sec. II to set up the background. The spin coefficients are for the sake of brevity listed in Appendix A. For the same reason the congruence of zero angular momentum (ZAMO) observers, which we will later use for splitting the electromagnetic field into the electric $\boldsymbol{E} = \boldsymbol{u} \cdot \boldsymbol{F}$ and magnetic $\boldsymbol{B} = \boldsymbol{u} \cdot \star\boldsymbol{F}$ field, is introduced in Appendix B. And the elliptic integrals are defined in Appendix C.

We shortly introduce the TMEs in Sec. III and the Debye potentials in Sec. IV. We introduce neither the NP nor the GHP formalism since these are standard methods nowadays and are covered in [3, 4, 22, 25].

In Sec. V we shortly recall the results of Linet [24, 26]. He cast the TMEs under the assumptions of stationarity and axisymmetry into the form of generalized Laplace equations and provided Green functions. He has also shown, how to obtain the Debye potential for such fields – using the generalized axially symmetric potential (GASP) theory. It is easy to obtain the values of potential (which is a solution of the Laplace equation) on the

* d.kofron@gmail.com
† kotlarik.petr@gmail.com

axis; then, the solution on the whole space is defined as a particular integral.

In Sec. VI we present the analytic solution of the Debye potential (which we call the superpotential). This superpotential gives rise to to a field with φ_0 given by the Green function of the Teukolsky operator. We discuss the structure of discontinuities which we found in this superpotential and their significance. The importance of this result is clear: a closed compact analytical formula seems to be much better than an infinite series expansion (which is difficult to treat numerically close to the radius at which the source is located).

In Sec. VI A we discuss the properties and charge induced by this superpotential on the Kerr black hole. Sections VI B and VI C are devoted to presentation of realistic physical fields of given sources: a charged ring or a current loop. We numerically check our results against the series expansion solutions presented in [17]. Again, for the sake of compactness the reader is asked to refer to this paper for particular coefficients of the series.

II. KERR BLACK HOLE

One of the most fundamental solution of the vacuum Einstein field equations — the rotating black hole — was discovered in 1963 by Roy Kerr [1]. Recent historical reviews can be found in [27, 28].

The metric itself in Boyer – Lindquist coordinates reads

$$\mathbf{d}s^2 = -\frac{\Delta}{\Sigma}\left(\mathbf{d}t - a\sin^2\theta\,\mathbf{d}\varphi\right)^2 + \frac{\Sigma}{\Delta}\mathbf{d}r^2 + \Sigma\,\mathbf{d}\theta^2 + \frac{\sin^2\theta}{\Sigma}\Big(\left(a^2+r^2\right)\mathbf{d}\varphi - a\,\mathbf{d}t\Big)^2, \quad (1)$$

with the standard definitions

$$\Delta = r^2 - 2Mr + a^2 = (r-r_p)(r-r_m)\,, \quad (2)$$

$$\Sigma = \rho\bar\rho = r^2 + a^2\cos^2\theta \quad (3)$$

$$\rho = r - ia\cos\theta\,. \quad (4)$$

The parameters have the following meaning: M is the mass of the black hole, Ma is its angular momentum, r_p is the position of outer black hole horizon whereas r_m is the position of inner black hole horizon. We will also frequently use parameter β which we define as[1]

$$\beta = \sqrt{M^2 - a^2} = (r_p - r_m)/2\,. \quad (5)$$

The Kinnersley NP[2] tetrad ($\boldsymbol{l}$, $\boldsymbol{m}$, $\bar{\boldsymbol{m}}$, $\boldsymbol{n}$) adapted to the principal null directions of the Weyl tensor reads as follows

$$\boldsymbol{l} = \frac{1}{\sqrt{2}\,\Delta}\left[\left(r^2+a^2\right)\boldsymbol{\partial_t} + \Delta\,\boldsymbol{\partial_r} + a\,\boldsymbol{\partial_\varphi}\right],$$
$$\boldsymbol{n} = \frac{1}{\sqrt{2}\,\Sigma}\left[\left(r^2+a^2\right)\boldsymbol{\partial_t} - \Delta\,\boldsymbol{\partial_r} + a\,\boldsymbol{\partial_\varphi}\right], \quad (6)$$
$$\boldsymbol{m} = \frac{1}{\sqrt{2}\,\bar\rho}\left(ia\sin\theta\,\boldsymbol{\partial_t} + \boldsymbol{\partial_\theta} + i\csc\theta\,\boldsymbol{\partial_\varphi}\right).$$

Total electric charge Q_e and magnetic charge Q_m can be calculated by integrating two-form $\boldsymbol{F}^* = \boldsymbol{F} - i\star\boldsymbol{F}$ over a closed 2-surface. This yields

$$iQ_e - Q_m = \frac{1}{4\pi}\oint \boldsymbol{F}^*\,. \quad (7)$$

After standard reconstruction of $\boldsymbol{F}^*$ from the NP components and the NP tetrad we get for surfaces of constant t and r following form of the Gauss law:

$$iQ_e - Q_m = \frac{1}{2}\int_0^\pi -\rho\,a\sin^2\theta\,\varphi_2 - 2i\sin\theta\left(r^2+a^2\right)\varphi_1 + \frac{a\Delta\sin^2\theta}{\rho}\,\varphi_0\;\mathrm{d}\theta\,, \quad (8)$$

where we already anticipated axial symmetry.

We will also employ the Weyl coordinates which are introduced as

$$z = {}^1\!/_2\Delta'(r)\cos\theta\,, \qquad \varrho = \sqrt{\Delta}\,\sin\theta\,. \quad (9)$$

III. TEUKOLSKY MASTER EQUATION

Let us write down TME [5] for φ_0 in the GHP formalism as

$$\left[(\text{þ} - \bar\varrho - 2\varrho)\left(\text{þ}' - \varrho'\right) - \left(\text{ð} - \bar\tau' - 2\tau\right)\left(\text{ð}' - \tau'\right)\right]\varphi_0 = J_0\,, \quad (10)$$

where the sources are encoded in J_0 which is given in terms of projections of the four-current onto the null tetrad as

$$J_0 = \left(\text{ð} - 2\tau - \bar\tau'\right)J_l - \left(\text{þ} - 2\varrho - \bar\varrho\right)J_m\,. \quad (11)$$

Once the Green function G is known the field of particular sources is then given by convolution of this Green function G with the particular source terms J_0 [26] as

$$\varphi_0 = \int_0^\infty\int_0^\pi G(r,\theta,r',\theta')J_0(r',\theta',r_0,\theta_0)\times \Sigma(r',\theta')\sin\theta'\,\mathrm{d}r'\mathrm{d}\theta'\,. \quad (12)$$

The Green function of the Teukolsky operator (the one on the l.h.s. of Eq. (10)) is easy to integrate and will be provided explicitly in the next Section.

To know the whole electromagnetic field, one has to seek for φ_1 as well. And this task is considerably more difficult. We can either (a) directly solve the ME in NP

[1] Out of parameters r_p, r_m, M, a, β only two are independent.

[2] Notice the boost given by $\sqrt{2}$ in contrast to standard textbook form. This makes the resulting expressions in terms of the Debye potentials to appear 'more symmetrical'.

formalism — which are presented in Appendix D in a simplified version for stationary and axially symmetric field; or (b) use the Debye potentials for the electromagnetic field. We will pursue the latter approach in Section VI.

IV. DEBYE POTENTIAL

There exist three distinct possibilities how to choose Debye potential for the electromagnetic field. We adhere to the most common one — a complex GHP scalar function $\bar{\psi}$ of GHP weight $[0,-2]$ which solves the the Debye equation. This equation in GHP formalism can be written as

$$\left[\left(\text{þ}' - \varrho'\right)\left(\text{þ} + \bar{\varrho}\right) - \left(\text{ð} - \tau\right)\left(\text{ð}' + \bar{\tau}\right)\right]\bar{\psi} = 0\,. \tag{13}$$

The Debye potential then gives rise to the solution of Maxwell equations. For stationary axisymmetric fields we have

$$\varphi_0 = \frac{1}{2}\frac{\partial^2\bar{\psi}}{\partial r^2}\,, \tag{14}$$

$$\varphi_1 = \frac{1}{2\sin\theta}\frac{\partial^2}{\partial r\partial\theta}\left(\frac{\sin\theta\,\bar{\psi}}{\rho}\right) - i\frac{a\sin\theta}{\rho^3}\,\bar{\psi}\,, \tag{15}$$

$$\varphi_2 = -\frac{\Delta}{\rho^2}\,\varphi_0\,, \tag{16}$$

where Eq. (16) results from axisymmetry and stationarity.

Let us just shortly comment on another possibilities in choosing the Debye potential. Using the Debye potential with GHP weights $[0,0]$ does not lead to the Laplace equation and thus is not suitable for our purposes. Whereas by using the one with GHP weights $[0,2]$ under the assumptions of stationarity and axisymmetry does not lead to anything new. We can prove that if $\bar{\psi}_{[0,-2]}$ solves the Debye equation (13), then $\bar{\chi}_{[2,0]} = \Delta^{-1}\bar{\psi}_{[0,-2]}$ solves the corresponding equation for this Debye potential and, moreover, it gives rise to exactly the same field.

V. GENERALIZED AXIALLY SYMMETRICAL POTENTIAL THEORY

It is straightforward to get the Green function of TME for φ_0, φ_2 since TME reduces to Laplace equation in a fiducial flat space of dimension $2s+3$ (where s is the spin weight of the particular NP field component) under the assumptions of axial symmetry and stationarity. This has been done by Linet in [24, 26]. The generalized Laplace equation is

$$\Delta_s g = \frac{1}{\varrho}\,\delta\left(\varrho - \varrho_0\right)\delta\left(z - z_0\right)\,, \tag{17}$$

where the Laplace operator Δ_s is defined as

$$\Delta_s \equiv \frac{\partial^2}{\partial z^2} + \frac{\partial^2}{\partial\varrho^2} + \frac{1+2s}{\varrho}\frac{\partial}{\partial\varrho}\,. \tag{18}$$

Using GASP, Linet has provided the Green function of Eq. (17) in term of the integral for general s. In our case, when $s=1$, we have

$$g = \frac{\varrho_0^2}{2\pi}\int_0^\pi \frac{\sin^2\alpha}{\left(\varrho^2 - 2\varrho\varrho_0\cos\alpha + \varrho_0^2 + (z-z_0)^2\right)^{3/2}}\,\mathrm{d}\alpha\,. \tag{19}$$

The Debye equation (13) can also be transformed to the Laplace equation. Yet, for DE we no longer seek for Green function. We need to find the Debye potential (which we call superpotential in this case and denote Ψ) of this Green function. It is given by twice integrating Eq. (14) with $\varphi_0 = G$.

Let us introduce function $\Xi_{\mathbf{r}}$ which is the Debye superpotential rescaled and cast in Weyl coordinates

$$\Psi_{\mathbf{r}}(r,\theta) = \sin\theta\,\Delta\,\Xi_{\mathbf{r}}(\varrho,z)\,. \tag{20}$$

The Debye equation transformed to the Weyl coordinates takes the form of generalized Laplace equation

$$\Delta_1\Xi_{\mathbf{r}} = 0\,. \tag{21}$$

In the Weyl coordinates Linet [24] obtained by simple integration values of the function $\Xi_{\mathbf{r}}$ on the axis of the symmetry

$$\Xi_{\mathbf{r}}(0,z) = \frac{\pi}{\sin\theta_0}\frac{\sqrt{(z-z_0)^2+\varrho_0^2}}{z^2-\beta^2}\,. \tag{22}$$

A general theorem ensures that the solution of Laplace equation is in the axisymmetric case completely determined by its values on the axis. From GASP it thus follows that the superpotential is obtained by integration

$$\begin{aligned}\Xi_{\mathbf{r}}(\varrho,z) &= \frac{2}{\pi}\int_0^\pi \Xi_{\mathbf{r}}\left(0, z + i\varrho\cos\alpha\right)\sin^2\alpha\,\mathrm{d}\alpha \\ &= \frac{2}{\sin\theta_0}\int_0^\pi \frac{\sqrt{\varrho_0^2 + \left(z + i\varrho\cos\alpha - z_0\right)^2}}{\left(z + i\varrho\cos\alpha\right)^2 - \beta^2}\,\sin^2\alpha\,\mathrm{d}\alpha\,.\end{aligned} \tag{23}$$

So far, the results of Linet.

VI. EXACT INTEGRALS

The integration of the Debye superpotential, Eq. (23), is long, involves several steps of simplification and extensive use of identities involving elliptic integrals. Therefore we present only the results and discuss the properties of the solution.

Although the φ_0 component does not carry any information about the monopole contribution of the central black hole, the Debye superpotential can contain

a monopole term – it arises during integration as an integration constant. Thus, the proper value of the monopole on the central black hole has to be evaluated later.

Let us introduce

$$h(z',\varrho') = z - z' + i\,(\varrho - \varrho')\,, \tag{24}$$

$$\begin{aligned} d(z',\varrho') &= \sqrt{h(z',\varrho')\bar{h}(z',\varrho')} \\ &= \sqrt{(z-z')^2 + (\varrho-\varrho')^2}\,; \end{aligned} \tag{25}$$

we may think of h as being a vector in complex plane connecting point (z,ϱ) and (z',ϱ'), then d is its norm.

The common form of elliptic modulus for circular sources is

$$m = \frac{4\varrho\varrho_0}{(z-z_0)^2 + (\varrho+\varrho_0)^2}\,. \tag{26}$$

However our results will be given also in terms of complementary modulus $m' = 1-m$ and reciprocal complementary modulus $\mu' = 1/m'$, explicitly

$$\mu'(\varrho_0) = 1 + \frac{4\varrho\varrho_0}{(z-z_0)^2 + (\varrho-\varrho_0)^2}\,, \tag{27}$$

$$m'(\varrho_0) = \mu'(-\varrho_0)\,. \tag{28}$$

Let us express our desired solution $\Xi_{\mathbf{r}}$ of the Laplace's equation in terms of an auxiliary function f which is defined as follows

$$\begin{aligned} f(\varrho_0) = \frac{1}{\varrho^2 d(z_0,\varrho_0)} \Bigg[& -id(z_0,\varrho_0)^2 E(\mu') + 2\varrho_0\,(4z - h(z_0,\varrho_0))\,K(\mu') - 4(z+z_0)\varrho_0 \Pi\left(\frac{h(z_0,-\varrho_0)}{h(z_0,\varrho_0)}\middle|\mu'\right) \\ & + \frac{2\varrho_0 d(\beta,0)^2}{\beta}\,\Pi\left(\frac{(z_0-\beta-i\varrho_0)\bar{h}(z_0,-\varrho_0)}{(z_0-\beta+i\varrho_0)\bar{h}(z_0,\varrho_0)}\middle|\mu'\right) - \frac{2\varrho_0 d(\beta,0)^2}{\beta}\,\Pi\left(\frac{(z_0+\beta-i\varrho_0)\bar{h}(z_0,-\varrho_0)}{(z_0+\beta+i\varrho_0)\bar{h}(z_0,\varrho_0)}\middle|\mu'\right)\Bigg]\,. \end{aligned} \tag{29}$$

Then, the Debye superpotential for the circular sources $\Xi_{\mathbf{r}}$ reads

$$\Xi_{\mathbf{r}} = \frac{1}{\sin\theta_0}\left(f(\varrho_0) + \bar{f}(-\varrho_0)\right)\,. \tag{30}$$

It is clearly a *real* function and has interesting structure of discontinuities as can be seen from the contourplot in Fig. 3. Two of these three discontinuities will be dealt with soon.

The existence of these discontinuities arise naturally from the behavior of elliptic integrals of the third kind $\Pi(n,m)$. Seen as a function of complex n it has a branch cut on the interval $(1,\infty)$. When the elliptic characteristic n crosses the real line for $n>1$ it thus has a step

$$\lim_{\epsilon\to+0}\Pi(n-i\epsilon|m) = \Pi(n|m)\,, \tag{31}$$

$$\lim_{\epsilon\to+0}\Pi(n+i\epsilon|m) = \Pi(n|m) + \frac{\pi}{\sqrt{1-n}\sqrt{1-\frac{m}{n}}}\,. \tag{32}$$

In our case, the discontinuities are located – in the Weyl coordinates – at two arcs connecting the north pole and south pole of the black hole with the source (curves $\boldsymbol{\gamma}_{\mathbf{n}}$ and $\boldsymbol{\gamma}_{\mathbf{s}}$) and a line from the source to infinity (curve $\boldsymbol{\gamma}_{\mathbf{i}}$).

The respective circles have centers $(0,z_{\mathbf{j}})$ and radii $R_{\mathbf{j}}$ where

$$\begin{aligned} z_{\mathbf{n}} &= \frac{1}{2}\frac{z_0^2+\varrho_0^2-\beta^2}{z_0-\beta}\,, & R_{\mathbf{n}} &= \frac{1}{2}\frac{(z_0-\beta)^2+\varrho_0^2}{z_0-\beta}\,, \\ z_{\mathbf{s}} &= \frac{1}{2}\frac{z_0^2+\varrho_0^2-\beta^2}{z_0+\beta}\,, & R_{\mathbf{s}} &= \frac{1}{2}\frac{(z_0+\beta)^2+\varrho_0^2}{z_0+\beta}\,. \end{aligned} \tag{33}$$

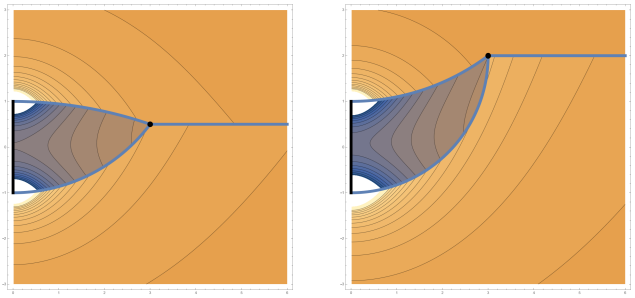

(a) $-\beta < z_0 < \beta, \beta = 1$ (b) $z_0 > \beta, \beta = 1$

FIG. 1: The contourplot of the Debye superpotential $\Xi_{\mathbf{r}}$ in the Weyl coordinates (ϱ, z). Discontinuities are present along the thick blue lines: $\boldsymbol{\gamma}_{\mathbf{n}}$, $\boldsymbol{\gamma}_{\mathbf{i}}$, $\boldsymbol{\gamma}_{\mathbf{s}}$ and they divide the space into three different regions whose characteristic function are $\Theta_{\mathbf{n}}$, $\Theta_{\mathbf{i}}$, $\Theta_{\mathbf{s}}$ (northern, inner and southern region). The outer horizon of the black hole stretches on the z axis from $-\beta$ to β.

We also define

$$\begin{aligned} r_{\mathbf{n}} &= \varrho^2 + (z-z_{\mathbf{n}})^2 - R_{\mathbf{n}}^2\,, \\ r_{\mathbf{s}} &= \varrho^2 + (z-z_{\mathbf{s}})^2 - R_{\mathbf{s}}^2\,, \end{aligned} \tag{34}$$

for the purpose of definition of region functions.

The Weyl plane is divided into the north, inner and

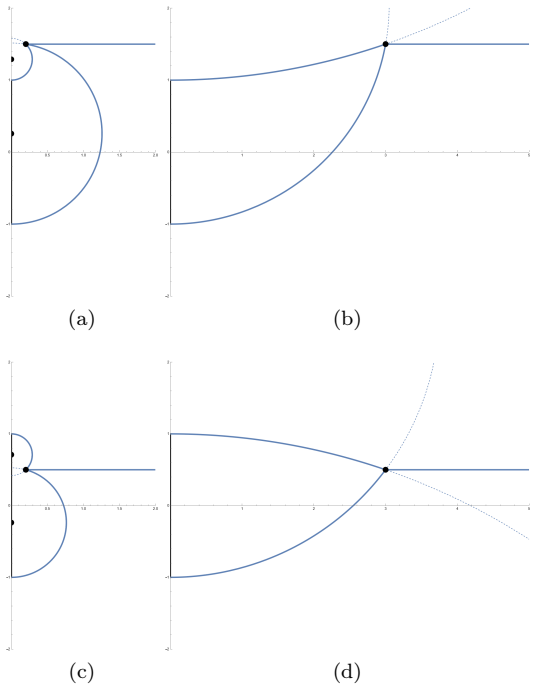

FIG. 2: Diagram showing different possibilities of the location of discontinuities depending on the mutual position of the horizon and the source in Weyl coordinates. The shape of inner region has nontrivial algebraic expression. The black hole horizon stretches on vertical axis from -1 to 1 and the location of the ring is denoted by a point. Wherever possible the centers of the circles are also shown (dots on the axis).

south region with the region functions defined as

$$\Theta_{\mathbf{n}} = \Theta(+z - z0) + \Theta(-r_{\mathbf{n}})\Theta(-(z - z_0)\,\mathrm{sign}(z_0 - \beta))\,,$$

$$\Theta_{\mathbf{i}} = \begin{cases} \Theta(-\,\mathrm{sign}(z_{\mathbf{s}} + \beta) r_{\mathbf{s}})\Theta(\mathrm{sign}(z_{\mathbf{n}} - \beta) r_{\mathbf{n}})\,, \\ \qquad \text{for } |z_{\mathbf{n}}| > \beta \text{ or } |z_{\mathbf{s}}| > \beta \\ \Theta(-r_{\mathbf{n}}) + \Theta(-r_{\mathbf{s}}) \\ -\Theta(-\,\mathrm{sign}(z_{\mathbf{s}} + \beta) r_{\mathbf{s}})\Theta(\mathrm{sign}(z_{\mathbf{n}} - \beta) r_{\mathbf{n}})\,, \\ \qquad \text{otherwise} \end{cases} \tag{35}$$

$$\Theta_{\mathbf{s}} = \Theta(-z + z0) + \Theta(-r_{\mathbf{s}})\Theta(-(z - z_0)\,\mathrm{sign}(z_0 + \beta))\,,$$

where $\Theta(x)$ stands for Heaviside step function.

We have realized that the discontinuities across the lines $\boldsymbol{\gamma}_{\mathbf{n}}, \boldsymbol{\gamma}_{\mathbf{i}}, \boldsymbol{\gamma}_{\mathbf{s}}$ corresponds to a contribution of the Debye potential of monopole in one part and zero in the other in the sense that

$$[\Xi_{\mathbf{r}}]\,|_{\boldsymbol{\gamma}_{\mathbf{j}}} = \Xi_{\mathbf{j}}|_{\boldsymbol{\gamma}_{\mathbf{j}}}\,, \tag{36}$$

for $\mathbf{j} \in \{\mathbf{n}, \mathbf{i}, \mathbf{s}\}$, where $[f(x)]$ represents the jump. Thus we may get rid of the discontinuities across the lines $\boldsymbol{\gamma}_{\mathbf{n}}$ and $\boldsymbol{\gamma}_{\mathbf{s}}$ by adding an appropriate monopole term in the

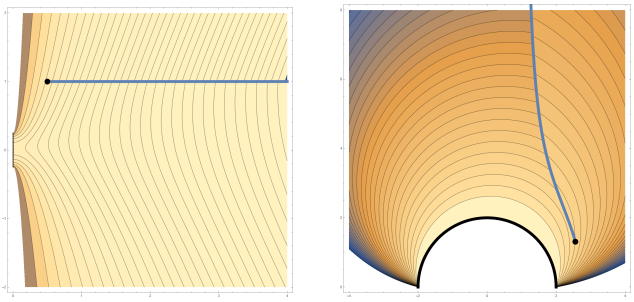

FIG. 3: The contourplot of the Debye superpotential (a) Ξ in Weyl coordinates (ϱ, z) and (b) Ψ in Boyer–Lindquist coordinates (r, θ). Discontinuity is still present along the line $\boldsymbol{\gamma}_{\mathbf{i}}$ — thick black line. The white regions are merely a cut-off of the values.

respective regions as

$$\Xi = \Xi_{\mathbf{r}} - \frac{4i\pi}{\sin\theta_0}\frac{(\beta + ia)\sqrt{(z_0 - \beta)^2 + \varrho_0^2}}{\beta}\,\Xi_{\mathbf{r}}\Theta_{\mathbf{n}} + \frac{4i\pi}{\sin\theta_0}\frac{(\beta - ia)\sqrt{(z_0 + \beta)^2 + \varrho_0^2}}{\beta}\,\Xi_{\mathbf{s}}\Theta_{\mathbf{s}}\,, \tag{37}$$

where the normalized — corresponding to unit charge — Debye potentials of the monopole read

$$\Xi_{\mathbf{n}} = -i\frac{\sqrt{(z - \beta)^2 + \varrho^2}}{2\,(\beta + ia)\,\varrho^2}\,, \tag{38}$$

$$\Xi_{\mathbf{i}} = -i\frac{z + z_0}{(r_p + r_m)\,\varrho^2}\,, \tag{39}$$

$$\Xi_{\mathbf{s}} = +i\frac{\sqrt{(z + \beta)^2 + \varrho^2}}{2\,(\beta - ia)\,\varrho^2}\,. \tag{40}$$

The Debye superpotential Ξ remains *real*.

Actually the discontinuity can be removed across arbitrary two of these three lines, yet it has to remain present on the third one. It has to be stressed that it is necessary to remove two of these three discontinuities – if this is not done, then the electromagnetic field component φ_1 generated from this superpotential is discontinuous.

This discontinuity is caused by a ramification of a multi-valued function. Yet, it can be also seen as a presence of distributional sources on the right hand side of the Laplace's equation, and we have decided to have these sources along $\boldsymbol{\gamma}_{\mathbf{i}}$.

The function Ξ is finally sufficiently smooth across $\boldsymbol{\gamma}_{\mathbf{n}}$ and $\boldsymbol{\gamma}_{\mathbf{s}}$; but the discontinuity across $\boldsymbol{\gamma}_{\mathbf{i}}$ is still present.

The Debye superpotential is

$$\Psi = \sin\theta\,\Delta(r)\,\Xi(r, \theta)\,, \tag{41}$$

where $\Xi(\varrho, z)$ given by Eq. (37) has to be transformed from Weyl coordinates to Boyer–Lindquist coordinates. The contourplot of Ξ and Ψ are in Fig. 3.

For stationary axisymmetric sources we may write

$$\boldsymbol{J} = j_0 \boldsymbol{\partial_t} + j_3 \boldsymbol{\partial_\varphi} \,, \tag{42}$$

where j_0 and j_3 are functions of r and θ only.

Simplified expression for the sources of TME reads as follows

$$J_0 = \frac{1}{2\rho\Sigma}\Bigg[-\frac{\partial}{\partial\theta}\left(\rho^2 j_0\right) + ia\sin\theta\frac{\partial}{\partial r}\left(\rho^2 j_0\right) \\ \frac{\partial}{\partial\theta}\left(a\sin^2\theta\,\rho^2\, j_3\right) - i\frac{\partial}{\partial r}\Big(\left(a^2+r^2\right)\sin\theta\,\rho^2\, j_3\Big)\Bigg] \tag{43}$$

and the Debye potential is given by convolution of the Debye superpotential with sources as

$$\bar{\psi} = \int_0^\pi \int_0^\infty \Psi(r,\theta,r',\theta') J_0(r',\theta',r_0,\theta_0) \\ \Sigma(r',\theta')\sin\theta'\,\mathrm{d}r'\mathrm{d}\theta' \,. \tag{44}$$

We can also explicitly integrate the Green function G of the Teukolsky operator which is

$$G = \frac{\sin\theta}{\sin\theta_0}\, g \,, \tag{45}$$

$$g = \frac{d(z_0,-\varrho_0)}{\varrho^2}\left[-E(m) + \left(1 + \frac{2\varrho_0\varrho}{d(z_0,-\varrho_0)^2}\right)K(m)\right] . \tag{46}$$

The function G solves TME and for g we have $\Delta_1 g = 0$. It can be checked that

$$G = \frac{1}{2}\frac{\partial^2\Psi}{\partial r^2} \,, \tag{47}$$

which is a consistency check following from the definition of the superpotential.

Let us also note that the position of discontinuities discussed so far is *natural* in the sense, that it is defined by the branch cuts of respective elliptic integrals of the third kind. But we are allowed to move the discontinuities wherever is desired. Thus, they can be moved to line $r = r_0$ on Boyer–Lindquist coordinates (which is an ellipse in Weyl coordinates). The reason we make this short comment is to draw a clear theoretical connection to the series expansion approach. In [17] the field is given by different series expansions in regions $r < r_0$ and $r > r_0$

$$\varphi_0 = 2\sum_{l=1}^{\infty}\frac{a_l}{l(l+1)}{}_1Y_{l0}\frac{\mathrm{d}^2 y_{l0}^{(1)}}{\mathrm{d}x^2} \,, \\ y_{l0}^{(1)} = x(x-1)F\left(l+2,1-l,2;x\right) \,, \quad \text{for } r<r_0 \,, \tag{48}$$

$$\varphi_0 = 2\sum_{l=1}^{\infty}\frac{b_l}{l(l+1)}{}_1Y_{l0}\frac{\mathrm{d}^2 y_{l0}^{(2)}}{\mathrm{d}x^2} \,, \\ y_{l0}^{(2)} = (-x)^l F\left(l,1+l,2l+2;x\right) \,, \quad \text{for } r>r_0 \,, \tag{49}$$

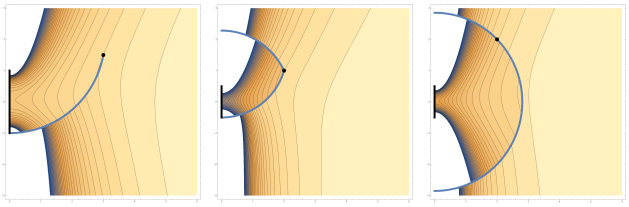

(a) $\Xi_{\mathbf{0}}$ (b) $\Xi_{\mathbf{1}}$ (c) $\Xi_{\mathbf{2}}$

FIG. 4: The contourplot of the Debye superpotential $\Xi_{\mathbf{j}}$, $\mathbf{j} \in (\mathbf{0},\mathbf{1},\mathbf{2})$ in Weyl coordinates with different positions of discontinuities. In (c) we can see the discontinuities corresponding to the series expansion case. The exact formulae can be found in Appendix E.

where $x = \frac{r-r_m}{r_p-r_m}$. Thus, this is almost ready to be twice integrated along r to obtain the series expansion of the Debye potential. As discussed in [17], for φ_1 a different monopole term has to be added in regions $r < r_0$ and $r > r_0$, so the discontinuity is present also in this formulation. In Fig. 4 another possible locations of discontinuities are visualized. The respective formulae are postponed to Appendix E.

We do not integrate the series expansion of the Debye potential since we already have found an exact closed solution. For particular sources, we have numerically checked the validity of our results.

A. The Debye superpotential

The Debye superpotential is itself a Debye potential for some electromagnetic field. What will be the electric and magnetic charge induced on the black hole? Recall that the charge within a topological sphere is given by the Gauss law – Eq. (8). Using Eq. (16) this simplifies to

$$iQ_e - Q_m = \int_0^\pi -i\sin\theta\left(r^2+a^2\right)\varphi_1 + \frac{a\Delta\sin^2\theta}{\rho}\varphi_0\,\mathrm{d}\theta \,, \tag{50}$$

which we would like to evaluate on the horizon.

First of all we may express the electromagnetic field in terms of the Debye superpotential $\varphi[\Psi_{\mathbf{r}}]$. The behavior of $\Psi_{\mathbf{r}}$ on the horizon[3] is of the form

$$\Psi_{\mathbf{r}} = 0 + S(\theta)(r-r_p) + O\left((r-r_p)^2\right) . \tag{51}$$

[3] Keep in mind that during the "regularization" of the Debye superpotential in Eq. (37) no charge has been added on the black hole.

In particular we have

$$\Psi_{\mathbf{r}} \doteq 0$$
$$-\pi \frac{\sqrt{4\Delta(r_0)\sin^2\theta_0 + (-2\beta\cos\theta + \cos\theta_0\,\Delta'(r_0))^2}}{\beta\sin\theta\,\sin\theta_0}(r-r_p) + \dots \quad (52)$$

Evaluating the flux on the horizon and simplifying the expressions yield a simple result which can be explicitly integrated

$$iQ_e - Q_m = \int_0^\pi -ir_p(r_p+r_m)\frac{\partial}{\partial\theta}\left(\frac{\sin\theta\,\partial_r\Psi_{\mathbf{r}}}{\rho(r_p,\theta)}\right)\mathrm{d}\theta = -ir_p(r_p+r_m)\left[\frac{\sin\theta\,S(\theta)}{\rho(r_p,\theta)}\right]_{\theta=0}^{\pi}. \quad (53)$$

Thus, the total charge upon the black hole is[4]

$$Q_{\mathbf{r}} = iQ_e - Q_m = -i\frac{\pi}{\beta\sin\theta_0}\left[\rho(r_p,\theta)\times \sqrt{4\Delta(r_0)\sin^2\theta_0 + (-2\beta\cos\theta + \cos\theta_0\,\Delta'(r_0))^2}\right]_{\theta=0}^{\pi}. \quad (54)$$

B. Charged ring

Let us consider the source of static charged ring in the form of Eq. (42) with

$$j_0 = \hat{j}_0(r_0,\theta_0)\frac{\delta(r-r_0)}{\Sigma(r_0,\theta_0)}\frac{\delta(\theta-\theta_0)}{\sin\theta_0}, \qquad j_3 = 0. \quad (55)$$

Then, the convolution of the sources with the superpotential as in the Eq. (44) leads to the Debye potential of charged ring

$$\bar{\psi}_{\mathbf{ring}} = \frac{\hat{j}_0(r_0,\theta_0)}{2\overline{\rho(r_0,\theta_0)}}\left(\cot\theta_0 + \frac{\partial}{\partial\theta_0} - ia\sin\theta_0\frac{\partial}{\partial r_0}\right)\Psi. \quad (56)$$

From this Debye potential the electromagnetic field is easily reconstructed by differentiation. Hence, we have

$$\begin{aligned}\varphi_0 &= \varphi_0[\bar{\psi}_{\mathbf{ring}}],\\ \varphi_1 &= \varphi_1[\bar{\psi}_{\mathbf{ring}}] + \frac{e_{\mathbf{ring}}}{\rho^2},\\ \varphi_2 &= \varphi_2[\bar{\psi}_{\mathbf{ring}}],\end{aligned} \quad (57)$$

where the value of the charge $e_{\mathbf{ring}}$ counterbalances the charge induced on the black hole by the presence of the ring. It is given by the same operator as in Eq. (56), i.e.

$$e_{\mathbf{ring}} = \frac{\hat{j}_0(r_0,\theta_0)}{2\overline{\rho(r_0,\theta_0)}}\left(\cot\theta_0 + \frac{\partial}{\partial\theta_0} - ia\sin\theta_0\frac{\partial}{\partial r_0}\right)Q_{\mathbf{r}}. \quad (58)$$

The integral lines of electric and magnetic field of a charged ring hovering above the equatorial plane on the Kerr background which would have been measured by congruence of ZAMO observers are visualized in Fig. 5.

We have numerically compared the values of φ_0 with the results given in [17] as an infinite series expansion and the results are identical (modulo normalization factor $\sqrt{2}\pi$).

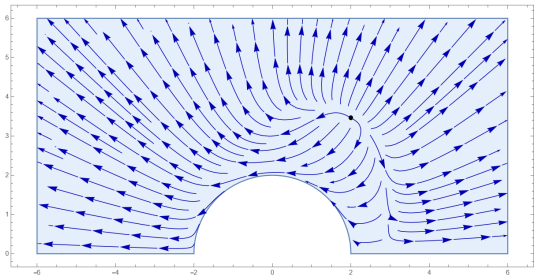

(a) Integral curves of $\boldsymbol{E}$.

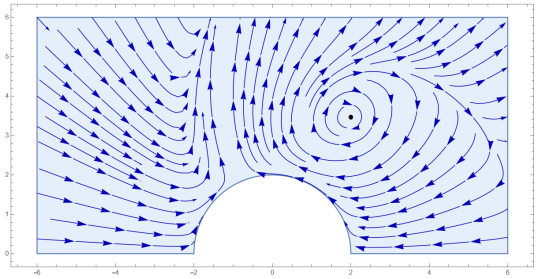

(b) Integral curves of $\boldsymbol{B}$.

FIG. 5: Integral curves of of the electric $\boldsymbol{E}$ and the magnetic $\boldsymbol{B}$ field of a charged ring (depicted by black dot) above the black hole as measured by ZAMO in the (r,θ) plane. The Meissner effect exhibits itself as well as the presence of both electric and magnetic field due to the almost extremal rotation of the black hole. The rotation axis is horizontal and the parameters are $r_p = 2, r_m = 1.999, r_0 = 4, \theta_0 = \pi/3$.

C. Current loop

Let the source of the electromagnetic field be an axially symmetric current loop defined as

$$j_0 = 0, \quad j_3 = \hat{j}_3(r_0,\theta_0)\frac{\delta(r-r_0)}{\Sigma(r_0,\theta_0)}\frac{\delta(\theta-\theta_0)}{\sin\theta_0}. \quad (59)$$

[4] Notice, that $\rho(r,0)\rho(r,\pi) = r^2 + r_p r_m$.

Evaluating the Eq. (12) leads to the Debye potential of the current loop

$$\bar{\psi}_{\mathbf{current}} = \hat{j}_3(r_0,\theta_0)\frac{\sin\theta_0}{2\overline{\rho(r_0,\theta_0)}} \left(-ir_0 - a\sin\theta_0\frac{\partial}{\partial\theta_0} + i\left(r_0^2+a^2\right)\frac{\partial}{\partial r_0}\right)\Psi\,. \quad (60)$$

Again, the results are in agreement with [17] if we set the normalization constant $\hat{j}_3 = 2\sqrt{2}r_0\sqrt{\Delta(r_0)/\Upsilon(r_0,\pi/2)}$ (in [17] the ring is only in equatorial plane).

The field can be reconstructed from the NP projections

$$\begin{aligned}\varphi_0 &= \varphi_0[\bar{\psi}_{\mathbf{current}}]\,,\\ \varphi_1 &= \varphi_1[\bar{\psi}_{\mathbf{current}}] + \frac{e_{\mathbf{current}}}{\rho^2}\,,\\ \varphi_2 &= \varphi_2[\bar{\psi}_{\mathbf{current}}]\,,\end{aligned} \quad (61)$$

where the monopole charge $e_{\mathbf{current}}$ has to be set to

$$e_{\mathbf{current}} = \hat{j}_3(r_0,\theta_0)\frac{\sin\theta_0}{2\overline{\rho(r_0,\theta_0)}} \left(-ir_0 - a\sin\theta_0\frac{\partial}{\partial\theta_0} + i\left(r_0^2+a^2\right)\frac{\partial}{\partial r_0}\right)Q_{\mathbf{r}}\,, \quad (62)$$

if we want the black hole to be uncharged.

The integral lines of the electric and magnetic fields which would have been measured by congruence of ZAMO observers are visualized in Fig. 6.

VII. CONCLUSIONS

We provided compact and closed form of the electromagnetic Debye superpotential for circular sources on the Kerr background. This superpotential is not unique as the necessary discontinuities can be moved to any line connecting the source to infinity/axis if viewed as a one-valued function after ramification. Therefore, also the distributional sources are not unique.

Having this superpotential at hand we discussed the field of the charged ring and the circular current loop.

We demonstrated that our results are in agreement with previous results obtained in a form of series.

ACKNOWLEDGMENTS

D.K. and P.K. acknowledge the support from the Czech Science Foundation, Grant 21-11268S. The calculations were performed using *Wolfram Mathematica*® as well as *MapleSoft Maple*®.

D.K. is also deeply indebted to Oldřich Semerák whose comments helped to improve the manuscript.

Data Availability Statement: Data sharing not applicable to this article as no datasets were generated or analyzed during the current study.

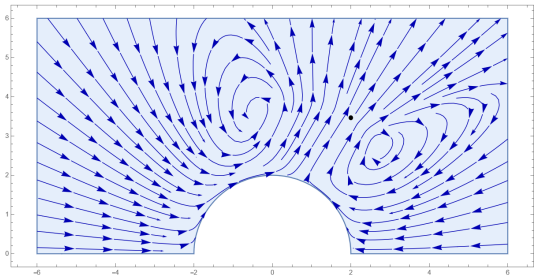

(a) Integral curves of $\boldsymbol{E}$.

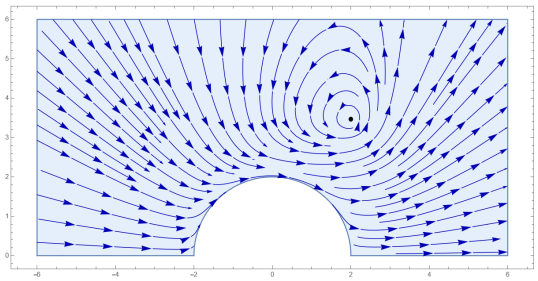

(b) Integral curves of $\boldsymbol{B}$.

FIG. 6: Integral curves of the electric and the magnetic field around the current loop (depicted by black dot) above the black hole as measured by ZAMO in the (r,θ) plane. The rotational axis is horizontal and the parameters are $r_p = 2, r_m = 1.999, r_0 = 4, \theta_0 = \pi/3$.

Appendix A: NP quantities of Kerr black hole

The nonzero NP spin coefficients corresponding to the tetrad (6) are

$$\begin{aligned}\pi &= \frac{i}{\sqrt{2}}\frac{a\sin\theta}{\rho^2}\,, & \mu &= \frac{-1}{\sqrt{2}}\frac{\Delta}{\Sigma\rho}\,,\\ \tau &= \frac{-i}{\sqrt{2}}\frac{a\sin\theta}{\Sigma}\,, & \varrho &= \frac{-1}{\sqrt{2}}\frac{1}{\rho}\,,\\ \gamma &= \mu + \frac{1}{\sqrt{2}}\frac{r-M}{\Sigma}\,, & \beta &= \frac{1}{\sqrt{2}}\frac{\cot\theta}{\bar{\rho}}\,,\\ \alpha &= \pi - \bar{\beta}\,,\end{aligned} \quad (A1)$$

and the only nonzero Weyl scalar reads

$$\psi_2 = -\frac{M}{\rho^3}\,. \quad (A2)$$

Appendix B: ZAMO congruence

The physical interpretation of the electromagnetic field is done by an observer who makes a local measurements. Physical measurements in GR are done by projections of the field onto an orthonormal tetrad. One of the most useful congruence of observers around the Kerr black hole are the ZAMO observers whose 4-velocity is defined by

$\boldsymbol{u}_a \propto (\boldsymbol{dt})_a$, the congruence is thus non-twisting and, as its name suggests, angular momentum of every particular observer vanishes, i.e. $L \equiv \boldsymbol{\eta}\cdot\boldsymbol{u} = 0$. The tetrad ($\boldsymbol{u} \equiv \boldsymbol{e}_{(t)}$) is given by

$$\begin{aligned} \boldsymbol{e}_{(t)} &= \frac{1}{N}\left(\boldsymbol{\partial_t} + \omega\,\boldsymbol{\partial_\varphi}\right), \quad & \boldsymbol{e}_{(r)} &= \sqrt{\frac{\Delta}{\Sigma}}\,\boldsymbol{\partial_r}\,, \\ \boldsymbol{e}_{(\theta)} &= \frac{1}{\sqrt{\Sigma}}\,\boldsymbol{\partial_\theta}\,, & \boldsymbol{e}_{(\varphi)} &= \frac{1}{\sin\theta}\sqrt{\frac{\Sigma}{\Upsilon}}\,\boldsymbol{\partial_\varphi}\,, \end{aligned} \tag{B1}$$

where

$$N = \sqrt{\frac{(\boldsymbol{\eta}\cdot\boldsymbol{\xi})^2}{\boldsymbol{\eta}\cdot\boldsymbol{\eta}} - \boldsymbol{\xi}\cdot\boldsymbol{\xi}}\,, \tag{B2}$$

$$\omega = -\frac{\boldsymbol{\xi}\cdot\boldsymbol{\eta}}{\boldsymbol{\eta}\cdot\boldsymbol{\eta}}\,, \tag{B3}$$

$$\Upsilon = \Delta\Sigma + r(r_p + r_m)\left(r^2 + r_p r_m\right)\,. \tag{B4}$$

The scalar product of two vectors $\boldsymbol{u}$ and $\boldsymbol{v}$ is denoted as $\boldsymbol{u}\cdot\boldsymbol{v} = \boldsymbol{u}^a\boldsymbol{g}_{ab}\boldsymbol{v}^b$. The Killing vectors of the Kerr metric are $\boldsymbol{\xi} = \boldsymbol{\partial_t}$ and $\boldsymbol{\eta} = \boldsymbol{\partial_\varphi}$. The projections

$$\mathcal{E}_{(k)} = \boldsymbol{e}_{(t)}\cdot\boldsymbol{F}^*\cdot\boldsymbol{e}_{(k)}\,, \qquad \text{for} \qquad k \in (r,\,\theta,\,\varphi)\,, \tag{B5}$$

written in compact form for $\boldsymbol{\mathcal{E}} = \boldsymbol{E} - i\boldsymbol{B}$ are

$$\begin{aligned} \mathcal{E}_{(r)} &= \frac{\frac{-ia\sin\theta\Delta}{\rho}\,\varphi_0 - 2\left(r^2+a^2\right)\varphi_1 + ia\sin\theta\,\rho\,\varphi_2}{\sqrt{\Upsilon}}\,, \\ \mathcal{E}_{(\theta)} &= \frac{r^2+a^2}{\sqrt{\Delta\Upsilon}}\left(\frac{\Delta}{\rho}\,\varphi_0 - \frac{2ia\sin\theta\Delta}{r^2+a^2}\,\varphi_1 - \bar{\varrho}\,\varphi_2\right), \\ \mathcal{E}_{(\varphi)} &= -\frac{i\sqrt{\Delta}}{\rho}\,\varphi_0 - \frac{i\rho}{\sqrt{\Delta}}\,\varphi_2\,. \end{aligned} \tag{B6}$$

Appendix C: Elliptic integrals

We use the same definition of complete elliptic integrals as the one implemented in *Wolfram Mathematica*®, i.e.

$$E(m) = \int_0^{\pi/2}\sqrt{1 - m\sin^2\theta}\,\mathrm{d}\theta\,, \tag{C1}$$

$$K(m) = \int_0^{\pi/2}\frac{1}{\sqrt{1 - m\sin^2\theta}}\,\mathrm{d}\theta\,, \tag{C2}$$

$$\Pi(n|m) = \int_0^{\pi/2}\frac{1}{\left(1 - n\sin^2\theta\right)\sqrt{1 - m\sin^2\theta}}\,\mathrm{d}\theta\,. \tag{C3}$$

Appendix D: Maxwell Equations in axisymmetric stationary case

Maxwell Equations in axisymmetric stationary case can be, using the the following rescaled NP quantities

$$\varphi_0 = \frac{\sqrt{2}\rho}{\sin\theta}\,\tilde{\varphi}_0\,, \quad \varphi_1 = \frac{\sqrt{2}}{\rho^2}\,\tilde{\varphi}_1\,, \quad \varphi_2 = \frac{\sqrt{2}\Delta}{\rho\sin\theta}\,\tilde{\varphi}_2\,, \tag{D1}$$

rewritten as

$$\frac{\frac{\partial}{\partial\theta}\,\tilde{\varphi}_0}{\sin\theta} - \frac{\frac{\partial}{\partial r}\,\tilde{\varphi}_1}{\rho^2} = -J_l\,, \quad \frac{\frac{\partial}{\partial r}\,(\Delta\tilde{\varphi}_0)}{\bar{\rho}\sin\theta} + \frac{\frac{\partial}{\partial\theta}\,\tilde{\varphi}_1}{\rho\Sigma} = J_m\,, \tag{D2}$$

$$\frac{\frac{\partial}{\partial\theta}\,\tilde{\varphi}_2}{\Sigma\sin\theta} + \frac{\Delta\frac{\partial}{\partial r}\,\tilde{\varphi}_1}{\rho^2\Sigma} = J_n\,, \qquad \frac{\frac{\partial}{\partial r}\,\tilde{\varphi}_2}{\rho\sin\theta} - \frac{\frac{\partial}{\partial\theta}\,\tilde{\varphi}_1}{\rho^3} = J_{\bar{m}}\,. \tag{D3}$$

Appendix E: Different discontinuities location

We may express

$$\begin{aligned} r &= \frac{1}{2}\left(r_p + r_m + \sqrt{(z-\beta)^2 + \varrho^2} + \sqrt{(z+\beta)^2 + \varrho^2}\right), \\ r_0 &= \frac{1}{2}\left(r_p + r_m + \sqrt{(z_0-\beta)^2 + \varrho_0^2} + \sqrt{(z_0+\beta)^2 + \varrho_0^2}\right) \end{aligned} \tag{E1}$$

and then define potentials

$$\begin{aligned} \Xi_{\mathbf{0}} &= \Xi_{\mathbf{r}} - \frac{4i\pi\mathcal{R}_+}{\beta\sin\theta_0}\,\Xi_{\mathbf{n}}\Theta_{\mathbf{n}} \\ &\quad - \left(\frac{4i\pi(r_p+r_m)}{\sin\theta_0}\,\Xi_{\mathbf{i}} + \frac{4i\pi\mathcal{R}_+}{\beta\sin\theta_0}\,\Xi_{\mathbf{n}}\right)\Theta_{\mathbf{s}}\,, \end{aligned} \tag{E2}$$

$$\begin{aligned} \Xi_{\mathbf{1}} &= \Xi_{\mathbf{r}} - \frac{2i\pi\mathcal{R}_+}{\beta\sin\theta_0}\,\Xi_{\mathbf{n}}\Theta_{\mathbf{n}}\left(1 + \Theta(r_0 - r)\right) \\ &\quad - \left(\frac{4i\pi(r_p+r_m)}{\sin\theta_0}\,\Xi_{\mathbf{i}} + \frac{2i\pi\mathcal{R}_+}{\beta\sin\theta_0}\,\Xi_{\mathbf{n}}\right)\Theta_{\mathbf{s}}\,, \end{aligned} \tag{E3}$$

$$\begin{aligned} \Xi_{\mathbf{2}} &= \Xi_{\mathbf{r}} - \frac{2i\pi\mathcal{R}_+}{\beta\sin\theta_0}\,\Xi_{\mathbf{n}}\Theta_{\mathbf{n}}\left(1 + \Theta(r_0 - r)\right) \\ &\quad - \left(\frac{4i\pi(r_p+r_m)}{\sin\theta_0}\,\Xi_{\mathbf{i}} + \frac{2i\pi\mathcal{R}_+}{\beta\sin\theta_0}\,\Xi_{\mathbf{n}}\right)\Theta_{\mathbf{s}}\Theta(r - r_0) \\ &\quad + \frac{4i\pi\mathcal{R}_-}{\beta\sin\theta_0}\Theta(r_0 - r)\Theta_{\mathbf{s}}\Xi_{\mathbf{s}}\,, \end{aligned} \tag{E4}$$

where

$$\begin{aligned} \mathcal{R}_+ &= (\beta + ia)\sqrt{(z_0-\beta)^2 + \varrho_0^2}\,, \\ \mathcal{R}_- &= (\beta - ia)\sqrt{(z_0+\beta)^2 + \varrho_0^2}\,. \end{aligned} \tag{E5}$$

All of these potential represent the same field. They differ just by the position of discontinuities — visualisations can be found in Fig 4. And, moreover, there is still a great freedom since one can add terms

$$a_{\mathbf{n}}\Xi_{\mathbf{n}} + a_{\mathbf{i}}\Xi_{\mathbf{i}} + a_{\mathbf{s}}\Xi_{\mathbf{s}}\,, \qquad a_{\mathbf{n}} + a_{\mathbf{i}} + a_{\mathbf{s}} = 0\,, \tag{E6}$$

i.e. Debye potential of field representing monopole with vanishing charge.

[1] R. P. Kerr, Gravitational Field of a Spinning Mass as an Example of Algebraically Special Metrics, Phys. Rev. Lett. **11**, 237 (1963).

[2] B. Punsly, *Black Hole Gravitohydromagnetics*, Astrophysics and Space Science Library, Vol. 355 (Springer Berlin Heidelberg, Berlin, Heidelberg, 2009).

[3] E. Newman and R. Penrose, An Approach to Gravitational Radiation by a Method of Spin Coefficients, J. Math. Phys. **3**, 566 (1962).

[4] R. Geroch, A. Held, and R. Penrose, A space-time calculus based on pairs of null directions, J. Math. Phys. **14**, 874 (1973), arXiv:1011.1669v3.

[5] S. A. Teukolsky, Rotating black holes: Separable wave equations for gravitational and electromagnetic perturbations, Phys. Rev. Lett. **29**, 1114 (1972).

[6] S. A. Teukolsky, Perturbations of a Rotating Black Hole. I. Fundamental Equations for Gravitational, Electromagnetic, and Neutrino-Field Perturbations, Astrophys. J. **185**, 635 (1973).

[7] E. D. Fackerell and J. R. Ipser, Weak Electromagnetic Fields Around a Rotating Black Hole, Phys. Rev. D **5**, 2455 (1972).

[8] J. Jezierski and T. Smołka, A geometric description of Maxwell field in a Kerr spacetime, Class. Quantum Gravity **33**, 125035 (2016), arXiv:1502.00599.

[9] A. Starobinski and S. Churilov, Amplification of electromagnetic and gravitational waves scattered by a rotating "black hole", Sov. J. Exp. Theor. Phys. **65**, 3 (1973).

[10] W. H. Press and S. A. Teukolsky, Perturbations of a Rotating Black Hole. II. Dynamical Stability of the Kerr Metric, Astrophys. J. **185**, 649 (1973).

[11] S. A. Teukolsky and W. H. Press, Perturbations of a rotating black hole. III - Interaction of the hole with gravitational and electromagnetic radiation, Astrophys. J. **193**, 443 (1974).

[12] J. A. Petterson, Magnetic field of a current loop around a schwarzschild black hole, Phys. Rev. D **10**, 3166 (1974).

[13] D. M. Chitre and C. V. Vishveshwara, Electromagnetic field of a current loop around a Kerr black hole, Phys. Rev. D **12**, 1538 (1975).

[14] J. A. Petterson, Stationary axisymmetric electromagnetic fields around a rotating black hole, Phys. Rev. D **12**, 2218 (1975).

[15] B. Linet, Electrostatics and magnetostatics in the Schwarzschild metric, J. Phys. A. Math. Gen. **9**, 1081 (1976).

[16] J. Bičák and L. Dvořák, Stationary electromagnetic fields around black holes, Czechoslov. J. Phys. **27**, 127 (1977).

[17] J. Bičák and L. Dvořák, Stationary electromagnetic fields around black holes. II. General solutions and the fields of some special sources near a Kerr black hole, Gen. Relativ. Gravit. **7**, 959 (1976).

[18] J. M. Cohen and L. S. Kegeles, Electromagnetic fields in curved spaces: A constructive procedure, Phys. Rev. D **10**, 1070 (1974).

[19] J. Cohen and L. Kegeles, Electromagnetic fields in general relativity: A constructive procedure, Phys. Lett. A **47**, 261 (1974).

[20] R. M. Wald, Construction of solutions of gravitational, electromagnetic, or other perturbation equations from solutions of decoupled equations, Phys. Rev. Lett. **41**, 203 (1978).

[21] L. S. Kegeles and J. M. Cohen, Constructive procedure for perturbations of spacetimes, Phys. Rev. D **19**, 1641 (1979).

[22] L. Andersson, T. Bäckdahl, and P. Blue, Spin geometry and conservation laws in the Kerr spacetime, Surv. Differ. Geom. **20**, 183 (2015), arXiv:1504.02069v1.

[23] S. Aksteiner and T. Bäckdahl, Symmetries of linearized gravity from adjoint operators, J. Math. Phys. **60**, 10.1063/1.5092587 (2019), arXiv:1609.04584.

[24] B. Linet, Stationary axisymmetry electromagnetic fields in the Kerr metric, J. Phys. A. Math. Gen. **12**, 839 (1979).

[25] R. Penrose and W. Rindler, *Spinors and Space-Time* (Cambridge University Press, 1984).

[26] B. Linet, Stationary axisymmetric test fields on a Kerr metric, Phys. Lett. A **60**, 395 (1977), arXiv:1011.1669v3.

[27] D. L. Wiltshire, M. Visser, and S. Scott, *The Kerr spacetime: Rotating black holes in general relativity*, edited by D. L. Wiltshire, M. Visser, and S. Scott (Cambridge University Press, Cambridge, 2009) p. 378.

[28] S. A. Teukolsky, The Kerr metric, Class. Quantum Gravity **32**, 10.1088/0264-9381/32/12/124006 (2015), arXiv:1410.2130.

CONCLUSIONS

In this thesis, we studied the influence of the environment on the gravitational field of a black hole. Under some simplifying assumptions, namely stationarity (or even staticity) and axial symmetry, we obtained several closed-form solutions describing the field of a black hole encircled by a thin disc or ring. Besides the basic geometrical properties, we analyzed the quasinormal response of such a non-isolated black hole.

First, we considered static spacetimes in Chap. 2, i.e. we neglected the overall rotation present in the spacetime. The metric of such a field can be described by just two functions: one that satisfies the linear Laplace equation (an analogue of the Newtonian gravitational potential) and the other is given by a simple, yet non-linear quadrature. We focused on thin-disc sources while also having their "superposition" with a black hole in mind. These discs are thus typically empty in their centre, having a density that is sufficiently smooth when approaching the disc's edges. We derived several analytical models of a black hole surrounded by a thin disc. In some cases, we even found the complete metric, solving the quadrature for the second metric function analytically.

In particular, we obtained several families of finite or infinite discs with polynomial and power-law density profiles in Sec. 2.6.1. Previously, some of these discs were known in terms of infinite series with slow convergence properties, while here we provided the solution in closed form using elliptic integrals. The second metric function has usually to be found by numerical integration, yet in some cases it has been possible to solve the problem completely analytically. In particular, this applies to the discs resulting from combinations of the Kuzmin-Toomre solutions we derived in Sec. 2.6.2. They smoothly extend from the horizon to infinity, with density appropriately vanishing at both limits, ensuring analytical behaviour everywhere above the horizon. Additionally, we proposed a novel method for generating thin-disc solutions in Sec. 2.6.3 using the Appell potential as a "seed" solution. The method successfully reproduced many results from the literature, and we were able to complete the metric for several disc families constructed from the relativistic Morgan-Morgan discs, including their superposition with the black hole.

Then, we studied the QNM spectrum of a black hole encircled by a gravitating disc in Chap. 3. To simplify the problem, we probed the geometry using a scalar field while assuming only a small deviation from the Schwarzschild black hole, thus keeping the mass of the disc small compared to the mass of the central black hole. We found that for a wide range of disc parameters, the QNM frequencies decreased while the damping time increased. Similar results were observed in the spherically symmetric case, indicating some kind of universal behaviour. If such a relation truly exists generically, it may help to distinguish environmental effects from those predicted by alternative theories of gravity.

Finally, we embarked on the stationary case in Chap. 4. Here, we chose the perturbative approach while using the tetrad formalism developed by Geroch, Held, Newman, and Penrose. Our initial investigation involved the electromagnetic field on a rotating black-hole background. We introduced the Debye superpotential, a single complex scalar function, which yields the Green function of the Teukolsky equation, representing the electromagnetic field of an elemental ring source. Subsequently, we applied these findings to two specific scenarios: the charged ring and the axial current around the Kerr black hole, see Sec. 4.4.3. By providing closed-form solutions we expect further generalization to extended bodies such as discs in future work. Finally, we outlined the procedure for also defining the Debye superpotential for gravitational perturbations.

The future outlook

The immediate next steps are clear. In particular, we plan to analyze the Debye super-potential of the gravitational perturbations. Additionally, we are eager to find stationary analogues of the static disc solutions by perturbatively adding rotational angular momentum to the disc or considering the Kerr black hole instead of the Schwarzschild solution. The subsequent analysis will also involve solving the related issue of finding the gauge transformation from the radiation gauges to the explicitly circular-type metric (1.6).

Another exciting topic to explore further is the problem of QNMs. There are, in fact, three directions we look forward:

1. Since astrophysical objects typically possess angular momentum, one natural extension is to consider stationary rather than static spacetimes. With some modifications, we can apply the same method we used to find the frequencies of QNMs in the static case. Therefore, if a suitable analytical model of a Kerr black hole perturbed by a rotating disc is found, we intend to perform a similar analysis of QNMs in such a spacetime.

2. The new generation of ground and space-based gravitational wave detectors may soon allow for a precise spectroscopy of the ring-down phase. For the spectroscopy to work reliably, the spectrum of QNMs should be stable against perturbations. However, it has been found that the QNM spectrum is destabilized when a second peak in the effective potential is present, although the frequencies of (at least) the fundamental mode can still be recovered from the time evolution. Whether ordinary matter can indeed produce a second peak in the effective potential is still an open question, as discussed in Chap. 3. This aspect deserves further investigation.

3. Another avenue is to extend the analysis from scalar-field QNMs to the behavior of gravitational perturbations. In this case, two kinds of perturbations will be involved: one that describes the geometry of the deformed black-hole spacetime and another that governs the propagation of gravitational QNMs. Their mutual interaction will be the main focus.

BIBLIOGRAPHY

Aksteiner, S., Andersson, L., Araneda, B., & Whiting, B. 2021, On the Geometry of Petrov Type II Spacetimes, Classical and Quantum Gravity, 38, 135023, doi: 10.1088/1361-6382/abf542

Andersson, L., Bäckdahl, T., & Blue, P. 2015, Spin Geometry and Conservation Laws in the Kerr Spacetime, Surveys in Differential Geometry, 20, 183, doi: 10.4310/SDG.2015.v20.n1.a8

Appell, P. 1887, Quelques remarques sur la théorie des potentiels multiformes, Mathematische Annalen, 30, 155, doi: 10.1007/BF01564536

Arnowitt, R., Deser, S., & Misner, C. W. 1962, The Dynamics of General Relativity, 227

Bach, R., & Weyl, H. 1922, Neue Lösungen der Einsteinschen Gravitationsgleichungen: B. Explizite Aufstellung statischer axialsymmetrischer Felder, Mathematische Zeitschrift, 13

Barausse, E., Cardoso, V., & Pani, P. 2015, Environmental Effects for Gravitational-wave Astrophysics, Journal of Physics: Conference Series, 610, 012044, doi: 10.1088/1742-6596/610/1/012044

Berti, E., Cardoso, V., Cheung, M. H.-Y., et al. 2022, Stability of the Fundamental Quasinormal Mode in Time-Domain Observations against Small Perturbations, Physical Review D, 106, 084011, doi: 10.1103/PhysRevD.106.084011

Bičák, J., & Dvořák, L. 1976, Stationary Electromagnetic Fields around Black Holes. II. General Solutions and the Fields of Some Special Sources near a Kerr Black Hole, General Relativity and Gravitation, 7, 959, doi: 10.1007/BF00766421

Bičák, J., Lynden-Bell, D., & Katz, J. 1993a, Relativistic Disks as Sources of Static Vacuum Spacetimes, Physical Review D, 47, 4334, doi: 10.1103/PhysRevD.47.4334

Bičák, J., Lynden-Bell, D., & Pichon, C. 1993b, Relativistic Discs and Flat Galaxy Models, Monthly Notices of the Royal Astronomical Society, 265, 126, doi: 10.1093/mnras/265.1.126

Birkhoff, G., & Langer, R. 1923, Relativity and Modern Physics (Harvard University Press, Cambridge)

Bičák, J., & Dvořák, L. 1977, Stationary Electromagnetic Fields around Black Holes, Czechoslovak Journal of Physics B, 27, 127, doi: 10.1007/BF01587004

Cano, P. A., Fransen, K., & Hertog, T. 2020, Ringing of Rotating Black Holes in Higher-Derivative Gravity, Physical Review D, 102, 044047, doi: 10.1103/PhysRevD.102.044047

Cardoso, V., Destounis, K., Duque, F., Macedo, R. P., & Maselli, A. 2022, Black Holes in Galaxies: Environmental Impact on Gravitational-Wave Generation and Propagation, Physical Review D, 105, L061501, doi: 10.1103/PhysRevD.105.L061501

Carter, B. 1969, Killing Horizons and Orthogonally Transitive Groups in Space-Time, Journal of Mathematical Physics, 10, 70, doi: 10.1063/1.1664763

Carter, B. 1970, The commutation property of a stationary, axisymmetric system, Communications in Mathematical Physics, 17, 233, doi: 10.1007/BF01647092

Chandrasekhar, S., & Detweiler, S. 1975, The Quasi-Normal Modes of the Schwarzschild Black Hole, Proceedings of the Royal Society of London A, Mathematical and Physical Sciences, doi: 10.1098/rspa.1975.0112

Chazy, J. 1924, Sur le champ de gravitation de deux masses fixes dans la théorie de la relativité, Bulletin de la Société Mathématique de France, 52, 17, doi: 10.24033/bsmf.1044

Chen, C.-Y., & Kotlařík, P. 2023, Quasinormal Modes of Black Holes Encircled by a Gravitating Thin Disk, Physical Review D, 108, 064052, doi: 10.1103/PhysRevD.108.064052

Cheung, M. H.-Y., Destounis, K., Macedo, R. P., Berti, E., & Cardoso, V. 2022, Destabilizing the Fundamental Mode of Black Holes: The Elephant and the Flea, Physical Review Letters, 128, 111103, doi: 10.1103/PhysRevLett.128.111103

Chitre, D. M., & Vishveshwara, C. V. 1975, Electromagnetic Field of a Current Loop around a Kerr Black Hole, Physical Review D, 12, 1538, doi: 10.1103/PhysRevD.12.1538

Chrzanowski, P. L. 1975, Vector Potential and Metric Perturbations of a Rotating Black Hole, Physical Review D, 11, 2042, doi: 10.1103/PhysRevD.11.2042

Čížek, P., & Semerák, O. 2017, Perturbation of a Schwarzschild Black Hole Due to a Rotating Thin Disk, The Astrophysical Journal Supplement Series, 232, 14, doi: 10.3847/1538-4365/aa876b

Cohen, J. M., & Kegeles, L. S. 1974, Electromagnetic Fields in Curved Spaces: A Constructive Procedure, Physical Review D, 10, 1070, doi: 10.1103/PhysRevD.10.1070

Cohen, J. M., & Kegeles, L. S. 1975, Space-Time Perturbations, Physics Letters A, 54, 5, doi: 10.1016/0375-9601(75)90583-6

Conway, J. T. 2000, Analytical Solutions for the Newtonian Gravitational Field Induced by Matter within Axisymmetric Boundaries, Monthly Notices of the Royal Astronomical Society, 316, 540, doi: 10.1046/j.1365-8711.2000.03523.x

Curzon, H. E. J. 1925, Cylindrical Solutions of Einstein's Gravitation Equations, Proceedings of the London Mathematical Society, 2-23, 477, doi: 10.1112/plms/s2-23.1.477

D'Afonseca, L. A., Letelier, P. S., & Oliveira, S. R. 2005, Geodesics around Weyl-Bach's Ring Solution, Classical and Quantum Gravity, 22, 3803, doi: 10.1088/0264-9381/22/17/028

Deadman, E., & Stewart, J. M. 2010, Linearized Perturbations of the Kerr Spacetime and Outer Boundary Conditions in Numerical Relativity, Classical and Quantum Gravity, 28, 015003, doi: 10.1088/0264-9381/28/1/015003

Demianski, M., & Francaviglia, M. 1981, Type-D Space-Times with a Killing Tensor, Journal of Physics A: Mathematical and General, 14, 173, doi: 10.1088/0305-4470/14/1/017

Edgar, S. B., Gómez-Lobo, A. G.-P., & Martín-García, J. M. 2009, Petrov D Vacuum Spaces Revisited: Identities and Invariant Classification, Classical and Quantum Gravity, 26, 105022, doi: 10.1088/0264-9381/26/10/105022

Evans, N. W., & de Zeeuw, P. T. 1992, Potential-Density Pairs for Flat Galaxies, Monthly Notices of the Royal Astronomical Society, 257, 152, doi: 10.1093/mnras/257.1.152

Fackerell, E. D., & Ipser, J. R. 1972, Weak Electromagnetic Fields Around a Rotating Black Hole, Physical Review D, 5, 2455, doi: 10.1103/PhysRevD.5.2455

Geroch, R., Held, A., & Penrose, R. 1973, A Space-time Calculus Based on Pairs of Null Directions, Journal of Mathematical Physics, 14, 874, doi: 10.1063/1.1666410

Gleiser, R. J., & Pullin, J. A. 1989, Appell Rings in General Relativity, Classical and Quantum Gravity, 6, 977, doi: 10.1088/0264-9381/6/7/005

Griffiths, J., & Podolský, J. 2009, Exact Space-Times in Einstein's General Relativity, Cambridge Monographs on Mathematical Physics, Cambridge (Cambridge University Press)

Israel, W. 1966, Singular Hypersurfaces and Thin Shells in General Relativity, Il Nuovo Cimento B, 44, 1, doi: 10.1007/BF02710419

Jaramillo, J. L., Macedo, R. P., & Sheikh, L. A. 2021, Pseudospectrum and Black Hole Quasinormal Mode Instability, Physical Review X, 11, 031003, doi: 10.1103/PhysRevX.11.031003

Kalnajs, A. J. 1976, Dynamics of Flat Galaxies. III. Equilibrium Models, The Astrophysical Journal, 205, 751, doi: 10.1086/154331

Kegeles, L. S., & Cohen, J. M. 1979, Constructive Procedure for Perturbations of Spacetimes, Physical Review D, 19, 1641, doi: 10.1103/PhysRevD.19.1641

Kerr, R. P. 1963, Gravitational Field of a Spinning Mass as an Example of Algebraically Special Metrics, Physical Review Letters, 11, 237, doi: 10.1103/PhysRevLett.11.237

Kinnersley, W. 1969, Type D Vacuum Metrics, Journal of Mathematical Physics, 10, 1195, doi: 10.1063/1.1664958

Kofroň, D., & Kotlařík, P. 2022, Debye Superpotential for Charged Rings or Circular Currents around Kerr Black Holes, Physical Review D, 106, 104022, doi: 10.1103/PhysRevD.106.104022

Kofroň, D., Kotlařík, P., & Semerák, O. 2023, Relativistic Disks by Appell-ring Convolutions, *submitted to Physical Review D*, arXiv, doi: 10.48550/arXiv.2310.16669

Komar, A. 1959, Covariant Conservation Laws in General Relativity, Physical Review, 113, 934, doi: 10.1103/PhysRev.113.934

Konoplya, R. A. 2021, Black Holes in Galactic Centers: Quasinormal Ringing, Grey-Body Factors and Unruh Temperature, Physics Letters B, 823, 136734, doi: 10.1016/j.physletb.2021.136734

Kotlařík, P., & Kofroň, D. 2022, Black Hole Encircled by a Thin Disk: Fully Relativistic Solution, The Astrophysical Journal, 941, 25, doi: 10.3847/1538-4357/ac9620

Kotlařík, P., Kofroň, D., & Semerák, O. 2022, Static Thin Disks with Power-law Density Profiles, The Astrophysical Journal, 931, 161, doi: 10.3847/1538-4357/ac6027

Kotlařík, P., Semerák, O., & Čížek, P. 2018, Schwarzschild Black Hole Encircled by a Rotating Thin Disc: Properties of Perturbative Solution, Physical Review D, 97, 084006, doi: 10.1103/PhysRevD.97.084006

Kuzmin, G. G. 1956, A stationary Galaxy model admitting triaxial velocity distribution, Astronomicheskiĭ Zhurnal, 33, 27

Ledvinka, T., & Bičák, J. 2019, Disk Sources of the Kerr and Tomimatsu-Sato Spacetimes: Construction and Physical Properties, Physical Review D, 99, 064046, doi: 10.1103/PhysRevD.99.064046

Lemos, J. P. S., & Letelier, P. S. 1994, Exact General Relativistic Thin Disks around Black Holes, Physical Review D, 49, 5135, doi: 10.1103/PhysRevD.49.5135

Lenells, J. 2011, Boundary Value Problems for the Stationary Axisymmetric Einstein Equations: A Disk Rotating around a Black Hole, Communications in Mathematical Physics, 304, 585, doi: 10.1007/s00220-011-1243-8

Letelier, P. S. 2007, Simple Potential–Density Pairs for Flat Rings, Monthly Notices of the Royal Astronomical Society, 381, 1031, doi: 10.1111/j.1365-2966.2007.12128.x

Leung, P. T., Liu, Y. T., Suen, W.-M., Tam, C. Y., & Young, K. 1997, Quasinormal Modes of Dirty Black Holes, Physical Review Letters, 78, 2894, doi: 10.1103/PhysRevLett.78.2894

Leung, P. T., Liu, Y. T., Suen, W. M., Tam, C. Y., & Young, K. 1999, Perturbative Approach to the Quasinormal Modes of Dirty Black Holes, Physical Review D, 59, 044034, doi: 10.1103/PhysRevD.59.044034

Linet, B. 1976, Electrostatics and Magnetostatics in the Schwarzschild Metric, Journal of Physics A: Mathematical and General, 9, 1081, doi: 10.1088/0305-4470/9/7/010

Linet, B. 1977, Stationary Axisymmetric Test Fields on a Kerr Metric, Physics Letters A, 60, 395, doi: 10.1016/0375-9601(77)90030-5

Linet, B. 1979, Stationary Axisymmetry Electromagnetic Fields in the Kerr Metric, Journal of Physics A: Mathematical and General, 12, 839, doi: 10.1088/0305-4470/12/6/013

Mestel, L. 1963, On the Galactic Law of Rotation, Monthly Notices of the Royal Astronomical Society, 126, 553, doi: 10.1093/mnras/126.6.553

Misner, C. W., Thorne, K. S., Wheeler, J. A., & Kaiser, D. I. 2017, Gravitation (Princeton Oxford: Princeton University Press)

Morgan, T., & Morgan, L. 1969, The Gravitational Field of a Disk, Physical Review, 183, 1097, doi: 10.1103/PhysRev.183.1097

Newman, E., & Penrose, R. 1962, An Approach to Gravitational Radiation by a Method of Spin Coefficients, Journal of Mathematical Physics, 3, 566, doi: 10.1063/1.1724257

Petrov, A. Z. 1954, Klassifikacya prostranstv opredelyayushchikh polya tyagoteniya, Uchenye Zapiski Kazanskogo Gosudarstvennogo Universiteta, 114, 55

Petterson, J. A. 1974, Magnetic Field of a Current Loop around a Schwarzschild Black Hole, Physical Review D, 10, 3166, doi: 10.1103/PhysRevD.10.3166

Petterson, J. A. 1975, Stationary Axisymmetric Electromagnetic Fields around a Rotating Black Hole, Physical Review D, 12, 2218, doi: 10.1103/PhysRevD.12.2218

Regge, T., & Wheeler, J. A. 1957, Stability of a Schwarzschild Singularity, Physical Review, 108, 1063, doi: 10.1103/PhysRev.108.1063

Schwarzschild, K. 1916, Über das Gravitationsfeld eines Massenpunktes nach der Einsteinschen Theorie, Sitzungsberichte der Königlich Preußischen Akademie der Wissenschaften (Berlin), 189

Semerák, O. 2002a, Thin Disc around a Rotating Black Hole, but with Support in-Between, Classical and Quantum Gravity, 19, 3829, doi: 10.1088/0264-9381/19/14/321

Semerák, O. 2002b, Towards gravitating discs around stationary black holes (World Scientific), 111–160, doi: 10.1142/9789812776938_0004

Semerák, O. 2003, Gravitating Discs around a Schwarzschild Black Hole: III, Classical and Quantum Gravity, 20, 1613, doi: 10.1088/0264-9381/20/9/302

Semerák, O. 2016, Static Axisymmetric Rings in General Relativity: How Diverse They Are, Physical Review D, 94, 104021, doi: 10.1103/PhysRevD.94.104021

Semerák, O., & Žáček, M. 2000, Oscillations of Static Discs around Schwarzschild Black Holes: Effect of Self-Gravitation, Publications of the Astronomical Society of Japan, 52, 1067, doi: 10.1093/pasj/52.6.1067

Semerák, O., Zellerin, T., & Žáček, M. 1999, The Structure of Superposed Weyl Fields, Monthly Notices of the Royal Astronomical Society, 308, 691, doi: 10.1046/j.1365-8711.1999.02748.x

Semerák, O., & Žáček, M. 2000, Gravitating Discs around a Schwarzschild Black Hole: I, Classical and Quantum Gravity, 17, 1613, doi: 10.1088/0264-9381/17/7/303

Starobinskii, A. A., & Churilov, S. M. 1974, Amplification of Electromagnetic and Gravitational Waves Scattered by a Rotating "Black Hole", Journal of Experimental and Theoretical Physics, 38

Stephani, H., Kramer, D., MacCallum, M., Hoenselaers, C., & Herlt, E. 2003, Exact Solutions of Einstein's Field Equations (Cambridge University Press), doi: 10.1017/CBO9780511535185

Stewart, J. M. 1979, Hertz-Bromwich-Debye-Whittaker-Penrose Potentials in General Relativity, Proceedings of the Royal Society of London A, Mathematical and Physical Sciences, 367, 527, doi: 10.1098/rspa.1979.0101

Stewart, J. M., Walker, M., & Penrose, R. 1997, Perturbations of Space-Times in General Relativity, Proceedings of the Royal Society of London A, Mathematical and Physical Sciences, 341, 49, doi: 10.1098/rspa.1974.0172

Teukolsky, S. A. 1972, Rotating Black Holes: Separable Wave Equations for Gravitational and Electromagnetic Perturbations, Physical Review Letters, 29, 1114, doi: 10.1103/PhysRevLett.29.1114

Teukolsky, S. A. 1973, Perturbations of a Rotating Black Hole. I. Fundamental Equations for Gravitational, Electromagnetic, and Neutrino-Field Perturbations, The Astrophysical Journal, 185, 635, doi: 10.1086/152444

Teukolsky, S. A. 2015, The Kerr Metric, Classical and Quantum Gravity, 32, 124006, doi: 10.1088/0264-9381/32/12/124006

Toomre, A. 1963, On the Distribution of Matter Within Highly Flattened Galaxies., The Astrophysical Journal, 138, 385, doi: 10.1086/147653

Vogt, D., & Letelier, P. S. 2009, Analytical Potential-Density Pairs for Flat Rings and Toroidal Structures, Monthly Notices of the Royal Astronomical Society, 396, 1487, doi: 10.1111/j.1365-2966.2009.14803.x

Wald, R. M. 1978, Construction of Solutions of Gravitational, Electromagnetic, or Other Perturbation Equations from Solutions of Decoupled Equations, Physical Review Letters, 41, 203, doi: 10.1103/PhysRevLett.41.203

Wald, R. M. 1984, General Relativity (Chicago: University of Chicago Press)

Wald, R. M. 1993, Black Hole Entropy Is the Noether Charge, Physical Review D, 48, R3427, doi: 10.1103/PhysRevD.48.R3427

Will, C. M. 1974, Perturbation of a Slowly Rotating Black Hole by a Stationary Axisymmetric Ring of Matter. I. Equilibrium Configurations, The Astrophysical Journal, 191, 521, doi: 10.1086/152992

Zerilli, F. J. 1970, Effective Potential for Even-Parity Regge-Wheeler Gravitational Perturbation Equations, Physical Review Letters, 24, 737, doi: 10.1103/PhysRevLett.24.737

Žáček, M., & Semerák, O. 2002, Gravitating Discs around a Schwarzschild Black Hole II, Czechoslovak Journal of Physics, 52, 19, doi: 10.1023/A:1013957512339

LIST OF PUBLICATIONS

Chen, C.-Y., & Kotlařík, P. 2023, Quasinormal Modes of Black Holes Encircled by a Gravitating Thin Disk, Physical Review D, 108, 064052, doi: 10.1103/PhysRevD.108.064052

Kofroň, D., & Kotlařík, P. 2022, Debye Superpotential for Charged Rings or Circular Currents around Kerr Black Holes, Physical Review D, 106, 104022, doi: 10.1103/PhysRevD.106.104022

Kofroň, D., Kotlařík, P., & Semerák, O. 2023, Relativistic Disks by Appell-ring Convolutions, *submitted to Physical Review D*, arXiv, doi: 10.48550/arXiv.2310.16669

Kotlařík, P., & Kofroň, D. 2022, Black Hole Encircled by a Thin Disk: Fully Relativistic Solution, The Astrophysical Journal, 941, 25, doi: 10.3847/1538-4357/ac9620

Kotlařík, P., Kofroň, D., & Semerák, O. 2022, Static Thin Disks with Power-law Density Profiles, The Astrophysical Journal, 931, 161, doi: 10.3847/1538-4357/ac6027

APPENDIX

A

GHP EQUATIONS

Here we list all GHP equations except those which follow from the prime transformation, complex conjugation or combination of both. The commutation relations for any GHP quantity φ of weights (p, q) are

$$\begin{aligned}\left[\text{Þ}\text{Þ}' - \text{Þ}'\text{Þ}\right]\varphi = \Big[&(\bar\tau - \tau')\eth + (\tau - \bar\tau')\eth' - p(\kappa\kappa' - \tau\tau' + \psi_2 + \Phi_{11} - \Lambda) - \\ &-q(\bar\kappa\bar\kappa' - \bar\tau\bar\tau' + \bar\psi_2 + \Phi_{11} - \Lambda)\Big]\varphi\,,\end{aligned} \tag{A.1}$$

$$\begin{aligned}\left[\text{Þ}\eth - \eth\text{Þ}\right]\varphi = \Big[&\bar\varrho\eth + \sigma\eth' - \bar\tau'\text{Þ} - \kappa\text{Þ}' - p(\varrho'\kappa - \tau'\sigma + \psi_1) - \\ &-q(\bar\sigma'\bar\kappa - \bar\varrho\bar\tau' + \Phi_{01})\Big]\varphi\,,\end{aligned} \tag{A.2}$$

$$\begin{aligned}\left[\eth\eth' - \eth'\eth\right]\varphi = \Big[&(\bar\varrho' - \varrho')\text{Þ} + (\varrho - \bar\varrho)\text{Þ}' + p(\psi_2 + \varrho\varrho' - \sigma\sigma' - \Phi_{11} - \Lambda) - \\ &-q(\bar\psi_2 + \bar\varrho\bar\varrho' - \bar\sigma\bar\sigma' + \bar\psi_2 - \Phi_{11} - \Lambda)\Big]\varphi\,.\end{aligned} \tag{A.3}$$

The Ricci equations are

$$\text{Þ}\varrho - \eth'\sigma = (\varrho - \bar\varrho)\tau + (\bar\varrho' - \varrho')\kappa - \psi_1 + \Phi_{01}\,, \tag{A.4}$$

$$\text{Þ}\varrho - \eth'\kappa = \varrho^2 + \sigma\bar\sigma - \bar\kappa\tau - \tau'\kappa + \Phi_{00}\,, \tag{A.5}$$

$$\text{Þ}\sigma - \eth\kappa = (\varrho - \bar\varrho)\sigma - (\tau + \bar\tau')\kappa + \psi_0\,, \tag{A.6}$$

$$\text{Þ}\tau - \text{Þ}'\kappa = (\tau - \tau')\varrho + (\bar\tau - \tau')\sigma + \psi_1 + \Phi_{01}\,, \tag{A.7}$$

$$\eth\tau - \text{Þ}'\sigma = -\varrho'\sigma - \bar\sigma'\varrho + \tau^2 + \kappa\bar\kappa' + \Phi_{02}\,, \tag{A.8}$$

$$\text{Þ}'\varrho - \eth'\tau = \varrho\bar\varrho' + \sigma\sigma' - \tau\bar\tau - \kappa\kappa' - \psi_2 - 2\Lambda\,, \tag{A.9}$$

and the Bianchi identities

$$\begin{aligned}\text{Þ}\psi_1 - \eth'\psi_0 - \text{Þ}\Phi_{01} + \eth\Phi_{00} = &-\tau'\psi_0 + 4\varrho\psi_1 - 3\kappa\psi_2 + \bar\tau'\Phi_{00} - 2\bar\varrho\Phi_{01} - \\ &- 2\sigma\Phi_{10} + 2\kappa\Phi_{11} + \bar\kappa\Phi_{02}\,,\end{aligned} \tag{A.10}$$

$$\text{Þ}\psi_2 - \eth'\psi_1 - \eth'\Phi_{01} + \text{Þ}'\Phi_{00} + 2\text{Þ}\Lambda = \sigma'\psi_0 - 2\tau'\psi_1 + 3\varrho\psi_2 - 2\kappa\psi_3 + \bar{\varrho}'\Phi_{00} - \\ - 2\bar{\tau}\Phi_{01} - 2\tau\Phi_{10} + 2\varrho\Phi_{11} + \bar{\sigma}\Phi_{02}\,, \tag{A.11}$$

$$\text{Þ}\psi_3 - \eth'\psi_2 - \text{Þ}\Phi_{21} + \eth\Phi_{20} - 2\eth'\Lambda = 2\sigma'\psi_1 - 3\tau'\psi_2 + 2\varrho\psi_3 - \kappa\psi_4 - 2\varrho'\Phi_{10} + \\ + 2\tau'\Phi_{11} + \bar{\tau}'\Phi_{20} - 2\bar{\varrho}\Phi_{21} + \bar{\kappa}\Phi_{22}\,, \tag{A.12}$$

$$\text{Þ}\psi_4 - \eth'\psi_3 - \eth'\Phi_{21} + \text{Þ}'\Phi_{20} = 3\sigma'\psi_2 - 4\tau'\psi_3 + \varrho\psi_4 - 2\kappa'\Phi_{10} + 2\sigma'\Phi_{11} + \\ + \bar{\varrho}'\Phi_{20} - 2\bar{\tau}\Phi_{21} + \bar{\sigma}\Phi_{22}\,, \tag{A.13}$$

and the contracted Bianchi identities

$$\text{Þ}\Phi_{11} + \text{Þ}'\Phi_{00} - \eth\Phi_{10} - \eth'\Phi_{01} + 3\text{Þ}\Lambda = (\varrho' + \bar{\varrho}')\Phi_{00} + 2(\varrho + \bar{\varrho})\Phi_{11} - \\ - (\tau' + 2\bar{\tau})\Phi_{01} - (2\tau + \bar{\tau}')\Phi_{10} - \\ - \bar{\kappa}\Phi_{12} - \kappa\Phi_{21} + \sigma\Phi_{20} + \bar{\sigma}\Phi_{02}\,, \tag{A.14}$$

$$\text{Þ}\Phi_{12} + \text{Þ}'\Phi_{01} - \eth\Phi_{11} - \eth'\Phi_{02} + 3\eth\Lambda = (\varrho' + 2\bar{\varrho}')\Phi_{01} + (2\varrho + \bar{\varrho})\Phi_{12} - \\ - (\tau' + \bar{\tau})\Phi_{02} - 2(\tau + \bar{\tau}')\Phi_{11} - \\ - \bar{\kappa}'\Phi_{00} - \kappa\Phi_{22} + \sigma\Phi_{21} + \bar{\sigma}'\Phi_{10}\,. \tag{A.15}$$

APPENDIX

B

PERTURBATION OF WEYL SCALARS

In a vacuum, the Weyl tensor reduces to the Riemann tensor. The linear perturbation reads

$$R^{\text{exact}}_{\mu\nu\rho\sigma} = R_{\mu\nu\rho\sigma} + \varepsilon \breve{R}_{\mu\nu\rho\sigma} = R_{\mu\nu\rho\sigma} + \epsilon(R^{\alpha}{}_{\nu\rho\sigma} h_{\alpha\mu} + h_{\mu[\sigma;\rho]\nu} + h_{\rho\sigma;[\mu\nu]} + h_{\nu[\rho;\sigma]\mu}) \,. \quad \text{(B.1)}$$

The Weyl scalars then follow from the projection onto the perturbed tetrad, i.e. onto the vector $l^\mu + \varepsilon \breve{l}^\mu$ etc. The terms linear in ε are then

$$\begin{aligned} \breve{\psi}_0 = {} & \breve{R}_{\alpha\beta\gamma\delta} l^\alpha m^\beta l^\gamma m^\delta + \\ & + R_{\alpha\beta\gamma\delta} \breve{l}^\alpha m^\beta l^\gamma m^\delta + R_{\alpha\beta\gamma\delta} l^\alpha \breve{m}^\beta l^\gamma m^\delta + \\ & + R_{\alpha\beta\gamma\delta} l^\alpha m^\beta \breve{l}^\gamma m^\delta + R_{\alpha\beta\gamma\delta} l^\alpha m^\beta l^\gamma \breve{m}^\delta \,, \end{aligned} \quad \text{(B.2)}$$

and similarly for the other Weyl scalars. We can project the perturbation of the vectors onto the background tetrad,

$$\breve{l}^{\hat{a}} = \eta^{\hat{a}\hat{b}} \breve{l}_{\hat{b}} = \eta^{\hat{a}\hat{b}} e_{\hat{b}\alpha} \breve{l}^\alpha \,, \qquad \text{etc,} \quad \text{(B.3)}$$

where $e_{\hat{b}\alpha} = g_{\alpha\beta} e^\beta_{\hat{a}}$. Consider now that the background is of the Petrov type D, i.e. $\psi_0 = \psi_1 = \psi_3 = \psi_4 = 0$. Using the symmetries of the Riemann tensor we find that $\breve{\psi}_0$ and $\breve{\psi}_4$ are given solely by the linear part of the Riemann tensor projected onto the background tetrad. Perturbation of the other Weyl scalars, however, contains additional terms,

$$\breve{\psi}_0 = \breve{R}_{\alpha\beta\gamma\delta} l^\alpha m^\beta l^\gamma m^\delta \,, \quad \text{(B.4)}$$

$$\breve{\psi}_1 = \breve{R}_{\alpha\beta\gamma\delta} l^\alpha n^\beta l^\gamma m^\delta + \breve{l}^{\bar{m}} (\bar{\psi}_2 - 2\psi_2) - \breve{m}^n (\psi_2 + \bar{\psi}_2) \,, \quad \text{(B.5)}$$

$$\breve{\psi}_2 = \breve{R}_{\alpha\beta\gamma\delta} l^\alpha m^\beta \bar{m}^\gamma n^\delta - \psi_2 (\breve{l}^l + \breve{m}^m + \breve{\bar{m}}^{\bar{m}} + \breve{n}^n) \,, \quad \text{(B.6)}$$

$$\breve{\psi}_3 = \breve{R}_{\alpha\beta\gamma\delta} l^\alpha n^\beta \bar{m}^\gamma n^\delta + \breve{\kappa}^m(\bar{\psi}_2 - 2\psi_2) - \breve{\bar{\sigma}}^l(\psi_2 + \bar{\psi}_2)\,, \tag{B.7}$$

$$\breve{\psi}_4 = \breve{R}_{\alpha\beta\gamma\delta} \bar{m}^\alpha n^\beta \bar{m}^\gamma n^\delta\,. \tag{B.8}$$

If the metric in the (exact) tetrad (4.4) should remain the same, we find the following conditions for the tetrad components

$$\breve{l}^l + \breve{\kappa}^n = h_{ln}\,, \qquad \breve{m}^n - \breve{l}^{\bar{m}} = h_{lm}\,, \qquad \breve{l}^n = \frac{1}{2}h_{ll}\,, \quad \breve{m}^{\bar{m}} = -\frac{1}{2}h_{mm}\,, \tag{B.9}$$

$$\breve{m}^l - \breve{\kappa}^{\bar{m}} = h_{nm}\,, \qquad \breve{\bar{m}}^n - \breve{l}^m = h_{l\bar{m}}\,, \qquad \breve{\kappa}^l = \frac{1}{2}h_{nn}\,, \quad \breve{\bar{m}}^m = -\frac{1}{2}h_{\bar{m}\bar{m}}\,, \tag{B.10}$$

$$\breve{\bar{m}}^l - \breve{\kappa}^m = h_{n\bar{m}}\,, \quad \breve{\bar{m}}^{\bar{m}} + \breve{m}^m = -h_{m\bar{m}}\,. \tag{B.11}$$

These conditions are satisfied by, e.g., the following choice

$$\breve{l}^{\hat{a}} = \frac{1}{2}(h_{ln}, h_{ll}, -h_{l\bar{m}}, -h_{lm})\,, \tag{B.12}$$

$$\breve{\kappa}^{\hat{a}} = \frac{1}{2}(h_{nn}, h_{ln}, -h_{n\bar{m}}, -h_{nm})\,, \tag{B.13}$$

$$\breve{m}^{\hat{a}} = \frac{1}{2}(h_{nm}, h_{lm}, -h_{m\bar{m}}, -h_{mm})\,, \tag{B.14}$$

$$\breve{\bar{m}}^{\hat{a}} = \frac{1}{2}(h_{n\bar{m}}, h_{l\bar{m}}, -h_{\bar{m}\bar{m}}, -h_{m\bar{m}})\,. \tag{B.15}$$

Hence, the linear contribution to the Weyl scalars are

$$\begin{aligned}
-2\breve{\psi}_0 = {} & \left[\text{ð}\text{ð} - 2\bar{\tau}'\text{ð}\right] h_{ll} + \left[\text{Þ}\text{Þ} - 2\bar{\varrho}\text{Þ}\right] h_{mm} \\
& - 2\left[\text{Þ}\text{ð} - \bar{\tau}'\text{Þ} - 2\bar{\varrho}\text{ð} - 2\bar{\varrho}\bar{\tau}'\right] h_{(lm)}\,,
\end{aligned} \tag{B.16}$$

$$\begin{aligned}
-4\breve{\psi}_1 = {} & \left[\text{Þ}'\text{ð} + (\tau - \bar{\tau}')\text{Þ}' + (2\varrho' - \bar{\varrho}')\text{ð} + 2\tau(2\varrho' + \bar{\varrho}')\right] h_{ll} \\
& + \left[-\text{Þ}\text{ð} + (\bar{\tau}' - \tau)\text{Þ} + (2\bar{\varrho} - \varrho)\text{ð} - 2\varrho\tau + 2\bar{\varrho}\bar{\tau}'\right] h_{(ln)} \\
& + \Big[-\text{Þ}\text{Þ}' - \text{ð}\text{ð}' + (2\bar{\varrho}' - 3\varrho')\text{Þ} + \bar{\varrho}\,\text{Þ}' + (2\bar{\tau} - 3\tau')\text{ð} + \bar{\tau}'\text{ð}' \\
& \quad + \frac{\varrho}{\bar{\varrho}}\bar{\psi}_2 - 2\frac{\bar{\varrho}}{\varrho}\psi_2 - 2\varrho\varrho' - 2\tau\tau' + 2\bar{\varrho}(2\varrho' + \bar{\varrho}') + 2\bar{\tau}'(\bar{\tau} + 2\tau')\Big] h_{(lm)} \\
& + \left[\text{ð}\text{ð} + 2(\tau - \bar{\tau}')\text{ð} + 2\tau(\tau - \bar{\tau}')\right] h_{(l\bar{m})} \\
& + \left[\text{Þ}\text{Þ} + 2(\varrho + \bar{\varrho})\text{Þ} + 2\varrho(\varrho + \bar{\varrho})\right] h_{(nm)} \\
& + \left[\text{Þ}\text{ð}' + (3\tau' - \bar{\tau})\text{Þ} - \bar{\varrho}\,\text{ð}' + 2\tau'(\varrho - \bar{\varrho})\right] h_{mm} \\
& + \left[-\text{Þ}\text{ð} + (\bar{\tau}' - \tau)\text{Þ} + (2\bar{\varrho} - \varrho)\text{ð} + 2\bar{\varrho}(\bar{\tau}' - \varrho)\right] h_{(m\bar{m})}\,,
\end{aligned} \tag{B.17}$$

$$\begin{aligned}
-6\breve{\psi}_2 = {} & \left[\frac{1}{2}\text{Þ}'\text{Þ}' + (2\varrho' - \bar{\varrho}')\text{Þ}' + \varrho'(3\varrho' - 2\bar{\varrho}')\right] h_{ll} \\
& + \Big[-\text{Þ}\text{Þ}' - \text{ð}\text{ð}' + (\bar{\varrho} - \varrho)\text{Þ}' + 2(\bar{\varrho}' - \varrho')\text{Þ} + (\bar{\tau}' - \tau)\text{ð}' + 2(\bar{\tau} - \tau')\text{ð} \\
& \quad - \frac{\varrho'}{\bar{\varrho}'}\bar{\psi}_2 + \left(3 + 2\frac{\bar{\varrho}'}{\varrho'}\right)\psi_2 + 4\varrho\varrho' + 4\tau\tau' - 2\bar{\varrho}(2\varrho' + \bar{\varrho}') - 2\bar{\tau}'(\bar{\tau} + 2\tau')\Big] h_{ln} \\
& + \left[-\text{Þ}'\text{ð}' + (\bar{\tau} - 2\tau')\text{Þ}' - 2(\varrho' - \bar{\varrho}')\text{ð}' + 2(\bar{\varrho}'\bar{\tau} - 3\varrho'\tau')\right] h_{lm} \\
& + \left[2\text{Þ}'\text{ð} + 2(2\tau - \bar{\tau}')\text{Þ}' + 2(\varrho' - \bar{\varrho}')\text{ð} + 8\varrho'\tau\right] h_{l\bar{m}}
\end{aligned}$$

$$
\begin{aligned}
&+\left[\frac{1}{2}\text{Þ}\text{Þ}+(2\varrho-\bar{\varrho})+\varrho(3\varrho-2\bar{\varrho})\right]h_{nn}\\
&+\left[2\text{Þ}\eth'-2(\bar{\tau}-2\tau')\text{Þ}+2(\varrho-\bar{\varrho})\eth'+8\varrho\tau'\right]h_{nm}\\
&+\left[-\text{Þ}\eth+(\bar{\tau}'-2\tau)\text{Þ}+2(\bar{\varrho}-\varrho)\eth+2(\bar{\varrho}\bar{\tau}'-3\varrho\tau)\right]h_{n\bar{m}}\\
&+\left[\frac{1}{2}\eth'\eth'+(2\tau'-\bar{\tau})\eth'-\tau'(2\bar{\tau}+3\tau')\right]h_{mm}\\
&+\Big[-\text{Þ}\text{Þ}'-\eth\eth'+2(\bar{\varrho}'-\varrho')\text{Þ}+(\bar{\varrho}-\varrho)\text{Þ}'+2(\bar{\tau}-\tau')\eth+(\bar{\tau}'-\tau)\eth'\\
&+\frac{\varrho'}{\bar{\varrho}'}\bar{\psi}_2-\left(3+2\frac{\bar{\varrho}'}{\varrho'}\right)\psi_2-4\varrho\varrho'-4\tau\tau'-2\bar{\varrho}(2\varrho'+\bar{\varrho}')+2\bar{\tau}'(\bar{\tau}+2\tau')\Big]h_{m\bar{m}}\\
&+\left[\frac{1}{2}\eth\eth+(2\tau-\bar{\tau}')\eth+\tau(3\tau-2\bar{\tau}')\right]h_{\bar{m}\bar{m}}\,,
\end{aligned}
\tag{B.18}
$$

and $\breve{\psi}_3, \breve{\psi}_4$ follow from the prime transformation

$$
\breve{\psi}_3=\breve{\psi}_1'\,,\qquad \breve{\psi}_4=\breve{\psi}_0'\,. \tag{B.19}
$$

The symmetric form (4.104) can be obtained from (B.16) using Ricci equations for the type-D spacetimes.